Theses and Dissertations

1-1-1975

Fracture analyses of full size beams with welded details.

Keith Dale Boyer

Follow this and additional works at: http://preserve.lehigh.edu/etd

Part of the Civil Engineering Commons

FRACTURE ANALYSES OF FULL SIZE BEAMS

WITH WELDED DETAILS

by

Keith Dale Boyer

A THESIS

Presented to the Graduate Committee

of Lehigh University

in Candidacy for the Degree of

Master of Science
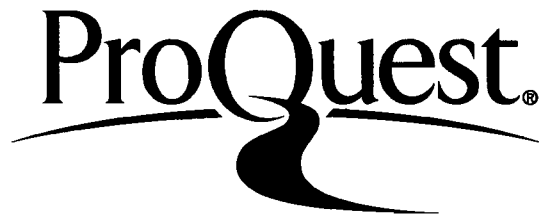
in

Civil Engineering

Lehigh University

May, 1976

ProQuest Number: EP76076

![ProQuest](ProQuest logo)

ProQuest EP76076

This thesis is accepted and approved in partial fulfillment

of the requirements for the degree of Master of Science.

May 5, 1976
(date)

Professor John W. Fisher
Professor in Charge

Professor David A. VanHorn
Chairman, Department
of Civil Engineering

ii

ACKNOWLEDGMENTS

TABLE OF CONTENTS

LIST OF TABLES

LIST OF FIGURES

ABSTRACT

Twelve full size beams with Category E welded details were fabricated from A36, A588 and A514 steels which met the current AASHTO toughness specifications. These beams were cyclically loaded at room temperature for 2 million cycles and then at temperatures - 40° F (-40° C) and lower until rapid fracture occurred. The fracture resistance of each beam was estimated using Linear Elastic Fracture Mechanics and compared to the material toughness test results. Current material toughness and fatigue specification were also checked for applicability to full scale beams.

Results of the beam fracture resistance estimations were in direct correlation with the slow bend (one second loading), 3 point bend, material tests. The welding residual stresses had a significant contribution to the fracture resistance estimation.

Category E of the current AASHTO fatigue specifications was found to be applicable to the 12 in. (305 mm) flange attachment. However, this category was observed to overestimate the fatigue strength of the full size cover plate beams. At the time of fracture most of the fatigue life of the welded girder was exhausted. Hence, fatigue resistance design is a major objective of any fracture control plan for bridge girders.

1. INTRODUCTION

Recent fractures of steel bridges in the United States, along with the current trend of designing welded details with thick high-strength steel has prompted FHWA to sponsor this project. Entitled "Determination of Tolerable Flaw Sizes in Full Size Bridge Weldments", the main objective is to correlate actual full size beam fractures with current material characterization tests. From these correlations, simple design guidelines and information are to be developed. Other objectives are to test present fracture toughness specifications and to develop guidelines for in-service bridge inspections.

A welded detail can be considered as a region of material with many small or microscopic flaws. Recent studies have revealed that these microscopic flaws can become macroscopic after repeated application of load. The major factors affecting crack initiation, crack growth and the eventual fatigue life of a welded bridge member are the stress range, the stress concentration, and the initial flaw condition[1,2].

The fabrication of a welded detail results in residual stresses. These residual stresses have large tensile components in or near the welds. This, in combination with the complex stress concentration and macroscopic fatigue flaws, can make welded details susceptible to rapid fracture. This is especially true of those details fabricated with thick high-strength steel.

This project consists of three parts. The first is the fatigue and fracture testing of 24 full size welded beam specimens with details which are commonly used in bridge design. The details were chosen from the AASHTO categories for fatigue design[3]. Two Category E details were chosen: the coverplate and the lateral attachment. The intermediate Category C detail was the transverse stiffener. The flange thickness transition provided the upper bound fatigue strength detail (Category B). Six beams were fabricated for each of the four detail categories. Each detail type was fabricated in three types of steel. A list of the details is shown in Table 1.1.

The second part of the study was a detailed material characterization. Materials from which these beams were fabricated were evaluated using several fracture toughness tests.

The third part is an analytical treatment of crack shapes which may be encountered during the beam tests. This has been completed in a report by Irwin and Tada[4]. The results of this study were used to estimate the critical stress intensity factor for the fractured beams.

This report contains the results and discussion of the 12 beam tests with lateral attachment details and cover plate details, and a summary of part of the material characteristics. Also included is a description of the tests and testing procedures.

2. DESCRIPTION OF TESTS

2.1 Test Specimens

The twelve welded beam specimens were fabricated by the Bethlehem Steel Corporation at their Bridge Division Fabrication Plant in Pottstown, Pennsylvania. All specimens were fabricated using current fabrication and inspection techniques.

Each thickness of material was furnished from the same heat for each of the three types of steel. Chemical composition, as defined by the mill reports, is shown in Tables 2.1. As beam components were flame cut from the larger rolled plates, a cutting schedule was maintained. Material testing samples were later cut from the same plate.

After the beam components were cut to size, the edges of the web plate were blast cleaned. The web and flange components were then assembled in a beam welder and the web to flange longitudinal fillet welds were then made by an automatic submerged-arc process. These welds were kept continuous. Any visible flaw such as excessive porosity was gouged out and rewelded.

The lateral attachment plates and the cover plates were connected after the cross section was completed. The groove weld lateral attachment plates were welded by a semi-automatic submerged arc process. The run-out tabs were then ground to an approximate radius of 0.75 in. (19.1 mm). The transverse fillet welds at the overlapped lateral attachment plate were made manually.

For each type of steel, ASTM A36, A588 Gr50, and A514, two beams were fabricated. A detailed drawing of beam specimen B4 is shown in Fig. 2.1a. Note that Beams B2 and B2A have smaller flange dimensions which were necessary to satisfy the jack capacity.

The cover plate beam specimens were also fabricated in three steel types. The A36 and A588 beams were rolled sections, W36 x 260 and W36 x 230 respectively, and the A514 was a built-up member. Each beam had two details, one with a transverse end weld and one without a transverse end weld. Detailed drawings of Beams B3 and B1 are shown in Figs. 2.1b and 2.1c. All measured beam dimensions are summarized in Table 2.2.

2.2 Test Setup

All beam testing was done on the dynamic test bed in Fritz Engineering Laboratory, Lehigh University. The test span length was 21 ft. (6.40 m). Two 110 kip (489.5 kN) Amsler jacks driven by a single pulsator were used for the 260 cpm (4.3 Hz) cyclic load. When needed to raise the level of maximum stress, a constant load jack was also used.

The latter jack was a 200 kip (890 kN) Parker-Hannifin jack loaded with an Amsler accumulator and maintained by a column of nitrogen. A schematic of the loading setup and geometry is shown in Fig. 2.2. Photographs of the setup are shown in Figs. 2.3 and 2.5.

2.3 Instrumentation

SR-4 strain gages were used extensively to control the strain during the fatigue and fracture tests. Also, electrical resistance temperature gages were used to monitor the beam's temperature.

Four electrical resistance strain gages were mounted on the tension flange and used as strain control when determining the beam deflections and loads. Two gages on the compression flange were used as a lateral buckling indicator. Since the strain gages were mounted close to the section to be cooled, temperature compensation plates were used to counteract thermal effects. The position of these gages is shown in Fig. 2.4 for the lateral attachment beam specimens. The cover plate beam specimens used a similar strain gage layout.

Initially, temperature gages were mounted directly on the steel beam at the critical section. After two fracture tests, it was found that the same surface temperature readings could be obtained by attaching the gages to steel plates, 1/16 in. x 1½ x 1½ in. (1.6 mm x 38.1 mm x 38.1 mm) and clamping these plates to the critical section of the beam. This procedure was very economical, since one gage could be reused for several tests. Usually three to five temperature gages were used on one beam section during a fracture test on the lateral attachment beam specimens. The position of these gages is also shown in Fig. 2.4. The cover plate beam fracture tests utilized only two temperature gages at the end of each cover plate on the outer flange surface.

To eliminate air temperature effects, the outer surface of the plates was covered with a 1/2 in. (12.7 mm) thick styrofoam insulation. The gages were positioned to avoid direct liquid nitrogen contact to assure accurate surface temperature.

2.4 Cooling Apparatus and Enclosure

Each beam was cooled from room temperature to a desired temperature with liquid nitrogen. The section or sections of the beam to be cooled were completely enclosed in a styrofoam box. The boxes were made relatively leak-proof by the use of sealing compound and duct tape. Inside each box was a copper tubing network which sprayed the top and both sides of the beam with liquid nitrogen.

Since cold gaseous nitrogen is heavy, the cold gas had a tendency to settle to the bottom of the cooling box. Without convective flow, this would cause a sharp temperature gradient across the beam section. Therefore, the inlet for the nitrogen was placed at the top of the beam. Connected to this inlet was a pressurized dewar of liquid nitrogen. By regulating the pressure within this container, the temperature in the box could be controlled.

An attempt was made to achieve uniform temperature throughout the beam cross-section. Since most of the nitrogen still in its liquid state remained in a tray at the bottom of the box, trays were also placed in the upper section of the box. This device made temperatures noticeably more uniform across the section being cooled. A sketch and photographs are shown in Figs. 2.2 and 2.5.

2.5 Design Stresses

In accordance with the 1974 Interim Specifications, the lateral attachment details and the cover plate details were classified as Category E. The allowable stress range for these types of details for two million design cycles is 8 ksi (55.2 MPa).

2.5.1 Lateral Attachment Details

Each beam had two different lateral attachment details as illustrated in Fig. 2.1a. One was an overlapped, 12 in. (305 mm) long attachment with transverse fillet welds on the inside of the tension flange, and a longitudinal fillet weld along the beam flange-tip. The other was a 12 in. (305 mm) long, groove weld attachment welded to the flange-tip. The 1 in. (25.4 mm) thick plate was flush with the outer surface of the flanges. The groove welded attachment had a sharp radius of about 0.75 in. (19.1 mm) where the reinforcement was removed by grinding at the weld ends.

The maximum stress was governed by the outermost fiber of the tension flange. The stress range was set on the inside of the tension flange. This yielded a nominal applied maximum stress and stress range at the overlapped fillet weld detail of (0.889) x (0.55 σ_Y) and 8 ksi (56.2 MPa) respectively. At the groove weld detail the maximum stress and stress range were 0.55 σ_Y and 9 ksi (62.1 MPa). These values were slightly different for Beams B2 and B2A. Actual values are shown in a schematic for each steel type in Figs. 2.6a, b and c.

2.5.2 Cover Plate Details

The maximum stress, .55 σ_Y, and the stress range, 8 ksi, were set on the outermost fiber of the tension flange at the cover plate ends. Actual values of these stresses are shown in Figs. 2.6 d, e, and f for each steel type.

2.6 Load and Deflection Control

Deflection control was used during the fatigue testing at room temperature. The desired stresses were obtained by averaging the four strain gages mounted on the tension flange. For each stress, deflections were obtained from a pair of deflection gages placed on either surface of the tension flange. When the maximum and minimum stresses were set, an appropriate set of deflections was obtained. The beam was then loaded cyclically between these deflections. Therefore, load adjustments for inertia forces were not required. A tolerance of ±0.003 in. (0.8 mm) deflection was maintained.

The fracture test loading could not be deflection controlled since any small temperature gradient across the beam section may have caused misleading deflections. Therefore, the dynamic loads were noted during the fatigue testing and these loads were then used to control loading during the fracture tests. Dynamic stress measurements confirmed the adequacy of the procedure.

2.7 General Testing Procedure

The first beam tested, B4A, served as a pilot study. Initially 1.5 million cycles of load were applied at a stress range of 8 ksi (55.25 MPa) at the fillet weld detail and 9 ksi (62.1 MPa) at the groove weld detail. At this point the beam section containing the largest fatigue cracks was tested at -40° F (-40° C) for one-half hour. No fracture occurred and the beam was fatigue cycled for an additional 250,000 cycles, at which time another -40° F (-40° C) test was run. This fatigue and fracture test sequence was repeated until a fracture occurred.

Failure did not occur when the fatigue cracks were small and still in the stress concentration area. The fatigue cracks destroyed about 70% of the tension flange area before fracture occurred. This extended fatigue and fracture sequence took considerable time to complete as altogether eight test sequences were carried out. For these reasons the test procedure was modified on subsequent tests as follows.

Each subsequent beam was cyclically loaded for two million cycles or until the fatigue cracks became a possible critical size, whichever occurred first. At this point each section of the beam containing the details was cooled to -40° F (-40° C). The beam was then cycled for at least one-half hour between a maximum stress of 0.55 σ_Y and a minimum stress of 0.55 σ_Y - σ_r. If no visible fatigue cracks existed after two million cycles the fracture test was discontinued and further fatigue cycles applied at room temperature.

If there was a possible critical fatigue crack at the beginning of the first fracture test and no fracture occurred in the first one-half hour, either an extended test at −40° F (−40° C) was run or the temperature was dropped below −40° F (−40° C). This temperature drop was done slowly to obtain accurate surface temperature readings. This extended test was continued until fracture or until the liquid nitrogen supply was depleted. If there was no fracture, the beam was again fatigue cycled at room temperature to increase the crack size.

The next low temperature test was run on the detail with the largest fatigue crack after the crack had grown a predetermined amount. This fatigue and fracture test sequence was continued until a fracture occurred.

2.8 Fatigue Testing

The stress range used in the fatigue test was in accordance with the 1974 AASHTO allowable range of stress for two million cycles at the fillet welded attachment for a Category E detail. An allowable stress range of 8 ksi (55.2 MPa) is permitted for a Category E detail.

It was initially intended to fatigue cycle between the same minimum and maximum stress limits as in the fracture tests. However, this was discontinued after three tests for several reasons. First, operating the constant load jack under cyclic deflection for such extended periods caused excessive wear and heating which caused damage to the hydraulic ram. In addition, it appeared that fatigue cracking at room temperature at the limit of allowable stress could cause effects

known as "warm prestressing"[5,6]. Such effects, if present, could result in a greater apparent fracture resistant condition. The earlier studies by Fisher, et al.[1,2] have demonstrated that the level of maximum stress has no appreciable affect on fatigue. Hence, in subsequent tests, the cyclic stress range was applied at a lower level of maximum stress.

During the fatigue test period, frequent checks were made for visible fatigue cracks. Mainly, visual inspections were made with a 10X magnifying glass and a clearner fluid. At times a magnetic particle probe was also used. Since the cycling was continued twenty-four hours a day, some of the cracks were 1 in. (25.4 mm) corner cracks before they were discovered.

An automatic shut-off switch was used to prevent extremely large edge cracks from occurring before the scheduled fracture tests. The switch was usually set for a 0.005 in. (.13 mm) deflection increase.

2.9 Fracture Testing

During the pilot study, the beam was tested at low temperatures after an initial 1.5 million cycles of loading. In subsequent tests, the initial fracture test was run after accumulating two million cycles of cyclic load, as it was apparent that no brittle fracture would occur at this stage of testing as the fatigue cracks were small.

In preparation for the fracture test, the moveable temperature gage plates were clamped to the beam at various points around

both beam sections to be cooled as shown in Fig. 4. The gages used for test control were placed at the crack planes on the exterior surface of the tension flange. Actual temperature gage placement is noted in Table 2.3.

The cooling apparatus was then put in place and the styrofoam boxes were sealed. Most leakage was stopped during the initial cooling period. The temperature was monitored constantly and recorded every five minutes. When the temperature at the test control gages reached $-40°$ F ($-40°$ C), the liquid nitrogen flow was regulated to maintain the test temperature.

During the first fracture test, both beam sections containing the welded details were cooled simultaneously. By regulating the liquid nitrogen flow, the temperature in each box was kept relatively close, $±5°$ F ($±2.8°$ C).

When the temperatures at the critical details became stable, cyclic loads were applied. Prior to applying the maximum allowable stress of $0.55 \sigma_Y$ and the full design stress range level, the crack tip was marked by applying cyclic stresses between the limits of $0.55 \sigma_Y - \sigma_r$ and $0.55 \sigma_Y - \sigma_r/2$. This cyclically applied stress was continuted for approximately thirty minutes, after which the full stress range was applied to the maximum nominal stress of $0.55 \sigma_Y$. In most cases, the initial set of dynamic loads yielded a minimum stress of $0.55 \sigma_Y - \sigma_r$ and a maximum stress of $0.55 \sigma_Y$. A load history for each beam is shown in Tables 2.4 through 2.15.

During each low temperature test, one of the tension flange strain gages was monitored on a memory oscilloscope. This trace showed both the sinusoidal loading rate and the fracture point. Since the triggering at failure was manual, only one trace was obtained at fracture and is shown in Fig. 2.7.

A sinusoidal loading rate of 260 cpm (4.3 Hz) was provided by the Amsler pulsator. This resulted in a loading rate of about 0.12 sec. from the minimum stress to maximum stress level. The sinusoidal nature of the cyclic load yielded a maximum loading rate of 100 ksi/sec. (690 MPa/sec.). As can be seen in Fig. 2.7 the fracture occurred at a point approximately 95% of the maximum load. This was typical of subsequent tests as well. However, the nominal maximum load will be used for the fracture analysis.

3. MATERIALS CHARACTERIZATION

3.1 Test Plan

For the purposes of material characterization Standard Charpy V-Notch (CVN) and Dynamic and Static Fracture Toughness (K_c) tests were carried out on each plate thickness. Mill test data for each plate was also available. Initially it was desirable to determine the fracture toughness of the flange plates {2 in. (51 mm) - A36 steel; 2 in. (51 mm) - A588 steel; and 1-1/2 in. (38 mm) - A514 steel}. The chemical composition and mill test data are summarized in Tables 2.1a, b, c and d. These plates were used to fabricate the test beams described in this report. In this section, a brief description of the experimental procedure and the test results are presented.

3.2 Charpy V-Notch Impact Tests

In order to determine the macroscopic brittle-ductile transition behavior of the plate materials, conventional ASTM standard A370-68 Type A Charpy V-Notch specimens were prepared from each of the three plates. The specimens were all transverse (LT) with notch direction perpendicular to the rolling direction. The impact test data was analyzed using a least squares best fit sigmoidal computer program developed at Lehigh University.

3.3 Fracture Toughness Measurements

The Charpy V-Notch data was used to select a test temperature range so that valid fracture toughness data could be acquired for the

plates. Temperatures of 0° F (18° C), -40° F (-40° C) and -80° F (-62° C) were chosen for dynamic testing. A lower temperature range based on the transition temperature shift[7] was selected for the slow bend (intermediate loading rate) tests. Equation 1 was used to estimate where additional tests were conducted at other temperatures

$$T_{shift} = 215 - 1.5 \, \sigma_Y \qquad (1)$$

T_{shift} = transition temperature shift (° F)

σ_Y = room temperature static yield stress (ksi)

3.3.1 Drop Weight Test Apparatus

The dynamic K_c testing was carried out using the Lehigh drop weight test machine (see Fig. 3.1). The details of this apparatus are described in Ref. 8. The impact loading of the three-point bend specimen (Fig. 3.2) was achieved by means of a falling mass (400 lbs.) guided vertically along two parallel rails. An instrumented loading tup[8] at the bottom of the mass was calibrated to act as a load-dynamometer. As the specimen was loaded the strain output from the tup was recorded. A typical load-time relationship is shown in Fig. 3.3. The drop weight mass in a given set of tests was chosen to minimize the test specimen inertia. In order to minimize the influence of the specimen inertia, 3/4 in. x 1/2 in. (19.1 mm x 12.7 mm) half-rounds were positioned on the test specimen. This cushioned the application of the load and increased the loading time to about one millisecond. The half round cushions were machined from unhardened drill rods. The test specimen

temperatures were controlled by a variety of means. All were held at the required test temperature for at least ten minutes prior to testing. A test was completed within ten seconds of the specimen's removal from the temperature bath.

3.3.2 Slow Bend Test Apparatus

Slow bend tests* were carried out on a standard 120 kip Tinius-Olsen screw-type tensile testing machine. The cross head of the machine could be moved at various speeds. The specimen was loaded with the same tup used for the dynamic testing. A loading rate of 20 kips per second was selected for all slow bend tests. This resulted in a loading time of about 1 second. Load-time data was recorded on x-y recorders. Fracture tests of the customary "static" type, with a loading time to fracture of several minutes, were not conducted.

3.3.3 K_c Specimen Preparation

The test specimen geometry for all K_c tests in this program is shown in Fig. 3.2. All specimens were saw cut from the original plate with their long dimension in the rolling direction. This resulted in the crack being perpendicular to the rolling direction.

---

* Tests in which the fracture load occurs about 1 second after the start of loading are not "slow" in the customary usage of the term. Such tests are sometimes termed "intermediate speed" tests. However, for simplicity of language in this report, the 1 second loading time tests will be termed "slow bend".

After the individual specimens were saw cut from the plates the cut surfaces were shaped so as to be normal to the plate surfaces. The thickness of the A36 and A588 steel specimens was reduced to 1-1/2 in. (38 mm). A notch with a 30° chevron front was machined at the center of the specimens to help initiate crack growth during the precracking process. The cyclic-loading for precracking was done on a 10 ton Amsler Vibrafore using three-point bending. The fatigue crack was formed in two stages. During the first stage, the crack was grown as quickly as possible. The final 1/8 in. (3 mm) of the crack was grown slowly so that the average crack growth rate was equal or less than 1 microinch per cycle (25.4 nm per cycle). The maximum K during fatigue precracking was about 40 ksi $\sqrt{in.}$ (44 MPa $\sqrt{m}$).

3.3.4 Fracture Toughness Data Evaluation

The fracture toughness, K_c, values were determined from the maximum load at the fracture of the three-point bend specimens[9]. K was determined from the relationship

$$Y = \frac{K\ B\ W^2}{1.5\ PL\ \sqrt{a'}} = 1.93 - 3.12 \left(\frac{a'}{W}\right) + 14.68 \left(\frac{a'}{W}\right)^2 - 25.3 \left(\frac{a'}{W}\right)^3 + 25.9 \left(\frac{a'}{W}\right)^4$$

(2)

where   Y = dimensionless ratio

B = specimen width

W = specimen depth (3.0 in.)

P = applied load

L = span length (10.0 in.)

a = effective crack length

r_y = plastic-zone size

a' = a + r_y

The plastic-zone size, r_y, was defined as

$$r_y = \frac{1}{2\pi} \left(\frac{K}{\sigma_Y}\right)^2 \tag{3}$$

where σ_Y is yield stress

Equations 2 and 3 were solved by a simple iteration method[9]. The value of σ_Y corresponded to the temperature and loading speed of the test conditions. This was determined by the following equation[10].

$$\sigma_{Yd} = \sigma_Y \Big|_{+ 75° F, t_o} + \frac{174,000}{(T + 459) \log (2 \times 10^{10}t)} - 27.4 \tag{4}$$

where   t = loading time to maximum load

t_o = time of load application for a static test (50 sec.)

T = testing temperature (°F)

σ_Y = yield stress (ksi)

σ_{Yd} = elevated yield stress (ksi) at test conditions

3.4 Drop Tear Energy Measurements

A method of direct measurement of fracture energy was described in Ref. 8. After the specimen is fractured the drop weight is

arrested by two cushions made from Type 1100-0 or 6061-0 electrical grade aluminum 1 in. (25.4 mm) diameter rods. Figure 3.1 shows the test setup. When the drop weight impacts the aluminum blocks, they are compressed inelastically and their difference in height is a measure of the energy absorbed. In addition, the drill rod cushions are subjected to permanent diamond shaped indentation during loading of the specimen. The length of the identation is also a function of the energy absorbed.

The initial potential energy in the system less the sum of the energies absorbed by the aluminum and drill rod cushions represents the net energy absorbed by the fractured specimen. This value divided by the fracture surface area yields the drop tear energy (DTE). Material behavior in terms of DTE as a function of temperature is obtained simultaneously with the K tests.

3.5 Results of Fracture Tests

3.5.1 Charpy V-Notch Tests

Figures 3.4 through 3.8 summarize the CVN test results in the form of standard Charpy V-Notch curves. For the three materials the energy absorption and the lateral expansion data, plotted against temperature, show a conventional form with relatively sharp transition behavior. The 15 ft.-lb. (20 joule) energy level and the 15 mil. (0.38 mm) lateral expansion transition temperatures are listed in Table 3.1 for each flange plate.

3.5.2 K_c Test Results

The dynamic and static fracture toughness for the flange plates are summarized in Figs. 3.9 through 3.13. Also shown is the limiting test validity requirement[10].

$$B > 2.5 \left(\frac{K_c}{\sigma_Y} \right)^2 \tag{5}$$

where B = specimen thickness

K_c = fracture toughness value

σ_Y = yield stress of the material at test conditions

In some cases, computed K_c values were obtained which did not satisfy the above ASTM thickness requirement. The trend curves for the limited test data were based on earlier results. Although from these curves it was possible to indicate the brittle-ductile transition temperatures, it appears that another independent method to evaluate fracture toughness values at these temperatures will be needed. The J-integral type tests with three-point bend specimens might provide the required data points to confirm the fracture behavior in the transition temperature range.

Barsom's temperature shift relationship (see Eq. 1) was used to determine the expected temperature shift caused by the change in loading rates between dynamic and static tests. These values are listed below for each steel.

| | Temperature Shift | |
	°F	°C
A36	149	65
A588	124	51
A514	32	0
A36 Rolled	129	54
A588 Rolled	115	46

The actual temperature shifts are shown in the K_c vs. temperature plots (Figs. 3.9 through 3.13) for the dynamic and intermediate loading rate tests used in this project. These actual values were in each case, larger than the shifts predicted by Barsom. Hence Eq. 1 is conservative.

The CVN and dynamic K_{IC} results were compared by using the relationship proposed by Barsom[7] for the transition temperature region of the CVN plots

$$K_{Id} = [5E \ (CVN)]^{\frac{1}{2}} \qquad (6)$$

E   = modulus of elasticity (psi)

K_{Id} = fracture toughness (psi $\sqrt{in.}$)

CVN = Charpy energy (ft.-lbs.)

These values are also plotted on the K_c vs. temperature plots in Figs. 3.9 through 3.13. There is a good correlation between the measured K_{Id} values and the plot given by Eq. 6 for A36 steel and the A588 rolled beam steel. However, the correlation is not as good for the A36 rolled beam steel and the A588 and A514 plates. Very conservative results were obtained for the A514 steel. Several unconservative points were obtained for the A588 steel and the A36 rolled beam steel.

-22-

3.5.3 Drop Tear Energy Test Results

The DTE data points were obtained simultaneously with the K_{Id} test data. A full DTE vs. Temperature plot was not obtained. Most of the points were on the lower shelf or in the transition region. The DTE vs. Temperature plots are presented in Figs. 3.14 through 3.16. Generally, the transition temperatures from these diagrams are higher and more conservative than the respective CVN transition temperature for the same plate.

4. LATERAL ATTACHMENT BEAM TEST RESULTS AND ANALYSES

4.1 Fatigue Cracks

The fatigue cracks at the groove weld lateral attachments were initially detected on the flange edge, at the sharp 0.75 in. (19.1 mm) or less radius, as 1/4 in. (6 mm) elliptical surface cracks. These surface cracks soon became elliptical corner cracks and then edge cracks. All final fractures at this detail were precipitated from an edge crack.

On the overlapped fillet weld detail, fatigue cracks were initiated at the toe of the transverse fillet weld. Most of these cracks were initially detected as several 0.5 in. (13 mm) elliptical surface cracks which eventually connected to form one large elliptical surface crack. As with the groove weld detail, these cracks then became corner cracks and finally edge cracks. Beam B6 was the only specimen to fracture from this detail.

The size of the fatigue cracks at each critical detail can be found by referencing the small letters on the fracture surface drawings in Figs. 4.1 to 4.6 with the load history tables given in Tables 2.4 to 2.9.

Many additional fatigue cracks existed at other details on the beams. Figures 4.7 and 4.8 show these fatigue cracks at all details at two million cycles and prior to the last fracture test. The surface measurements of these cracks is shown adjacent to the crack. The crack shapes are merely estimates from these surface measurements.

4.2 Remaining Fatigue Life

The number of cyclic loads needed to propagate an edge crack from its fracture initiation point to an edge crack size of 75% of the flange width, b, was defined as the remaining useful fatigue life had brittle fracture not occurred. The following crack growth relation-ship determined from earlier studies on welded details was used[12].

$$\frac{da}{dN} = 2 \times 10^{-10} \ \Delta K^3 \tag{7}$$

As defined in Section 4.5.2 the stress intensity range can be found from the following relationship

$$\Delta K = \sqrt{\frac{2b}{\pi a'} \ \tan \frac{\pi a'}{2b}} \ \Delta\sigma \ \sqrt{\pi a'} \tag{8}$$

Secondary stress intensity effects from residual stresses were ne-glected for this analysis. Also by this stage of growth the crack had grown out of the stress concentration zone. Through numerical inte-gration of Eq. 8 the remaining fatigue life was estimated. The results for each beam are listed in Table 4.1.

Figure 4.9 shows the mean S-N curve and its confidence limits for Category E details. The data base used to develop this curve utilized tests on 12 to 14 inch (35 to 36 mm) deep beams with a maxi-mum flange thickness of 1/2 in. (12.7 mm). The fatigue results for the lateral attachment beams, which had a maximum flange thickness of 2 in. (51 mm) are plotted on the same curve. The open figures repre-sent the point at which the fatigue cracks were first observed and the

closed figures represent the point of fracture. There is a good correlation between the fracture points and the Category E fatigue-life relationship.

As can also be seen from Fig. 4.9 and the additional life estimated and tabulated in Table 4.1, an incremental addition to the fatigue life was small and would not have significantly altered the strength as all the points were well within the 95% confidence limits. Hence even if rapid fracture had not occurred very little residual life would have remained. Fatigue resistance design is therefore a major objective of any fracture control plan in the design of bridge girders.

4.3 Beam Fracture Tests

Beam B4A

Eight fracture tests were carried out on Beam B4A as the test procedure was developed. Three of these tests were on the overlapped fillet weld detail while five were on the groove weld detail.

The first five fracture tests were run with fatigue cracks still in the stress concentration zone. After 1.5 million cycles the largest fatigue crack found was a 1 in. x 1/16 in. (25.4 mm x 1.6 mm) elliptical corner crack (see Fig. 4.7) at a transverse fillet weld. The first two fracture tests were on this detail. At two million cycles, a 3/8 in. x 1 in. (9.5 mm x 25.4 mm) elliptical corner crack was observed at a groove weld detail. The fracture tests were carried out at test temperatures between -40° F (-40° C) and -60° F (-51° C)

as can be seen in Table 2.7. No crack instability developed during any of these three tests.

A test was run on the fillet weld detail where a 1-7/8 in. x 9/16 in. (48 mm x 14 mm) elliptical corner crack existed. No fracture occurred there as well. With a 1-1/2 in. x 1-3/4 in. (38 mm x 44 mm) corner crack at the groove weld detail (test h) the next test reached a temperature of -170° F (112° C), however, no fracture occurred.

The cracks were extended by applying 250,000 cycles of fatigue loading at room temperature. The critical fatigue crack at the groove weld detail was grown to a ∿ 2-3/4 in. (70 mm) edge crack during this cyclic loading. At this point a -70° F (-56.5° C) fracture test was run. The test lasted 2.67 hours. During this test, the fatigue crack grew very rapidly through the high tensile residual stress region of the web to flange fillet welds. Finally, the beam fractured with an average edge crack size of 4.8 in. (122 mm) and temperature of -96° F (-71° C). Fatigue crack extension of approximately 2 in. (51 mm) was experienced during this test prior to crack instability.

Beam B4

It was apparent from experience with Beam B4A that rapid fracture was not likely to occur at -40° F (-40° C) with small cracks in the stress concentration zone. Therefore, the beam was cycled at room temperature for two million cycles. At this point several large elliptical corner cracks existed as shown in Figs. 4.3 and 4.7. The

first fracture test lasted for one-half hour and both details were tested simultaneously. No fracture occurred.

The beam was then cycled at room temperature to extend the fatigue cracks. When the crack at the critical detail became a ∿ 2-3/8 in. (60 mm) edge crack, a second fracture test was run. A temperature of -70° F (-56.5° C) was obtained before the cyclic load was applied. A stress range of 9 ksi (62.1 MPa) was applied for forty minutes. To speed the incipient fracture, the load range was increased to 9.8 ksi (67.6 MPa) while maintaining the same maximum stress. After one hour at this stress range and a nominal temperature of -70° F (-56.5° C) fracture occurred. At fracture, the temperature was -80° F (-62.0° C). A ∿ 3/4 in. (19 mm) fatigue crack extension was experienced during this test. The fracture occurred when the crack tip was in the high tensile residual stress zone of the web to flange weld.

Beam B6

The first fracture test was run on both details simultaneously after two million fatigue cycles. Since very small fatigue cracks existed (see Fig. 4.7) no fracture occurred. After 800,000 cycles of additional fatigue load the elliptical surface crack at the critical fillet weld detail grew to a large 2-3/8 in. x 1-1/2 in. (60 mm x 38 mm) elliptical corner crack. At this point two consecutive five hour fracture tests were run (test d and e, see Fig. 4.5) on this detail. Fracture occurred after the elliptical fatigue crack became an edge crack. The fracture temperature was -53° F (-47.0° C). This was the only fracture to occur at a fillet weld detail.

During the fatigue cycling of this beam, the ram in the constant load jack overheated. This caused the maximum load to decrease during the fatigue cycling overnight. Although the maximum load decreased, the stress range remained the same. The actual drop in maximum stress was 4.5 ksi (31.03 MPa) for 400,000 cycles.

Beam B2A

Five fracture tests were run on this beam (see Fig. 4.2) The first test at two million cycles was on both details. Both details contained large corner cracks at this point (see Fig. 4.7), however no fracture occurred at −40° F (−40° C). Since the elliptical corner crack at the groove weld detail grew quickly to a critical edge crack, the remainder of the fracture tests were conducted on this detail alone. During the last test, the temperature was maintained at −40° (−40° C) for 1½ hours. While the beam was still being cyclically loaded, the temperature was slowly dropped to −140° F (−95.5° C) in over 1½ hours. The −140° F (−95.5° C) temperature was maintained for another 1½ hours before fracture occurred at −144° F (−98° C). About 1/4 in. (6.4 mm) fatigue crack extension was experienced during the test prior to crack instability.

Note that the beam was fatigue cycled at a lower maximum stress than that during the fracture test. The same stress range was maintained during both fatigue and fracture testing. See Table 2.5 for the actual stresses and stress ranges used.

Beam B6A

The first fracture test was run on both details (see Fig. 4.7) at -40° F (-40° C). No fracture occurred. After an additional 730,000 cycles of fatigue load at room temperature, a corner crack at the groove weld detail became a ∿ 1-1/4 in. (32 mm) edge crack. The subsequent fracture test lasted 1.67 hours during which the temperature was slowly dropped from -40° F (-40° C) to -92° F (-69° C) at which point rapid fracture occurred. An average fatigue crack extension of 1/4 in. (6.4 mm) (see test d, Fig. 4.6) was experienced prior to fracture.

Beam B2

At two million cycles, a 1 in. (25 mm) edge crack existed at the groove weld detail while smaller elliptical corner cracks existed at the fillet weld detail (see Fig. 4.7). Both details were tested for forty minutes at -40° F (-40° C). At this time the cyclic load was stopped and the groove weld detail was cooled to -140° F (-95.5° C). After this temperature was obtained, the cyclic load was reapplied. After twenty minutes of cycling, fracture occurred at a temperature of -155° F (-104° C). A 1/4 in. (6.4 mm) fatigue crack extension was experienced during the last test (see test b, Fig. 4.1).

The beam was fatigue cycled at a lower maximum stress than that during the fracture test. The same stress range was maintained during both fatigue and fracture testing. See Table 2.4 for the actual stresses and stress ranges used.

4.4 Fracture Test Variables Affecting Fracture Toughness

Each fracture test had two major variables affecting the fracture resistance of the steel beam. These were the fatigue crack size and test temperature.

Since no beam fractured on the first cycle of load an effort was made to induce rapid fracture at $-40°$ F ($-40°$ C) by growing the fatigue crack to a critical size. As noted in Section 4.3, Beams B4, B4A, and B6 experienced average fatigue crack extensions of 0.65 in. (17 mm), 2.0 in. (51 mm), and 1.3 in. (33 mm), respectively, prior to brittle fracture. These large crack extensions took several hours to achieve.

Since time was a limiting factor, the test temperature was used as another variable. The slow cooling rate of approximately $1°$ F ($.6°$ C) per minute was used. Temperature at the critical details are shown graphically in Figs. 4.10 to 4.12 for the final 60 minutes of the last fracture test. In every case the temperature was slowly decreasing when fracture occurred.

Although large temperature gradients existed around the critical beam section, as shown in Table 2.3 an effort was made to keep accurate account of the surface temperature at the critical welded detail. The temperature gages were positioned at the critical detail on the exterior of the tension flange, thus being out of direct contact with the liquid nitrogen.

4.5 Stress Intensity Estimates

4.5.1 Introduction

All the flange cracks in the lateral attachment details were large edge cracks at fracture. This tended to simplify the calculations of the stress intensity factor. However, since the plates were flame cut and the beams and details were welded a rather complex residual stress pattern was present at the detail cross-section. Therefore several steps were used to estimate the value of the stress intensity factor, K.

By the method of superposition the following contributions were used to determine the magnitude of K. The primary contribution was from the applied stresses at failure. A secondary contribution was from the residual stresses at the detail cross-section. The residual stresses at the cracked section resulted from two contributions. One contribution to K was from the residual stresses at a typical cross-section of the welded beam. These stresses were caused by the web-to-flange welds and the flame cut plate edges. The other contribution was due to the residual stresses caused by the local detail welds. In this draft these residual stresses were estimated from available information.

In one case, the flange edge crack grew through the web-to-flange welds. The fatigue crack growth continued in two directions, upward into the web and across the flange. Therefore, when estimating the stress intensity, the web interaction had to be considered as well. The web restrained the large flange crack from opening. Thus the

contribution of this web restraint to the stress intensity estimate was negative.

The actual value of K was found to be the sum of three or four terms as shown in Eq. 9

$$K = K_{AS} + K_{RS} + K_{LW} + K_{WR} \tag{9}$$

The subscripts K_{ij} in Eq. 9 are the various contributions to the critical stress intensity. These include contributions from the applied stress, K_{AS}; the residual stress caused by flame cut edges and web-to-flange welds, K_{RS}; the residual stress caused by local detail welds, K_{LW}; and the web restraint of the flange in B4A, K_{WR}.

Plastic-zone corrections were made by using the following plane stress relationship.

$$r_y = \frac{1}{2\pi} \left(\frac{K_c}{\sigma_{Yd}} \right)^2 \tag{10}$$

Using an iterative process between Eqs. 9 and 10 values of K were obtained.

4.5.2 Contribution from the Applied Stress

To estimate the stress intensity from the applied stress for a flange edge crack, the following format was used. Generally,

$$K_{AS} = F(a') \, \sigma_{AS} \, \sqrt{\pi a'} \tag{11}$$

where F (a') consists of four parts as discussed by Albrecht and Yamada[13]

-33-

$$F(a') = F_E \ F_S \ F_W \ F_G$$

F_E = elliptical crack front correction

F_S = free surface correction

F_G = stress concentration correction

F_W = finite width correction

For this study F_E was taken as 1.0 since the cracks were edge cracks. F_S was assumed to be ~ 1.0 because of the lateral restraint offered by the lateral attachment. F_G was also taken as 1.0 for the large edge cracks in this study. This correction affects only small elliptical surface and corner cracks and will be discussed in the next section.

The finite width correction, F_W, was defined by Eq. 12[4].

$$F_W = \sqrt{\frac{2b}{\pi a'} \tan \frac{\pi a'}{2b}} \tag{12}$$

b = flange width

$a' = a + r_y$

a = crack size

r_y = plastic-zone correction

This finite width correction is exact for the model shown in Fig. 4.13. This is not exactly the situation with the flange edge cracks adjacent to the lateral attachment details, however it is a good approximation. The web was assumed to prevent in-plane bending of the flange and the

lateral attachment plates were assumed to partially prevent Poisson contractions on the flange tip as shown in Fig. 4.13b. For these reasons the dimensions used are those shown in Fig. 4.13b.

In the actual beam fractures, the stresses were not uniform through the plate thicknesses nor were the edge crack fronts. For these reasons the critical stress intensity was estimated for 1/3 levels through the flange thickness. The average crack size and stress were used for the respective one-third thickness of the flange. The measured values of the critical crack size, a, for each beam are listed in Table 4.2. The estimated values of K_{AS} are listed in Table 4.3.

4.5.3 Contributions from Stress Concentration

The stress concentrations for the groove weld details were determined from a current study at Fritz Engineering Laboratory. In this study, similar details were modeled using a three-dimensionsal finite element analysis[14]. By comparing certain dimensional parameters, the stress concentration for the uncracked detail was determined to be 2.22 for the groove weld detail with a .75 in. (19 mm) radius transition at the 1.5 in. x 6 in. (38 mm x 152 mm) flange. Similarly, the stress concentration for the groove weld detail attached to the 2 in. x 7 in. (51 mm x 178 mm) flange was estimated as 2.19. These stress concentration factors are lower bound estimates. Examination of the fabricated details showed that for the critical details that cracked, the transition was irregular and not a

smooth radius (see Fig. 4.14a). These irregularities were modeled for the most severe case, a 45° angle reentrant corner with 3/4 in. (19 mm) legs (see Fig. 4.14b). A stress concentration factor of about 7.9 was estimated for this case.

The overlapped fillet weld detail had a comparable stress concentration at approximately 7.1 for the 1-1/2 in. x 6 in. (38 mm x 156 mm) flange and 7.3 for the 2 in. x 7 in. (51 mm x 178 mm) flange. However, only one beam failed from this detail. There are at least two reasons for this. First, surface fabrication discontinuities at the radius elevated the apparent stress concentration. Second, the stress range at the groove weld detail was 12.5% higher than that at the fillet weld detail. The combination of these two differences made the groove weld detail more critical in all but one case.

The stress concentration, K_T, decays as a crack initiates and grows at the detail. This decay is also being studied at Fritz Engineering Laboratory by Zettlemoyer[14]. The study matches the decay described by Albrecht and Yamada[13], to an uncracked elliptical model. By varying the size of the ellipse in an infinite plate the effect of stress concentration decay can be matched. The purpose of this study is to develop a quick and inexpensive method to determine this decay for any detail and stress concentration situation. This analysis was used to model a groove weld detail for stress intensity variation with crack size.

The A514 steel groove weld detail on Beam B2A was examined for stress concentration effects on the stress intensity factor, K.

Results were obtained for two attachment-to-flange reentrant corner models: Case A was the smooth 3/4 in. (19 mm) radius transition (see Fig. 4.14a), Case B was the 3/4 in. (19 mm), 45° straight line transition shown in Fig. 4.14b. The stress concentration decay with crack size, F_G, is shown in Fig. 4.15 for both cases. Since the stress concentration value, K_T, in Case B was much higher than that used in Case A, the decay of K_T with crack growth for Case B was more rapid than Case A. Because of this the maximum stress intensity obtained for Case B was lower than the value obtained for Case A (see Fig. 4.16). Hence, this elevated stress concentration (Case B) at these details did not appreciably magnify the stress concentration, when compared to Case A results, but did cause a more rapid crack initiation.

The variation of stress intensity and crack size is summarized in Fig. 4.16 for both cases. It was conservatively assumed that the small cracks began as small elliptical corner cracks. The variation of the semi-major and semi-minor axes was defined by Eq. 13

$$C = 1.465 \, a^{0.202} \tag{13}$$

where   C = semi-major axis

         a = semi-minor axis

This relationship was determined from crack size measurement data. As can be seen in Fig. 4.16, the maximum stress intensity obtained for elliptical corner cracks was 126 ksi $\sqrt{in.}$ (139 MPa $\sqrt{m}$) for a crack size of .35 in. (9 mm). This value was less than the critical stress

intensity of 145 ksi $\sqrt{in.}$ (159.5 MPa $\sqrt{m}$) for Beam B2A. This value is also less than any slow bend material test result at $-40°$ F ($-40°$ C) (see Fig. 6.3).

4.5.4 Contribution From The Nominal Residual Stresses

K_{RS} is either positive or negative depending upon the magnitude and distribution of the cross-section residaul stresses and the crack size. When a crack grows through a tensile residual stress field there is an additional crack opening caused by the residual stresses which yields a positive K_{RS}. Similarly, when a crack grows through a compressive residual stress field there is crack closure and thus K_{RS} is negative. When a crack grows through both positive and negative residual stress fields, the residual stress condition near the crack tip, along the path of the crack, has an overriding effect.

The residual stress field through which the crack has grown can be approximated by superposition of small block stresses (see Fig. 4.17). K_{RS} can be obtained by using the following equation along with the method of superposition[15]

$$K_{RS} = \frac{2}{\pi} \sigma_{rs} \sqrt{\pi a'} \sqrt{\frac{2b}{\pi a'} \tan \frac{\pi a'}{2b}} \sin^{-1} \left(\frac{\sin \frac{\pi c}{2b}}{\sin \frac{\pi a'}{2b}} \right) \tag{14}$$

a' = edge crack size + plastic zone correction

   (see Table 4.2)

c = dimension from the plate edge to the end or beginning

   of the approximated block of residual stress

b = plate width

-38-

σ_{rs} = magnitude of the residual stress block

To obtain a good approximation of K_{RS}, stress block widths of 0.02 in. (.5 mm) were used over the entire crack length. Results of K_{RS} for each beam fracture are listed in Table 4.3 and plotted as a function of crack size in Figs. 4.18 to 4.23.

Actual measured residual stresses of the nominal beam sections were not available at the time of the lateral attachment detail analyses. The flange residual stresses were estimated from previous studies with similar plate thicknesses[16],[17]. Two assumptions were made in this estimation. First, the distribution of residual stresses through the plate thickness was assumed to be linear. Second, the residual stresses in the flange alone were assumed to be in equilibrium. The estimated residual stress distributions are shown in Figs. 4.25a to 4.27a for each steel. The actual measured residual stress distributions are also shown in Figs. 4.25b to 4.27b.

4.5.5 Contribution from the Local Weld Residual Stresses

The local detail welds change the nominal section residual stress pattern over the entire cross-section at the detail. Ideally, there should be only one residual stress contribution from the actual residual stresses at this critical section. Since there was no available data on residual stress state at this section, a two step procedure was used to estimate the effect along with the principle of superposition.

After the nominal beam section residual stresses were estimated, an additional local residual stress was assumed to account for

the detail welds. Both the nominal residual stresses and the local residual stresses are being measured. Pending completion of these measurements, the local welding effect was simulated in the following manner.

The residual stress distribution along the flange tip at the groove weld detail was assumed as is shown in Fig. 4.28. The decay of the stress along the flange tip was assumed to be very rapid beyond the attachment edge. The stress at the location where most of the cracks initiated was assumed to be about $\sigma_Y/4$. This stress was assumed to be distributed over 1/2 in. (12.7 mm) of the flange tip as shown in Fig. 4.28. Equation 14 was again used to determine the contribution from local welding. These values are also listed in Table 4.3.

The fillet weld detail, top one-third analysis included a different local residual stress distribution because the detail had a fillet weld along the inside surface of the flange. It was assumed that the magnitude of the local residual stress, $\sigma_Y/4$, at the flange tip decayed to $\sigma_Y/8$ at the end of the transverse weld (see Fig. 4.29). The middle and bottom third levels were treated similar to the groove weld details because there was also a longitudinal fillet weld made along the flange tip.

4.5.6 Contribution From The Web Restraint

Only beam B4A was observed to develop web restraint since the fatigue crack at fracture had grown as an edge crack through the web-to-flange welds and then became a two ended crack. This is shown

in Fig. 4.4. The analysis of the web restraint and the apparent reduction of the stress intensity is an iterative solution which is very involved. The actual analysis is discussed in detail in Appendix A. The web restraint was predicted to decrease K by -12 ksi $\sqrt{in}$. (-13.2 MPa $\sqrt{m}$).

4.5.7 Summary and Discussion of the Various Contributions

The values of K_{AS}, K_{RS}, K_{LW} and K_{WR} are listed in Table 4.3 for each one-third level of the flange thickness for each critical fatigue crack. The critical value for each beam was taken as the maximum value. Some modification of these values will be made when actual residual stress measurements are available. Plots showing the variation of each K_{ij} parameter with crack size are presented in Figs. 4.18 to 4.23 for the critical one-third level of flange thickness.

The estimated residual stress diagrams shown in Figs. 4.25 to 4.27 were used to determine the average residual stress distribution for each one-third level of flange thickness. A linear distribution was assumed through the thickness. The upper one-third level had the greatest residual stress influence while the bottom one-third level had the least.

For crack growth less than approximately 1.1 in. (28 mm), the crack shape was an elliptical corner crack as described in Section 4.5.3 for the groove weld details. The local weld tensile residual stresses and the nominal section tensile residual stresses on

the flange tip both influenced the total stress intensity value in addition to the applied stress magnification by the stress concentration parameter, F_G. These variations with crack size, a, are shown in Fig. 4.16 for Beam B2A. When the crack size for the elliptical corner cracks was approximately 1.1 in. (28 mm) the semi-major axis became equal to the flange thickness. At this point the crack rapidly became a 1.1 in. (28 mm) edge crack and the stress intensity suddenly increased. This discontinuity is shown in Fig. 4.16.

The residual stress effects on stress intensity for edge cracks can readily be seen in the K_{RS} vs. Edge Crack Size plots (see Figs. 4.18 to 4.23). As the edge crack grew a size of 1.1 in. (28 mm) into the negative residual stress zone there was a decrease in K_{RS} which extended over the next 2 in. of crack growth. In most cases this decrease in K_{RS} held the total stress intensity value, K, constant over this region.

Continued crack growth resulted in a rapid increase in K_{RS} as the fatigue crack grew into the high tensile residual stress region caused by the web-to-flange fillet welds. This also caused K to increase rapidly. This residual stress influence on K greatly affected the fracture of Beam B4 (top one-third analysis, Fig. 4.20) and B6 (top one-third analysis, Fig. 4.22). Each beam fractured with a crack size at or near the peak K value caused by K_{RS}. The fracture of beam B6A, was caused by a rising K_{RS} and K, (see Fig. 4.23). The point of fracture is marked on each "K vs. a" plot.

K_{AS} increased at a near constant rate for edge crack growth. Since the applied stresses were very high in the A514 beams this parameter had an overriding effect on K_{RS} and K_{LW}. This is shown in the bottom one-third analysis for Beams B2 and B2A, Figs. 4.18 and 4.19 respectively.

K_{LW} had its greatest influence on small elliptical corner cracks (see Fig. 4.16). For edge cracks at the groove weld details this contribution became constant and comparatively small. This contribution was slightly higher for the overlapped fillet weld detail.

The fracture of B4 was precipitated by the presence of the high tensile residual stress area at the web-to-flange welds. Beam B4A Beam B4A had a fatigue crack which grew through the same area during a fracture test and at a 6% higher applied stress but did not fail. This can only be explained by a difference in test temperatures when the fatigue cracks grew into this critical area. As can be seen from the material tests K vs. Temperature plot for A36 steel (Fig. 6.1), a slight difference in the test temperatures would cause a large change in the critical stress intensity factor, K_c. This was the case as the Beam B4A test temperature $\{-70° F (-57° C)\}$ was warmer than the temperature of Beam B4 $\{-80° F (-62° C)\}$ when the fatigue crack grew into this region. As the fatigue crack in Beam B4A grew through the web-to-flange welds K_{RS} was continually increasing. However, this was counter balanced by the flange crack opening restraint of the web. Only when the crack grew $\sim 1\frac{1}{4}$ in. (~ 32 mm) past the web did fracture

occur. K_{RS} had only a small effect on the estimated stress intensity since, at the time of fracture, the critical K was determined at the bottome one-third level of flange thickness.

5. COVER PLATE BEAM TEST RESULTS AND ANALYSES

5.1 Fatigue Cracks

The fatigue cracks on the end-weld cover plate beams were initially detected as ½ in. (13 mm) surface cracks. As these surface cracks grew larger they became either elliptical corner cracks (see Beam B1A, Fig. 5.2) or through cracks (see B3, Fig. 5.3).

On the cover plate detail without end weld the fatigue cracks were detected as ½ in. (13 mm) surface cracks at the end of the longitudinal fillet weld. After extended crack growth the fatigue cracks became elliptical corner cracks and then quickly edge cracks.

The size of the fatigue cracks at each critical detail can be found by referencing the small letters on the crack surface drawings in Figs. 5.1 to 5.6 with the load history tables given in Tables 2.10 to 2.15.

Additional fatigue cracks existed at the other detail on each beam. Fig. 5.7 shows the fatigue cracks at all details prior to the last fracture test. The surface measurements of these cracks are shown adjacent to the crack. The crack shapes were estimated from these surface measurements.

5.2 Fatigue Life

The number of cycles needed to propagate an elliptical surface crack from its fracture initiation point to a through thickness

flange crack was defined as the remaining useful fatigue life had brittle fracture not occurred. The remaining fatigue life was estimated by a numerical integration routine using Equations 7 and 11 as presented in Section 4.2. Secondary stress intensity effects from the residual stresses were neglected. Appropriate correction factors, F_S, F_W, F_G and F_E were used for the cover plate details.

Beams B1A, B3 and B3A had no appreciable remaining fatigue life at the time of fracture. Beams B1, B5 and B5A had 106,000, 607,000 and 70,000 cycles of remaining fatigue life, respectively.

Figure 5.8 shows the mean S-N curve and its confidence limits for the Category E details. The data base used to develop this curve utilized tests on 12 to 14 in. (305 to 356 mm) deep beams with a maximum flange thickness of ½ in. (13 mm). The fatigue results for the cover plate beams, which had flange thicknesses between 1.25 in. (32 mm) and 1½ in. (38 mm), are plotted on the same curve. The open figures represent the point at which the cracks were first observed and the closed figures represent the point of fracture.

Each cover plate details fatigue life at fracture was near or below the lower 95% confidence limit which corresponds to the design strength for category E details. The rapid fatigue crack initiation and growth was apparently caused by the higher stress concentration which existed at these full size details. These fatigue results were similar to those obtained in Reference 18 to 30 smaller scale cover plate beams with cover plates wider than the flange and no end

welds. The lower confidence limit for these details is also shown in Fig. 5.8. All cover plate details presented in this section had fatigue lives between the mean and the upper 95% confidence limit for this lower fatigue life detail type. This study has indicated that additional tests are needed on the fatigue behavior of full size welded cover plate details, particularly at low stress range levels.

5.3 Beam Fracture Tests*

Beam B1

Since the fatigue crack at the end-weld detail initiated and grew very rapidly (see Fig. 5.1), the first fracture test was conducted before the beam reached its 2 million cycle fatigue design life. At this point only a small 5/8 in. (16 mm) long elliptical surface crack existed at the no-end-weld detail (see Fig. 5.7).

Only one fracture test was run on this beam. Both the end-weld detail and the no-end-weld details were tested at -40°F(-40°C) for ½ hour. Since no fracture occurred at this point, the critical detail was cooled further while being cyclically loaded for 2¼ hours until fracture occurred at -200°F (-129°C). The fatigue crack extension during this fracture test was approximately 1/8 in. (3 mm) as can be seen in Fig. 5.1.

---

*Temperature at the critical details are shown graphically in Figs. 5.9 to 5.11 for the final 60 minutes of the last fracture test.

Beam B1A

A very large 5-7/8 in. x 1-1/4 in. (149 mm x 32 mm) el-
liptical corner crack existed at the end-weld detail after 1.134
million cycles (see Fig. 5.2). No cracks were found at the unwelded
end.

Only one fracture test was run on Beam B1A. Both details
were cooled to -40°F (-40°C) and then cyclically loaded. Just as
the maximum stress and stress range was obtained, fracture occurred at
the end-weld detail. The temperature at fracture was -48°F (-44°C).

Beam B3

After 2 million cycles a large 12 in. (305 mm) elliptical
surface crack existed along the weld toe of the end-weld detail. Two
1-1/4 in. (32 mm) long elliptical shaped cracks also existed at the
detail without a transverse end weld.

Both details were cooled to -40°F (-40°C) and cyclically
tested for 1/2 hour. No fracture occurred. An additional 162,000
fatigue cycles were applied at room temperature. At this stage of
crack growth the large elliptical surface crack at the end welded de-
tail became a through-thickness crack (see Figs. 5.3 and 5.7). Both
details were again cooled to -40°F (-40°C) and cyclically loaded.
Fracture occurred while loading. A maximum stress of 17.2 ksi
(118.6 MPa) and stress range of 5.4 ksi (37.2 MPa) was applied at the
time of fracture.

Beam B3A

After 1.79 million cycles of fatigue loading at room temperature, a 5 in. (127 mm) edge crack existed at the unwelded detail (see Figs. 5.4 and 5.7). A series of small elliptical shaped surface cracks also existed along the weld toe of the end-weld detail (see Fig. 5.7).

Both details were cooled to -40°F (-40°C) and cyclically loaded for 1 hour. No fracture occurred at either detail during this phase of testing. Testing was continued at the unwelded end with the large edge crack. The detail was slowly cooled to -96°F (-71°C) at which point fracture occurred.

Beam B5

A series of small elliptical surface flaws existed at the end-welded detail while only a small 1-1/4 in. (32 mm) surface flaw existed at the no-end-weld detail (see Figs. 5.5 and 5.7) after application of 2,000,000 load cycles.

Only the end-weld detail was cooled to -40°F (-40°C). The beam was then cyclically loaded for 30 min. without any sign of distress. After loading was removed, the detail was then cooled further to -140°F (-96°C). Then the cyclic load was reapplied and in 20 minutes fracture occurred at approximately -150°F (-101°C).

Beam B5A

After 1.863 million cycles of fatigue loading there was a
2 1/2 in. (64 mm) elliptical surface crack at the unwelded end. At
the end-welded detail there also existed a 2 in. (51 mm) long ellip-
tical surface crack (see Figs. 5.6 and 5.7). Both details were cooled
to -123°F (-86°C) and cyclic load was applied for 1 hour during which
time the temperature was slowly lowered to -190°F (-123°C). No frac-
ture occurred.

Additional cyclic loading (.123 million) was applied at room
temperature until the 2 million cycle fatigue design life was reached.
Little fatigue crack growth was experienced (see Figs. 5.6 and 5.7).
At this time both details were cooled to -40°F (-40°C) and cyclically
loaded for 1/2 hour. Since no fracture occurred, the unwelded end was
cooled further to -99°F (-73°C) while being cyclically loaded. Frac-
ture occurred at -99°F (-73°C).

5.4 Stress Intensity Estimates for Cover Plate Details

5.4.1 Introduction

All the cover plate beam specimens, except Beam B3A, frac-
tured from an elliptical surface crack or an elliptical corner crack.
The method of superposition was used to estimate the effects of ap-
plied load and residual stresses. This method was presented in sec-
tion 4.5 for the lateral attachment detail edge cracks. Beam B3A and
the elliptical cracks in Beams B1 and B1A were also analyzed using

the edge crack relationships presented in Section 4.5. This section summarizes the relationships used to evaluate the elliptical cracks encountered at the cover plate details.

Several contributions to the stress intensity were estimated separately as presented in Equation 9. The contribution from the applied stress, K_{AS}, was estimated from known solutions under uniform applied stress. Both the nominal section residual stress contribution, K_{RS}, and the local weld residual stress contribution, K_{LW}, had non-uniform stresses over an elliptical crack surface. To estimate these effects a stress-free state was created on the crack surface as was done with the flange attachments. A numerical integration method was used which is presented in Section 5.4.4.

The variation of stress intensity with crack size was not obtained since many of the elliptical cracks had different crack geometry relationships. Therefore, the semimajor axis, C, and the semiminor axis, a, values were used as ahown in the fatigue and fracture surface sketches (Figs. 5.1 to 5.6) for the crack size at fracture. C was held constant while the semiminor axis, a, was varied $\pm$ 0.3 in. ($\pm$ 8 mm) to calculate several values of K to incorporate the plastic zone correction.

The plastic zone correction, r_y, (see Equation 9) was used when possible when evaluating the stress intensity, K. Several stress intensity estimates for the critical crack sizes would not converge when this correction was used (see Tables 5.2 a,b).

5.4.2 Contribution from the Applied Stress

The stress intensity for elliptical crack shapes is defined by Equation 11 (see Section 4.5.2). The factor,

$$F(a') = F_E \, F_G \, F_S \, F_W$$

can be determined for the elliptical cracks encountered at the cover plate details as:

F_E = Crack shape correction

where $F_E = \dfrac{1}{E_k} [1 - k^2 \cos^2 \Phi]^{\frac{1}{4}}$

E_k, k, and Φ are defined in Figure 5.12.

F_G = Stress concentration correction

F_S = Free surface correction

F_W = Finite width or thickness correction

For this study F_E varied between 1.0 and $\dfrac{2}{\pi}$ for an elliptical crack growing from a shallow semi-elliptical crack to a semi-circular crack. F_G varied with crack size as shown in Figure 5.13. For crack sizes greater than 0.9 in. (10 mm), $F_G \simeq 1.0$. F_S was taken as 1.0 because of the lateral restraint offered by the cover plate in the through thickness direction of the flange. F_W was defined as a function of plate thickness, t_f, and crack sizes as equal to:

$$F_W = \sqrt{\frac{2t_f}{\pi a'} \tan \frac{\pi a'}{2t_f}} \qquad (15)$$

where $a' = a + r_y$

F_W approaches infinity when a' approaches t_f.

5.4.3 Contribution from the Stress Concentration

In a recent study at Fritz Engineering Laboratory, Zettlemoyer[14] developed a relationship for stress concentration factors, K_T at uncracked cover plate details. Values equal to about 6.5 were determined for the various cover plate beam specimens from Equation 16.

$$K_T = \log_e \left[\left(\frac{Z}{T_f} \right)^{-1.54} \left(\frac{T_{cp}}{T_f} \right)^{0.86} \right] + 5.80 \qquad (16)$$

T_f = Thickness of flange

T_{cp} = Thickness of cover plate

Z = Fillet weld leg size

The stress concentration effect decays rapidly as the crack size increases. This is discussed in more detail in Section 4.5.2. A plot of the decay with crack size, a, is shown in Fig. 5.13 for a typical end-weld cover plate beam specimen (W36x260). The decay is quite rapid. For crack sizes, a, of 0.01 in. (.3 mm) and 0.10 in. (3 mm), the stress concentration is 4.56 and 1.73 respectively.

The effect of stress concentration on stress intensity is shown in Fig. 5.14 for an elliptical crack growing at the toe of an end-welded cover plate. Because of the rapid decay of the stress concentration, K_T, crack instability did not develop at small

elliptical cracks. However the stress concentration significantly affected the fatigue strength of the beams.

5.4.4 Contibution from the Nominal Residual Stresses

The nominal beam cross section residual stresses were estimated from measurements on a beam section cut from a length of a typical beam. The results shown in Figs. 4.27b, 5.17 and 5.18 were determined by using the sectioning method. [19] The stresses were adjusted for equilibrium and variation through the flange thickness was assumed to be linear.

The contribution to stress intensity from the cross-section residual stresses, K_{RS} , will be positive or negative depending on the orientation of the crack and the residual stress distribution. An edge crack growing through the residual stress field can be analyzed in the same manner presented in Section 4.5.6. However, the estimate of K_{RS}, becomes more involved when an elliptical crack grows in the non-uniform residual stress field.

To estimate K_{RS} for an elliptical crack, a numerical integration procedure was developed. An approximate solution for the stress intensity, at a point on the crack front from applied splitting forces at a point on the crack surface was presented in Reference 4 and is shown in Fig. 5.15. A computer program was developed using this point by point approximation of K, to numerically integrate over the area of an elliptical crack. The crack surface was approximated

by a 0.03 in. (0.8 mm) mesh. The stress at each mesh point was esti-

mated by assuming a linear variation between the flange surfaces. This

permitted the average force acting on each mesh point to be determined.

5.4.5 Contribution from the Local Weld Residual Stresses

The local stresses at the ends of the cover plate were es-

timated by using the hole drilling method.[20] By drilling several

holes near each detail a good estimate of the local residual stresses

at the crack plane could be made. Results of these studies are pre-

sented in Figs. 5.19 to 5.21 for coverplated beams with and without

end welds.

Using the same numerical integration procedure as pre-

sented in Section 5.4, the local weld contribution, K_{LW}, to stress

intensity was estimated.

5.4.6 Summary and Discussion of the Various Contributions

The values of K, K_{AS}, K_{RS}, and K_{LW} are summarized in

Tables 5.2 a,b for each cover plate beam specimen. The stress in-

tensity values listed for Beams B1, B1A, B3 and B5A are for the

actual crack size at fracture. The plastic zone correction to the

semiminor crack size, a, would not converge for these beams.

Each estimate of K_{RS} and K_{LW} was checked by numerically

integrating a uniform stress over the same crack size mesh. The

stress intensity values obtained were compared with the stress

intensity results for uniform stress from the known solutions presented in Section 5.4   Table 5.1 shows the sensitivity of this numerical integration technique to the a/c ratio and Φ. Generally, the errors encountered were less than 10%. However, when a/c was less than 0.25 and Φ other than 90°, large errors were encountered. When comparing the solutions of the stress intensity estimated by numerical integration and a direct solution for Beam B1A, there was an 80.3% overestimate in the numerical integration solutions. To account for this gross overestimate the values obtained for K_{RS} and K_{LW} were scaled by a factor of 1.0/1.803.

Because of this overestimate and the small a/c ratio, the large elliptical cracks in Beams B1 and B1A were also analyzed as edge cracks for the center third of the flange width (see Figs. 5.1 and 5.2). The nominal section and local weld residual stresses were averaged over the central third width and assumed to vary linearly through the flange thickness. An analysis similar to that presented in Section 4.5 was used. The results shown in Table 5.2 are very similar to the results obtained by the elliptical crack numerical integration method presented in Section 5.4.4.

The major contribution was from the applied stress, K_{AS}. Values of K_{AS} were at least 40% of the total stress intensity values obtained for each beam fracture analysis.

The contribution from the nominal residual stress, K_{RS}, was much less than K_{AS}. Values of K_{RS} were less than 25% of the total

stress intensity estimate, K. The elliptical cracks present in these welded cover plate details grew in both positive and negative nominal residual stress areas which tended to compensate and minimize their effect.

The contribution from the local weld residual stress, K_{LW}, was approximately 50% of the total stress intensity estimate, K, for beams B1, B1A and B3 if the full local residual stress was applied. The remaining beams had K_{LW} estimates which were less than 20% of the total stress intensity.

There are two areas of uncertainty related to the local weld residual stress estimates. First, the stress measurements made by the hole drilling method were made ¼ in. (6 mm) away from the weld toe. Hence, the actual stresses at the crack growth planes were not known. Second, the stresses measured were only surface residual stresses. Therefore, the distribution through the thickness was unknown. The assumptions made in determining the local weld residual stress distribution shown in Figs. 5.19 to 5.21 were conservative. A lower bound estimate of K_{LW} was then made by taking 50% of the calculated value. These values are also listed in Tables 5.2 a,b.

The stress concentration effects had a negligible effect on the stress intensity factor. The stress concentration was predicted to decay rapidly with crack growth. At the fracture point the stress stress concentration correction, F_G, was approximately 1.0 for each cover plate fracture.

All of the analyses in this study utilized linear elastic fracture mecahnics. Whenever the net ligament at an elliptical crack, or flange thickness at an edge crack, becomes less than the plastic zone size using ½ the value of Equation 10, the validity of this method is diminished. Beam B1A had obvious plasticity on the fracture surface at the ¼ in. (6 mm) net ligament (see Fig. 5.2.). An elastic plastic method might have been more applicable for this case even though the estimated fracture resistance was in agreement with the material resistance. Table 5.3 shows the net ligament sizes for all the cover plate beam specimens.

6. COMPARISON OF BEAM K ESTIMATES AND MATERIAL K_c TESTS

6.1 Lateral Attachment Details

The beam fracture stress intensity estimates were correlated with the static and dynamic material toughness characterizations. Both the A36 and A588 beam fractures occurred at temperatures in the transition temperature region of the slow bend K_{IC} material tests. As can be seen in Figs. 6.1 to 6.3, there is a very good correlation between the beam K estimates and the slow bend material tests. The A514 beam fractures occurred at temperatures below the slow bend curve transition temperature region. The beam stress intensity estimates, however, were conservative since these points were above the K_{IC} value.

The good correlation between the beam stress intensity estimates and the slow bend K_{IC} material tests can be attributed to their similar loading rates. As discussed in Section 2.9, the beam fracture test loading rate was between 70 and 100 ksi/sec. and occurred as the crack front was being advanced under cyclic loading. The slow bend, three-point bend specimens were loaded at a rate of 20 kips/sec. which is 50 ksi/sec. at the crack tip. The dynamic K_{ID} specimens were fractured in approximately 4×10^{-4} sec. The beam tests demonstrated that the fracture resistance of these welded bridge details corresponded to the fracture toughness measurements which used a loading time of about one second.

Also plotted in Figs. 6.1 to 6.3 are the beam stress intensity estimates from the applied stress alone (K_{AS}). There is good correlation between K_{AS} for Beams B2, B2A, B4A, and B6A and their respective slow bend material test results. This demonstrates that in these tests, the residual stresses from welding and flame cutting did not significantly alter the fracture resistance. However the contribution to the stress intensity estimate from the residual stress field, K_{RS} should be considered when the crack tip is in the high tensile residual stress region of the web-to-flange welds. This can readily be seen in Figs. 4.3 and 4.5 for Beams B4 and B6, respectively. In both of these cases K_{RS} was nearly 50% of the total stress intensity estimate.

6.2 Cover Plate Details

The cover plated beam stress intensity estimates at fracture were correlated with the static and dynamic fracture toughness characterizations. Beams B1A (A514) B3, B34 (A36, rolled) and B5A (A588, rolled) fractured at temperatures in the transition region of the slow bend K_{IC} material tests. As can be seen in Figs. 6.4 to 6.6, there is good correlation between the predicted stress intensity estimates, K, and the extrapolated portion of the material test curve. Also plotted in these figures is the stress intensity value using only $\frac{1}{2} K_{LW}$. From these test analyses no distinction can be made as to which of the local weld effects, K_{LW} or $\frac{1}{2} K_{LW}$, is the better estimate. Material

tests were run at temperatures in this region, however there was no convergence in the test analyses between Eqs. 2 and 3.

Both B1 (A514) and B5 (A588, rolled) fractured at temperatures lower than the transition temperatures for the slow bend material tests. The stress intensity estimate, K, for Beam B5 was in direct correlation with the K_{IC} material tests results (see Fig. 6.5). However, the stress intensity estimate, K, for Beam B1 was quite conservative (see Fig. 6.6).

With the exception of Beam B3, the stress intensity estimates of beam fractures which precipitated from the large fatigue cracks in Beams B1, B1A, and B3A, were adequately predicted by K_{AS} alone (see Figs. 6.4 and 6.6). The stress intensity estimates of beam fractures which precipitated from small elliptical cracks (Beams B5 and B5A) were best estimated by including all of the residual stress contributions, K_{RS} and K_{LW} (see Fig. 6.5). Generally, a good estimation of stress intensity was obtained by considering only the applied stress contribution, K_{AS}, and the nominal section residual stress distribution, K_{RS}. These points are also shown in Figs. 6.4 to 6.6.

The beam fracture toughness was in good correlation with the slow bend K_{IC} material test results. This can be attributed to the similarities in the loading rates and the reasonableness of the critical K estimates as was discussed in Section 6.1.

7. CONCLUSIONS

This report summarizes the fatigue and fracture resistance of full scale welded beams with lateral attachments and cover plates. The fatigue test results were correlated with available test data obtained from smaller beams. The beam fracture resistance was correlated with fracture control tests made on the same material.

1. The stress intensity estimates from the beam fractures were best modeled by the slow bend K_{IC} fracture toughness. The beam fracture tests and the slow bend K_{IC} tests had similar loading rates. These tests have demonstrated the applicability of the one second loading time to measurements of fracture resistance of bridge beams.

2. For relatively large edge cracks, at the lateral attachment details, a good approximation of the critical stress intensity factor, K, for beam fractures can be estimated by only considering the applied stress. However if the edge crack tip has moved into the high tensile residual stress field near the web-to-flange welds, the residual stress contribution, K_{RS}, should be included. Fracture usually occurred when the crack tip was in this region. In one instance there was rapid fatigue crack growth through this region due to a rise in K, however, fracture did not occur until the fatigue crack was larger.

3. For the cover plated beam details, a good approximation of the critical stress intensity factor, K, for beam fractures was obtained by considering only the applied stress contribution, K_{AS}, and the nominal section residual stress contribution, K_{RS}.

4. Category E of the current AASHTO fatigue specifications was found to be applicable to the 12 in. (305 mm) flange attachment. However, this category was observed to overestimate the fatigue strength of the full size cover plated beam details. The fatigue life for each cover plate detail was at or below the design fatigue strength which was based on the lower confidence limit of tests of smaller scale cover plated beams[18].

5. The stress concentration effects for small elliptical corner cracks at a groove weld detail was analyzed. The maximum stress intensity was at an elliptical corner crack with a semi-minor axis of 0.4 in. (10 mm). The predicted stress intensity factor was less than the estimated resistance at fracture. This value was also less than the predicted fracture toughness value from the slow bend material tests at a service temperature of −40° F (−40° C). Similar results and comparisons were obtained for the cover plate details. Hence small fatigue cracks in materials satisfying the AASHTO toughness specification should not become unstable.

6. The Charpy V-notch data in the transition zone was converted to stress intensity values by Barsom's equation. Excellent correlation was found for the A36 steel and the A588 rolled beam steel. However, nonconservative values were predicted for the A588 steel and A36 rolled beam steel, and very con- servative results were predicted for the A514 steel.

7. The measured loading rate temperature shift was always greater than the empirical approximation suggested by Barsom. Hence this approximation is a conservative estimate.

8. <u>TABLES</u>

TABLE 1.1 LIST OF TEST SPECIMENS

Detail Type / Steel Type	Beam Numbers		
	A36	A588	A514
Lateral Attachment	B4	B6	B2
Category E	B4A	B6A	B2A
Cover Plate	B3*	B5*	B1
Category E	B3A*	B5A*	B1A
Transverse Stiffener			B7
Category C	B9A	B11A	B7A
Flange Transition	B10	B12	B8
Category B	B10A	B12A	B8A

* Rolled Beams

All Others Welded

24 Beams - Total

TABLE 2.1a RESULTS OF MILL TESTS

Plate t	Steel	Heat Number	Yield Pt. (ksi)	Tensile Strength (ksi)	Elong. Gage/%	C	M_n	P	S	S_i	C_u	N_i	C_r	V	M_o	B
1/2"	A36	401P1041	44.10	66.20	8/31	.14	1.06	.013	.017	.19						
1"	A36	411P4511	40.70	61.40	8/32	.14	1.06	.014	.032	.19						
2"	A36	402P7031	44.00	70.00	2/34	.17	1.06	.013	.022	.21						
3"	A36	432N4711	45.00	72.00	2/32	.17	1.09	.015	.024	.21						
1/2"	A588	401N6061	57.20	74.70	8/26	.13	1.09	.019	.028	.28	.28	.37	.57	.038		
1/2"	A588	432N2461	53.50	74.60	8/27	.12	1.17	.011	.023	.25	.29	.34	.50	.031		
2"	A588	401P8161	56.50	78.50	2/33	.12	1.09	.013	.019	.24	.26	.32	.54	.033		
2"	A588	402P7731	61.00	80.00	8/33	.10	1.12	.011	.025	.28	.29	.28	.55	.030		
3"	A588	494N5681	57.50	79.50	2/30	.12	1.08	.010	.027	.29	.29	.31	.51	.028		
3/8"	A514/J	801P03810	113.63	118.50	2/24	.17	.61	.008	.023	.27					.57	.0025
1/2"	A514/J	801P03810	113.00	120.25	2/30	.17	.61	.008	.023	.27					.57	.0025
1"	A514/J	801P03810	114.55	121.80	2/32	.17	.61	.008	.023	.27					.57	.0025
1-1/2"	A514/M	802P50780	125.10	134.15	2/31	.18	.61	.008	.023	.31		1.40			.52	.0028
1-1/2"	A514/ RQ1008	802N80660	117.00	129.50	2/21	.17	.59	.008	.021	.29		1.37			.49	.0022
2	A514/M	801N18640	110.00	122.25	2/19	.18	.66	.007	.023	.26		1.33			.50	.0036

TABLE 2.1b RESULTS OF MILL TESTS

Plate t	Steel	Heat Number	Yield Pt. (MPa)	Tensile Strength (MPa)	Elong. Gage/%	C	M_n	P	S	S_i	C_u	N_i	C_r	V	M_o	B
1/2"	A36	401P1041	304	456	8/31	.14	1.06	.013	.017	.19						
1"	A36	411P4571	281	423	8/32	.14	1.06	.014	.032	.19						
2"	A36	402P7031	303	483	2/34	.17	1.06	.013	.022	.21						
3"	A36	432N4711	310	496	2/32	.17	1.09	.015	.024	.21						
1/2"	A588	401N6061	394	515	8/26	.13	1.09	.019	.028	.28	.28	.37	.57	.038		
1/2"	A588	432N2461	369	514	8/27	.12	1.17	.011	.023	.25	.29	.34	.50	.031		
2"	A588	401P8161	390	541	2/33	.12	1.09	.013	.019	.24	.26	.32	.54	.033		
2"	A588	402P771	421	552	8/33	.10	1.12	.011	.025	.28	.29	.28	.55	.030		
3"	A588	494N5681	396	548	2/30	.12	1.08	.010	.027	.29	.29	.31	.51	.028		
3/8"	A514/J	801P03810	783	817	2/24	.17	.61	.008	.023	.27					.57	.0025
1-1/2"	A514/J	801P03810	779	829	2/30	.17	.61	.008	.023	.27					.57	.0025
1"	A514/J	801P03810	790	840	2/32	.17	.61	.008	.023	.27					.57	.0025
1-1/2"	A514/M	802P50780	863	925	2/31	.18	.61	.008	.023	.31		1.40			.52	.0028
1-1/2"	A514/RQ1008.	802N80660	807	893	2/21	.17	.59	.008	.021	.29		1.37			.49	.0022
2	A514/M	801N18640	758	843	2/19	.18	.66	.007	.023	.26		1.33			.50	.0036

TABLE 2.1 a,b (CONT'D)   RESULTS OF MILL TESTS

Steel	Heat Number	Yield Pt (ksi)	Tensile Strength (ksi)	Elong. Gage/%	C	M_n	P	S	S_i	C_u	N_i	C_r	V
A36 W36X260	122N478	57.9	75.4	8/28.5	.16	1.23	.015	.012					
A588 W36X230	185N056	66.4	85.2	8/25.2	.16	.94	.012	.024	.24	.31	.34	.55	.02

(b)

Steel	Heat Number	Yield Pt (ksi) (MPa)	Tensile Strength (MPa)	Elong. Gage/%	C	M_n	P	S	S_i	C_u	N_i	C_r	V
A36 W36X260	122N478	399	520	8/28.5	.16	1.23	.05	.012					
A588 W36X230	185N056	458	587	8/25.5	.16	.94	.012	.024	.24	.31	.34	.55	.02

TABLE 2.1c   MILL TEST CVN RESULTS

Plate t	Steel	Heat Number	Charpy Results (Ft-lbs.)			Test Temp. (°F)	Spec. Ft-lbs. @ °F	Charpy Results (Joules)			Test Temp. (°C)	Spec. Joules @ °C
			1	2	3			1	2	3		
1/2"	A36	401P1041	157	170	163	40	15 @ 40	213	231	221	4.5	20 @ 4.5
1"	A36	411P4571	68	53	34	40	15 @ 40	92	72	46	4.5	20 @ 4.5
2"	A36	402P7031	39	54	53	40	15 @ 40	53	73	72	4.5	20 @ 4.5
3"	A36	432N4711	74	75	60	40	15 @ 40	100	102	81	4.5	20 @ 4.5
1/2"	A588	401N6061	52	46	49	40	15 @ 40	71	62	67	4.5	20 @ 4.5
1/2"	A588	432N2461	48	44	22	40	15 @ 40	65	60	30	4.5	20 @ 4.5
2"	A588	401P8161	82	65	83	40	15 @ 40	111	88	113	4.5	20 @ 4.5
2"	A588	402P7731	65	77	40	40	15 @ 40	88	105	54	4.5	20 @ 4.5
3"	A588	494N5681	37	41	57	40	15 @ 40	50	56	77	4.5	20 @ 4.5
3/8"	A514/5	801P03810	28/39	20/34	19/28	0	25 @ 0	38/53	27/46	26/38	-18	34 @ -18
1/2"	A514/5	801P03810	32	32	34	0	25 @ 0	43	43	46	-18	34 @ -18
1"	A514/5	801P03810	62/26	56/26	47/26	0	25 @ 0	84/35	76/35	64/35	-18	34 @ -18
1-1/2"	A514/5	802P50780	55	56	49	0	25 @ 0	75	76	67	-18	34 @ -18
1-1/2"	A514/ RQ100B	802N80660	28	27	27	0	25 @ 0	38	37	37	-18	34 @ -18
2	A514/M	801N18610	64	62	60	0	25 @ 0	87	84	81	-18	34 @ -18

TABLE 2.1c (CONT'D) MILL TEST CVN RESULTS

Steel	Heat Number	Charpy Results (Ft-lbs)			Test Temp (°F)	Spec Ft-lbs @ °F	Charpy Results (Joules)			Test Temp. °C	Spec. Joules @ °C
		1	2	3			1	2	3		
A36 W36X260	122N478	239	239	239	40	15@40	324	324	324	4.5	20@4.5
A588 W36X230	185N056	87	75	60	40	15@40	118	102	81	4.5	20@4.5

TABLE 2.2a   CROSS-SECTIONAL PROPERTIES OF TEST SPECIMENS

Beam Number	Steel	Flange Width (in.)	Flange Thickness (in.)	Web Thickness (in.)	Total Depth (in.)	Nominal Moment of Inertia (in.^{4})	Nominal Section Modulus (in.^{3})
B2	A514	5.97	1.567	0.385	36.08	6482	360.1
B2A	A514	6.15	1.561	0.386	36.19	6482	360.1
B4	A36	6.97	2.019	0.375	35.98	9125	506.9
B4A	A36	7.00	2.016	0.375	35.91	9125	506.9
B6	A588	7.03	2.035	0.387	36.00	9125	506.9
B6A	A588	6.98	2.032	0.393	35.98	9125	506.9
B3	A36 W36X260	16.50	1.478	0.883	36.25	17300	952
B3A	A36 W36X260	16.56	1.493	0.867	36.25	17300	952
B5	A588 W36X230	16.41	1.234	0.780	35.94	15000	837
B5A	A588 W36X230	16.50	1.246	0.777	35.94	15000	837
B1	A514	5.94	1.570	.376	36.06	6482	360.1
B1A	A514	6.00	1.573	.376	36.09	6482	360.1

TABLE 2.2b   CROSS-SECTIONAL PROPERTIES OF TEST SPECIMENS

Beam Number	Steel	Flange Width (mm)	Flange Thickness (mm)	Web Thickness (mm)	Total Depth (mm)	Nominal Moment of Inertia (cm^4)	Nominal Section Modulus (cm^3)
B2	A514	152	39.67	9.78	916	269,667	5901
B2A	A514	156	39.65	9.80	919	269,667	5901
B4	A36	177	51.28	9.53	914	379,623	8307
B4A	A36	178	51.21	9.53	912	379,623	8307
B6	A588	179	51.69	9.83	914	379,623	8307
B6A	A588	177	51.61	9.98	914	379,623	8307
B3	A36 W36X260	419	37.54	22.43	921	720,080	15645
B3A	A36 W36X260	421	37.92	22.02	921	720,080	15645
B5	A588 W36X230	417	31.34	19.81	913	624,347	13702
B5A	A588 W36X230	419	31.65	19.74	913	624,347	13702
B1	A514	151	39.88	9.55	916	269,667	5901
B1A	A514	152	39.95	9.55	917	269,667	5901

TABLE 2.3a   CROSS-SECTION TEMPERATURES AT FRACTURE

(Lateral Attachment Beams)

Beam Number	Order of Test	Temperatures at Fracture**							
		Bottom Flange T1 (°F)	Web Stiff. T2 (°F)	Top Flange T3 (°F)	Bottom Flange T4 (°F)	Top Flange T5 (°F)	Bottom Flange T6 (°F)	Web Stiff. T7 (°F)	Top Flange T8 (°F)
B2	6	-155*	-106	-102	-171	---	---	---	---
B2A	4	-61	-71	---	-144*	-67	---	---	---
B4	2	-80*	-59	-45	---	---	---	---	---
B4A	1	---	-40	---	-105/-96*	-36	---	---	---
B6	3	---	---	---	---	---	-53*	-19	-08
B6A	5	-43	-77	---	-90/-94*	-68	---	---	---

*   Denotes test control gage at critical detail

** See Fig. 2.4 for gage locations

TABLE 2.3b CROSS-SECTION TEMPERATURES AT FRACTURE

(Lateral Attachment Beams)

Beam Number	Order of Test	Temperatures at Fracture**							
		Bottom Flange T1 (°C)	Web Stiff. T2 (°C)	Top Flange T3 (°C)	Bottom Flange T4 (°C)	Top Flange T5 (°C)	Bottom Flange T6 (°C)	Web Stiff. T7 (°C)	Top Flange T8 (°C)
B2	6	-104*	-77	-74	-113	---	---	---	---
B2A	4	-52	-57	---	-98*	-55	---	---	---
B4	2	-62	-51	-43	---	---	---	---	---
B4A	1	---	-40	---	-76/-71*	-38	---	---	---
B6	3	---	---	---	---	---	-47*	-28	-22
B6A	5	-42	-61	---	-68/-70*	-56	---	---	---

* Denotes test control gage at critical detail

** See Fig. 2.4 for gage locations

-75-

TABLE 2.4a   LOAD HISTORY FOR BEAM B2 (A514)

Testing Event	ID *	Subtotal N	Cumm. N	Fracture Test Data						Fatigue Data	
				Detail Tested	No.	** Temp. °F	Fract. Temp. °F	σ_r ksi	σ_{max} ksi	σ_r ksi	σ_{max} ksi
Fatigue	a	2,009,100	2,009,100							G 8.7 F 8.0	26.0
Fracture	b	10,000	2,019,100	F,G	1	-40		8.7 8.0	55.0		
Fracture	b	5,000	2,024,100	G	1	-130 to -155	-155	8.7	55.0		

* See fracture surface sketches for banding identification

F - Fillet welded detail

G - Groove welded detail

Steel type A514

** Temperatures at controling gages

TABLE 2.4b LOAD HISTORY FOR BEAM B2 (A514)

Testing Event	ID *	Subtotal N	Cumm. N	Fracture Test Data						Fatigue Data	
				Detail Tested	No.	** Temp. °C	Fract. Temp. °C	σ_r MPa	σ_{max} MPa	σ_r MPa	σ_{max} MPa
Fatigue	a	2,009,100	2,009,100							G 60 F 55	179
Fracture	b	10,000	2,019,100	F,G	1	-40		60 55	379		
Fracture	b	5,000	2,024,100	G	1	-90 to -104	-104	60	379		

*   See fracture surface sketches for banding identification

F – Fillet welded detail

G – Groove welded detail

Steel type A514

** Temperatures at controling gages .

TABLE 2.5a LOAD HISTORY FOR BEAM B2A (A514)

Testing Event	ID *	Subtotal N	Cumm. N	Detail Tested	No.	Temp. °F **	Fract. Temp. °F	Fracture Test Data σ_r ksi	Fracture Test Data σ_{max} ksi	Fatigue Data σ_r ksi	Fatigue Data σ_{max} ksi
Fatigue	a	1,982,800	1,982,800							G 8.7 / F 8.0	26.0 / 23.8
Fracture	b	15,000+ / 35,000	2,017,800	G / F / G / F	1 / 1 / 1 / 1	-40 / -40 / -40 / -40		4.3 / 4.0 / 8.7 / 8.0	50.6 / 46.4 / 55.0 / 50.4		
Fracture	c	13,800+ / 55,000	2,072,800	G / G	2 / 2	-40 / -40		4.3 / 8.7	50.6 / 55.0		
Fatigue	d	407,500	2,480,300								
Fracture	e	12,500+ / 48,750	2,529,050	G / G	3 / 3	-40 / -40		4.3 / 8.7	50.6 / 55.0		
Fracture	f	87,500	2,616,550	G	4	-40		8.7	55.0		
Fatigue	g	180,400	2,796,950							G 8.7 / F 8.0	26.0 / 23.8
Fracture	h	68,750	2,865,700	G	5	-40 to -144	-144	8.7	55.0		

* See fracture surface sketches for banding identification
** Temperature at controlling gages.
   Steel Type – A514

G – Groove welded detail
F – Fillet welded detail
+ – Cycles for marking crack front

-78-

TABLE 2.5b LOAD HISTORY FOR BEAM B2A (A514)

Testing Event	ID *	Subtotal N	Cumm. N	Detail Tested	Fracture Test Data					Fatigue Data	
					No.	** Temp. °C	Fract. Temp. °C	σ$_r$ MPa	σ MPa	σ$_r$ MPa	σ$_{max}$ MPa
Fatigue	a	1,982,800	1,982,800							G 60 / F 55	179 / 164
Fracture	b	15,000+ / 35,000	2,017,800	G / F / G / F	1 / 1 / 1 / 1	-40 / -40 / -40 / -40		30 / 28 / 60 / 55	349 / 320 / 379 / 348		
Fracture	c	13,800+ / 55,000	2,072,800	G / G	2 / 2	-40 / -40		30 / 60	349 / 379		
Fatigue	d	407,500	2,480,300							G 60 / F 55	179 / 164
Fracture	e	12,500+ / 48,750	2,529,050	G / G	3 / 3	-40 / -40		30 / 60	349 / 379		
Fracture	f	87,500	2,616,550	G	4	-40		60	379		
Fatigue	g	180,400	2,796,950							G 60 / F 55	179 / 164
Fracture	h	68,750	2,865,700	G	5	-40 to -98	-98	60	379		

*   See fracture surface sketches for banding identification

** Temperature at controlling gages

   Steel type – A514

G – Groove welded detail

F – Fillet welded detail

+ – Cycles for marking crack front

TABLE 2.6a   LOAD HISTORY OF BEAM B4   (A36)

Testing Event	ID *	Subtotal N	Cumm. N	Fracture Test Data						Fatigue Data	
				Detail Tested	No.	** Nominal Temp. °F	Fract. Temp. °F	σ_r ksi	σ_{max} ksi	σ_r ksi	σ_{max} ksi
Fatigue	a	2,001,800	2,001,800							G 9.0 F 8.0	19.8 17.6
Fracture	b	10,000⁺ 7,500	2,009,300	G F G F	1 1 1 1	−40 −40 −40 −40		4.5 4.0 9.0 8.0	15.3 13.6 19.8 17.6		
Fatigue	c	299,200	2,308,500							G/F 9.0/8.0	19.8/17.6
Fatigue	d	36,700	2,345,200							G/F 6.0/5.3	15.0/13.3
Fracture	e	5,000⁺ 10,000 14,500	2,355,200 2,369,700	G G G	2 2 2	−55 −70 −70	−80	4.5 9.0 9.8	15.3 19.8 19.8		

*   See fracture surface sketches for banding identification

** Temperature at controlling gages

G – Groove welded detail

F – Fillet welded detail

+ – Cycles for marking crack front

  Steel type – A36

TABLE 2.6b LOAD HISTORY OF BEAM B4 (A36)

Testing Event	ID *	Subtotal N	Cumm. N	Fracture Test Data						Fatigue Data	
				Detail Tested	No.	Nominal Temp. °C **	Fract. Temp. °C	σ_r MPa	σ_{max} MPa	σ_r MPa	σ_{max} MPa
Fatigue	a	2,001,800	2,001,800							G 62 F 55	137 121
Fracture	b	10,000+		G F	1 1	-40 -40		31 28	105 94		
		7,500	2,009,300	G F	1 1	-40 -40		62 55	137 121		
Fatigue	c	299,200	2,308,500							G/F 62/55	137/121
Fatigue	d	36,700	2,845,200							G/F 41/37	103/92
Fracture	e	5,000+ 10,000 14,500	2,355,200 2,369,700	G G G	2 2 2	-48 -57 -57	-62	31 62 68	105 137 137		

* See fracture surface sketches for banding identification
** Temperature at controlling gages
G - Groove welded detail
F - Fillet welded detail
+ - Cycles for marking crack front
    Steel type A36

TABLE 2.7a LOAD HISTORY OF BEAM B4A (A36)

Testing Event	ID*	Subtotal N	Cumm. N	Detail Tested	No.	**Temp. °F	Fract. Temp. °F	S_r ksi	σ_{max} ksi	S_r ksi	σ_{max} ksi
								Fracture Test Data		Fatigue Data	
Fatigue	a	1,500,000	1,500,000							G/F 9.0/8.0	1.98/17.6
Fracture	a	7,500+		F	1	-40		4.0	13.6		
	a	7,500	1,507,500	F	1	-40		8.0	17.6		
Fatigue	a	250,000	1,757,500							G/F 9.0/8.0	19.8/17.6
Fracture	a	7,500+		F	2	-40		4.0	13.6		
	a	7,500	1,765,000	F	2	-40		8.0	17.6		
Fatigue	a	250,000	2,015,000							G/F 9.0/8.0	19.8/17.6
Fracture	b	7,500+		G	3	-40		4.5	15.3		
	b	7,500	2,022,500	G	3	-40		9.0	19.8		
Fatigue	c	250,000	2,272,500							G/F 9.0/8.0	19.8/17.6
Fracture	d	7,500+		G	4	-40		4.5	15.3		
	d	7,500	2,280,000	G	4	-40		9.0	19.8		
Fatigue	e	250,000	2,530,000							G/F 9.0/8.0	19.8/17.6
Fracture	f	7,500+		G	5	-60		4.5	15.3		
	f	18,750	2,548,750	G	5	-60		9.0	19.8		
Fatigue	g	352,000	2,900,750							G/F 9.0/8.0	19.8/17.6
Fracture	g	7,500+		F	6	-40		4.0	13.6		
	g	7,500	2,908,250	F	6	-40		8.0	17.6		
Fatigue	g	67,900	2,976,150							G/F 9.0/8.0	19.8/17.6
Fracture	g	7,500+		G	7	-40		4.5	15.3		
	h	7,500	2,983,650	G	7	-40		9.0	19.8		
		5,000	2,988,650	G	7	-120 to -170		4.5	15.3		
		27,500+		G	7	-170 to -100		9.0	19.8		
Fatigue	i	243,100	3,231,750							G/F 9.0/8.0	19.8/17.6
		8,700+								G/F 4.5/4.0	15.3/13.6
Fracture	j	5,000	3,236,750	G	8	-70		4.5	15.3		
	j	40,000	3,276,750	G	8	-70 to -96	-96	9.0	19.8		

*   See fracture surface sketches for banding identification
** Temperature at controlling gages
    Steel type - A36

G - Groove welded detail
F - Fillet welded detail
+ - Cycles for marking crack front

TABLE 2.7b LOAD HISTORY OF BEAM B4A (A36)

Testing Event	ID*	Subtotal N	Cumm. N	Detail Tested	No.	Temp.** °C	Fract. Temp. °C	σr MPa	σmax MPa	Fatigue Data σr MPa	Fatigue Data σmax MPa
Fatigue	a	1,500,000	1,500,00							G/F 62/55	137/121
Fracture	a	7,500+	7,500	F	1	-40		28	94		
		7,500	1,507,500	F	1	-40		55	121		
Fatigue	a	250,000	1,757,500							G/F 62/55	137/121
Fracture	a	7,500+		F	2	-40		28	94		
		7,500	1,765,000	F	2	-40		55	121		
Fatigue	a	250,000	2,015,000							G/F 62/55	137/121
Fracture	b	7,500+		G	3	-40		31	105		
		7,500	2,022,500	G	3	-40		62	137		
Fatigue	c	250,000	2,272,500							G/F 62/55	137/121
Fracture	d	7,500+		G	4	-40		31	105		
		7,500	2,280,000	G	4	-40		62	137		
Fatigue	e	250,000	2,580,000							G/F 62/55	137/121
Fracture	f	7,500+		G	5	-51		31	105		
		18,750	2,548,750	G	5	-51		62	137		
Fatigue	g	352,000	2,900,750							G/F 62/55	137/121
Fracture	g	7,500+		F	6	-40		28	94		
		7,500	2,908,250	F	6	-40		55	121		
Fatigue	g	67,900	2,976,150							G/F 62/55	137/121
Fracture	h	7,500+		G	7	-40		31	105		
		7,500	2,983,650	G	7	-40		62	137		
		5,000	2,988,650	G	7	-84 to -112		31	105		
		27,500+		G	7	-112 to -73		62	137		
Fatigue	i	243,100	3,231,750							G/F 62/55	137/121
		8,700+								G/F 31/28	105/94
Fracture	j	5,000	3,236,750	G	8	-57		31	105		
		40,000	3,276,750	G	8	-57 to -71	-71	62	137		

* See fracture surface sketches for banding identification
** Temperature at controlling gages
Steel type – A36

G – Groove welded detail
F – Fillet welded detail
+ – Cycles for marking crack front

TABLE 2.8a   LOAD HISTORY OF BEAM B6 (A588)

Testing Event	ID *	Subtotal N	Cumm. N	Fracture Test Data						Fatigue Data	
				Detail Tested	No.	** Temp. °F	Fract. Temp. °F	σ_r ksi	σ_{max} ksi	σ_r ksi	σ_{max} ksi
Fatigue	a	1,999,800	1,999,800							G 9.0 F 8.0	27.5 24.4
Fracture	b	5,000+ 7,500	2,007,300	G F G F	1 1 1 1	-30 -30 -40 -40		4.5 4.0 9.0 8.0	23.0 20.4 27.5 24.4		
Fatigue	c	797,400	2,804,700							G 9.0 F 8.0	27.5[x] 24.4
Fracture	d	18,750+ 75,000	2,879,700	F F	2 2	-40 -40		4.0 8.0	20.4 24.4		
Fracture	e	7,500 75,000	2,954,700	F F	3 3	-40 -40	-53	4.0 8.0	20.4 24.7[y]		

*   See fracture surface sketches for banding identification
** Temperature at controlling gages
G – Groove welded detail
F – Fillet welded detail
+ – Cycles for marking crack front
x – Static jack dropped load maximum stress changed from 27.5 to ≈23 for 400,000 cycles of load
y – Static jack increased load
   Steel type – A588

TABLE 2.8b LOAD HISTORY OF BEAM B6 (A588)

Testing Event	ID*	Subtotal N	Cumm. N	Fracture Test Data — Detail Tested	No.	**Temp. °C	Fract. Temp. °C	σ_r MPa	σ_{max} MPa	Fatigue Data σ_r MPa	Fatigue Data σ_{max} MPa
Fatigue	a	1,999,800	1,999,800							G 62 F 55	190 168
Fracture	b	5,000+ 7,500	2,007,300	G F G F	1 1 1 1	-34 -34 -40 -40		31 28 62 55	159 141 190 168		
Fatigue	c	797,400	2,804,700							G 62 F 55	190[x] 168
Fracture	d	18,750+ 75,000	2,879,700	F F	2 2	-40 -40		28 55	141 168		
Fracture	e	7,500 75,000	2,954,700	F F	3 3	-40 -40	-47	28 55	141 170[y]		

*   See fracture surface sketches for banding identification
** Temperature at controlling gages
G – Groove welded detail
F – Fillet welded detail
+ – Cycles for marking crack front
x – Static jack dropped load maximum stress changed from 27.5 to ≈23 for 400,000 cycles of load
y – Static jack increased load
    Steel type – A588

-85-

TABLE 2.9a LOAD HISTORY OF BEAM B6A (A588)

Testing Event	ID *	Subtotal N	Cumm. N	Fracture Test Data						Fatigue Data	
				Detail Tested	No.	** Temp. °F	Fract. Temp. °F	σ_r ksi	σ_{max} ksi	σ_r ksi	σ_{max} ksi
Fatigue	a	2,042,600	2,042,600							G 9.0 F 8.0	19.0 16.9
Fracture	b	22,500	2,065,100	G F	1 1	-40 -40		9.0 8.0	27.5 24.4		
Fatigue	c	732,400	2,797,500							G 9.0 F 8.0	19.0 16.9
Fracture	d	25,000	2,822,500	G	2	-40/-90	-92	9.0	28.3^x		

*   See fracture surface sketches for banding identification
** Temperature at controlling gages
G – Groove welded detail
F – Fillet welded detail
x – Static jack increased load
     Steel type – A588

TABLE 2.9b. LOAD HISTORY OF BEAM B6A (A588)

Testing Event	ID *	Subtotal N	Cumm. N	Fracture Test Data						Fatigue Data	
				Detail Tested	No.	** Temp. °C	Fract. Temp. °C	σ_r MPa	σ_{max} MPa	σ_r MPa	σ_{max} MPa
Fatigue	a	2,042,600	2,042,600							G 62 F 55	131 117
Fracture	b	22,500	2,065,100	G F	1 1	−40 −40		62 55	190 168		
Fatigue	c	732,400	2,797,500							G 62 F 55	131 117
Fracture	d	25,000	2,822,500	G	2	−40/−68	−69	62	195[x]		

*   See fracture surface sketches for banding identification
** Temperature at controlling gages
G - Groove welded detail
F - Fillet welded detail
x - Static jack increased load
    Steel type - A588

-87-

TABLE 2.10a LOAD HISTORY/BEAM B1 (A514)

Testing Event	*ID	Subtotal N	Cumm. N	Fracture Test Data						Fatigue Data	
				Detail Tested	No.	**Temp. °F	Fract. Temp. °F	σ_r ksi	σ_{max} ksi	σ_r ksi	σ_{max} ksi
Fatigue	a	1,765,000	1,765,000							8.0	26.0
Fracture	b	7,500	1,772,500	E,N	1	-40		8	55		
		33,800	1,806,300	E	1	-40/-200	-200	8	55		

TABLE 2.10b

Testing Event	*ID	Subtotal N	Cumm. N	Fracture Test Data						Fatigue Dat	
				Detail Tested	No.	**Temp. °C	Fract. Temp. °C	σ_r MPa	σ_{max} MPa	σ_r MPa	σ_{max} MPa
Fatigue	a	1,765,000	1,765,000							55	179
Fracture	b	7,500	1,772,500	E,N	1	-40		55	379		
		33,800	1,806,300	E	1	-40/-129	-129	55	379		

* See Fracture Surface Sketches for banding identification
 E - End Weld Coverplate
 N - No End Weld Coverplate
** Temperatures at controlling gage

TABLE 2.11a LOAD HISTORY/BEAM B1A (A514)

Testing Event	*ID	Subtotal N	Cumm. N	Fracture Test Data						Fatigue Data	
				Detail Tested	No.	**Temp. °F	Fract. Temp. °F	σ_r ksi	σ_{max} ksi	σ_r ksi	σ_{max} ksi
Fatigue	a	1,134,200	1,134,200							8.0	26.0
Fracture	b		1,134,200	E†,N	1	-48	-48	8	55		

TABLE 2.11b

Testing Event	*ID	Subtotal N	Cumm. N	Fracture Test Data						Fatigue Data	
				Detail Tested	No.	**Temp. °C	Fract. Temp. °C	σ_r MPa	σ_{max} MPa	σ_r MPa	σ_{max} MPa
Fatigue	a	1,134,200	1,134,200							55	179
Fracture	b		1,134,200	E†,N	1	-44	-44	55	379		

* See Fracture Surface Sketches for banding identification
E – End Weld Coverplate
N – No End Weld Coverplate
** Temperature at controlling gage
† Critical Detail

-89-

TABLE 2.12a   LOAD HISTORY/BEAM B3

Testing Event	*ID	Subtotal N	Cumm. N	Fracture Test Data						Fatigue Data	
				Detail Tested	No.	** Temp. °F	Fract. Temp. °F	σ_r ksi	σ_{max} ksi	σ_r ksi	σ_{max} ksi
Fatigue	a	2,001,200	2,001,200							8.0	9.8
Fracture	b	7,500	2,008,700	E,N	1	-40		8.0	19.8		
Fatigue	c	162,000	2,170,700							8.0	9.8
Fracture	d		2,170,700	E†,N	2	-40	-45	5.4	17.2		

TABLE 2.12b

Testing Event	*ID	Subtotal N	Cumm. N	Fracture Test Data						Fatigue Data	
				Detail Tested	No.	** Temp. °C	Fract. Temp. °C	σ_r MPa	σ_{max} MPa	σ_r MPa	σ_{max} MPa
Fatigue	a	2,001,200	2,001,200							55	68
Fracture	b	7,500	2,008,700	E,N	1	-40		55	136		
Fatigue	c	162,000	2,170,700							55	68
Fracture	d		2,170,700	E†,N	2	-40	-43	37	119		

* See Fracture Surface Sketches for banding identification
E – End Weld Coverplate
N – No End Weld Coverplate
** Temperature at controlling gage
† Critical Detail

-90-

TABLE 2.13a   LOAD HISTORY/BEAM B3A (A36, W36x260)

Testing Event	*ID	Subtotal N	Cumm. N	Fracture Test Data						Fatigue Data	
				Detail Tested	No.	**Temp. °F	Fract. Temp. °F	σ_r ksi	σ_{max} ksi	σ_r ksi	σ_{max} ksi
Fatigue	a	1,790,900	1,790,900							8.0	9.8
Fracture	b	15,000	1,805,900	E,N	1	-40		8.0	19.8		
		11,300	1,817,200	E	1	-43/-96	-96	8.0	19.8		

TABLE 2.13b

Testing Event	*ID	Subtotal N	Cumm. N	Fracture Test Data						Fatigue Data	
				Detail Tested	No.	**Temp. °C	Fract. Temp. °C	σ_r MPa	σ_{max} MPa	σ_r MPa	σ_{max} MPa
Fatigue	a	1,790,900	1,790,900							55	68
Fracture	b	15,000	1,805,900	E,N	1	-40		55	137		
		11,300	1,817,200	E	1	-42/-71	-71	55	137		

* See Fracture Surface Sketches for banding identification
E – End Weld Coverplate
N – No End Weld Coverplate
** Temperature at controlling gage

-91-

TABLE 2.14a LOAD HISTORY/BEAM B5 (A588, W36x230)

Testing Event	*ID	Subtotal N	Cumm. N	Fracture Test Data						Fatigue Data	
				Detail Tested	No.	** Temp. °F	Fract. Temp. °F	σ$_r$ ksi	σ$_{max}$ ksi	σ$_r$ ksi	σ$_{max}$ ksi
Fatigue	a	2,000,000	2,000,000							8.0	10.5
Fracture	b	7,500	2,007,500	E	1	~40		8.0	27.5		
		5,000	2,012,500	E	1	~150	~150	8.0	27.5		

TABLE 2.14b

Testing Event	*ID	Subtotal N	Cumm. N	Fracture Test Data						Fatigue Data	
				Detail Tested	No.	** Temp. °C	Fract. Temp. °C	σ$_r$ MPa	σ$_{max}$ MPa	σ$_r$ MPa	σ$_{max}$ MPa
Fatigue	a	2,000,000	2,000,000							55	72
Fracture	b	7,500	2,007,500	E	1	~40		55	190		
		5,000	2,012,500	E	1	~101	~101	55	190		

*   See Fracture Surface Sketches for banding identification
E – End Weld Coverplate
N – No End Weld Coverplate
** Temperature at controlling gage

-92-

TABLE 2.15a   LOAD HISTORY/BEAM B5A (A588, W36x230)

Testing Event	*ID	Subtotal N	Cumm. N	Detail Tested	No.	**Temp. °F	Fract. Temp. °F	Fracture Test Data σr ksi	σmax ksi	Fatigue Data σr ksi	σmax ksi
Fatigue	a	1,862,500	1,862,500							8.0	12.9
Fracture	b	15,000	1,877,000	E,N	1	-129/-190		8.0	27.5		
Fatigue	c	123,000	2,000,000							8.0	12.9
Fracture	c	7,500	2,007,500	E,N	2	-40/		8.0	27.5		
		10,000	2,017,500	E		-40/	-99				
						-99					

TABLE 2.15b

Testing Event	*ID	Subtotal N	Cumm. N	Detail Tested	No.	**Temp. °C	Fract. Temp. °C	Fracture Test Data σr MPa	σmax MPa	Fatigue Data σr MPa	σmax MPa
Fatigue	a	1,862,500	1,862,500							55	89
Fracture	b	15,000	1,877,000	E,N	1	-40		55	190		
Fatigue	c	1,230,000	2,000,000							55	89
Fracture	c	7,500	2,007,500	E,N	2	-40/		55	190		
		10,000	2,017,500	E		-40/	-73				
						-73					

* See Fracture Surface Sketches for banding identification
E – End Weld Coverplate
N – No End Weld Coverplate
** Temperature at controlling gage

-93-

TABLE 3.1a   TRANSITION TEMPERATURE DATA FOR FLANGE PLATES

		Transition Temperature (°F)	
Material		(15 ft.-lb.)	(15 mil)
A36	(2" Pl)	-16	-26
A588	(2" Pl)	-24	-15
A514	(1-1/2" Pl)	-133	-102
A36	(1-7/16" Pl)	-37	-46
A588	(1-1/4" Pl)	-73*	-74

(a)

TABLE 3.1b

		Transition Temperature (°C)	
Material		(20 Joule)	(0.38 mm)
A36	(51 mm Pl)	-26.5	-32
A588	(51 mm Pl)	-31	-26
A514	(38 mm Pl)	-91.5	-74.5
A36 W36X260	(37 mm Pl)	-38	-43
A588 W36X260	(32 mm Pl)	-58*	-59

(b)

*Transition Temperature of 17 ft-lbs (23 Joules)

TABLE 4.1   REMAINING FATIGUE LIFE:
LATERAL ATTACHMENT DETAILS

Steel	Beam Number	Remaining Fatigue Life* (Cycles)
A514	B2	1,168,100
	B2A	576,500
A36	B4	175,200
	B4A	9,800
A588	B6	408,000
	B6A	669,600

* Fatigue failure defined at an edge
crack size = $\frac{3}{4}$ flange width
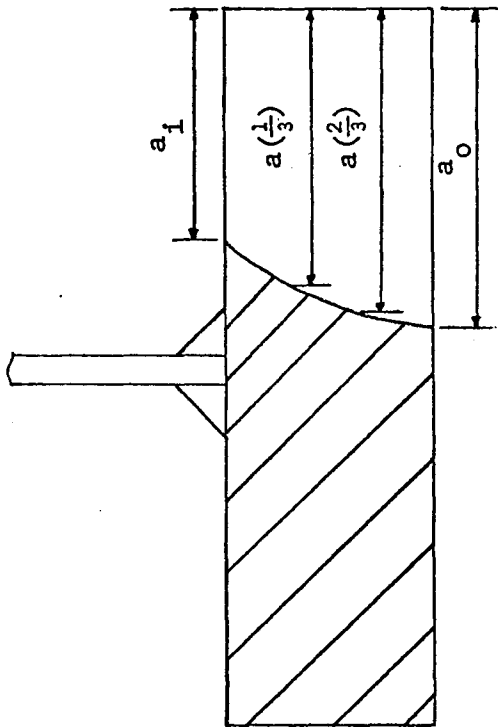
TABLE 4.2a CRACK SIZE MEASUREMENTS :
LATERAL ATTACHMENT DETAILS

Beam Number	Measured Crack Sizes				Averaged Crack Sizes (in.)				r_y* Correction Pl. Stress (in.)
	(1) a_1 (in.)	(2) $a'(\tfrac{1}{3})$ (in.)	(3) $a'(\tfrac{2}{3})$ (in.)	(4) a_o (in.)	$\dfrac{(1)+(2)+(3)+(4)}{4}$ a_{ave}	$\dfrac{(1)+(2)}{2}$ a_T	$\dfrac{(2)+(3)}{2}$ a_M	$\dfrac{(3)+(4)}{2}$ a_B	
B2	0.60	0.90	1.17	1.26	0.98	0.75	1.04	1.21	0.09
B2A	1.37	1.64	1.78	1.80	1.65	1.51	1.71	1.79	0.14
B4	2.92	3.12	3.32	3.38	3.19	3.02	3.22	3.35	0.41
B4A	4.62	4.90	5.03	4.93	4.87	4.76	4.96	4.98	0.47
B6	2.97	2.85	2.58	2.19	2.65	2.93	2.72	2.39	1.27
B6A	0.93	1.41	1.82	1.96	1.53	1.17	1.61	1.87	0.10

* Correction used at critical flange $\tfrac{1}{3}$ thickness (see Table 4.3)
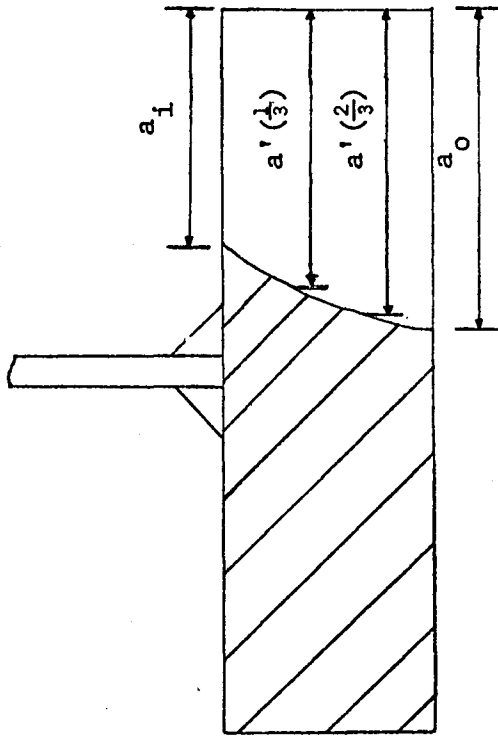
TABLE 4.2b   CRACK SIZE MEASUREMENTS: LATERAL ATTACHMENT DETAILS

Beam Number	Measured Crack Sizes				Averaged Crack Sizes (mm)				r_y* Correction Pl. Stress (mm)
	(1) a_i (mm)	(2) $a'(\frac{1}{3})$ (mm)	(3) $a'(\frac{2}{3})$ (mm)	(4) a_o (mm)	$\frac{(1)+(2)+(3)+(4)}{4}$ a_I	$\frac{(1)+(2)}{2}$ a_T	$\frac{(2)+(3)}{2}$ a_M	$\frac{(3)+(4)}{2}$ a_B	
B2	15	23	30	32	25	19	26	31	2
B2A	35	42	45	46	42	38	43	45	4
B4	74	79	84	86	81	77	82	85	10
B4A	117	124	128	125	124	120	126	126	12
B6	75	72	66	56	67	74	69	61	32
B6A	24	36	46	50	39	30	41	48	3

* Correction used at critical flange $\frac{1}{3}$ thickness (see Table 4.3)

TABLE 4.3a STRESS INTENSITY ESTIMATES:
LATERAL ATTACHMENT DETAILS

Beam No./ Flange Thickness Level	Applied Stress (ksi)	Crack Size $a+r_y$ (in.)	(1) K_{AS} (ksi√in)	(2) K_{RS} (ksi√in)	(3) K_{LW} (ksi√in)	(4) K_{WR} (ksi√in)	(1)+(2)+ (3)+(4) K (ksi√in)
B2 (σ_{yd}=155.6 ksi)							
TOD	46.5	0.78	74	−28	21	NA	67
MID	47.8	1.10	92	−16	17	NA	93
*BOT	49.2	1.30	101	−3	16	NA	114
B2A(σ_{yd}=153.5 ksi)							
TOP	51.2	1.56	118	50	15	NA	83
MID	52.7	1.80	130	−29	14	NA	115
*BOT	54.2	1.93	139	−9	14	NA	144
B4 (σ_{yd}=65.5 ksi)							
*TOP	16.8	3.43	62	39	4	NA	105
MID	17.5	3.54	66	23	4	NA	93
BOT	18.2	3.57	69	4	4	NA	77
B4A(σ_{yd}=67.7 ksi)							
TOP	18.0	5.20	103	15	5	−12	112
MID	18.7	5.43	116	0	5	−6	115
*BOT	19.4	5.45	102	9	5	0	116
B6 (σ_{yd}=79.3 ksi)							
*TOP	25.0	4.20	110	83	30	NA	223
MID	26.0	2.92	85	−3	6	NA	88
BOT	27.0	2.54	81	−8	6	NA	79
B6A(σ_{yd}=84.1 ksi)							
TOP	25.0	1.18	49	−38	8	NA	19
MID	26.0	1.64	61	−30	7	NA	38
*BOT	27.0	1.99	70	−11	7	NA	66

* Denotes critical flange thickness level

σ_{yd} = Yield stress at test temperature and loading rate (Eq. 4)

TABLE 4.3b   STRESS INTENSITY ESTIMATES:
LATERAL ATTACHMENT DETAILS

Beam No./ Flange Thickness Level	Applied Stress (MPa)	Crack Size $a+r_y$ (mm)	(1) K_{AS} (MPa√m)	(2) K_{RS} (MPa√m)	(3) K_{LW} (MPa√m)	(4) K_{WR} (MPa√m)	(1)+(2)+(3)+(4) K (MPa√m)
B2 (σ_{yd}=1073 MPa)							
TOP	321	20	81	−31	23	NA	73
MID	330	30	101	−18	19	NA	102
*BOT	339	33	111	−3	18	NA	126
B2A (σ_{yd}=1058 MPa)							
TOP	353	40	130	−55	17	NA	92
MID	363	46	143	−32	15	NA	126
*BOT	374	49	153	−10	15	NA	158
B4 (σ_{yd} = 452 MPa)							
*TOP	116	87	68	43	4	NA	115
MID	121	90	73	25	4	NA	102
BOT	125	91	76	4	4	NA	84
B4A (σ_{yd} = 467 MPa)							
TOP	124	132	113	17	6	−13	123
MID	129	138	128	0	6	−7	127
*BOT	134	138	112	10	6	0	128
B6 (σ_{yd} = 547 MPa)							
*TOP	172	91	121	91	33	NA	245
MID	179	74	94	−3	7	NA	98
BOT	186	65	89	−9	7	NA	87
B6A (σ_{yd} = 580 MPa)							
TOP	172	30	54	−42	9	NA	21
MID	179	42	67	−33	8	NA	42
*BOT	186	51	77	−12	8	NA	73

*   Denotes Critical Flange Thickness Level

σ_{yd} = Yield stress at test temperature and loading rate (Eq. 4)

TABLE 5.1   NUMERICAL INTEGRATION ERRORS, COVER PLATE DETAILS

Beam No.	Crack Size $a + r_y$ (in/mm)	Semi Major axis C (in/mm)	$(a+r_y)/C$	Φ Degree	Percent Error in K_{LW}, K_{RS}
B1	1.05/27	2.95/75	.36	90°	+5.8
B1A	1.25/52	5.9/150	.21	120°	+80.3*
B3	2.1/53	7.15/182	.29	90°	+9.6
B3A	N.A.	N.A.	N.A.	N.A.	N.A.†
B5	0.61/15	1.175/30	.52	90°	−1.3
B5A	1.13/29	1.95/50	.58	46.2°	−7.9

* K_{RS} and K_{LW} were scaled down in proporation to this overestimate.

† Flange Edge Crack Analysis

Table 5.2a Stress Intensity Estimates, Cover Plate Details

Beam No	Steel Type	Crack size, a in	Plastic zone size r_y in	Applied Stress ksi	σ_{rd} ** ksi	Fracture Temp. °F	1 K_{AS} ksi√in	2 K_{RS} ksi√in	3 K_{LW} + ksi√in	1 + 2 + 3 K ksi√in
++B1	A514	1.0	*	52.71	159	-200	113	5	187/93	305/211*
B1	A514	1.05	*	52.71	159	-200	118	11	104/52	233/181*
++B1A	A514	1.1	*	52.71	133	-48	125	13	196/98	334/236*
B1A	A514	1.25	*	52.71	133	-48	160	16	124/62	300/238*
B3	A36 Rolled	2.10	*	17.2	71	-45	70	49	74/37	193/156
B3A	A36 Rolled	5.63	0.47	19.8	78	-96	80	21	15/7	116/109
B5	A588 Rolled	0.55	0.05	26.54	96	-150	36	12	14/7	62/55
B5A	A588 Rolled	1.13	*	26.54	87	-99	82	29	14/7	125/118*

* No convergence was obtained when the plastic zone correction was used. Results shown are for the actual crack size at fracture.

** From equation 4 with t = 0.12 sec. σ_{rd} = 95% of the mill report yield stress. (See Table 2.1a,b) σ_{ys} value listed on right side of /.

+ Local weld contribution reduced 50%,

++ Edge crack analysis on center third of flange width.

Table 5.2b Stress Intensity Estimates, Cover Plate Details

Beam No	Steel Type	Crack size, a_i mm	Plastic zone size r_y mm	Applied Stress MPa	σ_{yd}** MPa	Fracture Temp. °C	1 K_{AS} MPa√m	2 K_{RS} MPa√m	3+ K_{LW} MPa√m	1+2+3 K MPa√m
++B1	A514	25.4	*	363	1096	-129	124	6	206/102	336/232
B1	A514	26.7	*	363	1096	-129	130	12	114/57	256/199
++B1A	A514	27.9	*	363	917	-44	138	14	216/108	367/260
B1A	A514	31.8	*	363	917	-44	176	18	136/68	330/262
B3	A36 Rolled	53.3	*	119	490	-43	77	54	81/41	212/172
B3A	A36 Rolled	143.0	11.9	137	538	-71	88	23	17/8	128/120
B5	A588 Rolled	14.2	1.3	183	662	-101	40	13	15/8	68/61
B5A	A588 Rolled	28.7	*	183	600	-73	90	32	15/8	138/130

* No convergence was obtained when the plastic zone correction was used. Results shown are for the actual crack size at fracture.

** From equation 4 with t = 0.12 sec. σ_{ys} = 95% of the mill report yield stress. (See Table 2.1a,b)

+ Local weld contribution reduced 50%, value listed on right side of /.

++ Edge crack analysis on center third of flange width.

TABLE 5.3 NET LIGAMENT SIZES

Beam No.	Steel Type	$\frac{1}{4\pi}\left(\frac{K}{\sigma_{Yd}}\right)^2$ (in.)/(mm)	Net Ligament B-a (in.)/(mm)
B1	A514	.17/4	.5/13
B1A	A514	.40/10	.35/9
B3	A36 (W36X260)	.59/15	.84/21**
B3A	A36 (W36X260)	.18/5	1.44/37*
B5	A588 (W36X230)	.03/.8	
B5A	A588 (W36X230)	.16/4	.1/3

*   Flange Thickness – Edge Crack (see Fig. 5.4)

** Web Thickness   – (see Fig. 5.3)

-103-

9. <u>FIGURES</u>

Fig. 2.1a Beam B4

Fig. 2.1b   Beam B3

22'-0" (6705.6 mm)

9'-6" (2895.6 mm)

3'-0" (914.4 mm)

9'-6" (2895.6 mm)

¾ ∇ Top and Bottom Flange

4 Cover Plates

No Weld, Top and Bottom Flanges

¾ ∇

6" (152.4 mm)

6" (152.4 mm)

8'-0" (2438.4 mm)

2'-6" (762 mm)

2'-6" (762 mm)

8'-0" (2438.4 mm)

6" (152.4 mm)

Typ⟩ 3/8

3/8

3/8

℞ 1½ x 6 x 22'-0" (2/Beam)

℞ 3/8 x 33 x 22'-0"

℞ 4 x 1 x 9'-6" (4/Beam)

3'-0" (914.4 mm)

Fig. 2.1c Beam B1

-107-
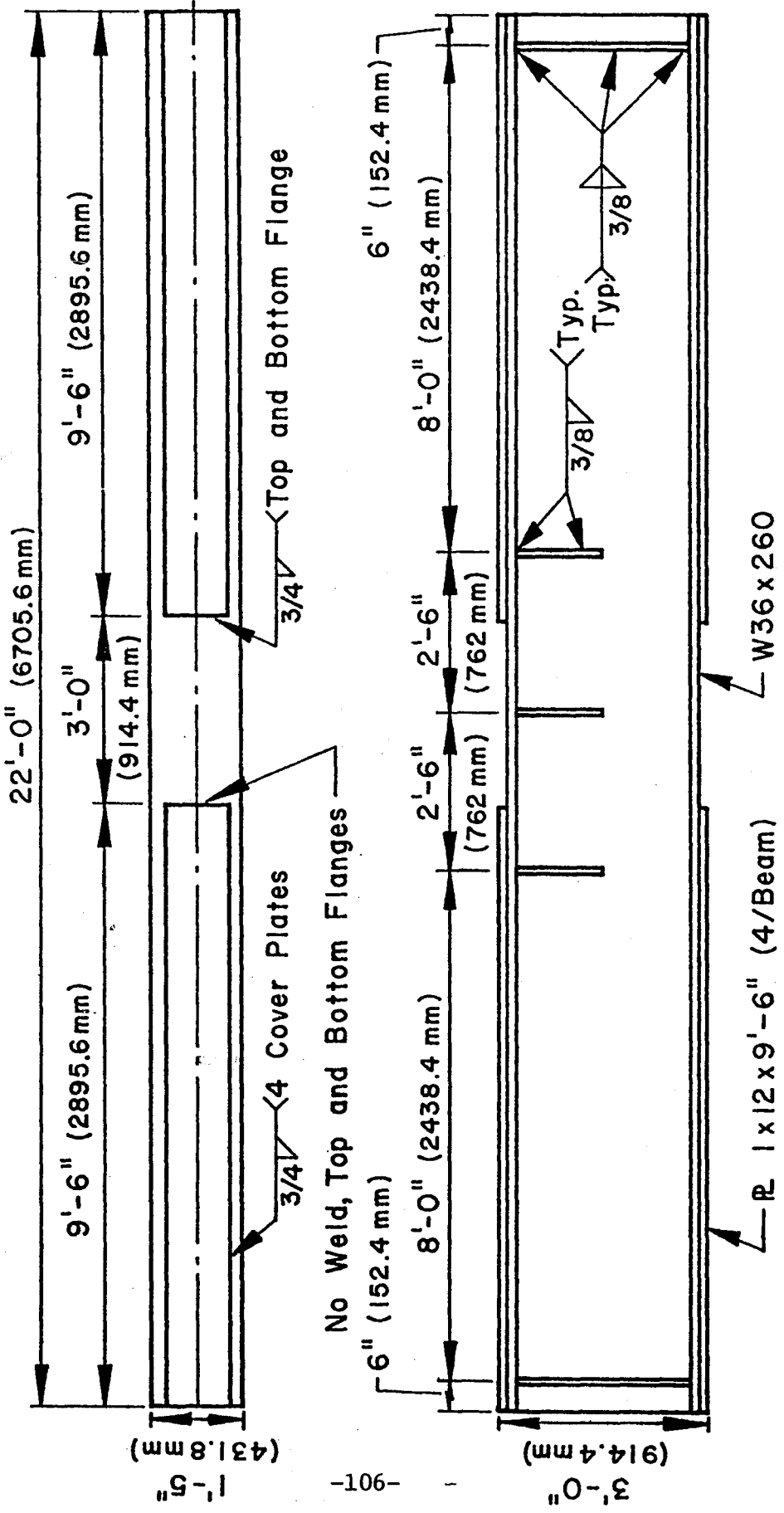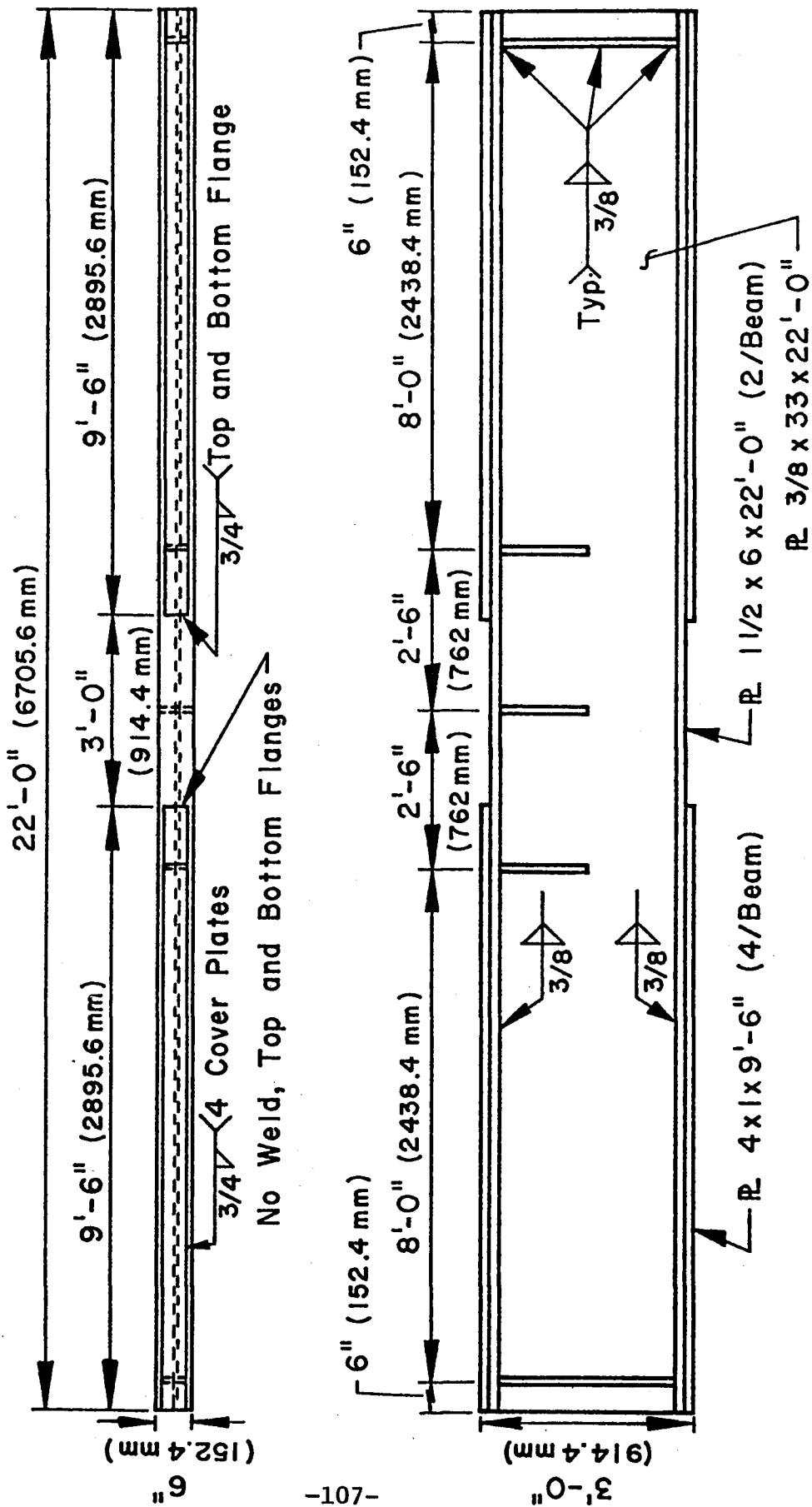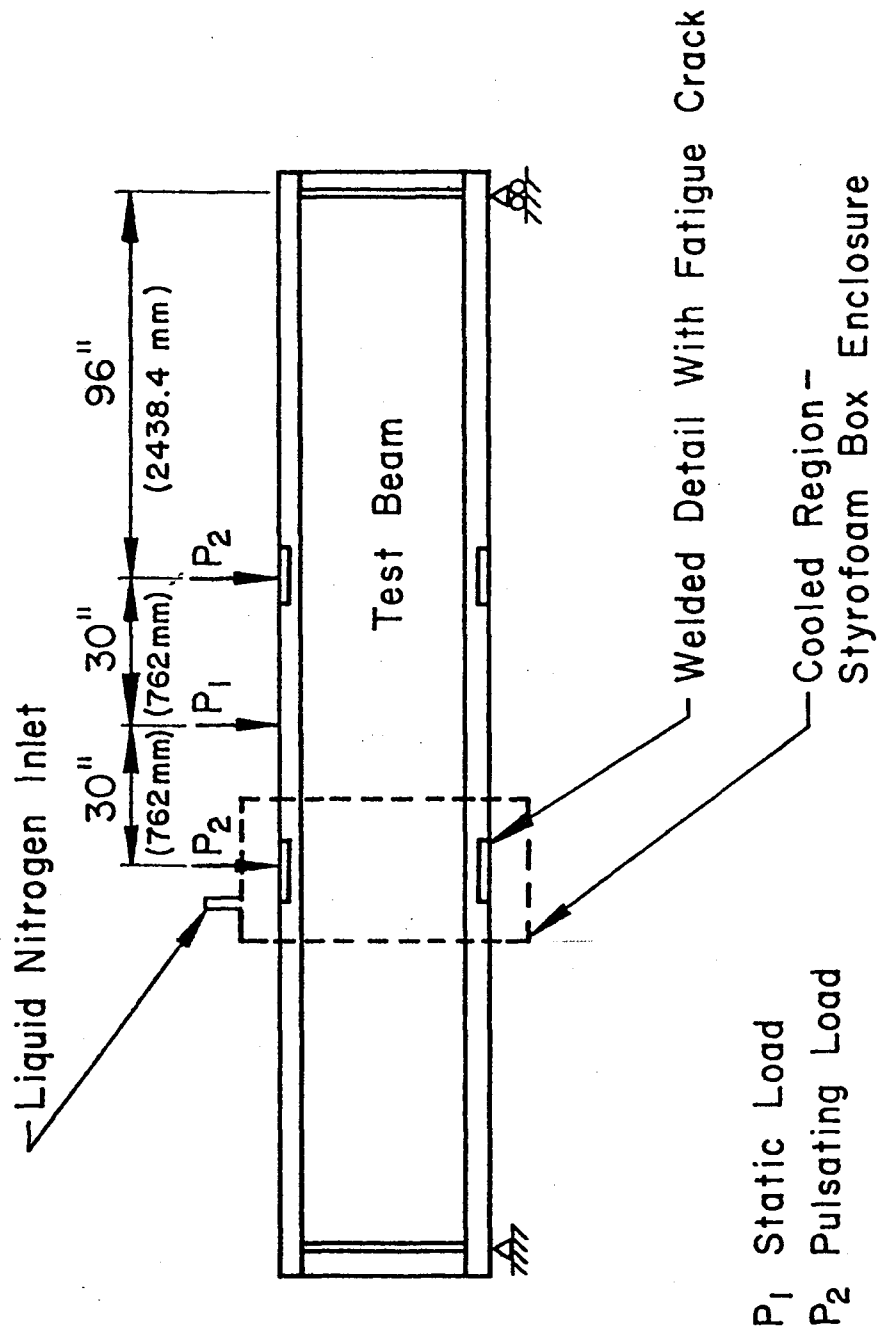
Fig. 2.2   Schematic of Fracture Test Setup
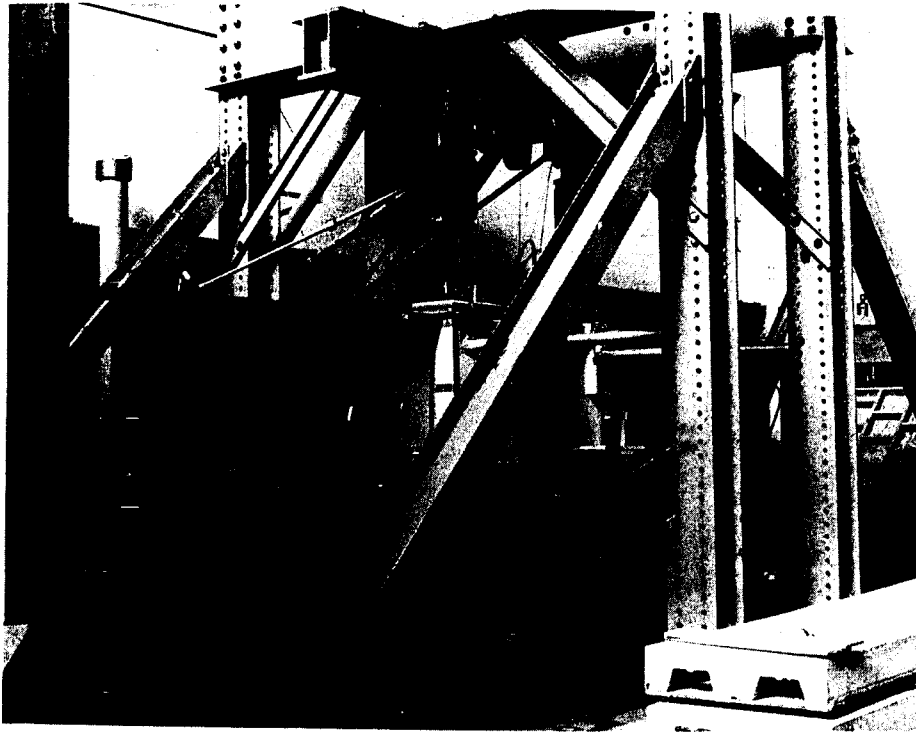
Fig. 2.3 Photograph of Test Setup
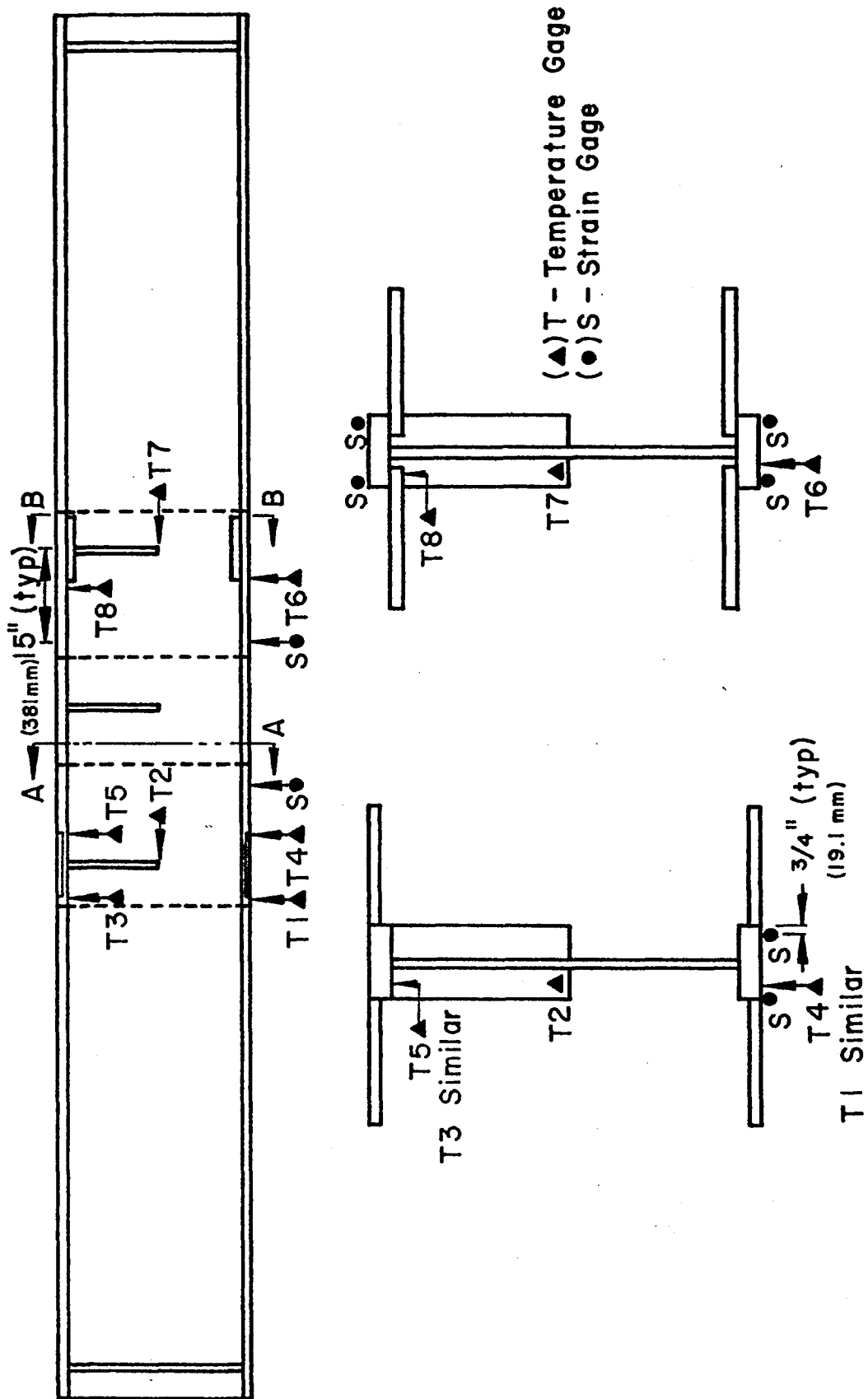
Fig. 2.4 Positions of Temperature and Strain Gages
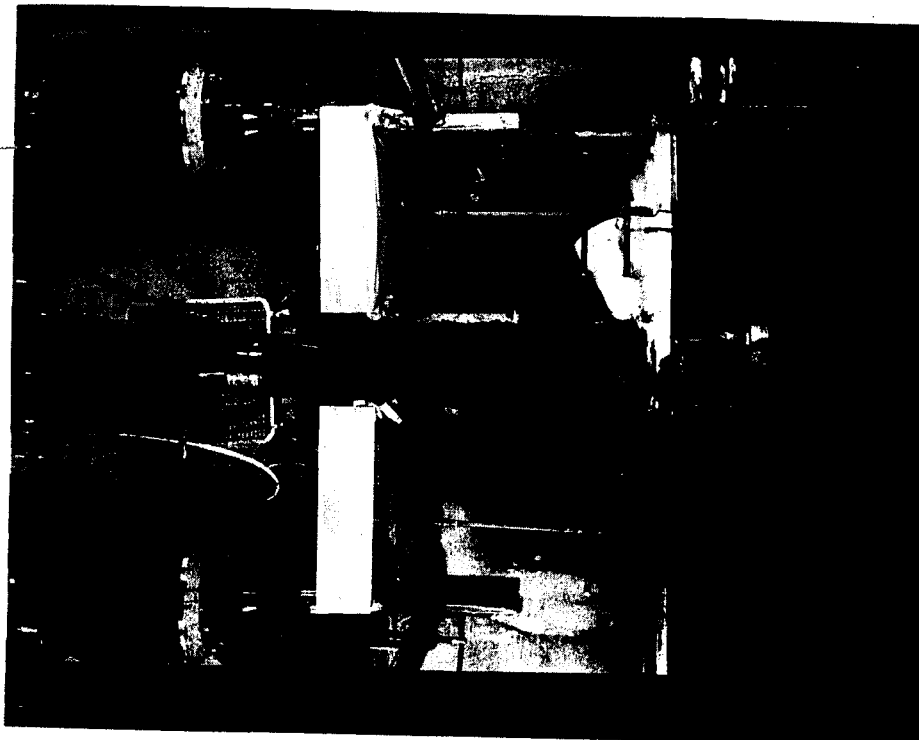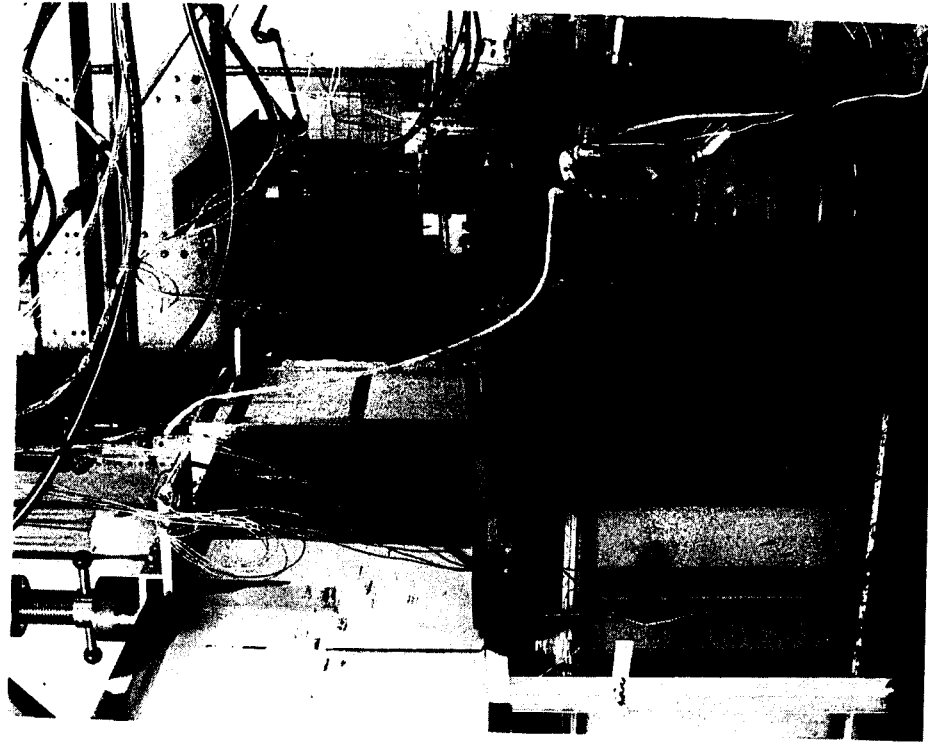
Fig. 2.5 Photographs of Cooling Network
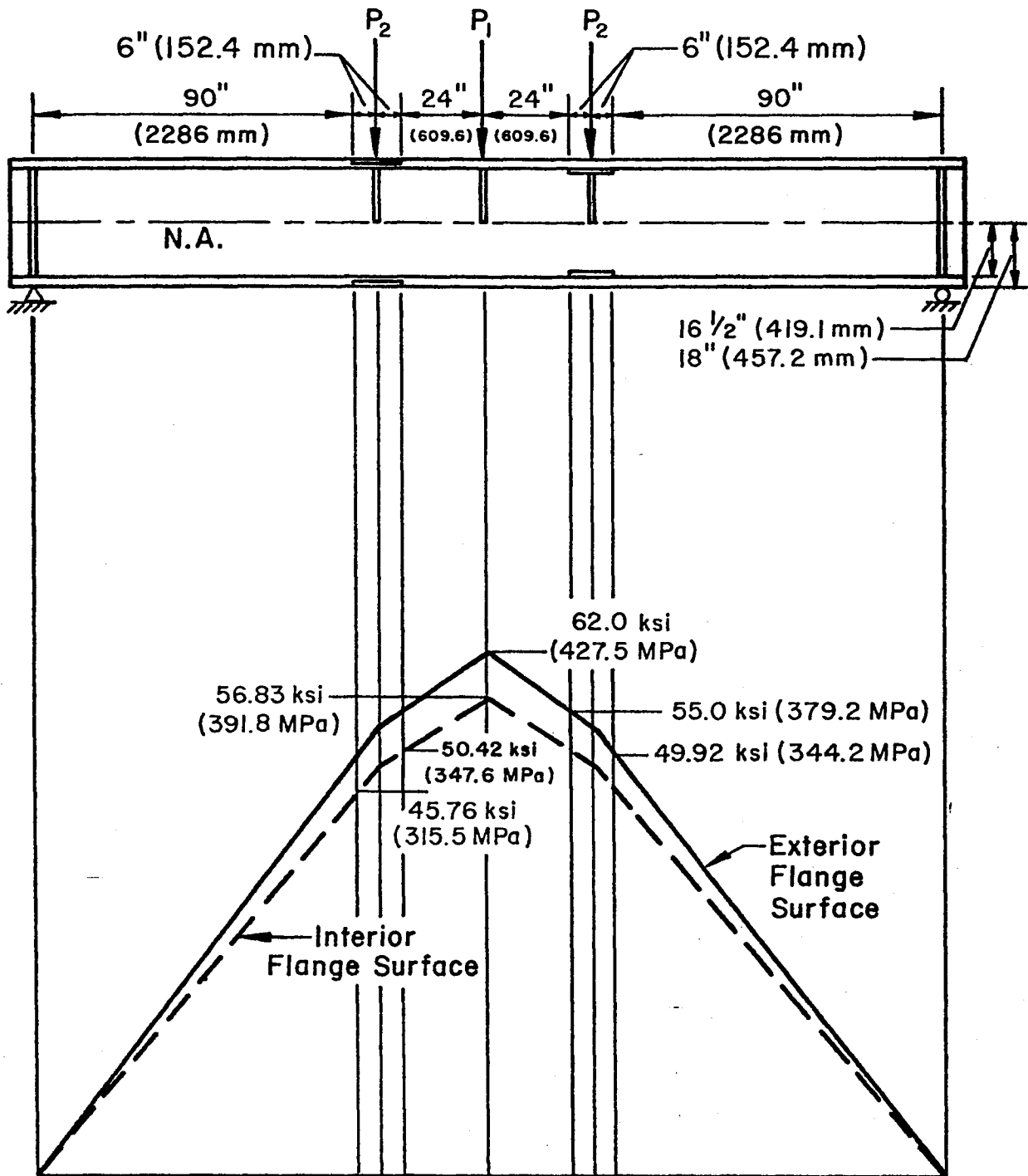
Fig. 2.6a Maximum Stress on Interior and Exterior Flange
Surfaces of Beams B2 and B2A (A514)
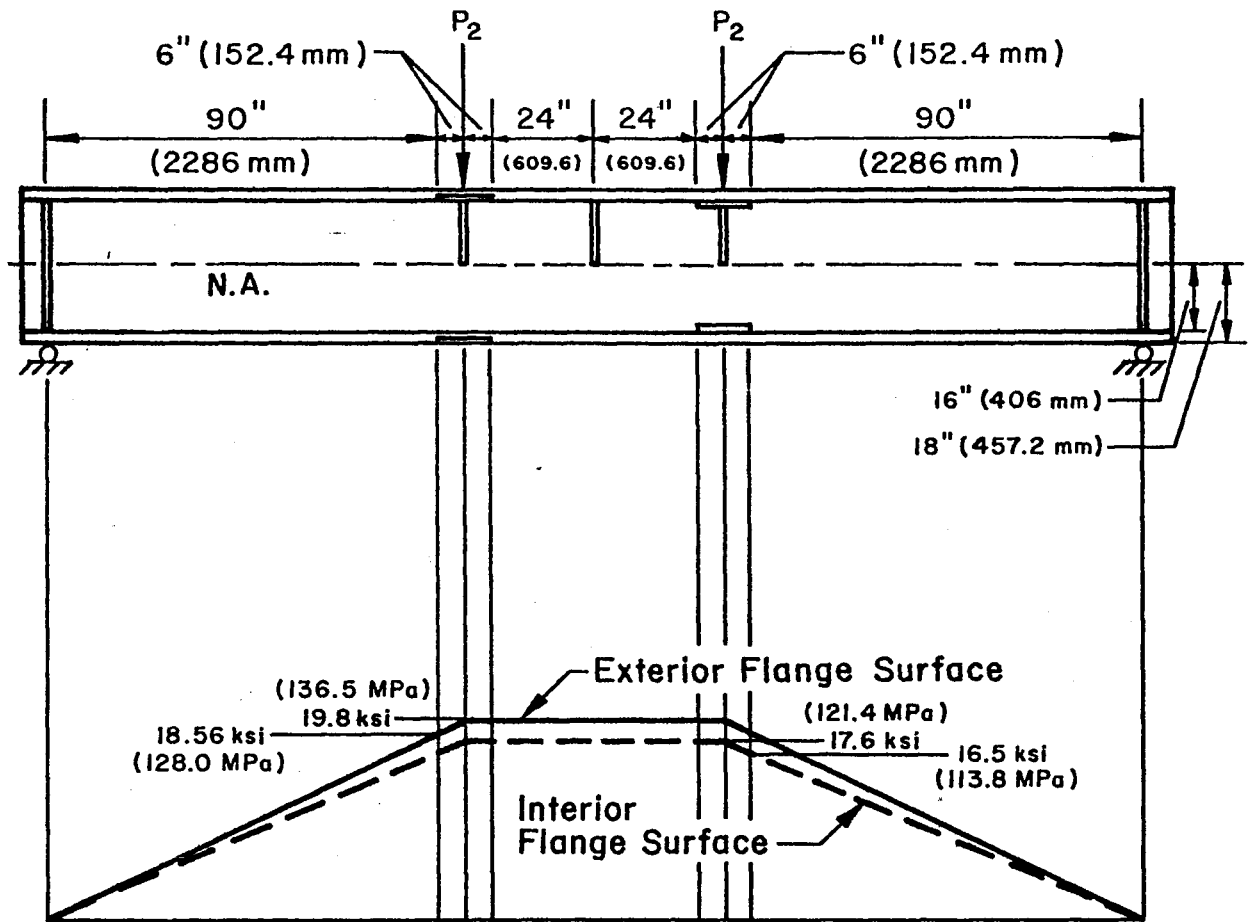
Fig. 2.6b   Maximum Stress on Interior and Exterior Flange
Surfaces of Beams B4 and B4A (A36)
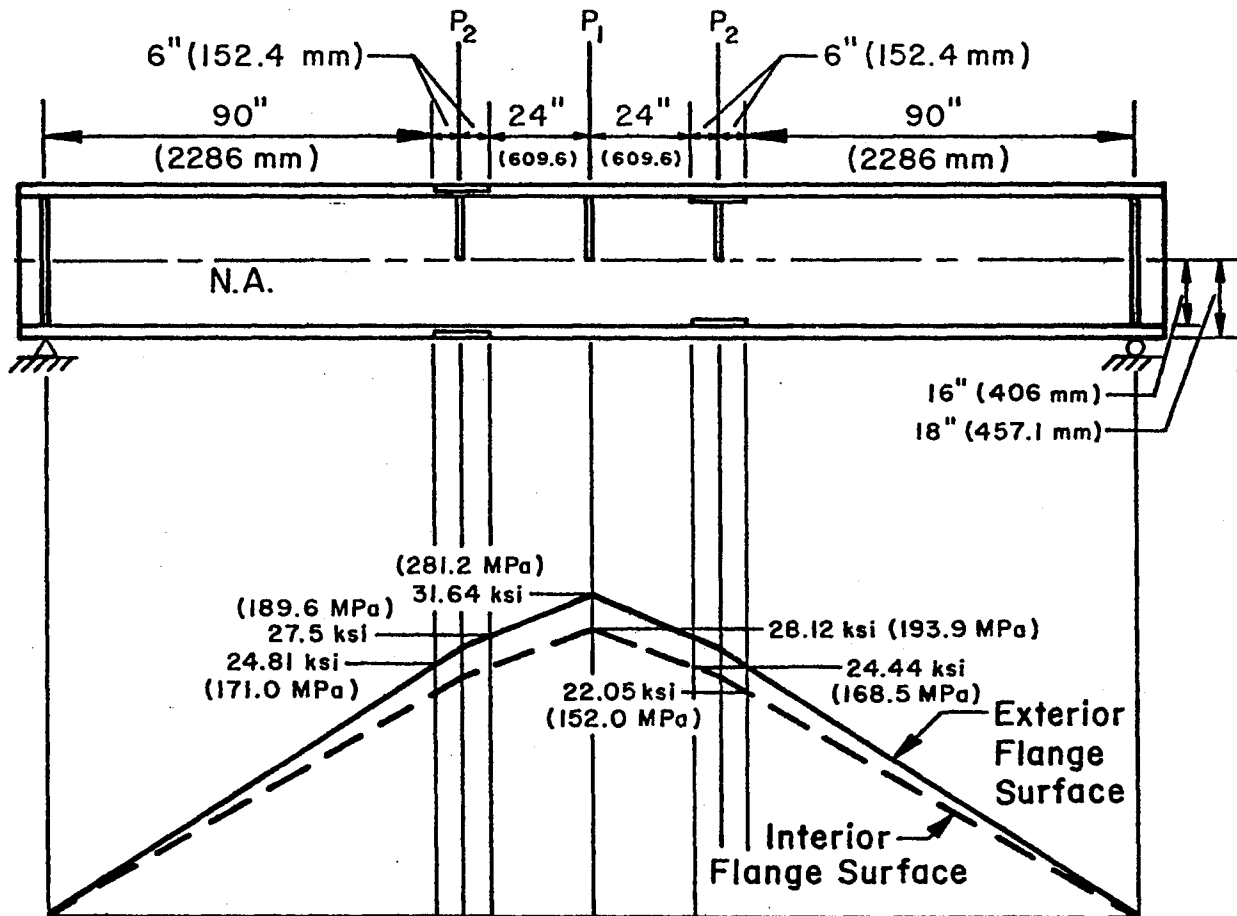
Fig. 2.6c Maximum-Stress on Interior and Exterior Flange
Surfaces of Beams B6 and B6A (A588)
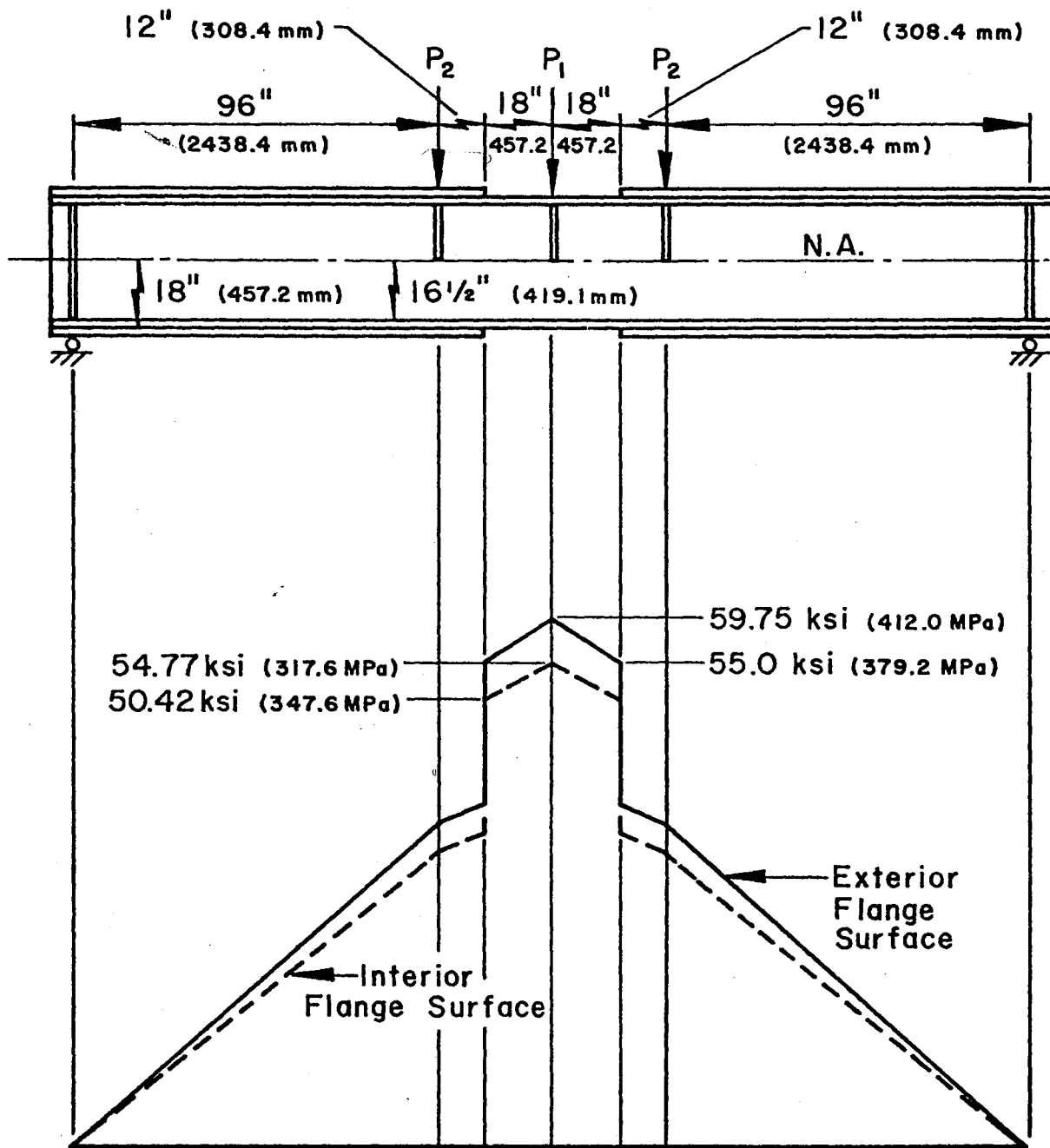
Fig. 2.6d   Maximum Stress on Interior and Exterior Flange
Surfaces of Beams B1 and B1A (A514)
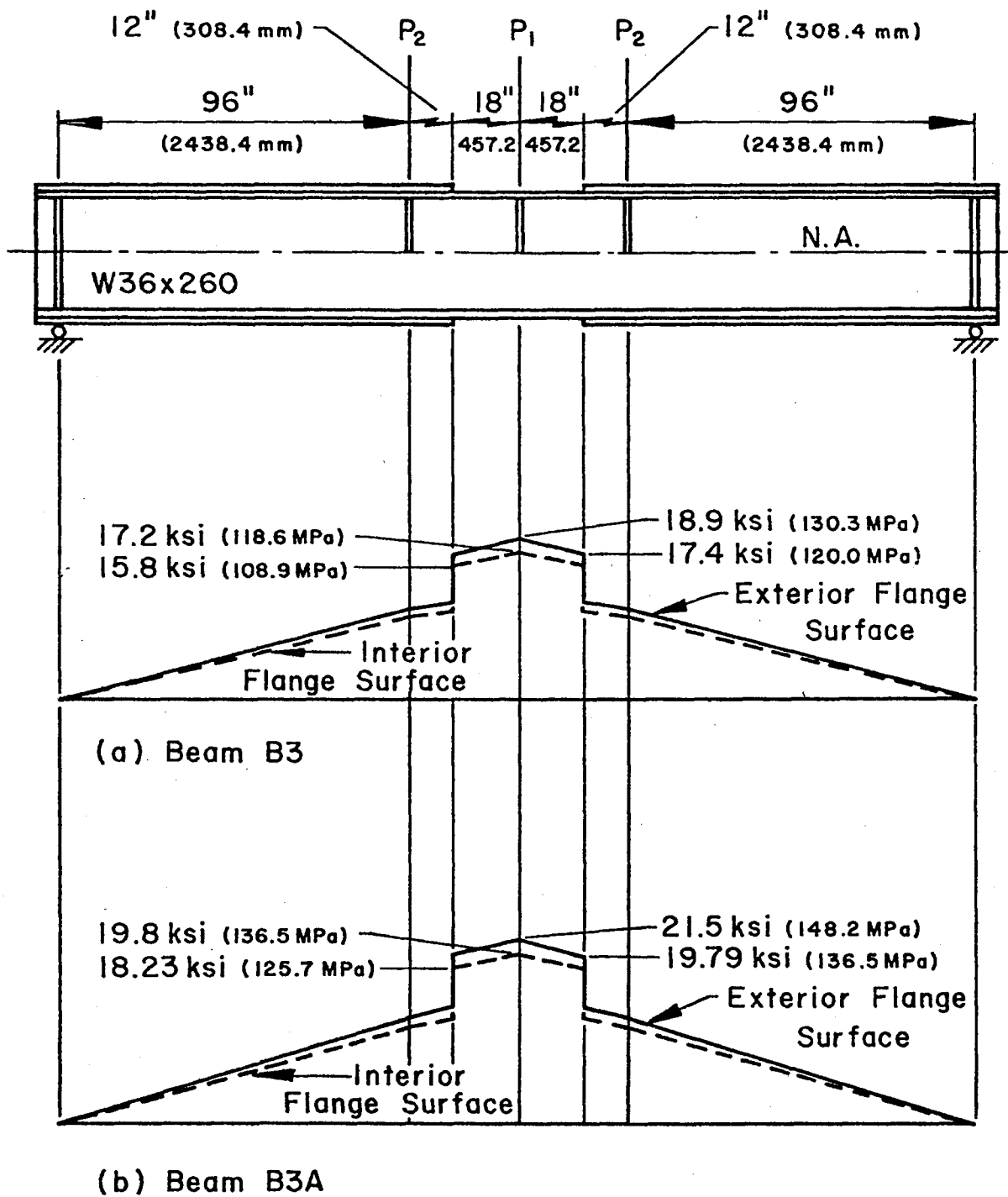
Fig. 2.6e   Maximum Stress on Interior and Exterior Flange
            Surfaces of Beams B3 and B3A (A36, W36 x 260)
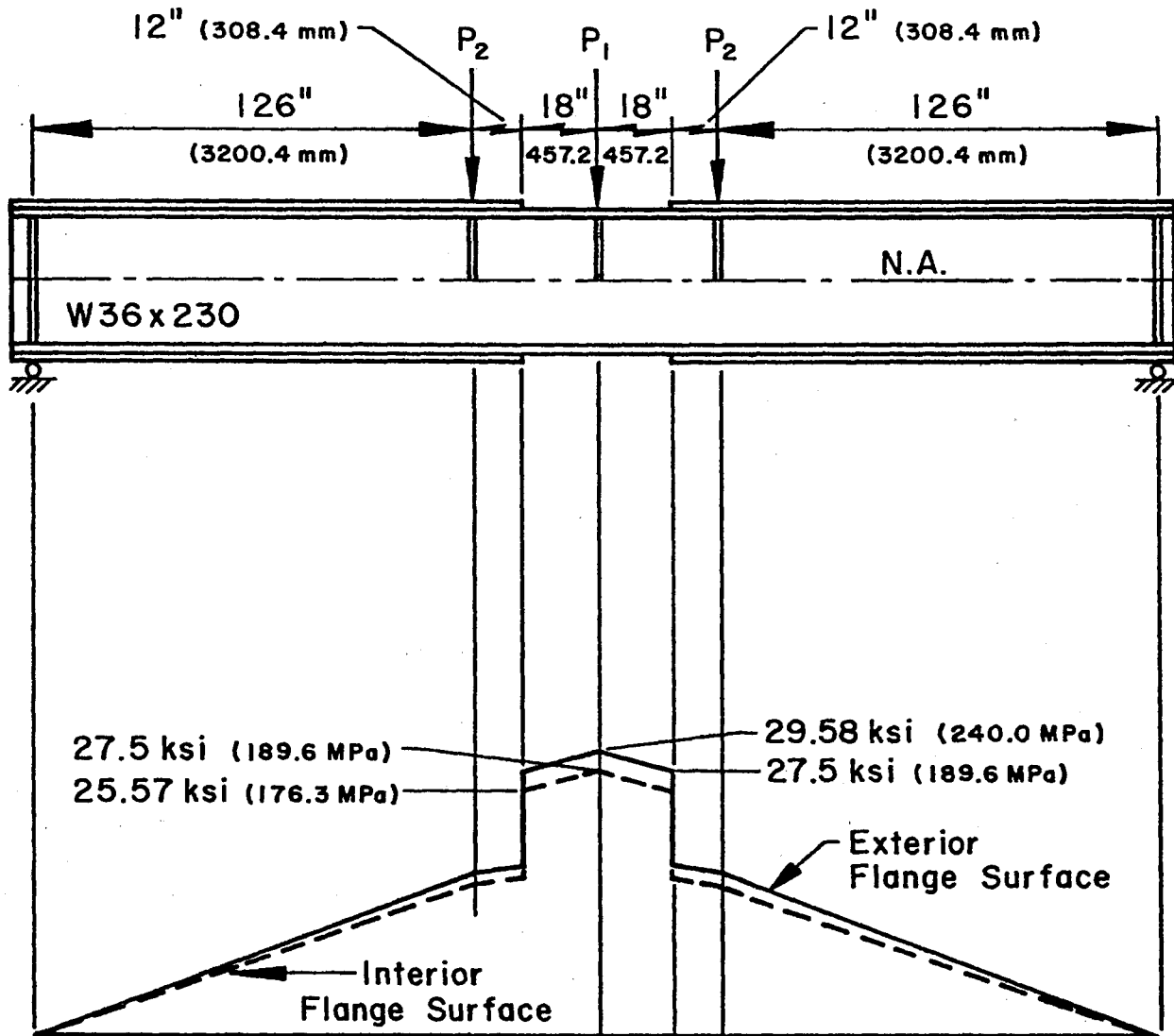
Fig. 2.6f Maximum Stress on Interior and Exterior Flange
Surfaces of Beams B5 and B5A (A588, W36 x 230)
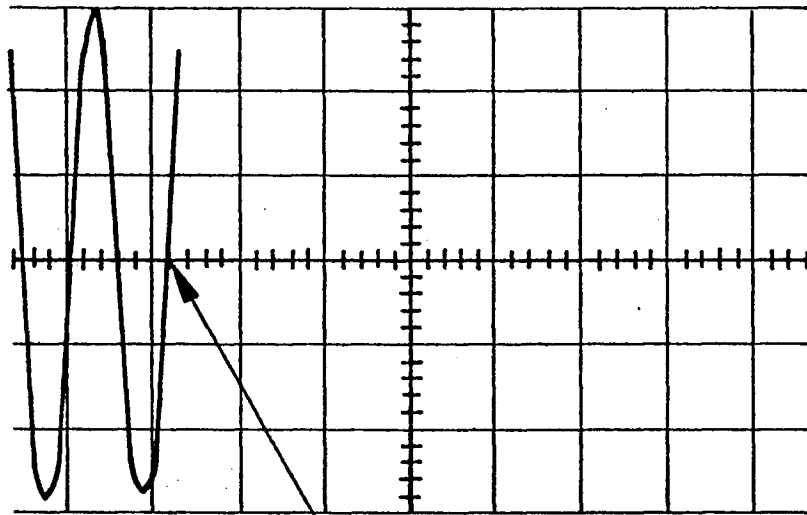
‑Maximum Slope
100 ksi/sec (689.5 MPa/Sec)

Note: Horizontal Scale: 0.2 sec/cm

Fig. 2.7 Strain Rate Trace at Fracture

Fig. 3.1 Photograph of Lehigh Drop Weight Test Machine

See Detail B

A

3" (76.2 mm)

12" (304.8 mm)

$\alpha = 30° \pm 1/2°$

1 1/2" (38.1 mm)

Section A-A

1/16" (1.5875 mm)

90 Chevron Notch
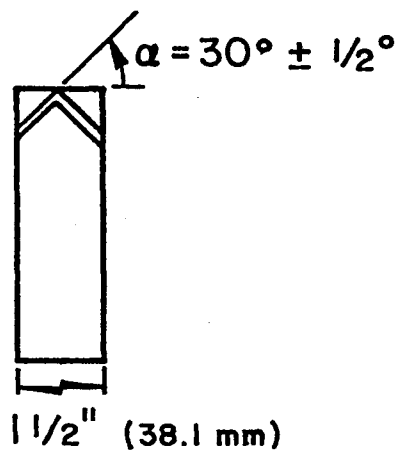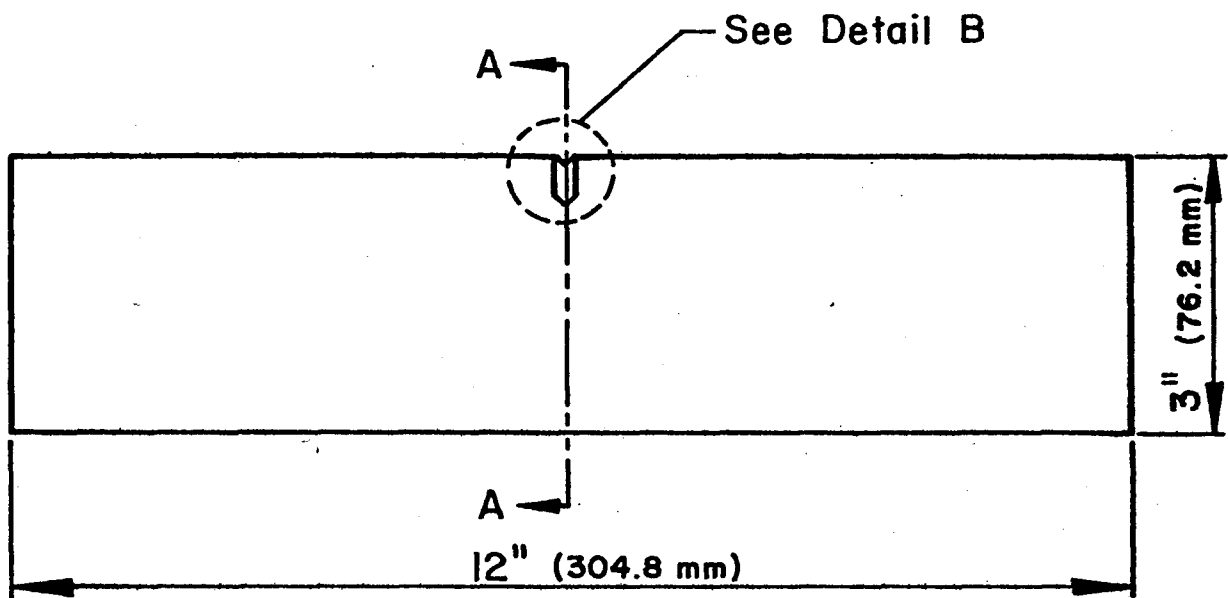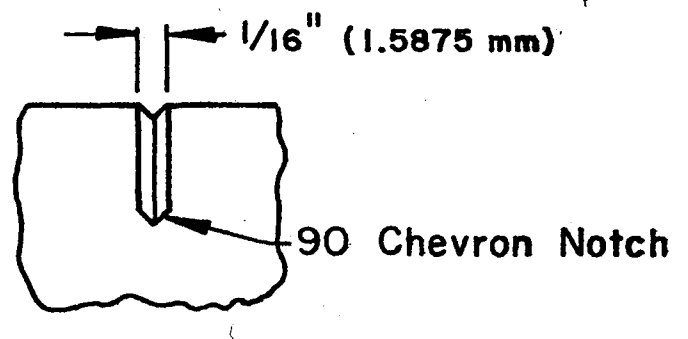
Detail B

Fig. 3.2 Three-Point Bend Specimen

-120-

Load (4 kips/cm)

Time (0.5 ms/cm)
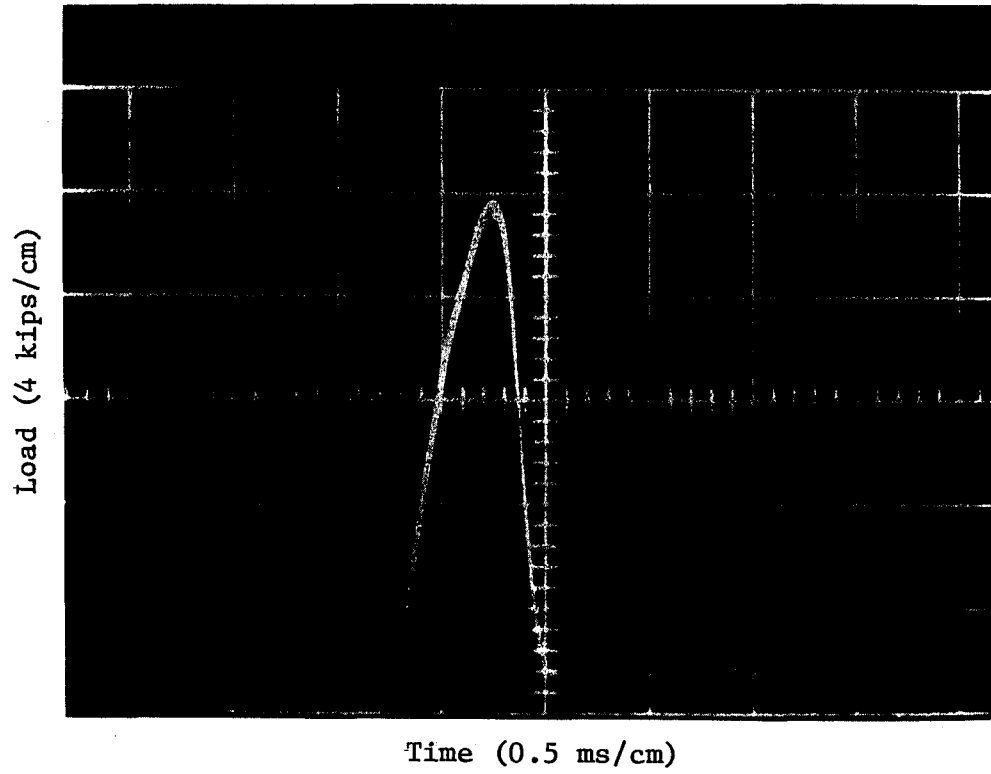
Fig. 3.3 Typical Load Time Relationship
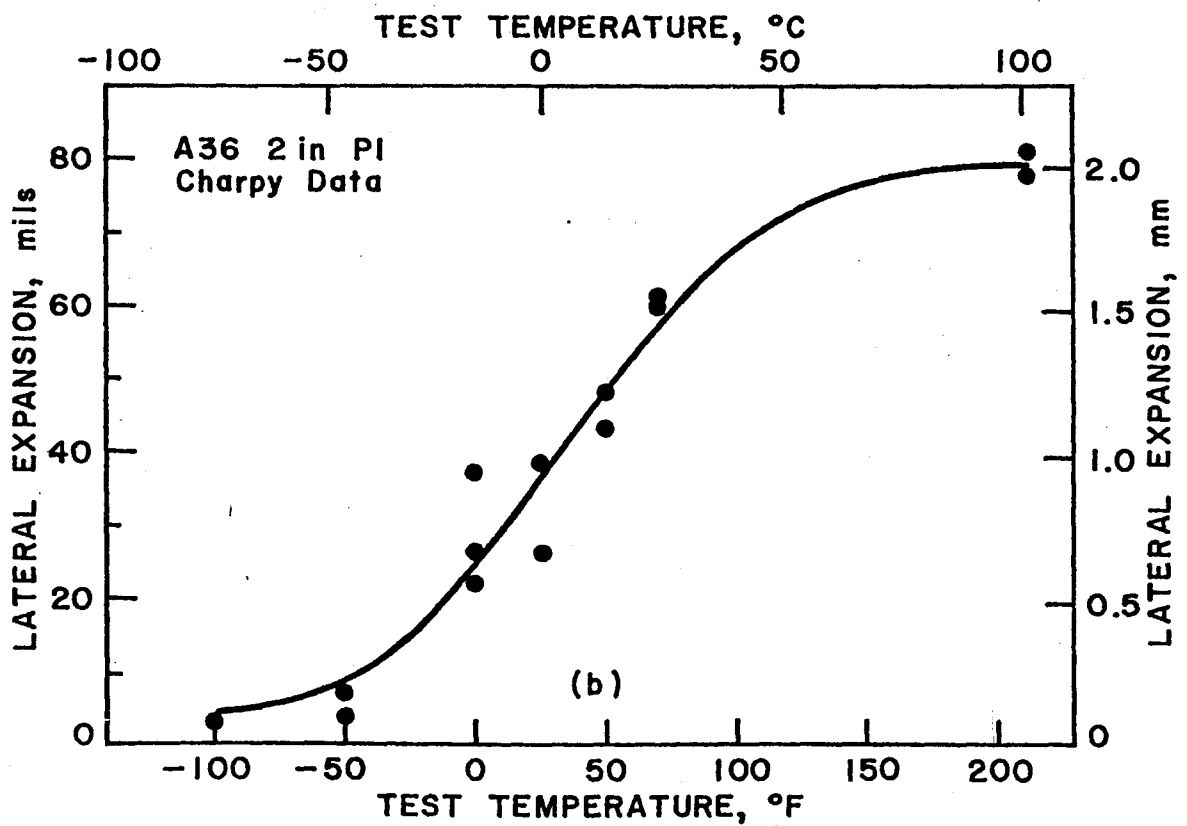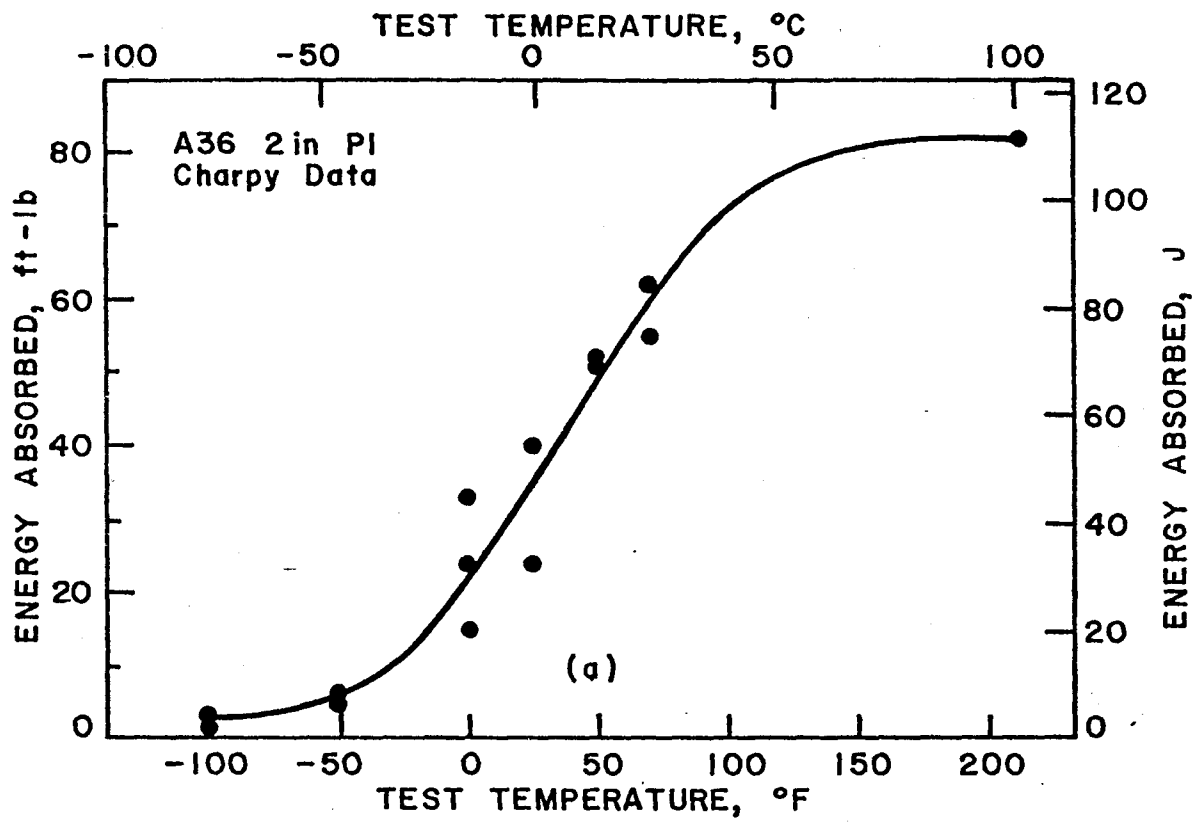
Fig. 3.4 Plotted CVN Data (A36/2 in. P1)
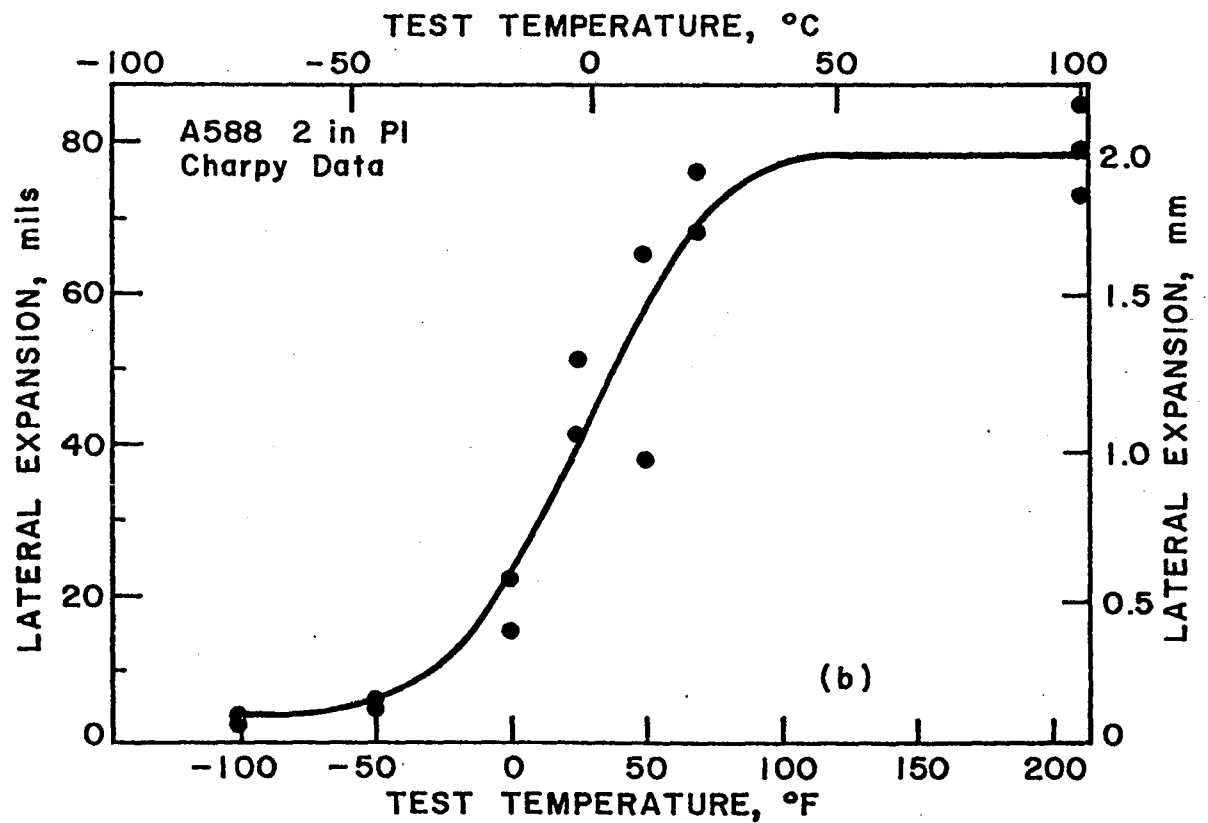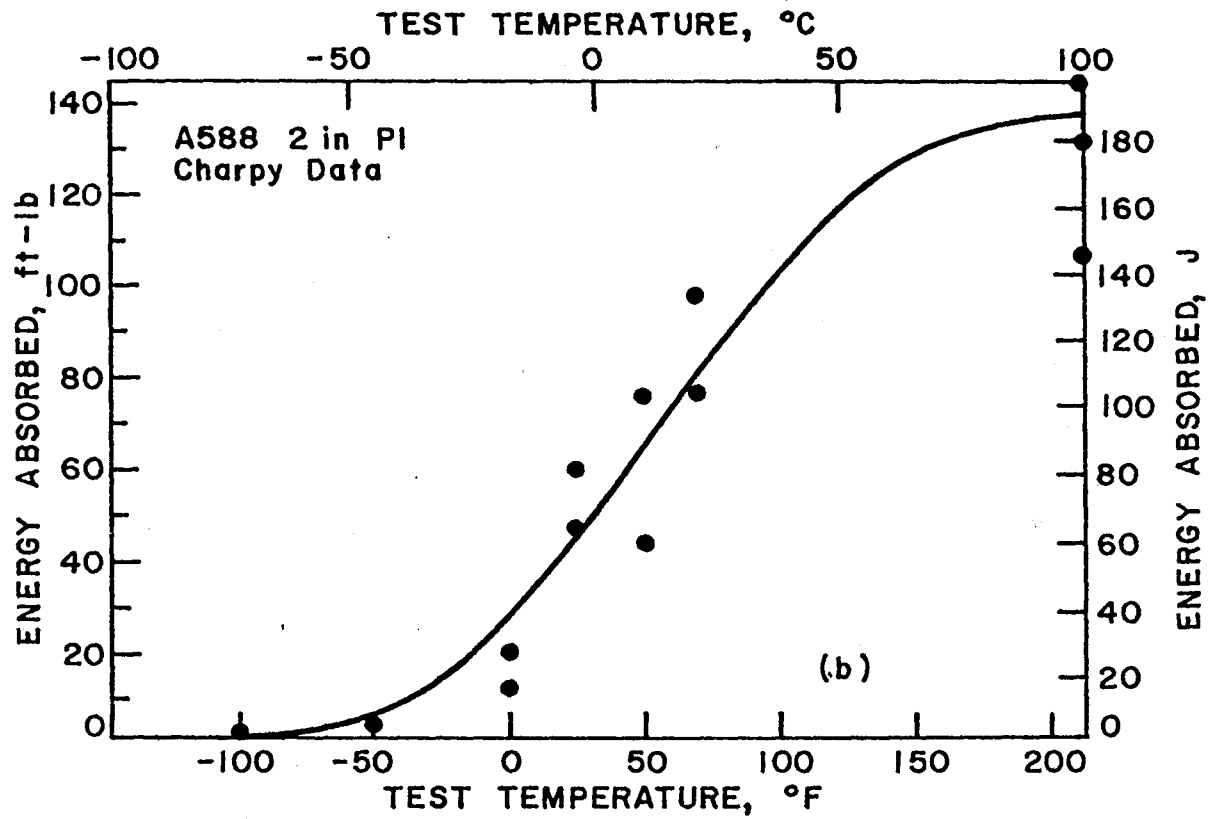
Fig. 3.5 Plotted CVN Data (A588/2 in. Pl)
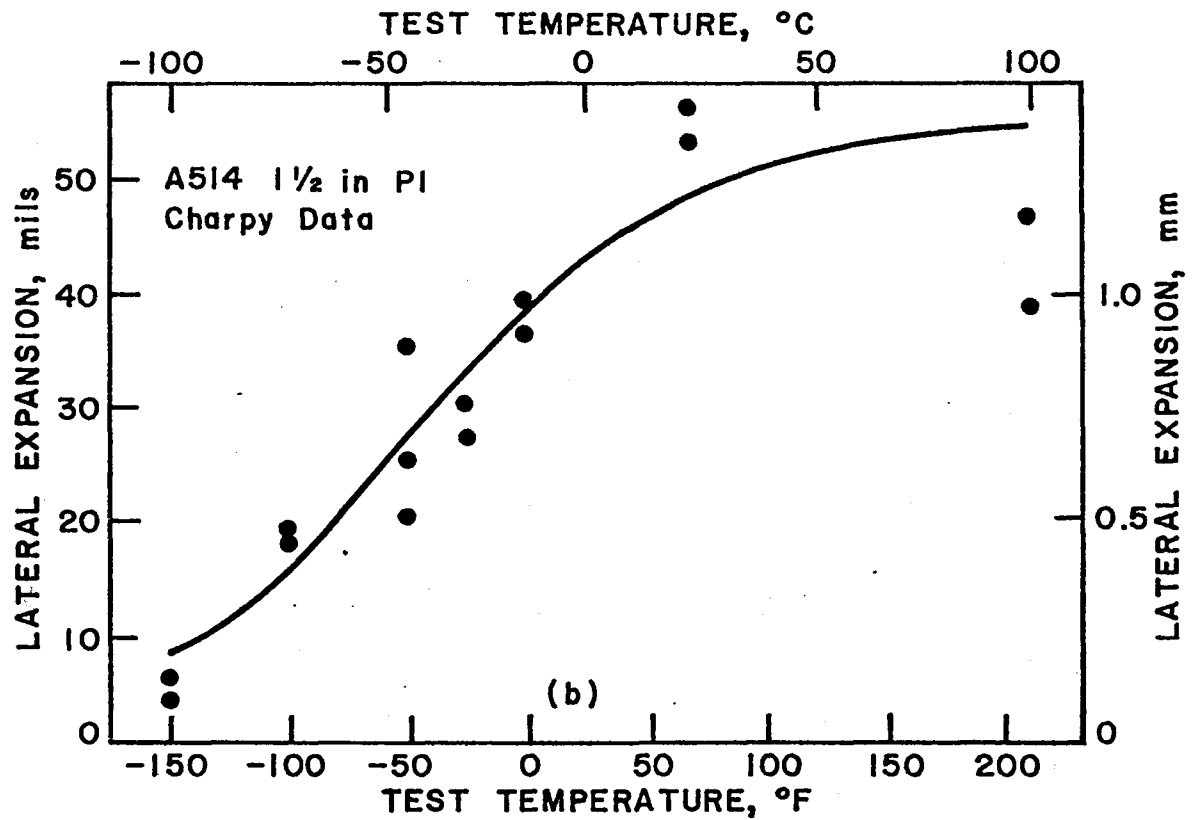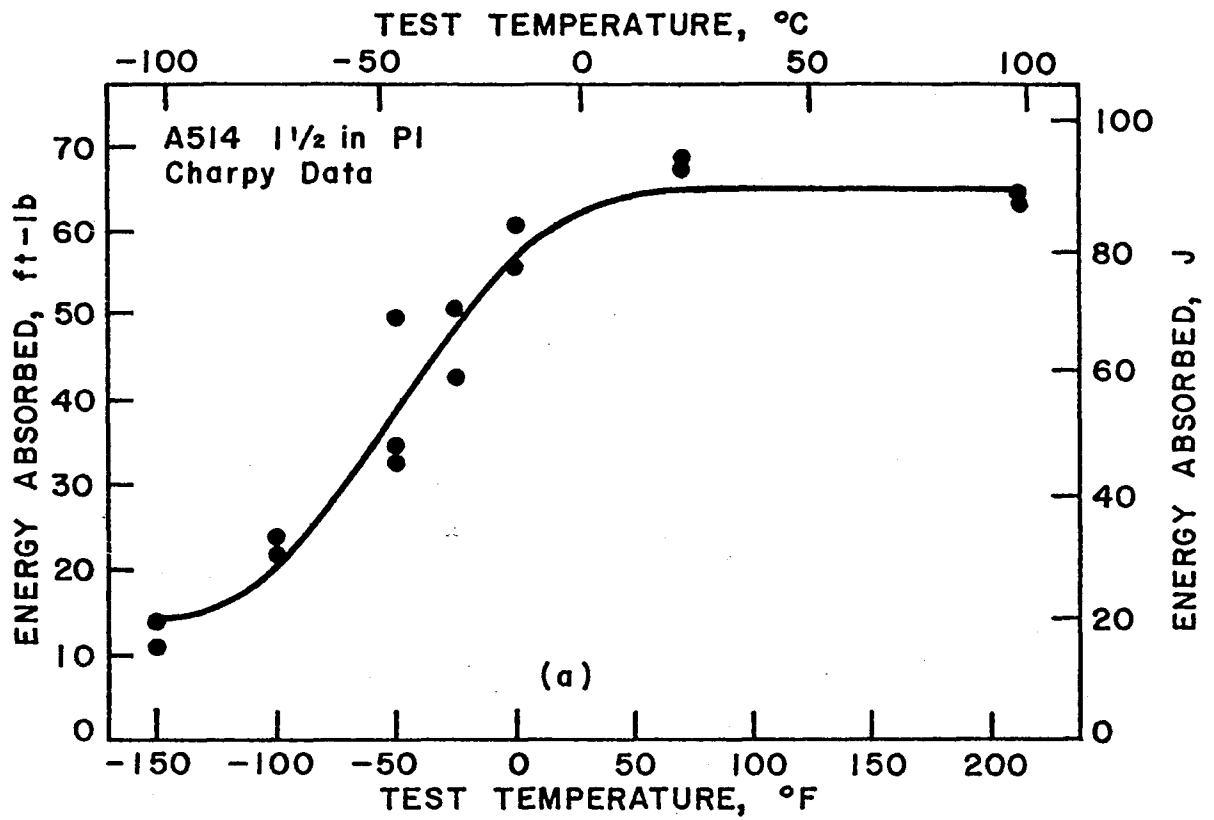
Fig. 3.6 Plotted CVN Data (A514/1½ in. P1)
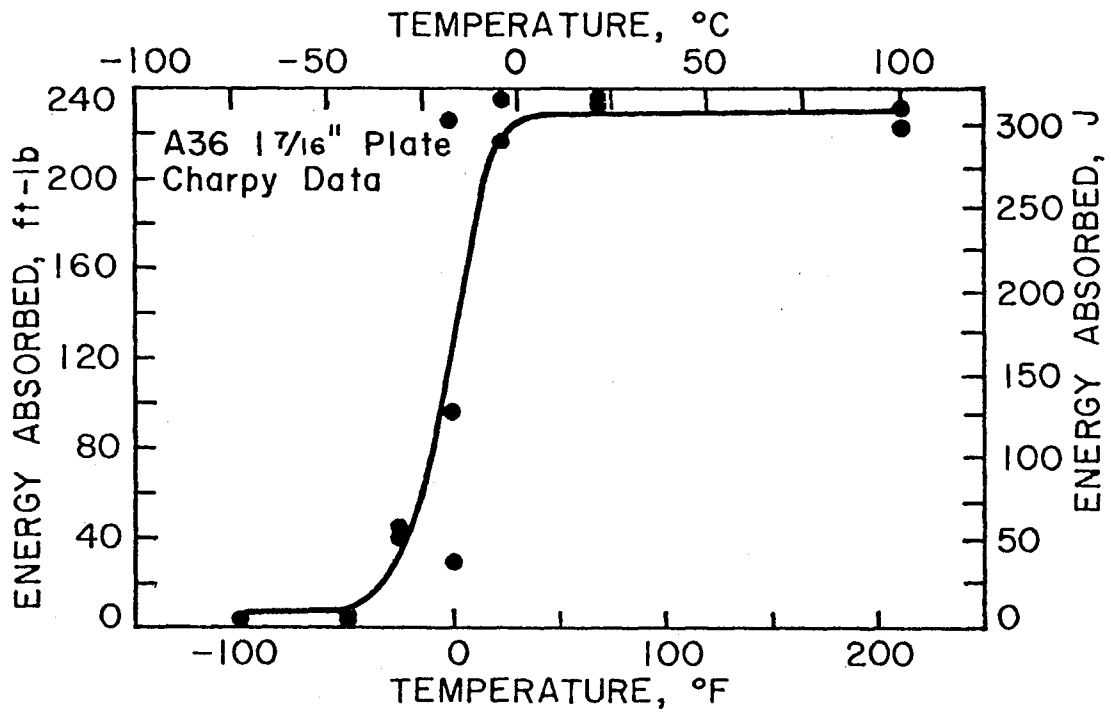
(a)
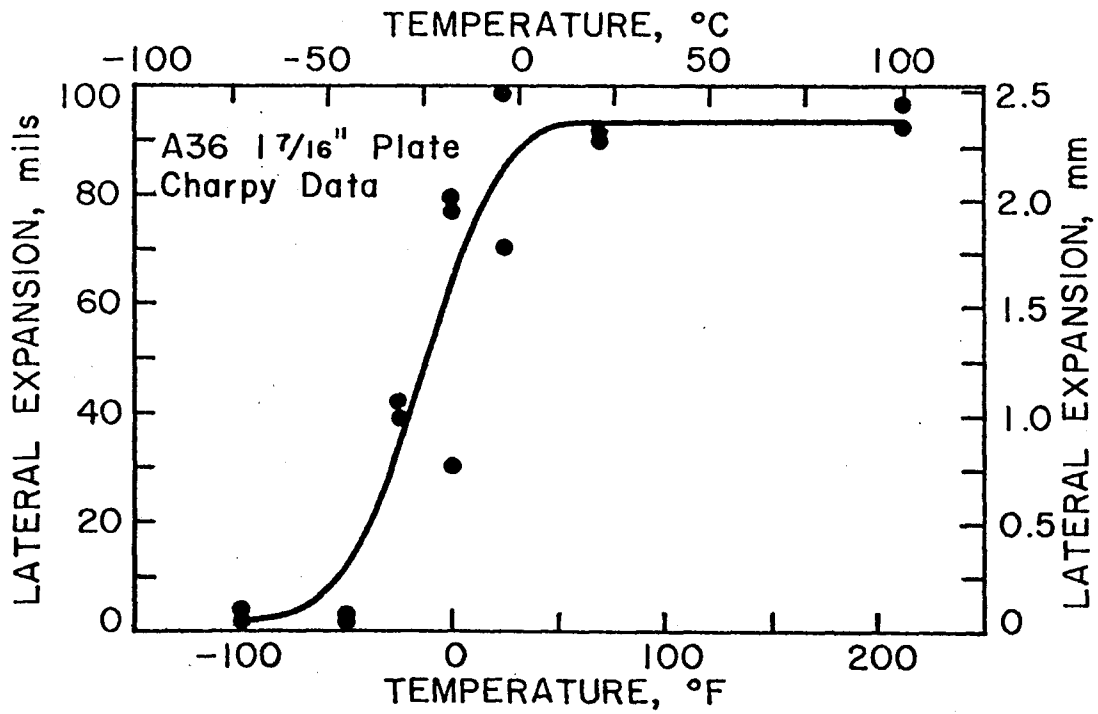
(b)

Fig. 3.7 Plotted CVN Data (A36, W36 x 260, Flange)
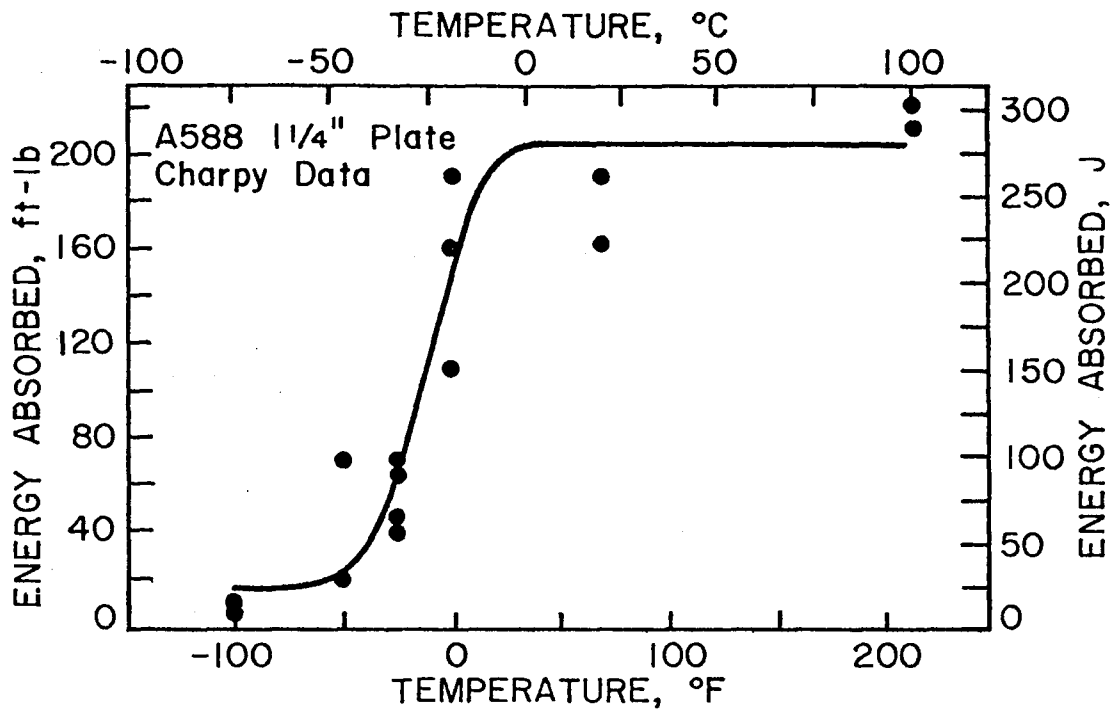
(a)
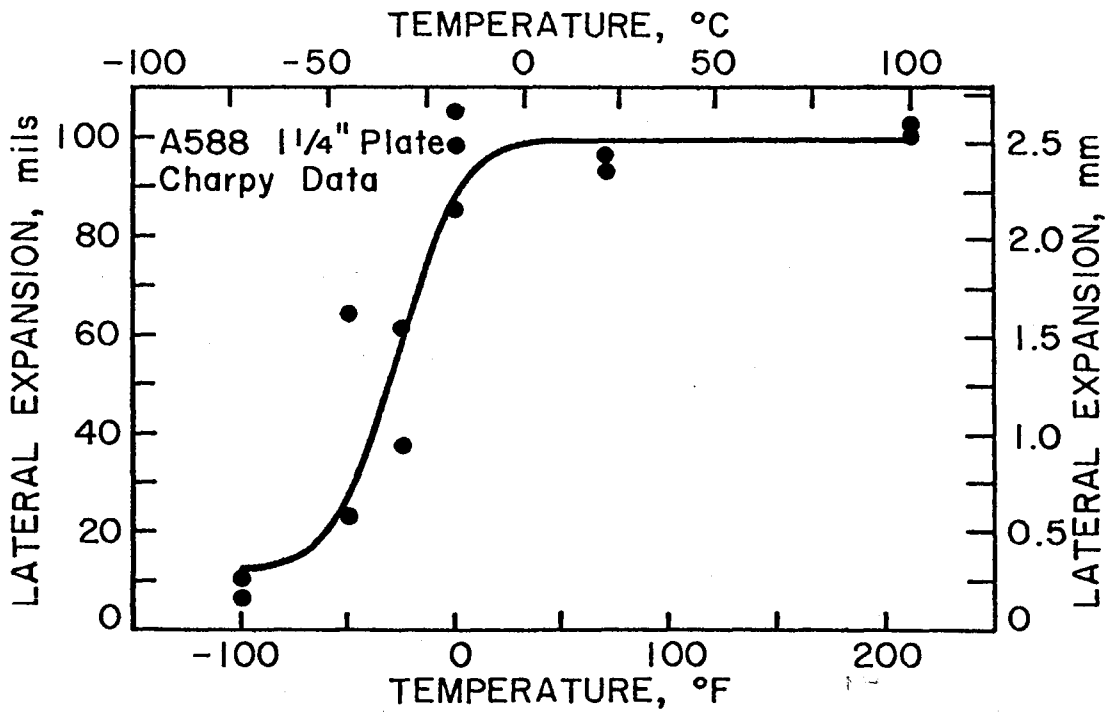
(b)

Fig. 3.8 Plotted CVN Data (A588, W36 x 230, Flange)

Fig. 3.9 Fracture Toughness vs. Temperature (A36/2 in. P1)

FRACTURE TOUGHNESS, MPa$\sqrt{m}$

Points from CVN Data
$K_{Id} = (5ECVN)^{1/2}$

Dynamic

Valid

Static

Valid
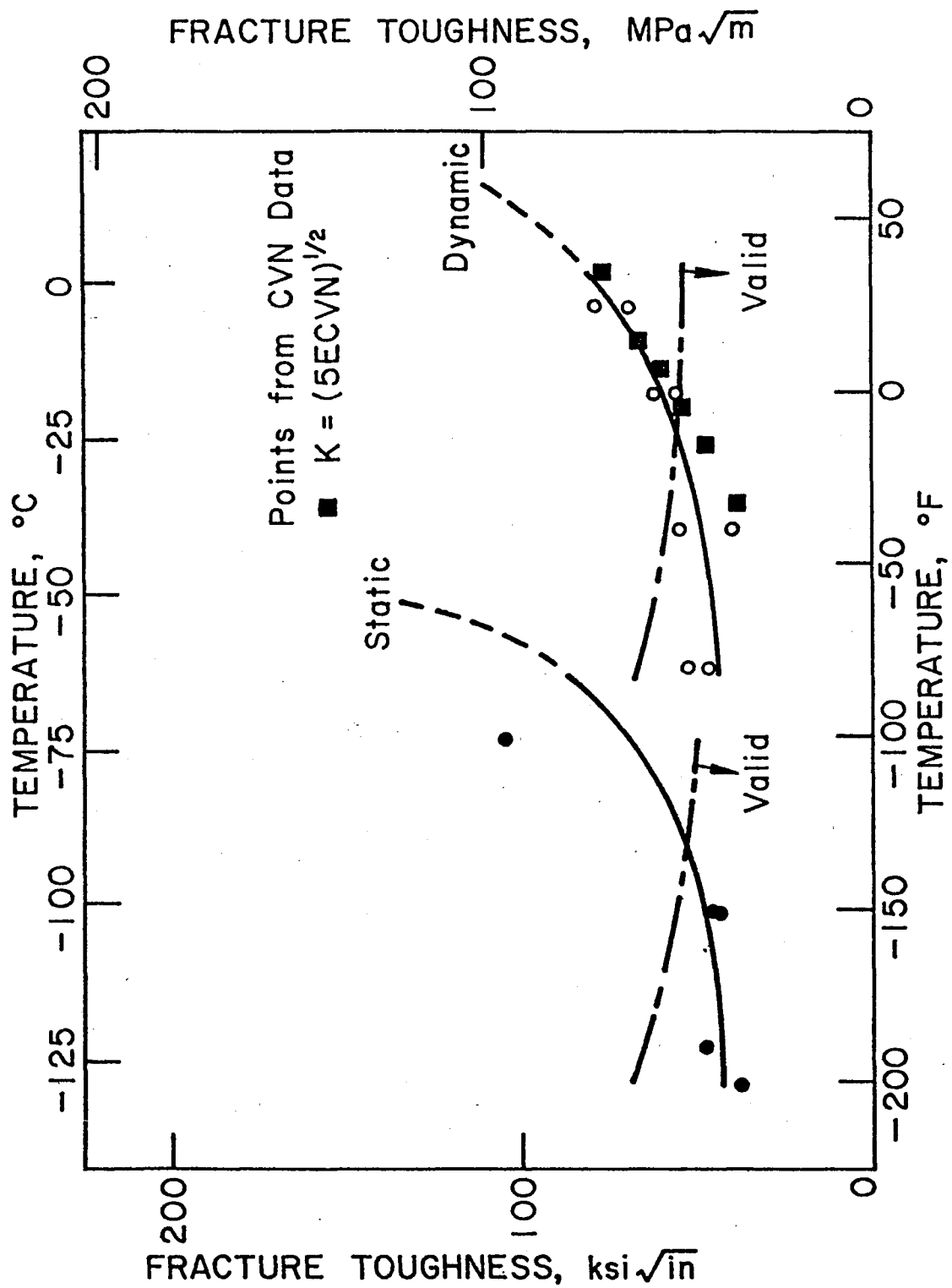
TEMPERATURE, °C

TEMPERATURE, °F

FRACTURE TOUGHNESS, ksi$\sqrt{in}$
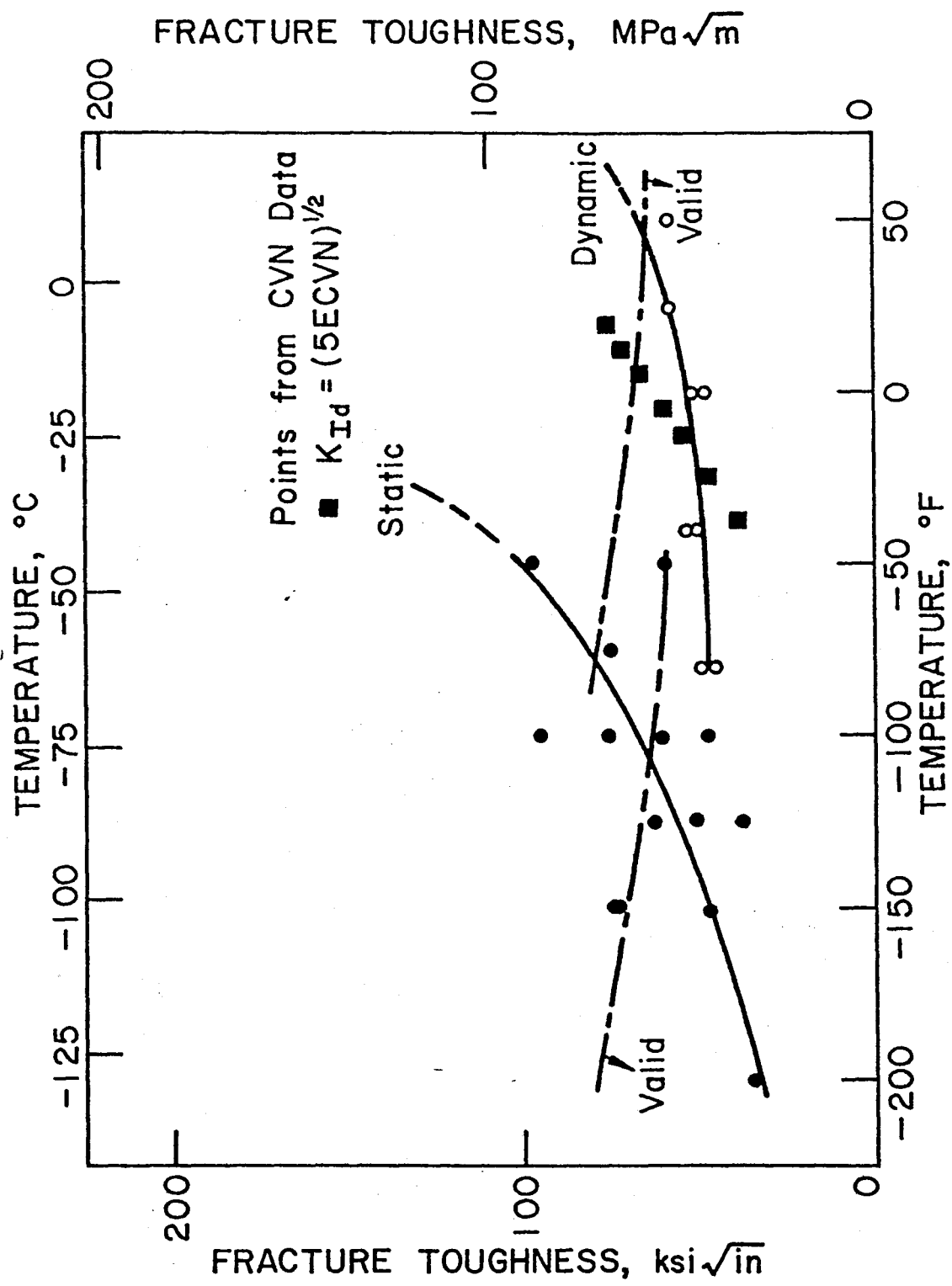
Fig. 3.10 Fracture Toughness vs. Temperature (A588/2 in. Pl)
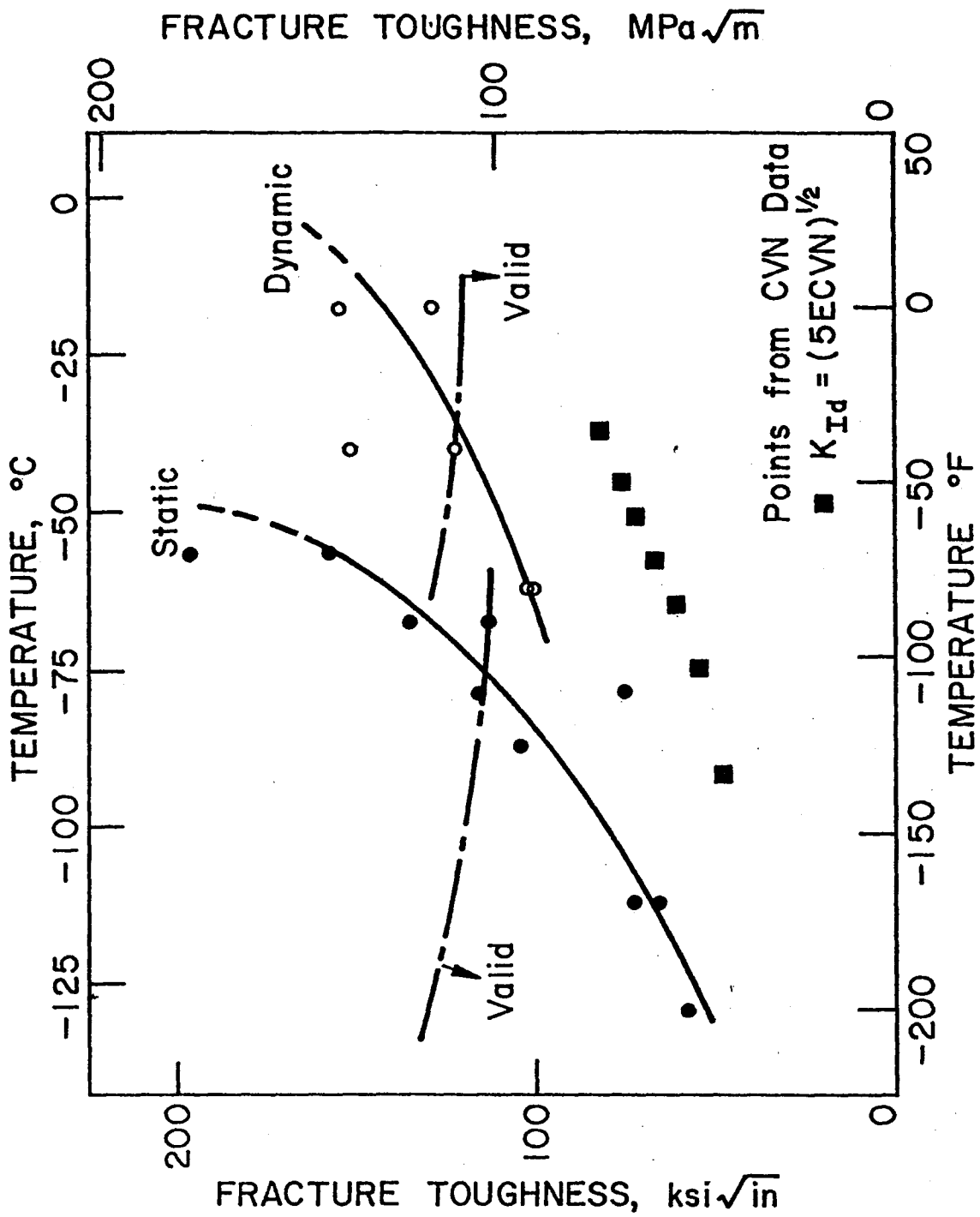
Fig. 3.11 Fracture Toughness vs. Temperature (A514/1½ in. Pl)
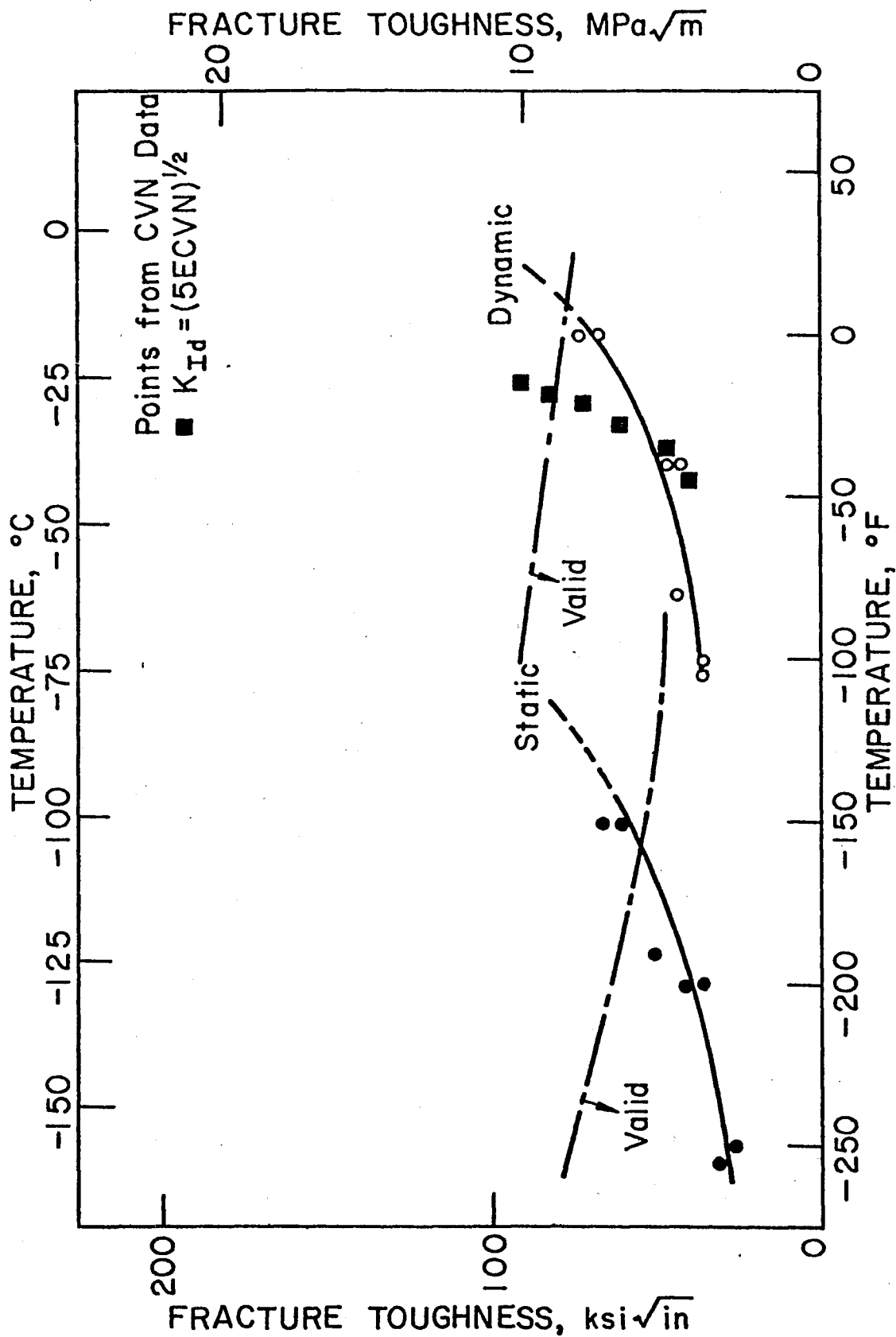
Fig. 3.12 Fracture Toughness vs. Temperature (A36, W36 x 260, Flange Material)
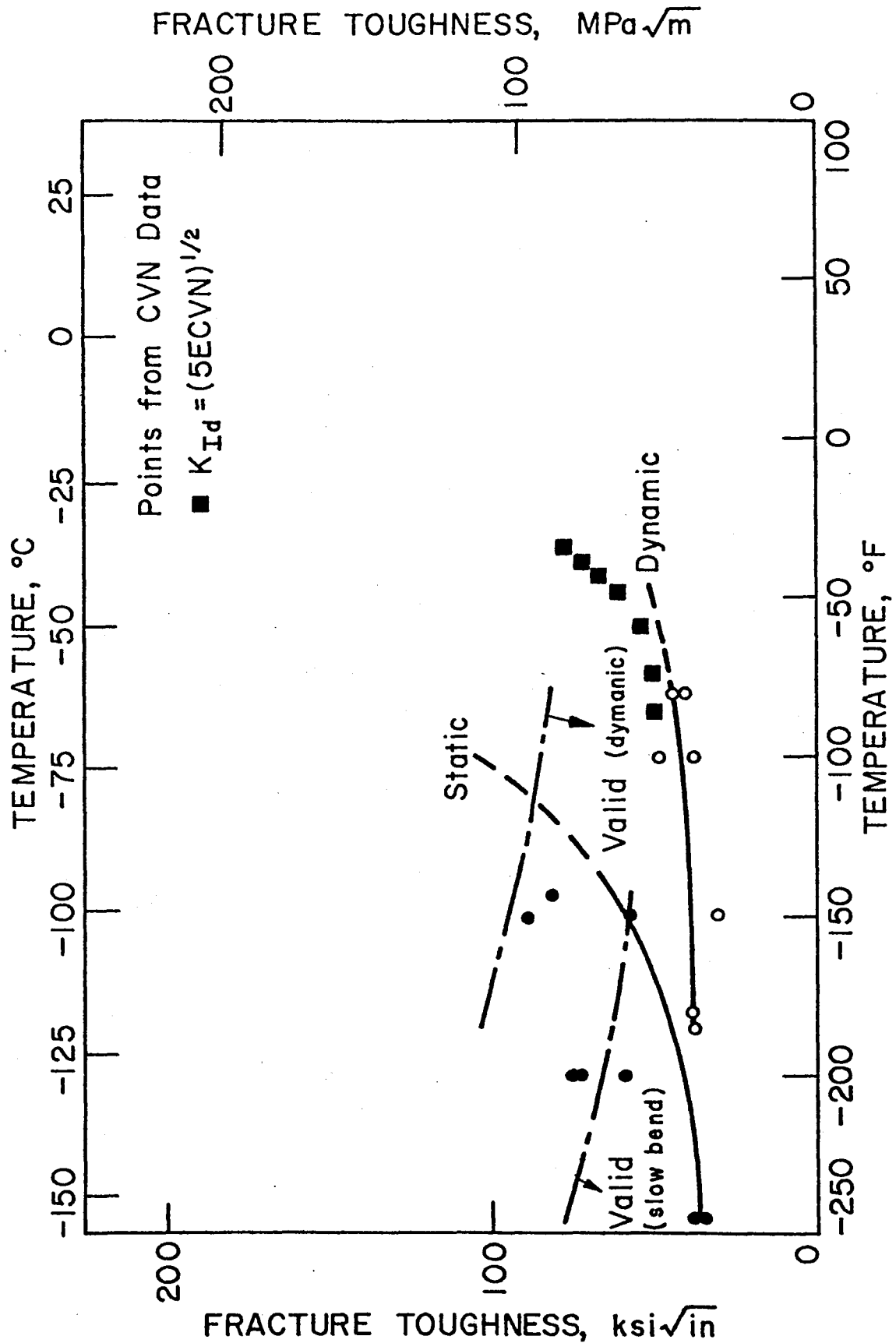
Fig. 3.13 Fracture Toughness vs. Temperature (A588, W36 x 230, Flange Material)
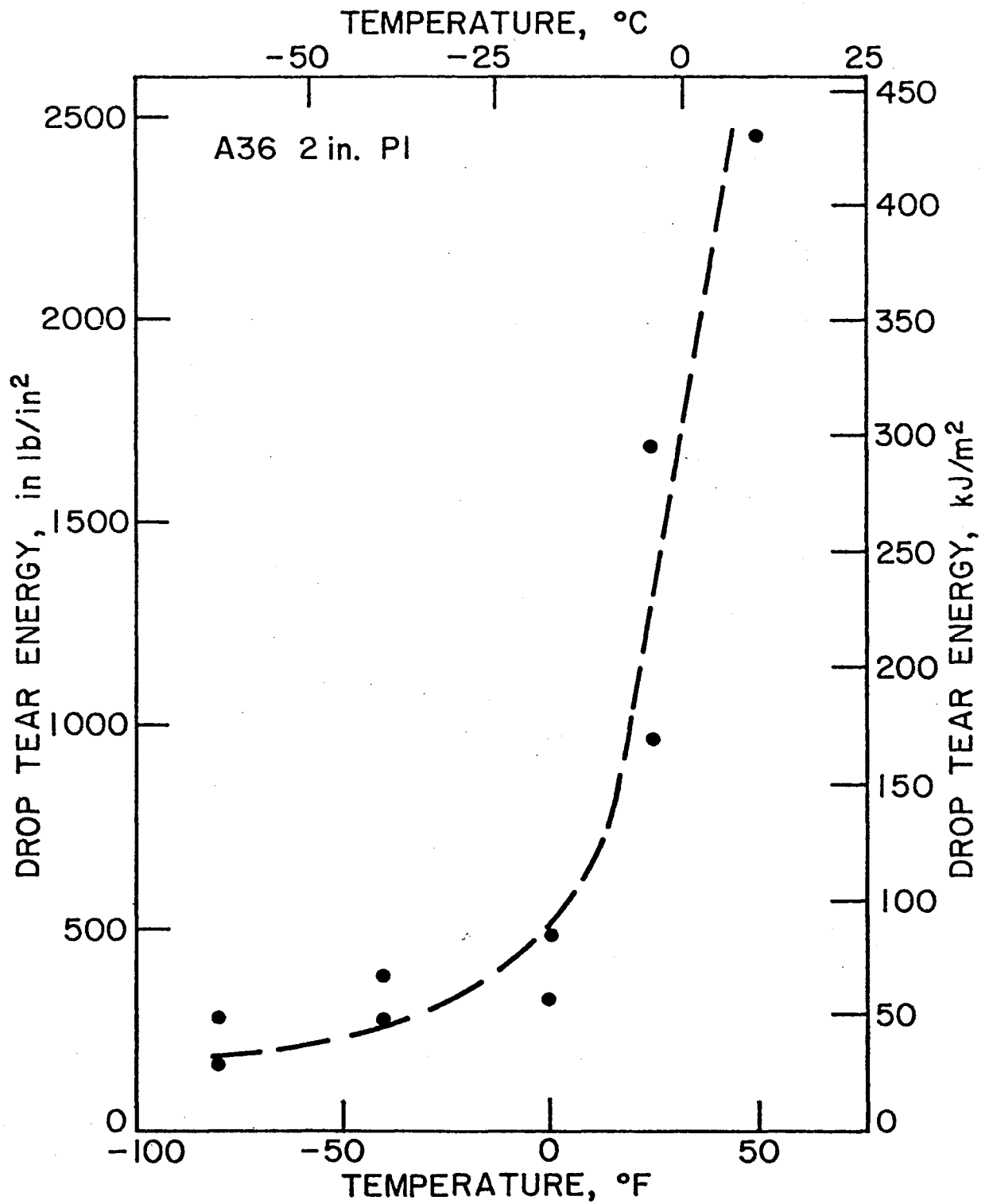
Fig. 3.14. Drop Tear Energy vs. Temperature (A36/2 in. P1)
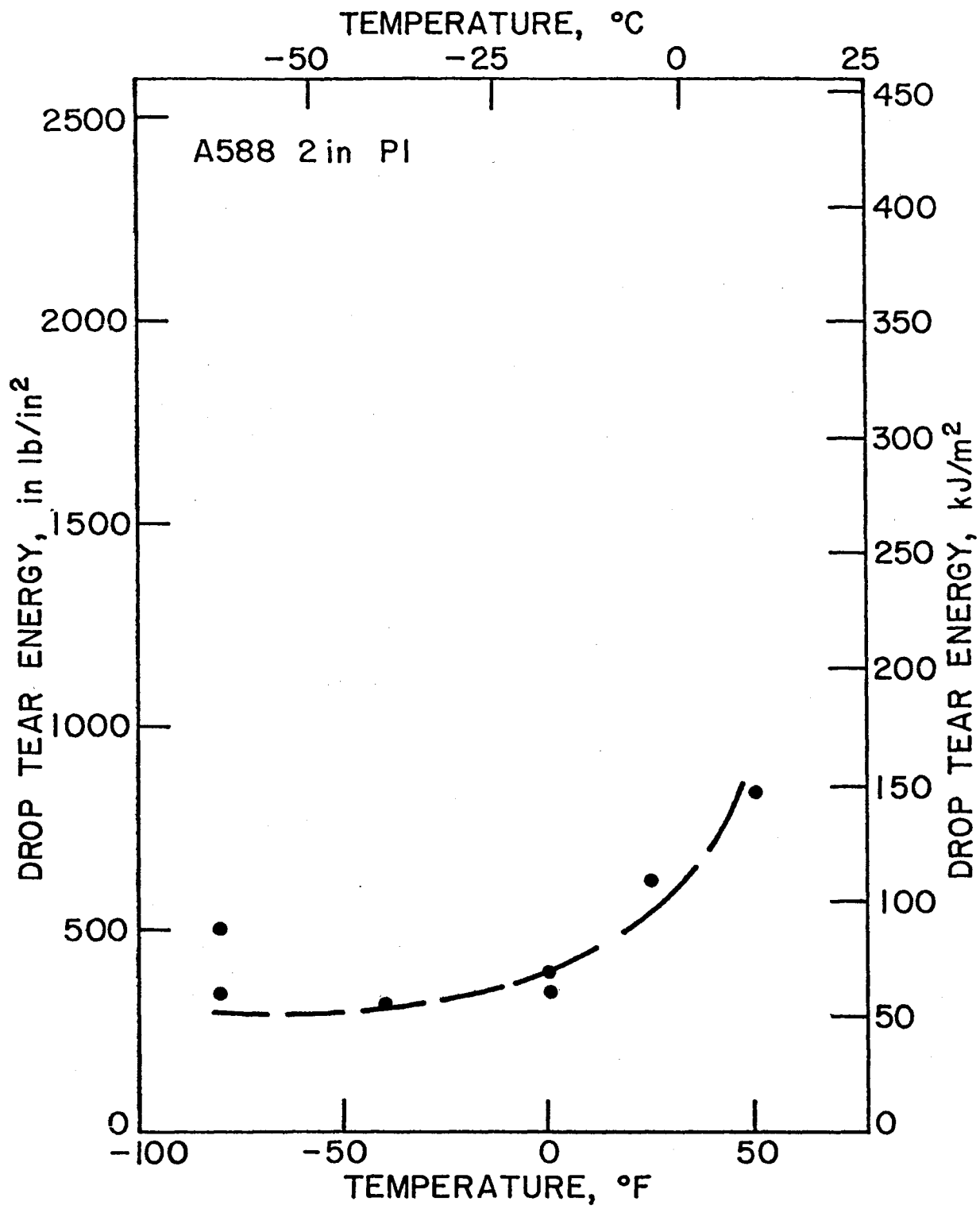
Fig. 3.15 Drop Tear Energy vs. Temperature (A588/2 in. P1)
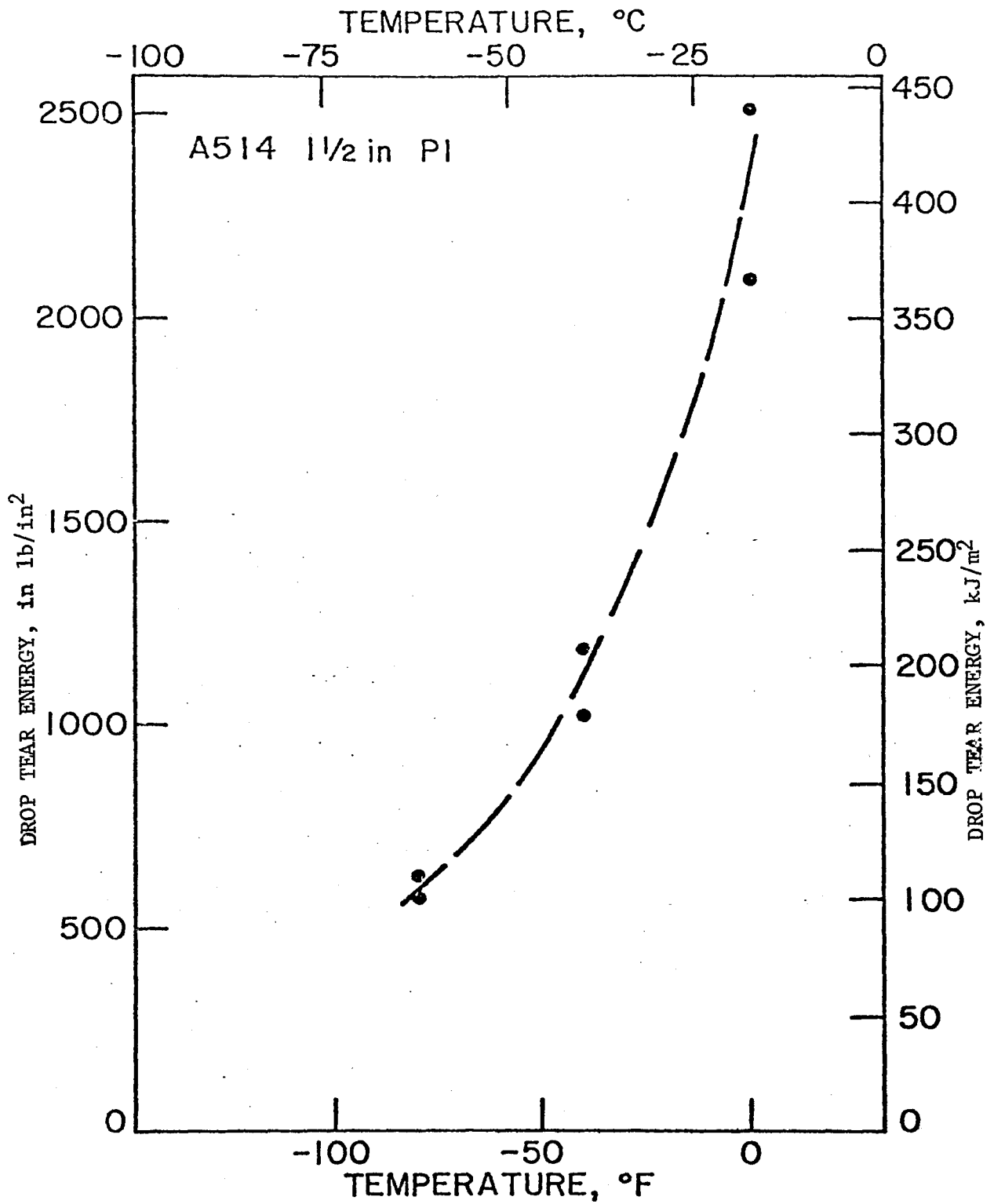
Fig. 3.16 Drop Tear Energy vs. Temperature (A514/1½ in. P1)

Beam B2

Critical Detail

Section AA
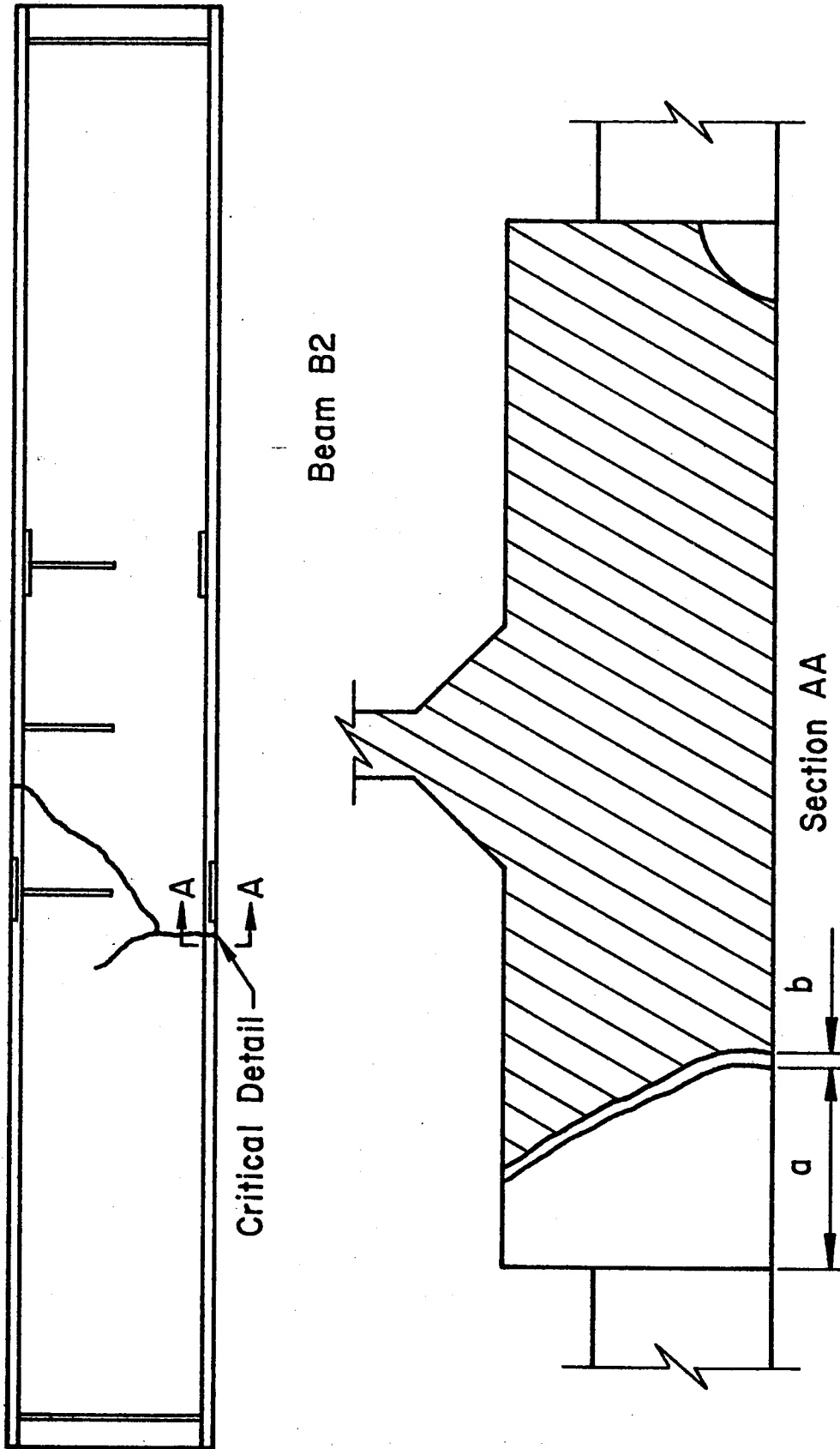
Fig. 4.1 Fatigue and Fracture Surface, B2 (A514)

Beam B2A

Critical Detail

A
A

Section AA

b+c
a
e
c
f
g
h
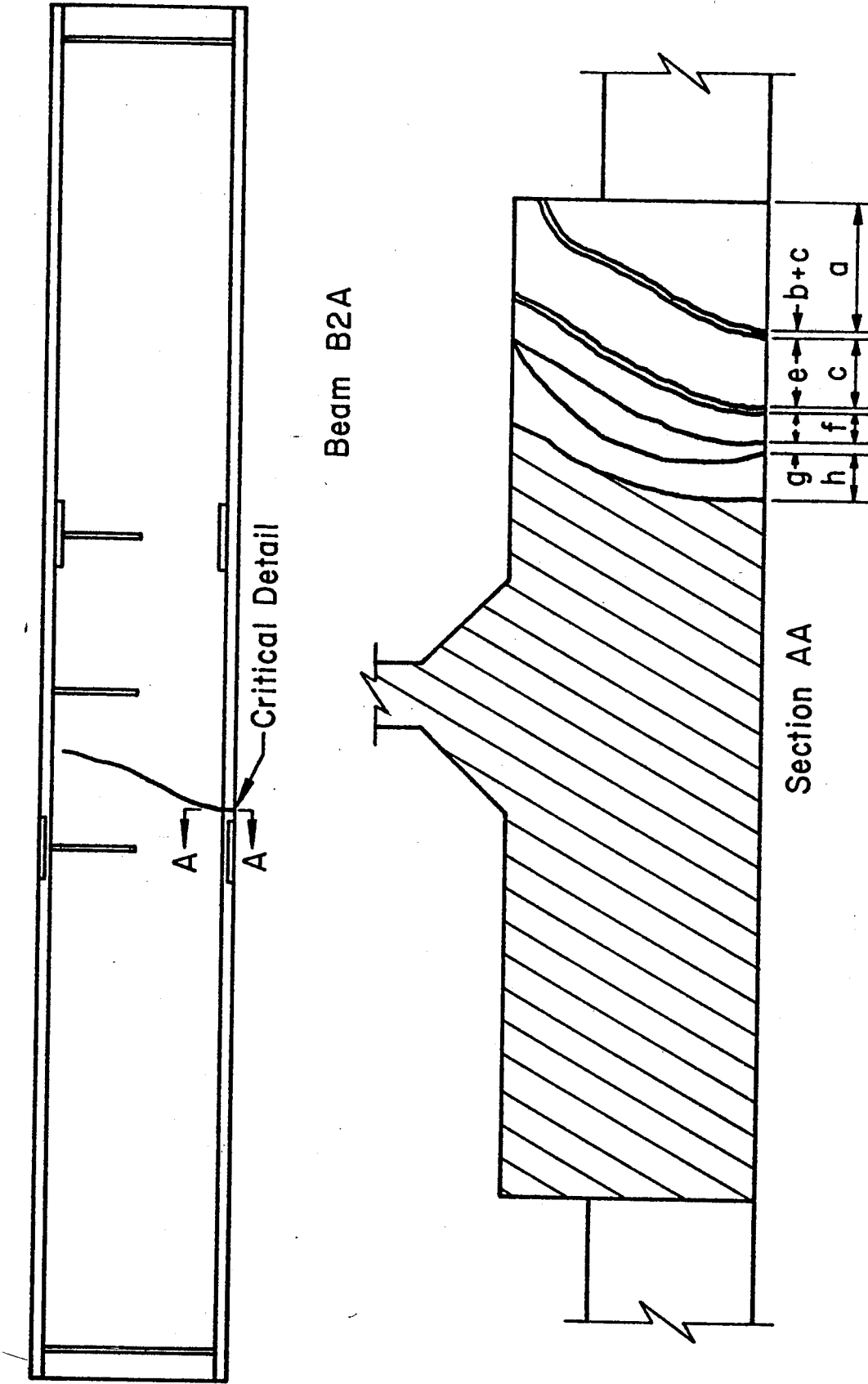
Fig. 4.2 Fatigue and Fracture Surface, B2A (A514)

-136-

Beam B4

Critical Detail
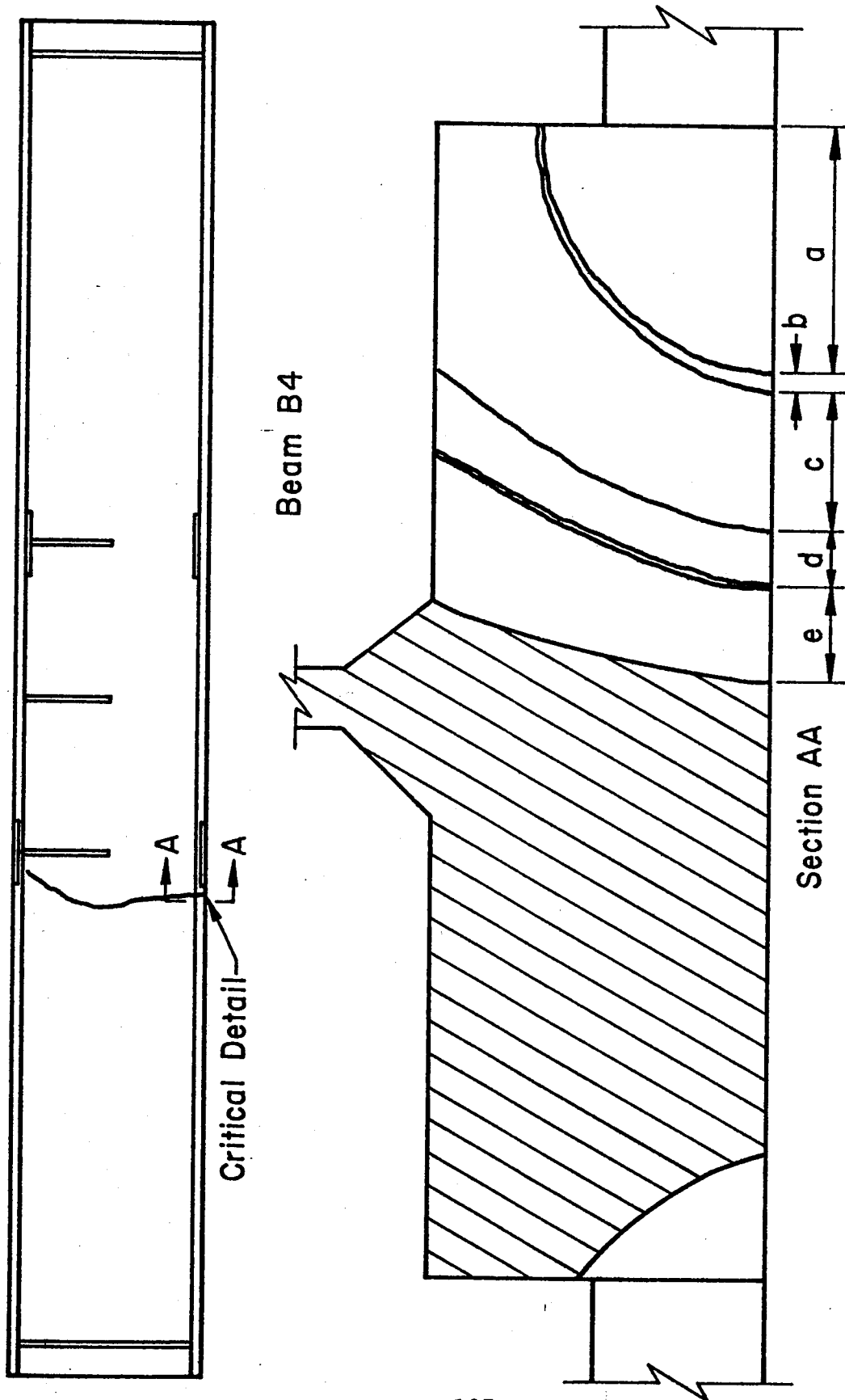
Section AA

Fig. 4.3 Fatigue and Fracture Surface, B4 (A36)

Beam B4A

Critical Detail

A

A

Section AA

j

j

i

h

g

f

d e

c

b

a
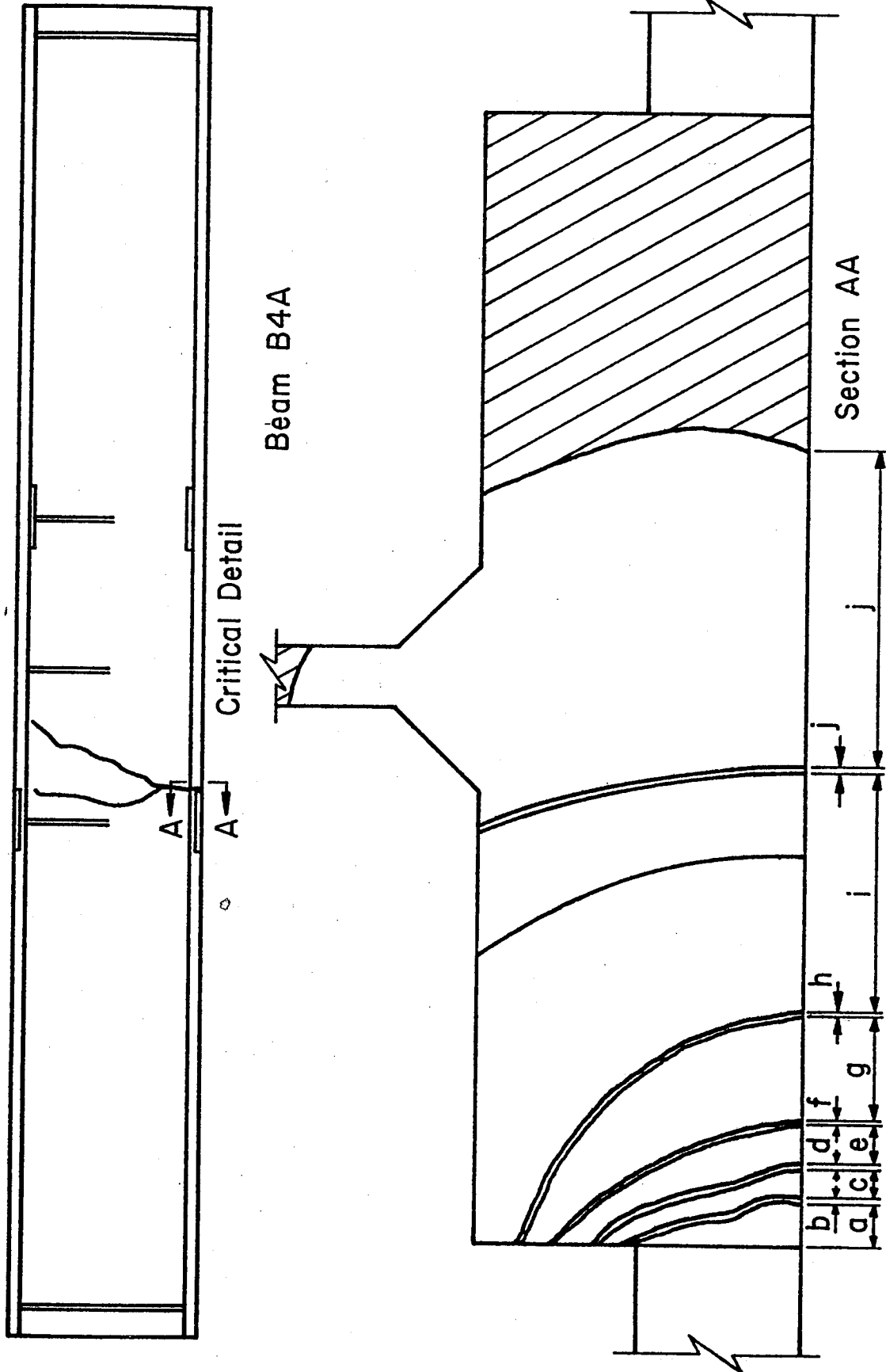
Fig. 4.4 Fatigue and Fracture Surface, B4A (A36)

-138-

Beam B6

Critical Detail
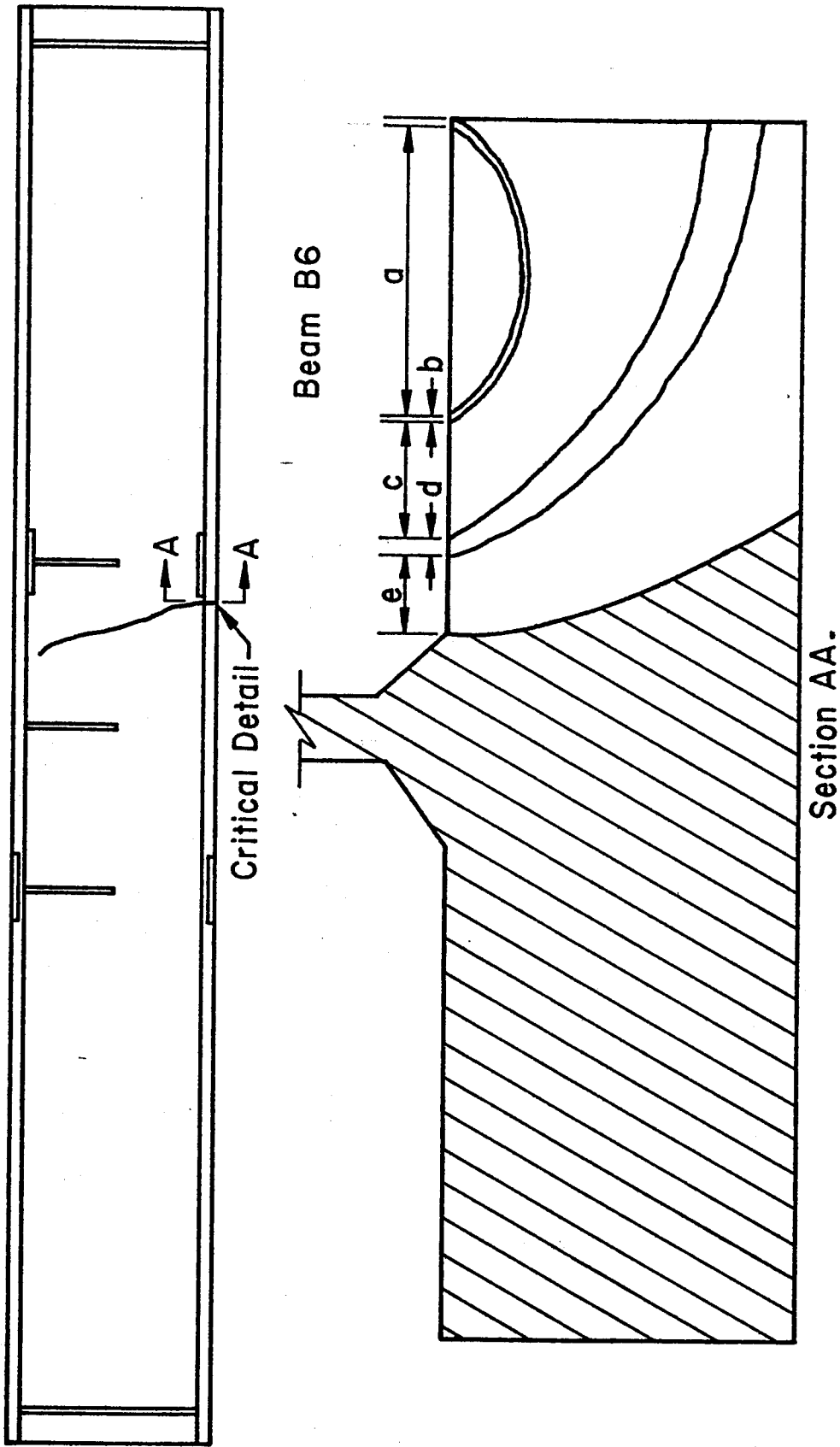
Section AA.

Fig. 4.5   Fatigue and Fracture Surface, B6 (A588)

Beam B6A

Critical Detail

A

A

Section AA

a

b

c

d
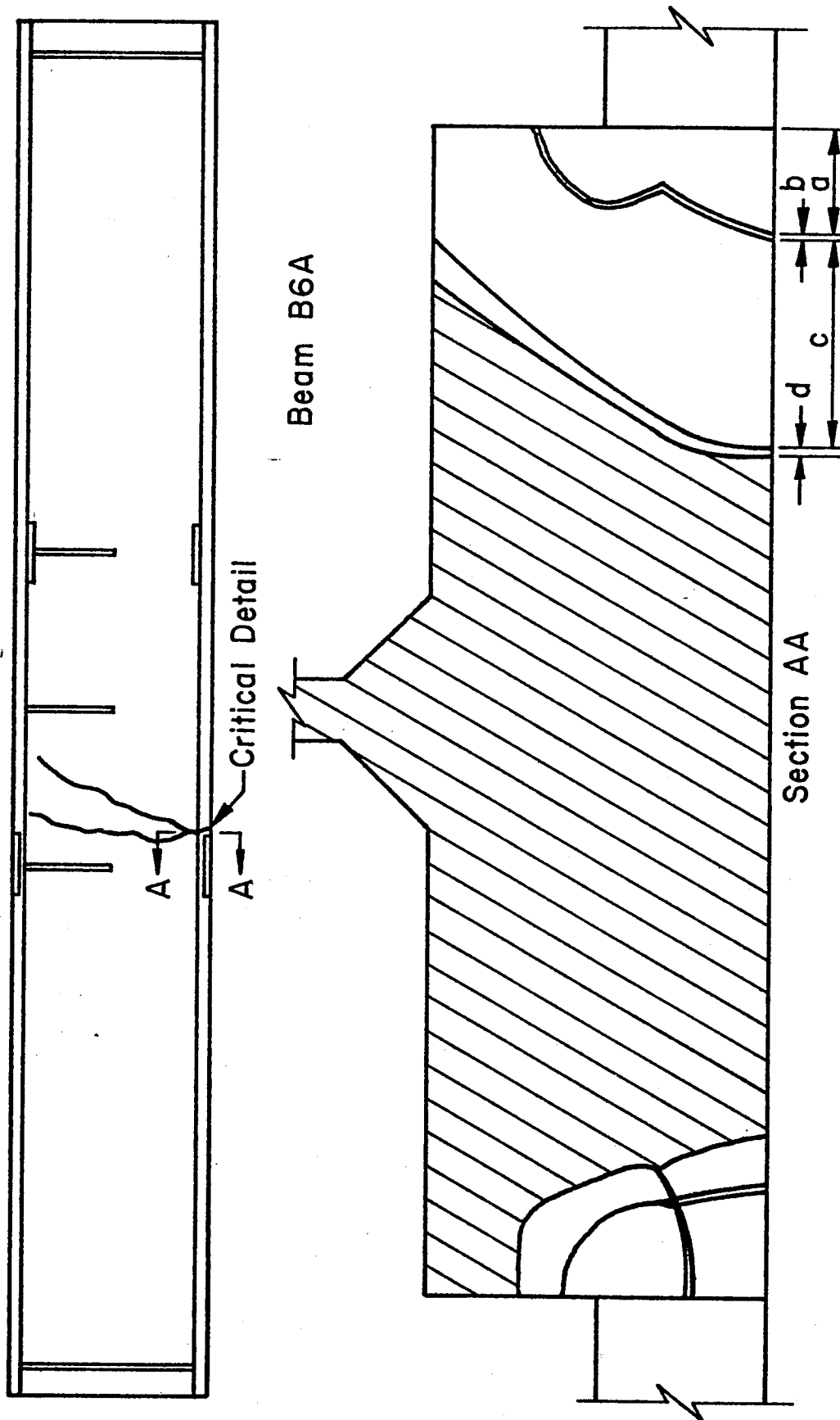
Fig. 4.6 Fatigue and Fracture Surface, B6A (A588)
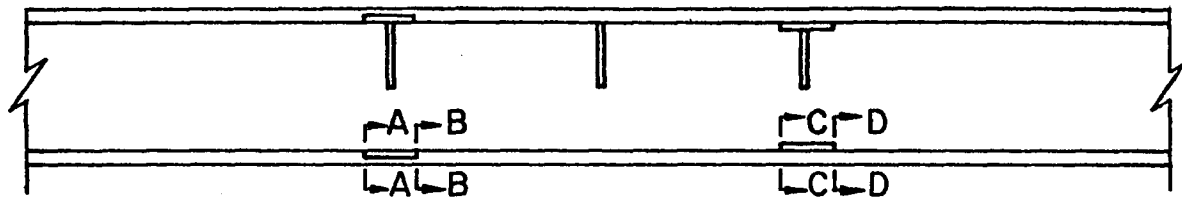
Beam	Section AA	Section BB	Section CC	Section DD
B2	✳ 5/8" — 3/8" — 1 1/4"	3/4" — 1" — 1/8"	2" 2" 3/4"	1 1/2" 1 3/4" 7/16"
B2A	1 1/4" — 7/8" — 7/16"	✳ 3/4" — 1 5/16" — 7/8"	2" 7/8"	1"
B4	✳ 1" — 1 13/32" — 1/2" — 1/2"	5/16" 1/2" — 7/8" — 1/4"	2 1/8" 1/4"	1/2" 2 1/4" 3/8"
B4A		✳ 1 1/4" 3/8"		
B6	3/8" — 7/8"	5/8" — 3/16"	2" 3/4" ✳	1 1/2"
B6A	1" — 1 3/16" 1/4" 3/8"	✳ 1 3/8" 1 1/4" 5/8" 3/4"	1"	

Table Scale 1 1/2"=1'-0"

✳ Beam Fractured At This Section

Fig. 4.7a   Fatigue Cracks at Two Million Cycles
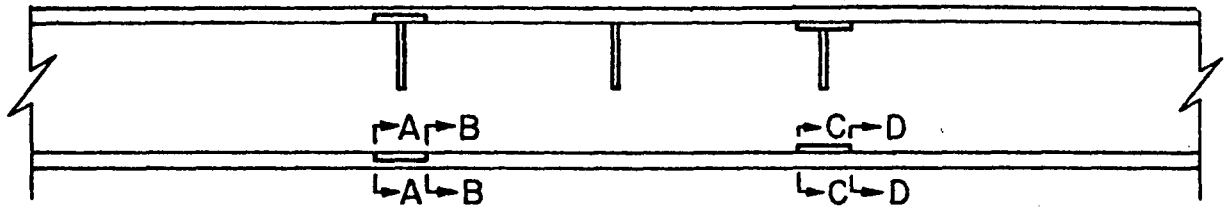
Beam	Section AA	Section BB	Section CC	Section DD
B2	✳ 15.9 / 31.8 ... 9.5	6.4 ... 25.4	50.8 50.8 ... 19.1	38.1 44.5 ... 11.1
B2A	31.8 ... 22.2	✳ 19.1 ... 33.3 / 22.2	50.8 ... 22.2	25.4
B4	✳ 25.4 ... 35.7 / 12.7 38.1	7.9 ... 22.2 / 12.7 6.4	54.0 ... 6.4	12.7 57.2 ... 9.5
B4A		✳ 31.8 / 9.5		
B6	9.5 ... 22.2	15.9 / 4.8	50.8 44.5	38.1
B6A	25.4 ... 30.2 / 6.4 9.5	✳ 34.9 ... 31.8 / 15.9 19.1	25.4	

✳ Beam Fractured At This Section
Crack Measurements In mm

Fig. 4.7b   Fatigue Cracks at Two Million Cycles

-142-

Beam	Section AA	Section BB	Section CC	Section DD
B2	✳ 5/8" 1 1/4" — 2.0 2.0	1/4" 1" 1/4" — 2.0 2.0	2" 2" 3/4" — 2.0 2.0	1 1/4" 1 3/4" 7/16" — 2.0 2.0
B2A	5/16" 5/8" 3/4" — 2.7 2.48	7/8" ✳ 13/16" 1 1/2" — 2.48 2.8	2 3/8" 1 3/16" — 2.8 2.8	1 1/4" — 2.8 2.8
B4	2" ✳ 1 1/8" 1/2" 2 3/4" — 2.37 2.37	1 1/2" 1" 3/4" 1/8" — 2.37 2.37	2 5/16" 3/8" — 2.37 2.37	1 7/8" 2 1/4" 3/8" — 2.37 2.37
B4A	1 1/4" 1 3/8" 3/8" 3/8" — 3.3 3.3	1/2" ✳ 3/8" 3" — 3.3 3.3	2" 1 1/4" 3/4" — 3.3 3.3	1 1/4" 5/8" 3/8" — 3.3 3.3
B6	3/8" 1 1/2" 5/8" — 2.7 2.92	1/8" 1/2" — 2.92 2.92	2" 2 1/2" ✳ 1 3/4" — 2.7 2.92	1 1/8" 1 3/4" — 2.7 2.7
B6A	1 1/8" 1 3/8" 1 1/2" 5/8" — 2.8 2.8	✳ 5/8" 1 3/8" 1 3/4" 1 3/8" — 2.8 2.8	1" 2 1/8" 1/4" — 2.8 2.8	2.8 2.8

Table Scale 1 1/2 = 1'-0"
Measurements Taken At Cycles Listed At Bottom
Of Cross Section (in millions of cycles)
✳ Beam Fractured At This Section

Fig. 4.8a Fatigue Cracks Prior to Last Fracture Test

-143-
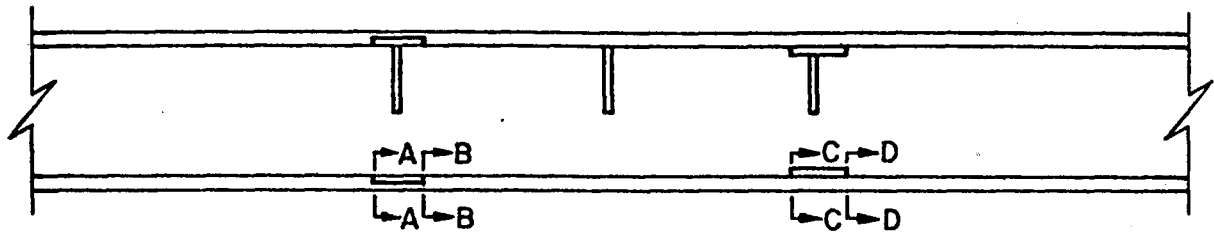
Beam	Section AA	Section BB	Section CC	Section DD
B2	✱ 15.9 / 31.8 / 2.0 2.0	6.4 25.4 / 2.0 2.0	50.8 50.8 19.1 / 2.0 2.0	31.8 44.5 11.1 / 2.0 2.0
B2A	7.9 / 19.1 15.9 / 2.7 2.48	22.2 ✱ / 20.6 38.1 / 2.48 2.8	60.3 30.2 / 2.8 2.8	31.8 / 2.8 2.8
B4	50.8 ✱ / 28.6 12.7 69.9 / 2.37 2.37	38.1 19.1 / 2.37 2.37	58.7 9.5 / 2.37 2.37	47.6 57.2 9.5 / 2.37 2.37
B4A	31.8 34.9 / 9.5 9.5 / 3.3 3.3	53.5 ✱ / 9.5 76.2 / 3.3 3.3	50.8 31.8 / 3.3 3.3	31.8 15.9 9.5 / 3.3 3.3
B6	9.5 38.1 12.7 / 2.7 2.92	28.6 12.7 / 2.92 2.92	50.8 63.5 ✱ 44.5 / 2.7 2.92	28.6 44.5 / 2.7 2.7
B6A	28.6 34.9 38.1 15.9 / 2.8 2.8	✱ 15.9 34.9 44.5 34.9 / 2.8 2.8	25.4 54.0 6.4 / 2.8 2.8	2.8 2.8

Measurements Taken At Cycles Listed At Bottom
Of Cross Section (In millions of cycles)
✱ Beam Fractured At This Section
Crack Measurements In mm

Fig. 4.8b Fatigue Cracks Prior to Last Fracture Test

-144-
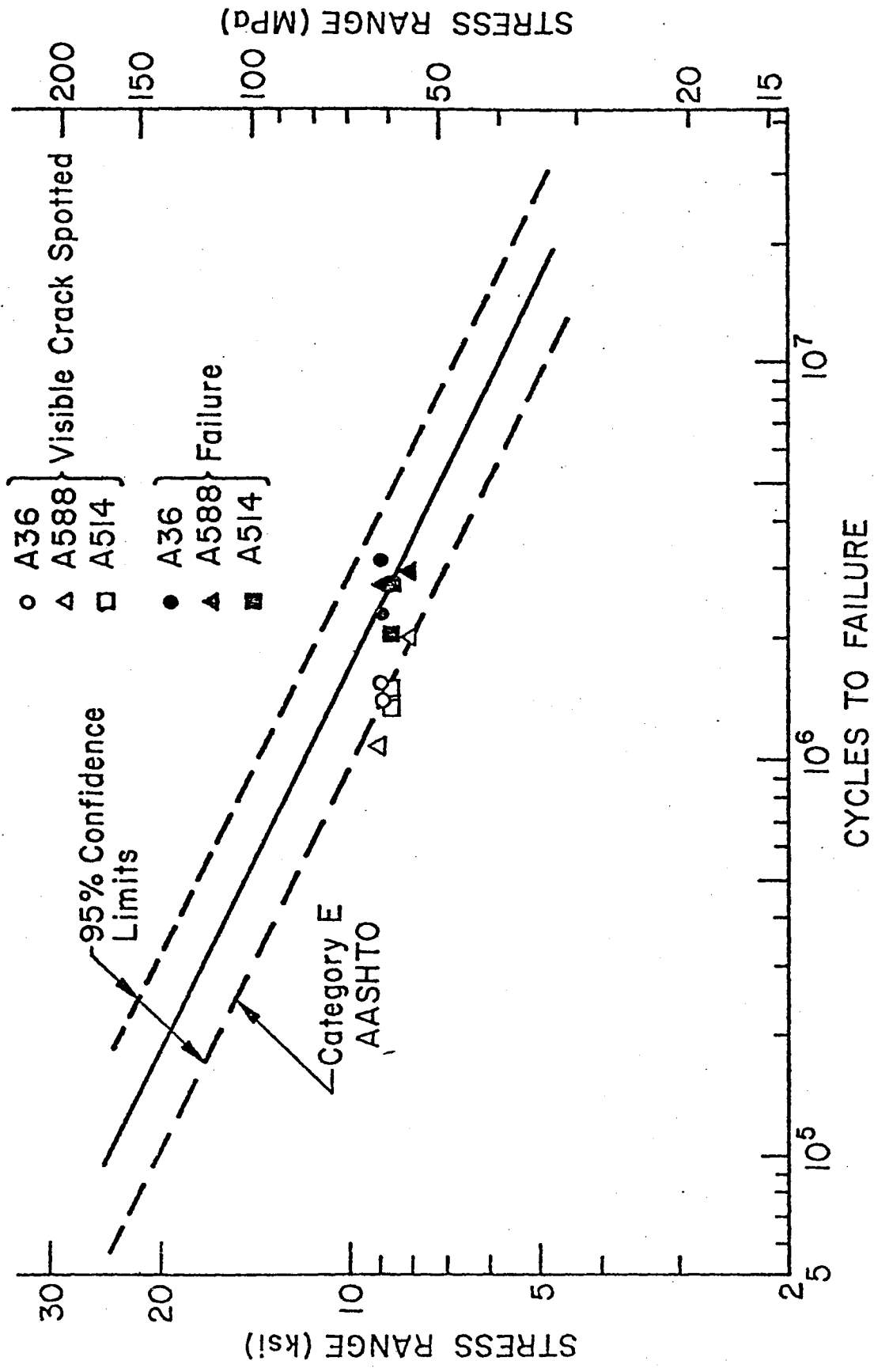
Fig. 4.9 Category E S-N Plot, Lateral Attachment Beams
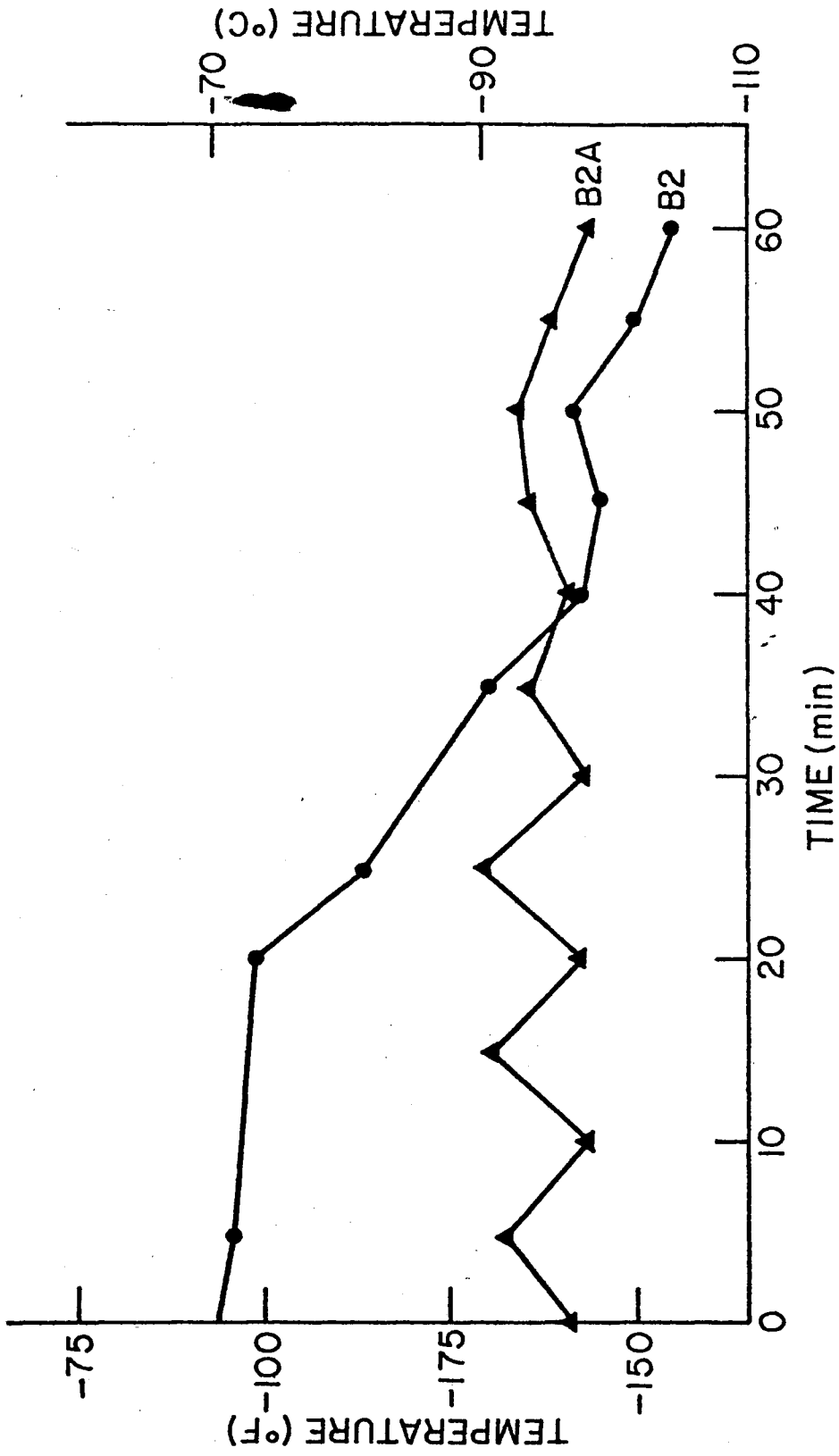
Fig. 4.10 Critical Detail Temperature/60 Minutes Prior to Fracture (A514)
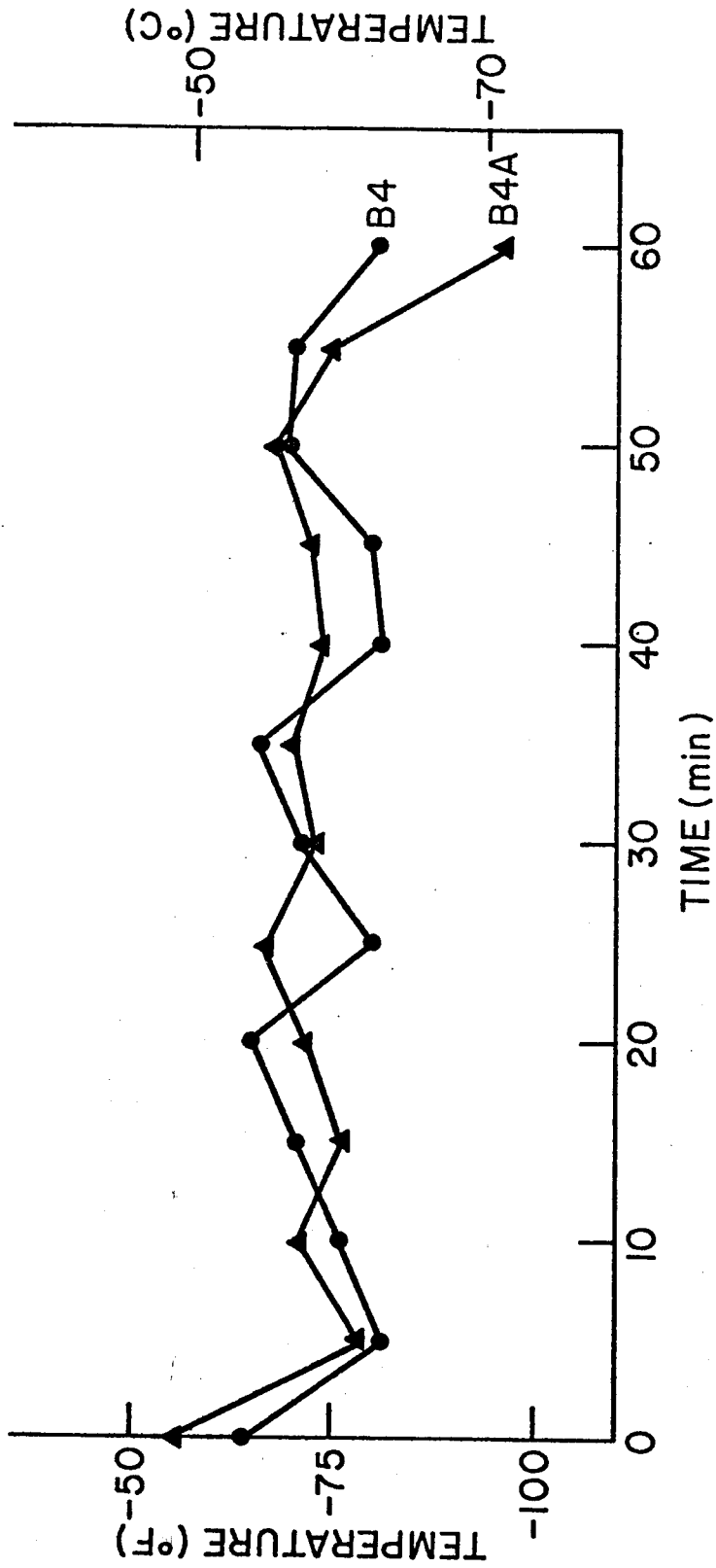
Fig. 4.11   Critical Detail Temperature/60 Minutes Prior to Fracture (A36)
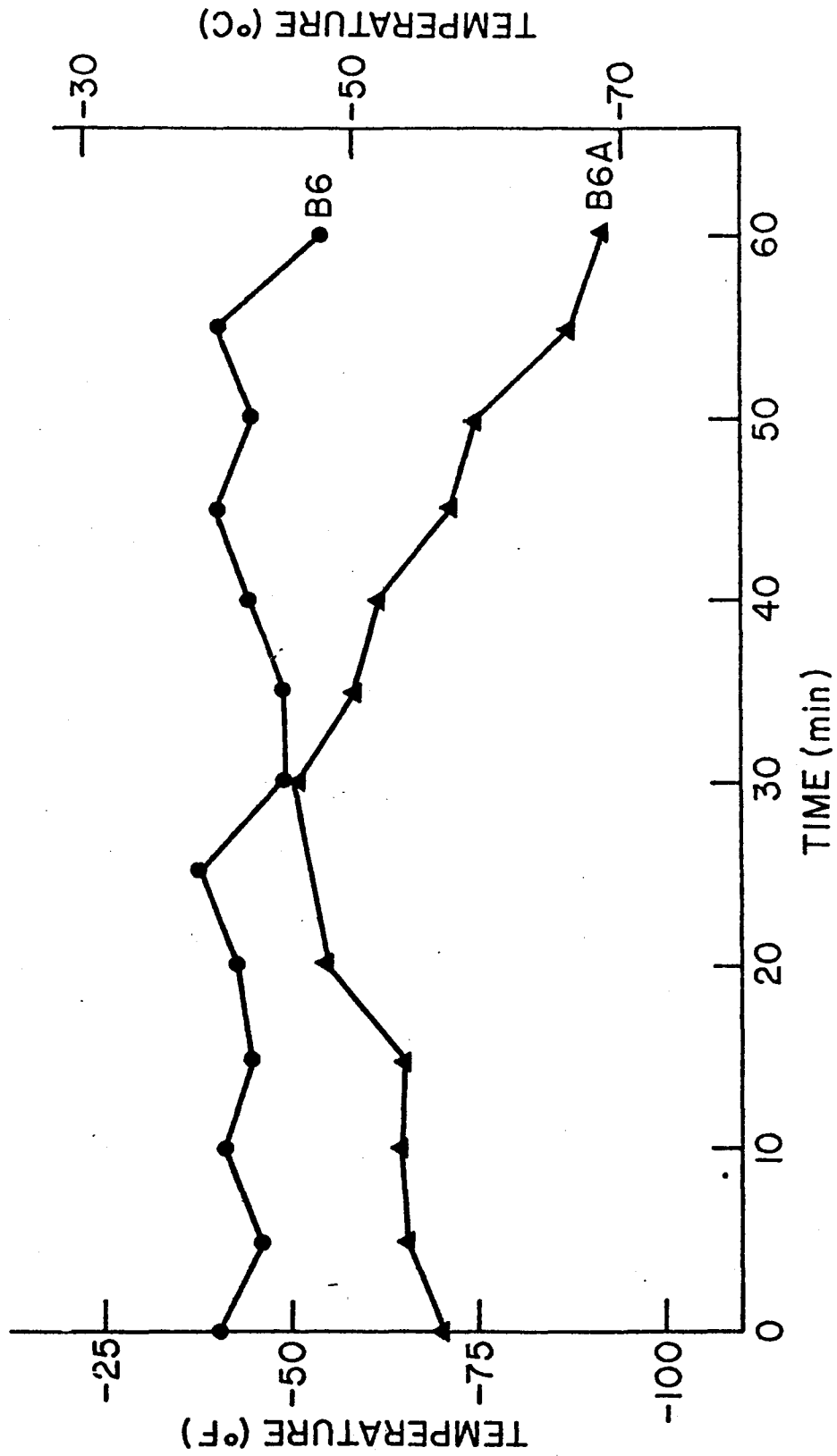
Fig. 4.12 Critical Detail Temperature/60 Minutes Prior to Fracture (A588)
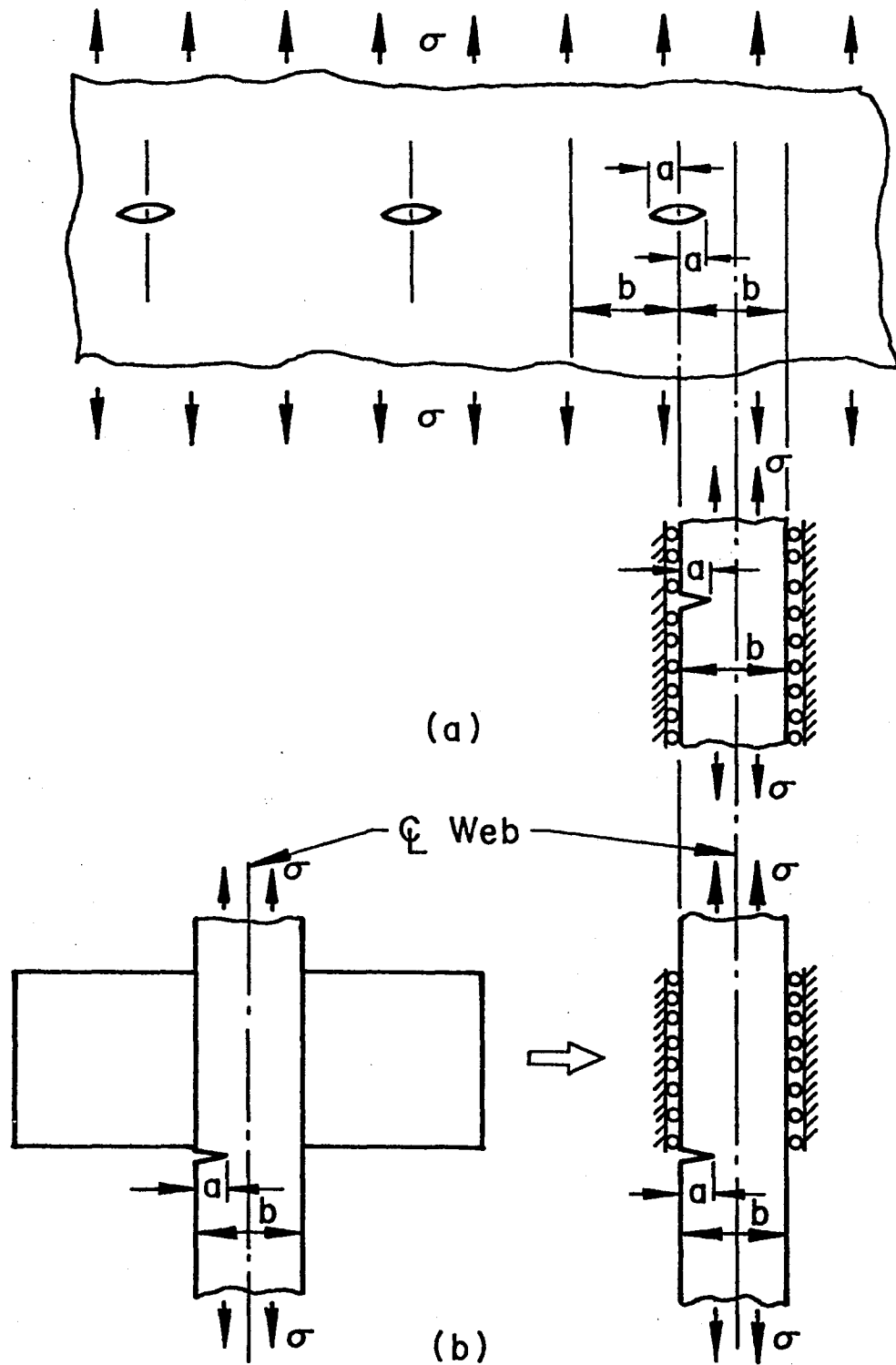
Fig. 4.13 Stress Intensity Model for Flange Edge Crack
For Applied Stress

Lateral Attachment

R 3/4"

Fracture Edge

(a)

Lateral
Attachment

45°

Flange

3/4" (19 mm)
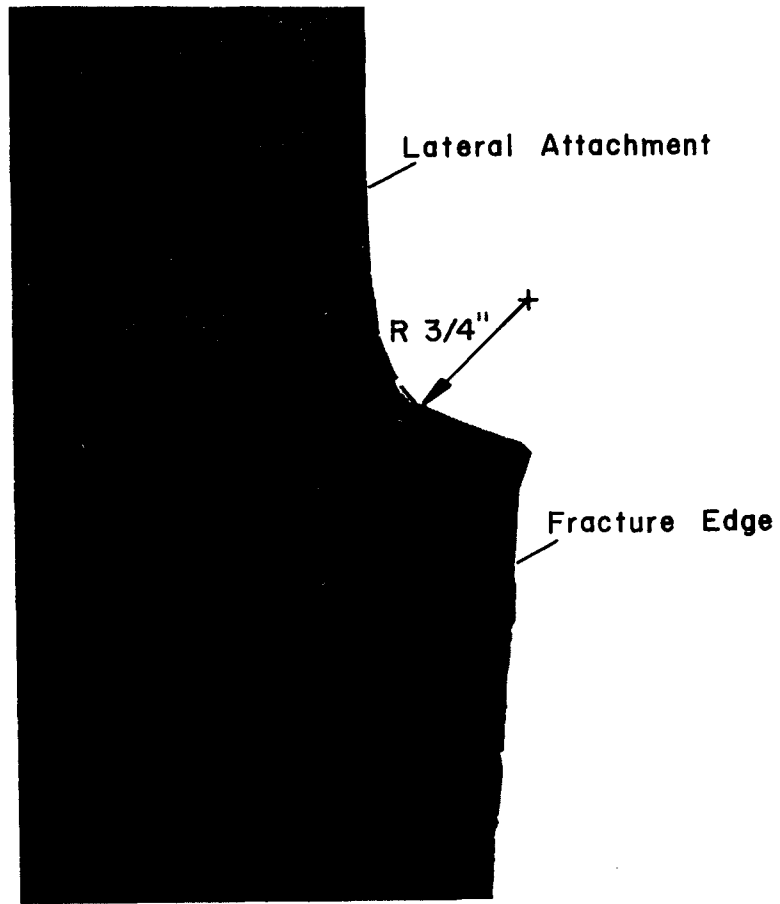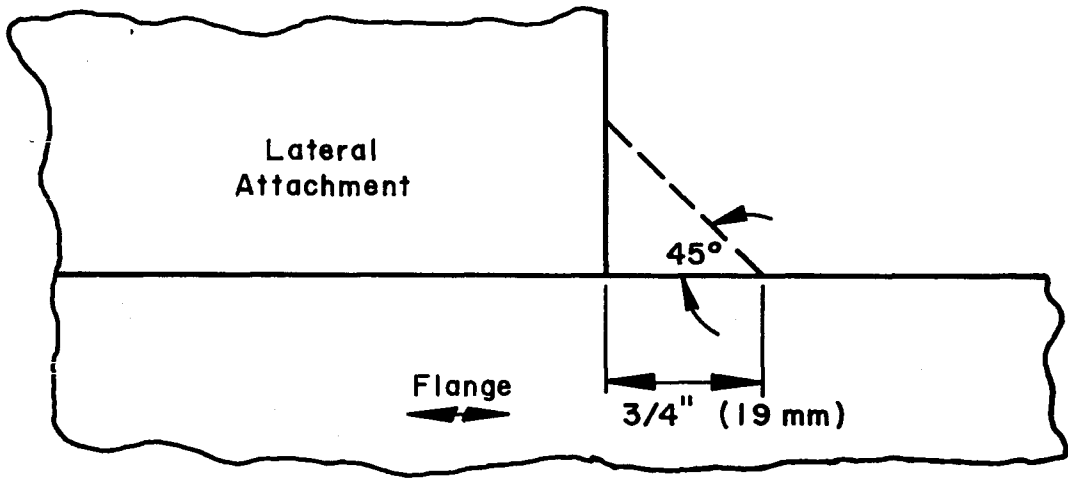
(b)

Fig. 4.14 Groove Weld Detail Reentrant Corners

-150-
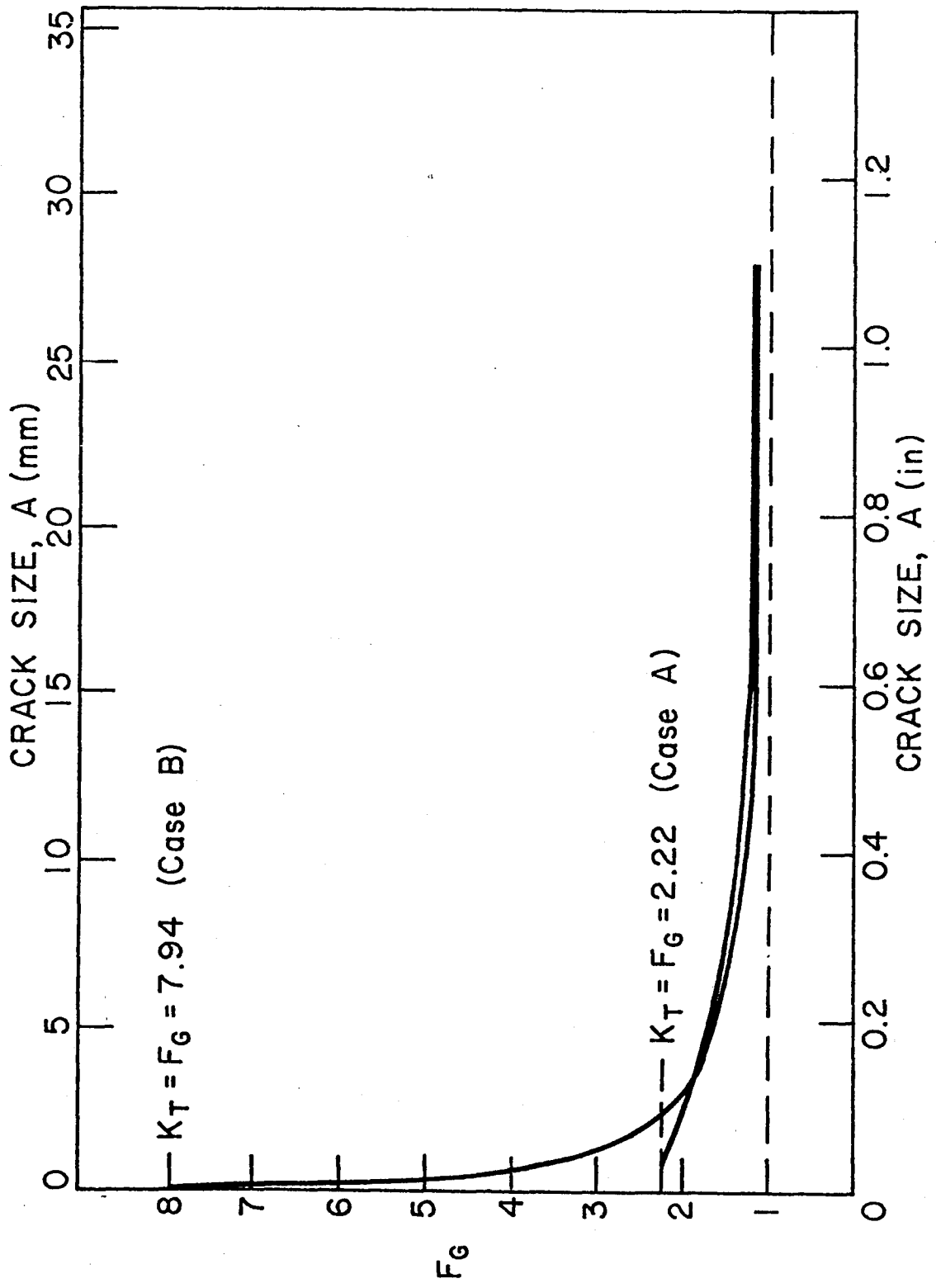
Fig. 4.15 Stress Concentration Decay With Crack Size (Beam B2A)
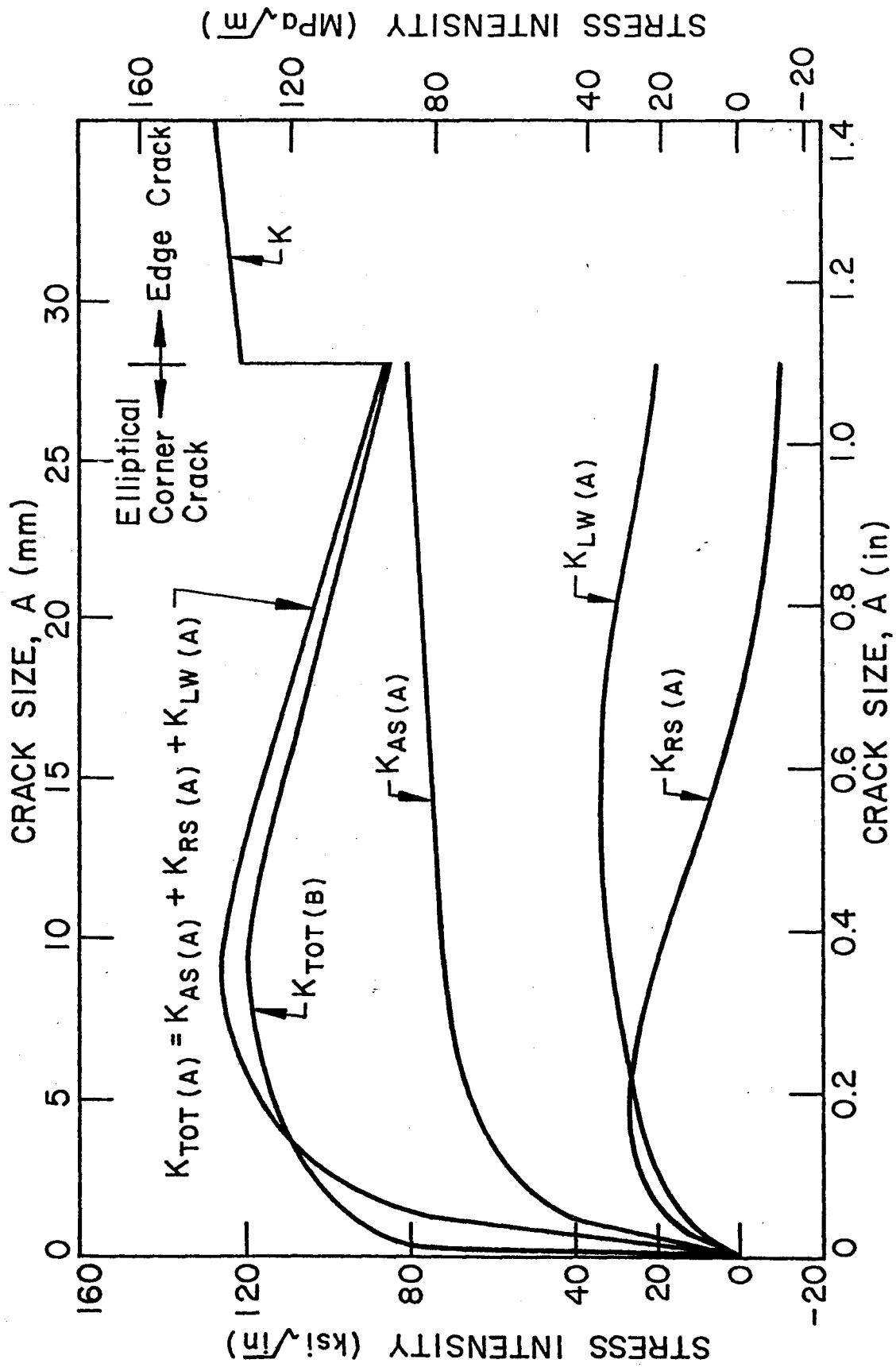
Fig. 4.16 Stress Intensity vs. Crack Size for Elliptical Corner Cracks (B2A, A514)
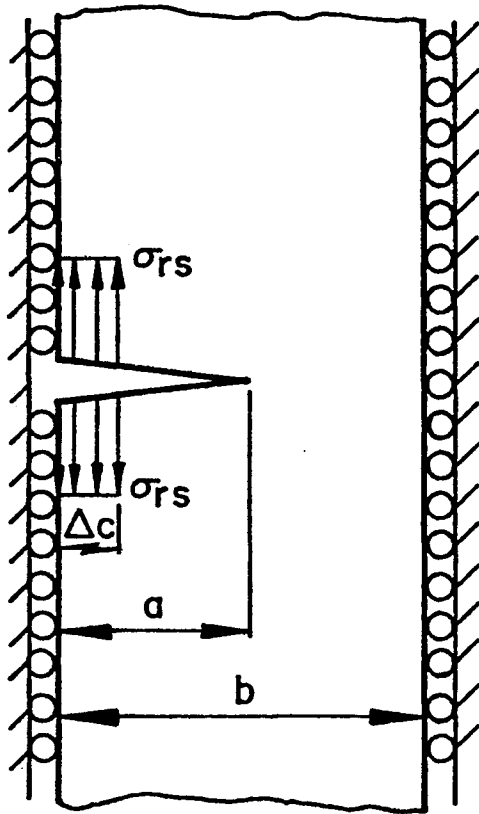
$$K_{RS} = 2/\pi \ \sigma_{rs}\sqrt{\pi a} \ F(a/b) \ F(c/a)$$

$$F(a/b) = \sqrt{\frac{2b}{\pi a} \ \tan \frac{\pi a}{2b}}$$

$$F(c/a) = \sin^{-1} \left(\frac{\sin \frac{\pi c}{2b}}{\sin \frac{\pi a}{2b}} \right)$$

$$\Delta c = 0.02"$$

Fig. 4.17 Superposition Model for Residual Stress
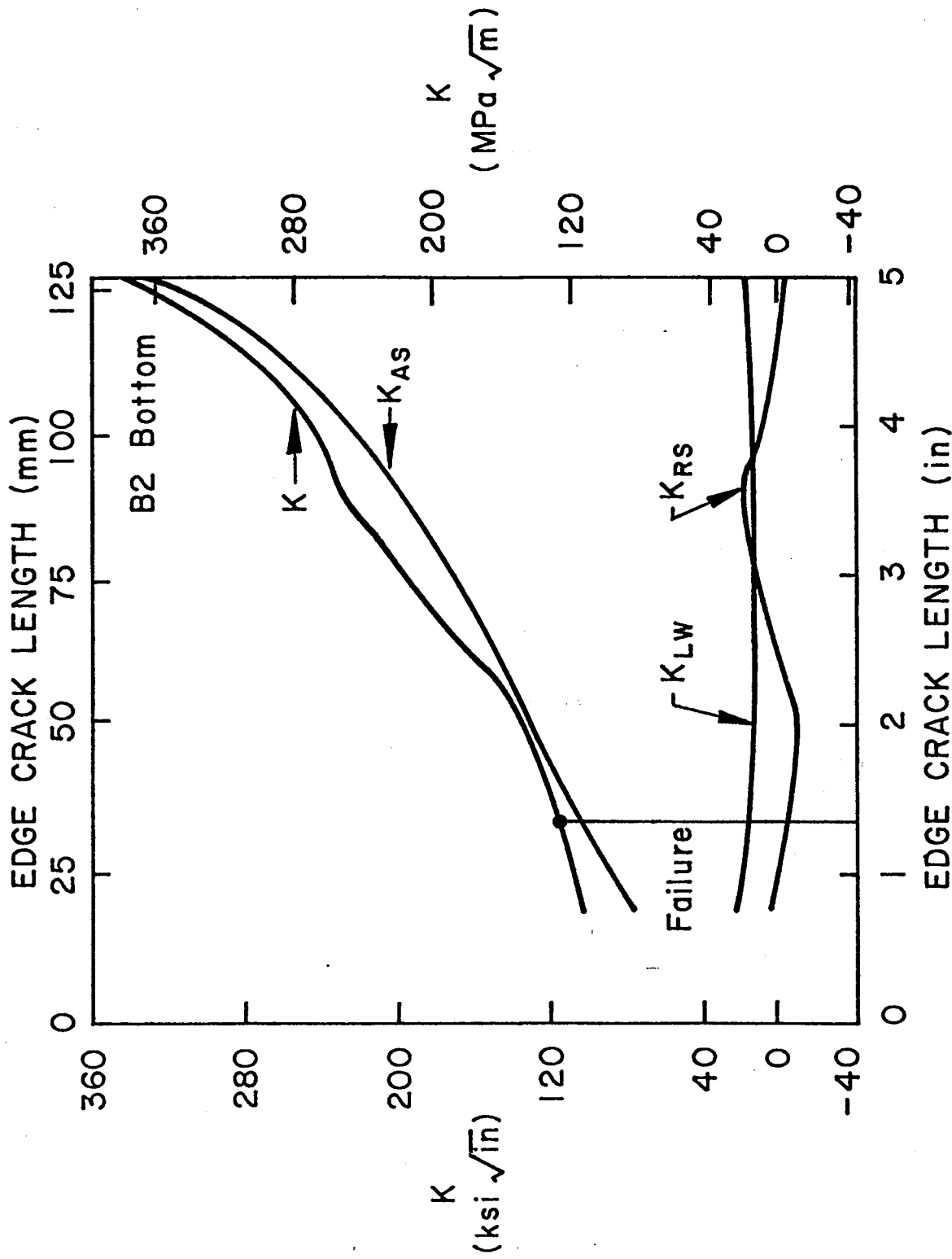
Fig. 4.18 K vs. Edge Crack Size (B2, A514)
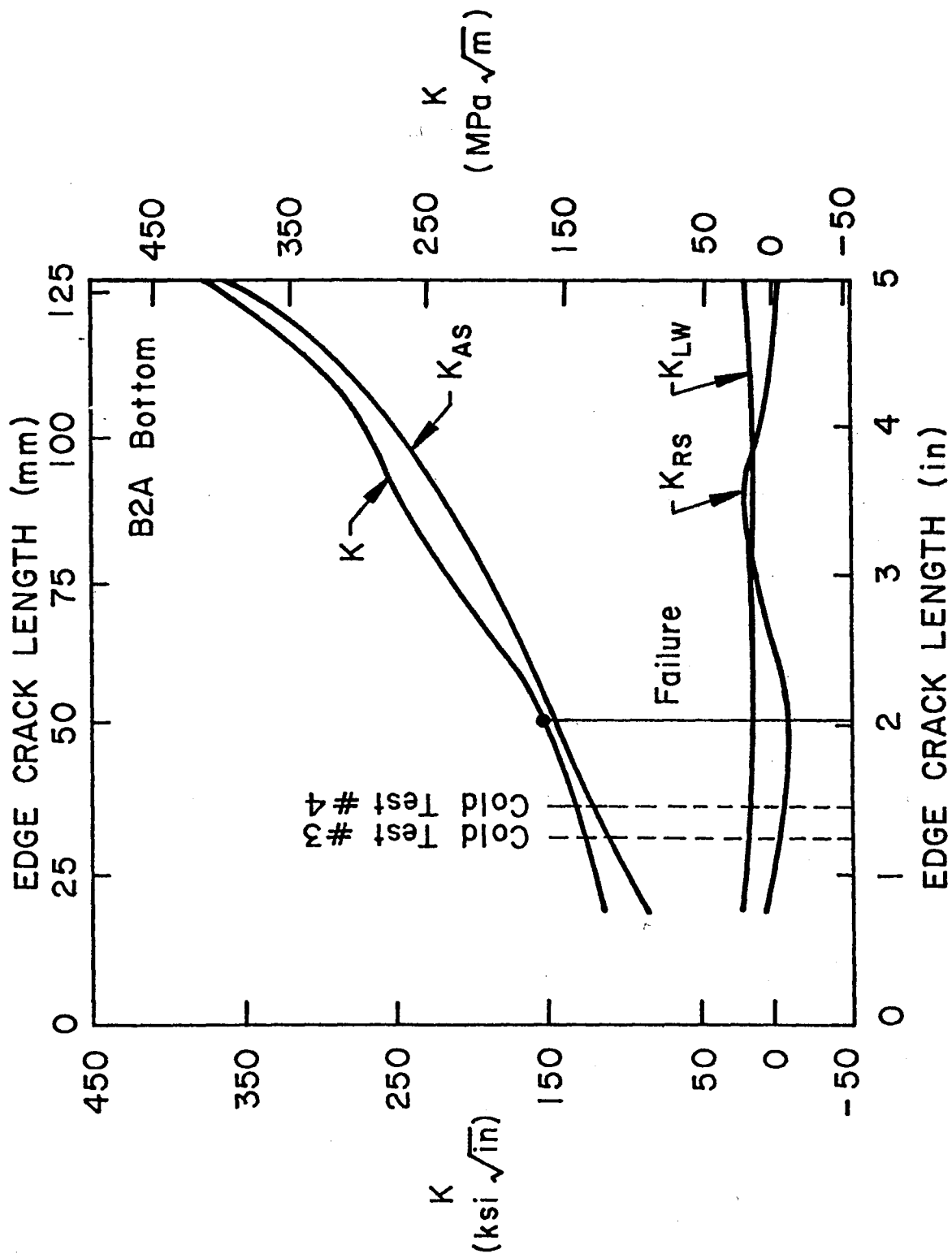
Fig. 4.19 K vs. Edge Crack Size (B2A, A514)
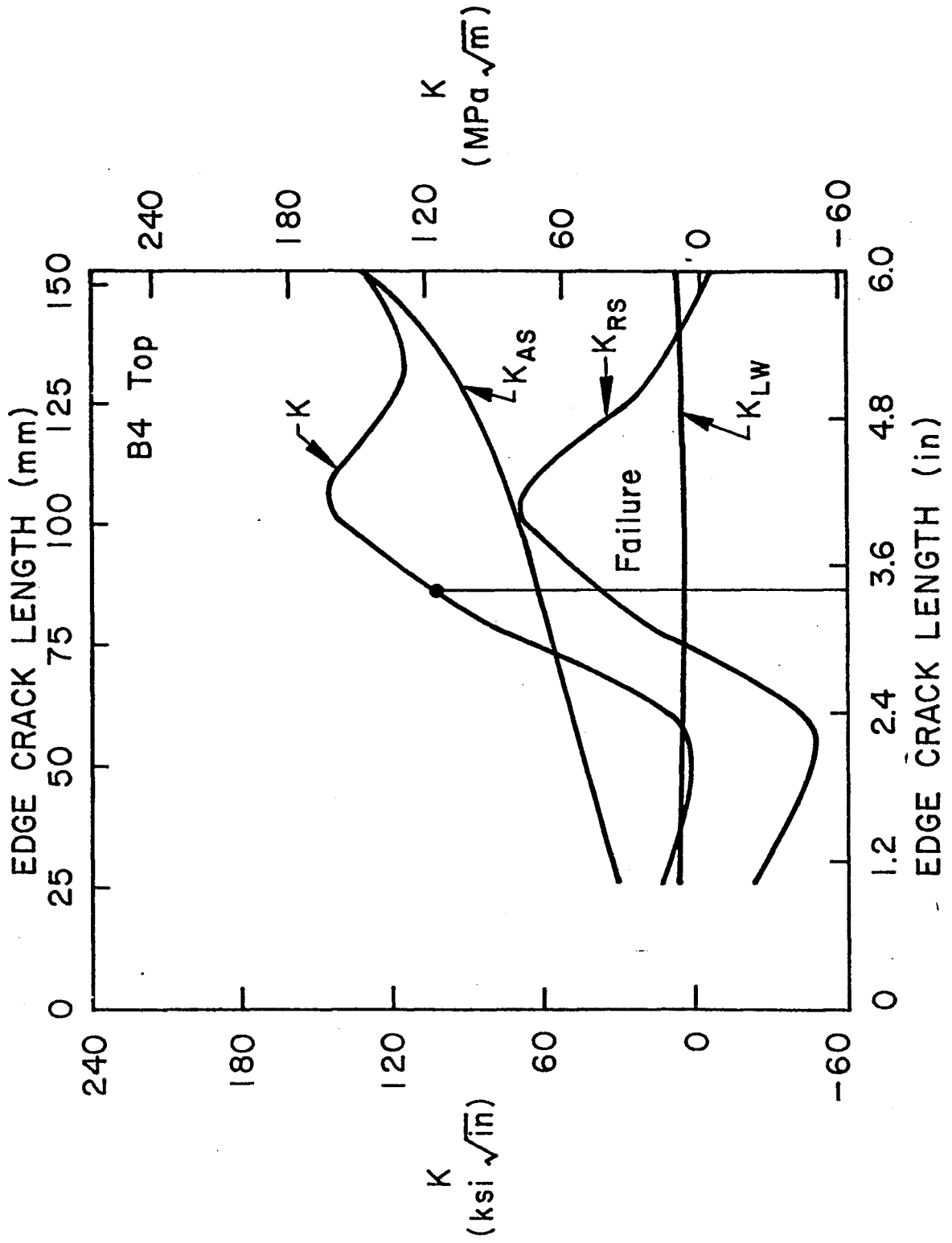
Fig. 4.20 K vs. Edge Crack Size (B4, A36)
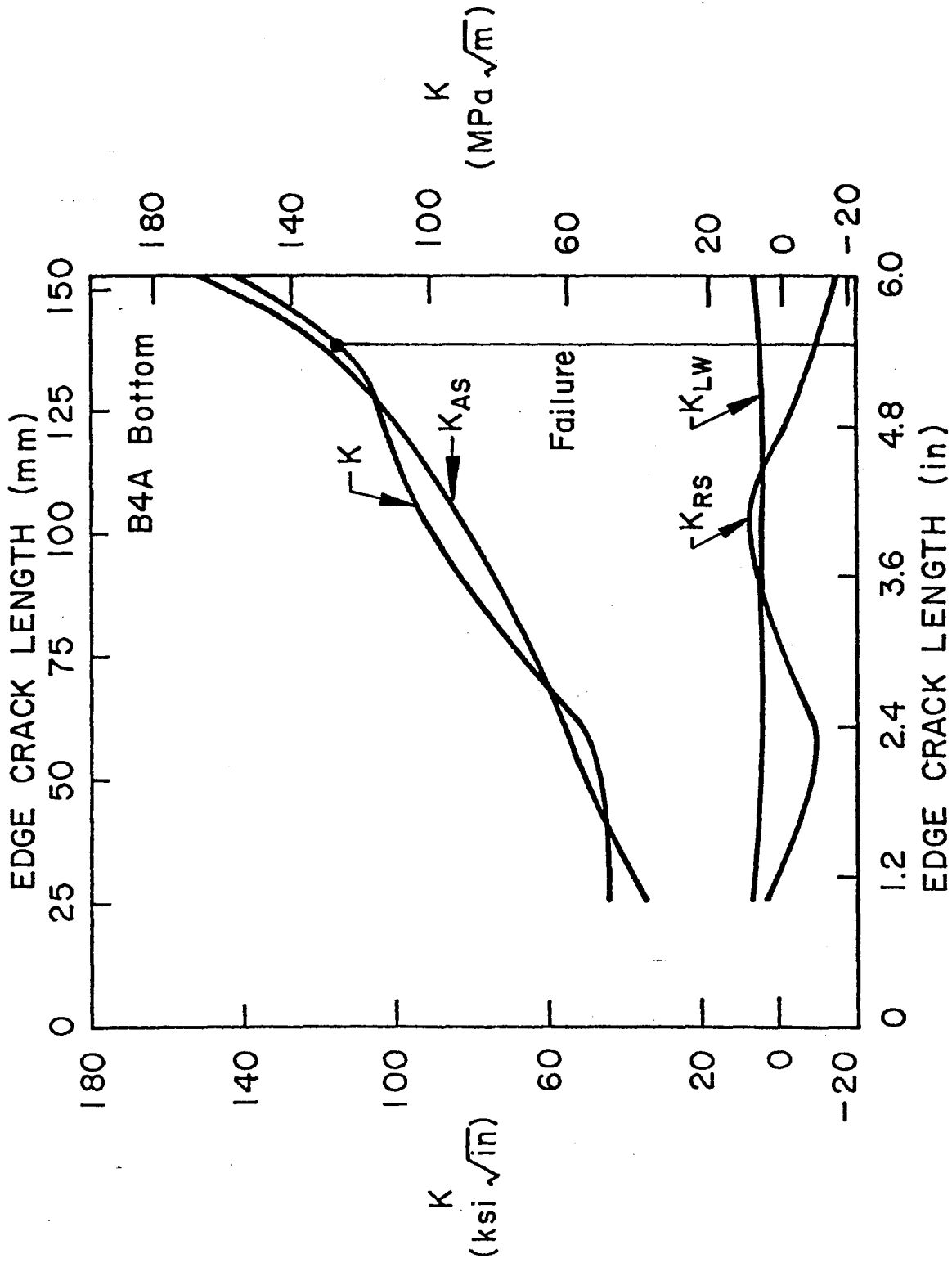
Fig. 4.21 K vs. Edge Crack Size (B4A, A36)
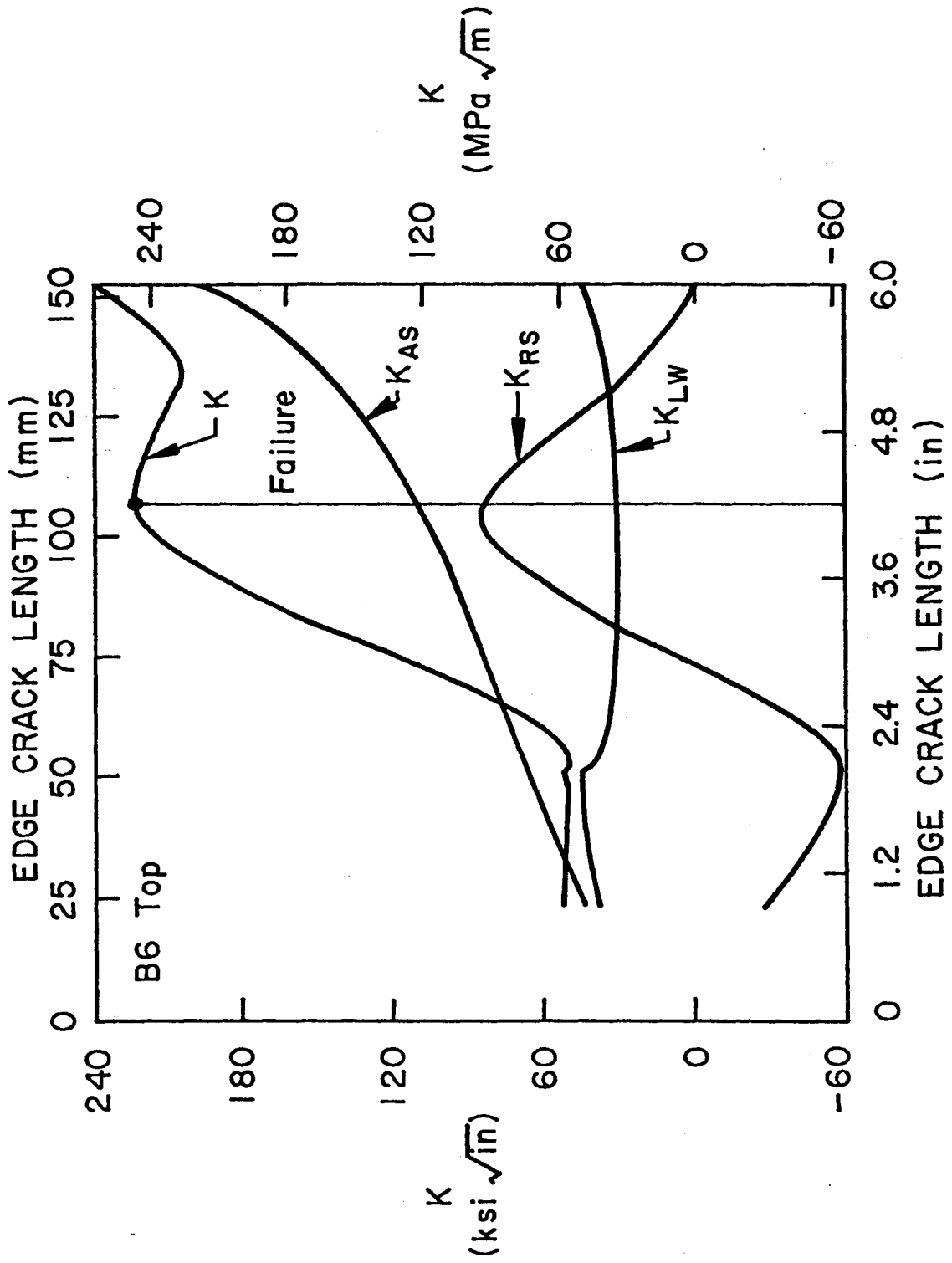
Fig. 4.22 K vs. Edge Crack Size (B6, A588)
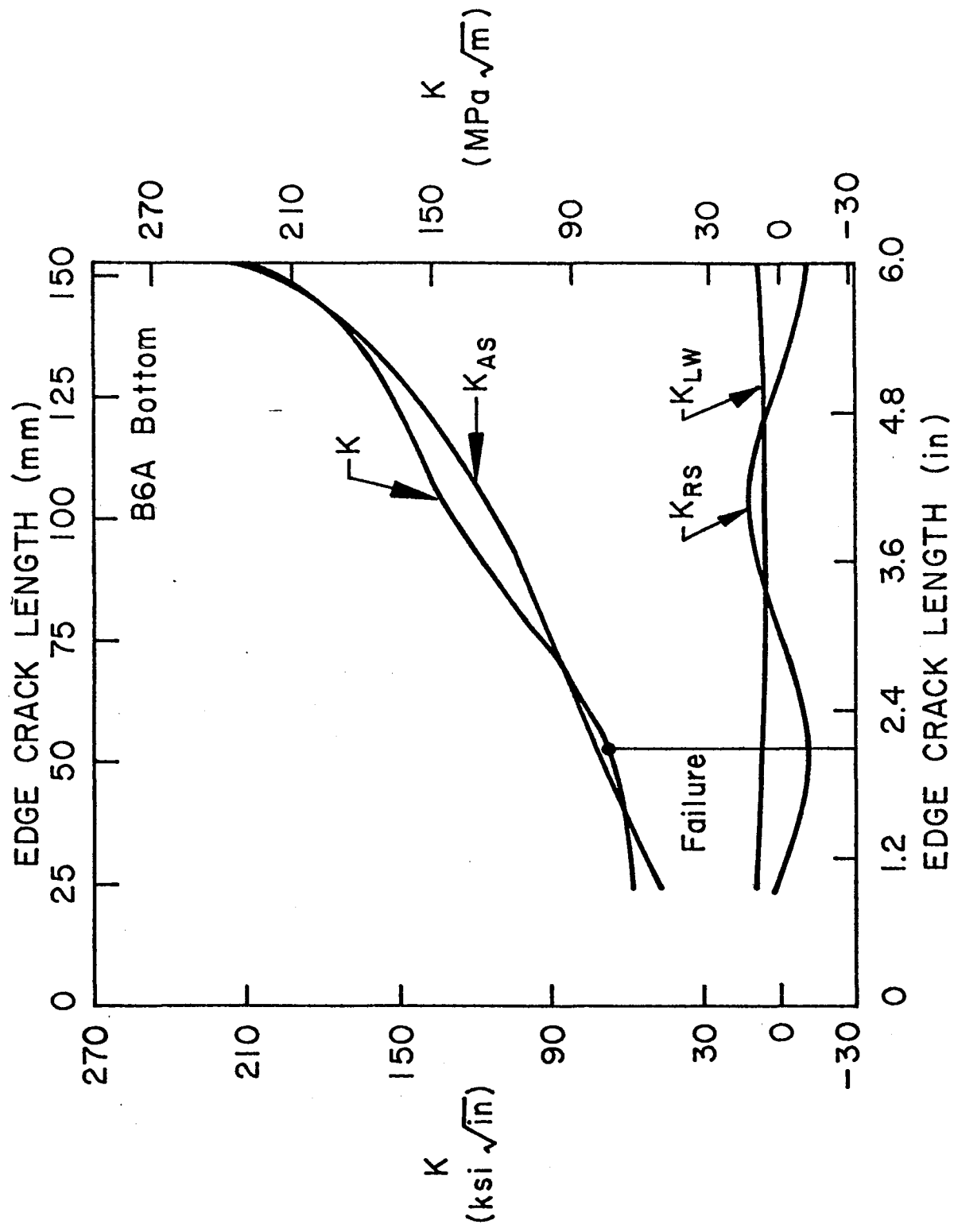
Fig. 4.23 K vs. Edge Crack Size (B6A, A588)

σ_{max}	= 49.2 ksi	= 344 MPa	
σ_{yd}	= 155.6 ksi	= 1087 MPa	
a	= 1.21 in	= 31 mm	
r_y	= 0.09 in	= 2.3 mm	
T_c	= −155°F	= −104°C	
K_c	= 114 ksi $\sqrt{in}$	= 125 MPa $\sqrt{m}$	
N	= 2,024,100		

B2 (A514)

σ_{max}	= 54.2 ksi	= 379 MPa	
σ_{yd}	= 153.5 ksi	= 1072 MPa	
a	= 1.79 in	= 45 mm	
r_y	= 0.14 in	= 3.6 mm	
T_c	= −144°F	= −98°C	
K_c	= 145 ksi $\sqrt{in}$	= 160 MPa $\sqrt{m}$	
N	= 2,865,700		

B2A (A514)

σ_{max}	= 16.8 ksi	= 117 MPa	
σ_{yd}	= 65.5 ksi	= 458 MPa	
a	= 3.02 in	= 77 mm	
r_y	= 0.41 in	= 10.4 mm	
T_c	= −80°F	= −62°C	
K_c	= 105 ksi $\sqrt{in}$	= 116 MPa $\sqrt{m}$	
N	= 2,369,700		

B4 (A36)

σ_{max}	= 19.4 ksi	= 136 MPa	
σ_{yd}	= 67.7 ksi	= 473 MPa	
a	= 4.98 in	= 125 mm	
r_y	= 0.47 in	= 11.9 mm	
T_c	= −96°F	= −71°C	
K_c	= 116 ksi $\sqrt{in}$	= 128 MPa $\sqrt{m}$	
N	= 3,276,750		

B4A (A36)

σ_{max}	= 25.0 ksi	= 175 MPa	
σ_{yd}	= 79.3 ksi	= 554 MPa	
a	= 2.93 in	= 74 mm	
r_y	= 1.27 in	= 32 mm	
T_c	= −53°F	= −47°C	
K_c	= 223 ksi $\sqrt{in}$	= 245 MPa $\sqrt{m}$	
N	= 2,954,700		

B6 (A588)

σ_{max}	= 27.0 ksi	= 189 MPa	
σ_{yd}	= 84.1 ksi	= 587 MPa	
a	= 1.89 in	= 48 mm	
r_y	= 0.10 in	= 2.5 mm	
T_c	= −92°F	= −69°C	
K_c	= 66 ksi $\sqrt{in}$	= 73 MPa $\sqrt{m}$	
N	= 2,822,500		

B6A (A588)

Fig. 4.24 Fracture Surface Sketches and Data Summary
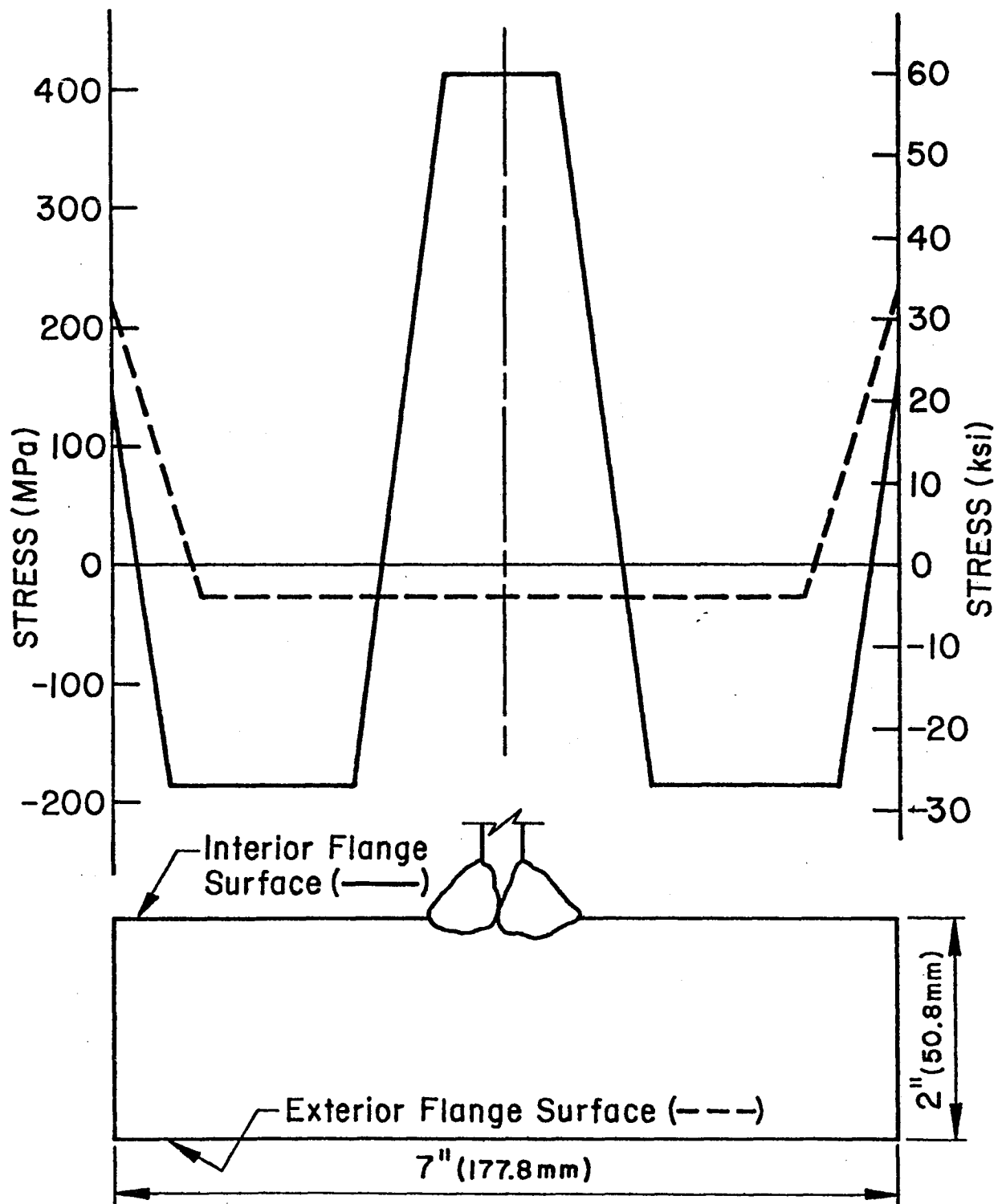
Fig. 4.25a Estimated Residual Stress Distribution for A36 Flange
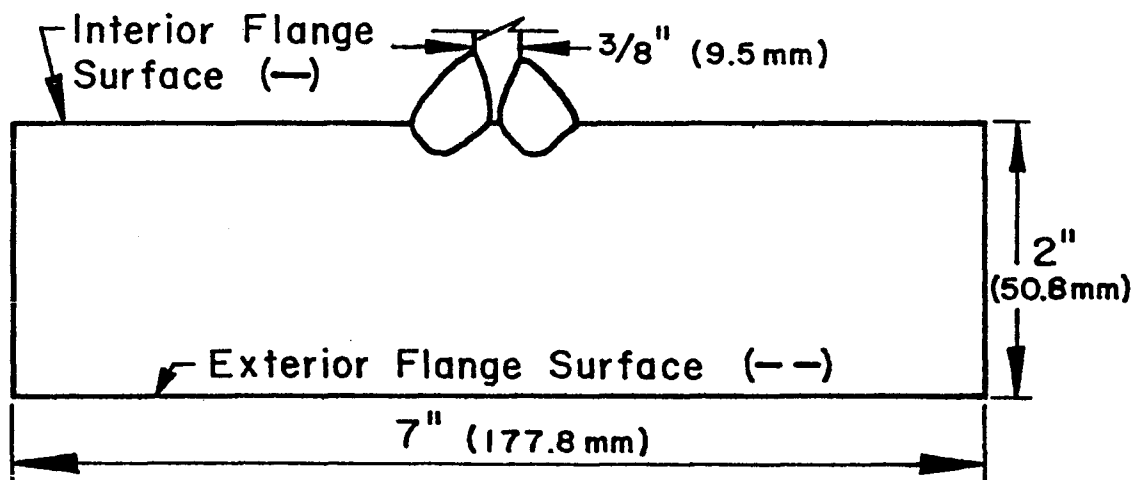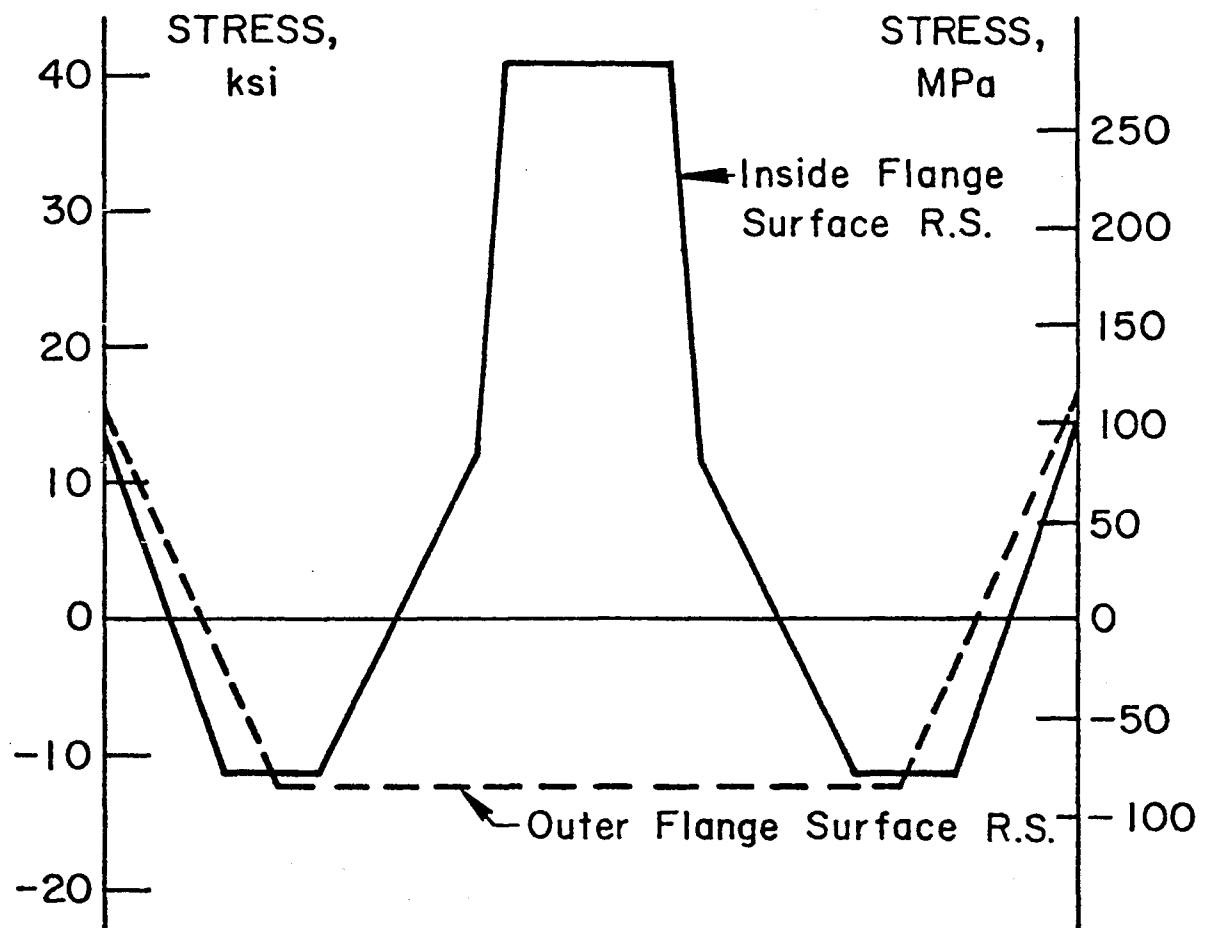
Fig. 4.25b Measured Residual Stress Distribution for A36 Flange
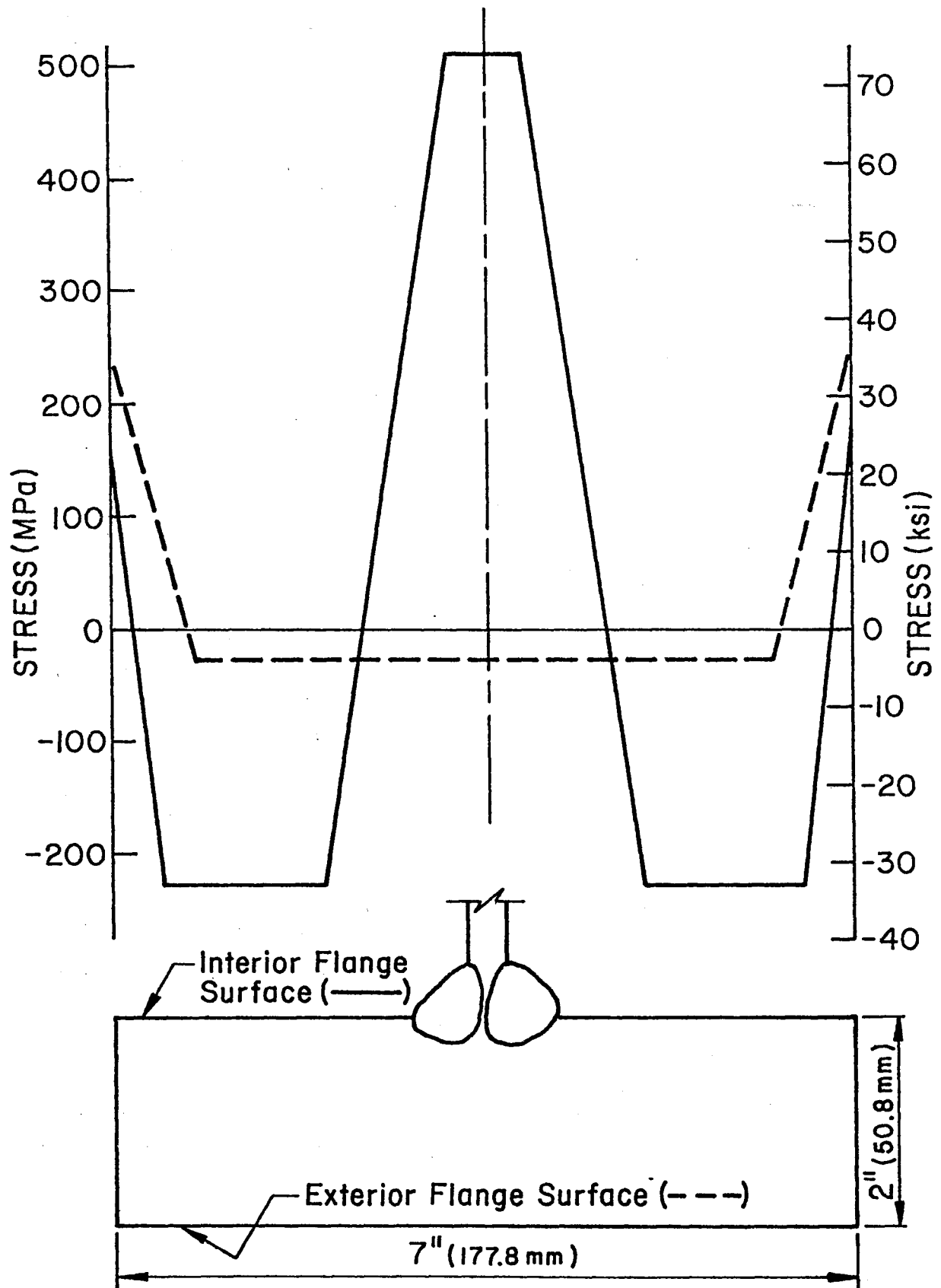
Fig. 4.26a Estimated Residual Stress Distribution for A588 Flange
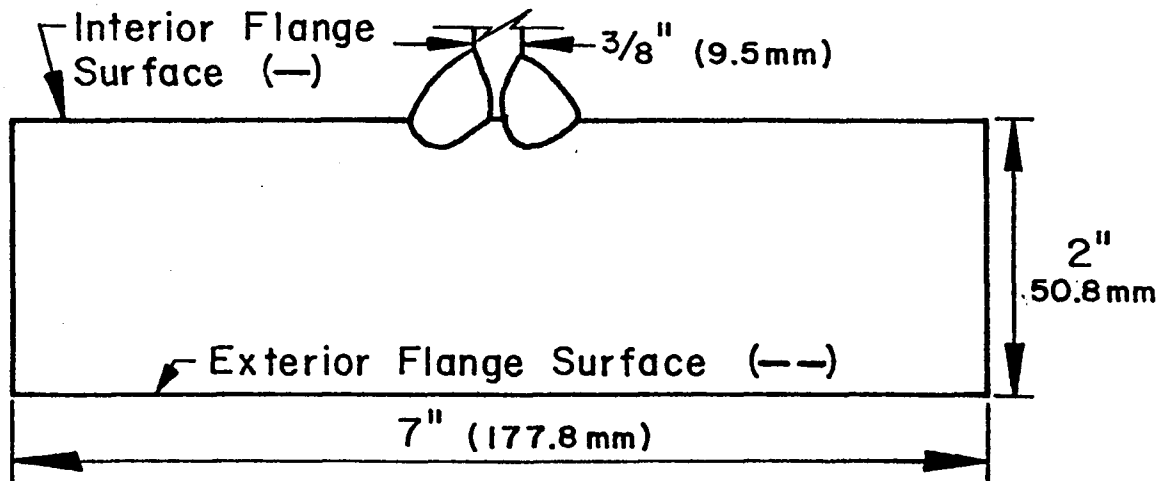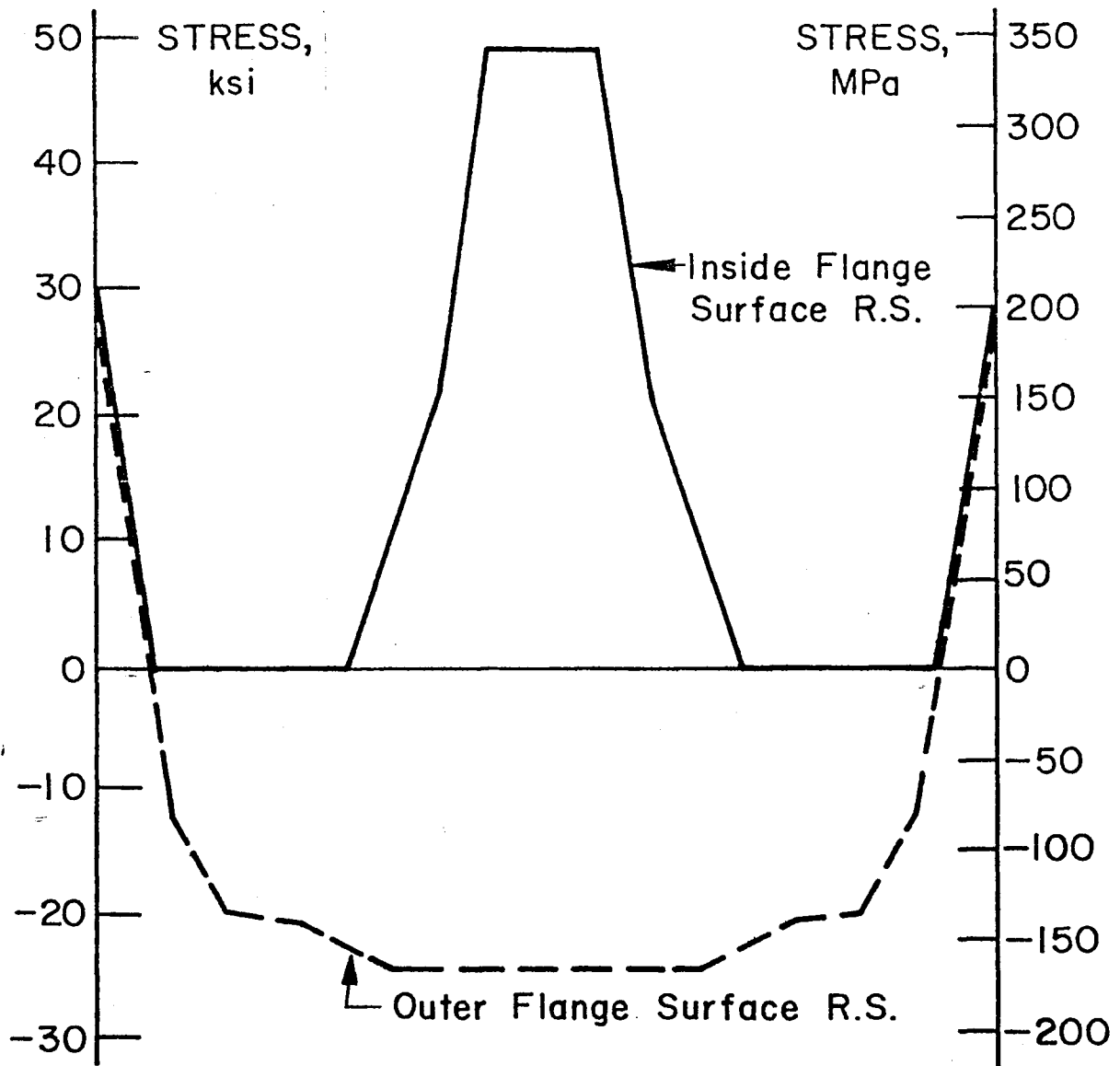
Fig. 4.26b   Measured Residual Stress Distribution for A588 Flange

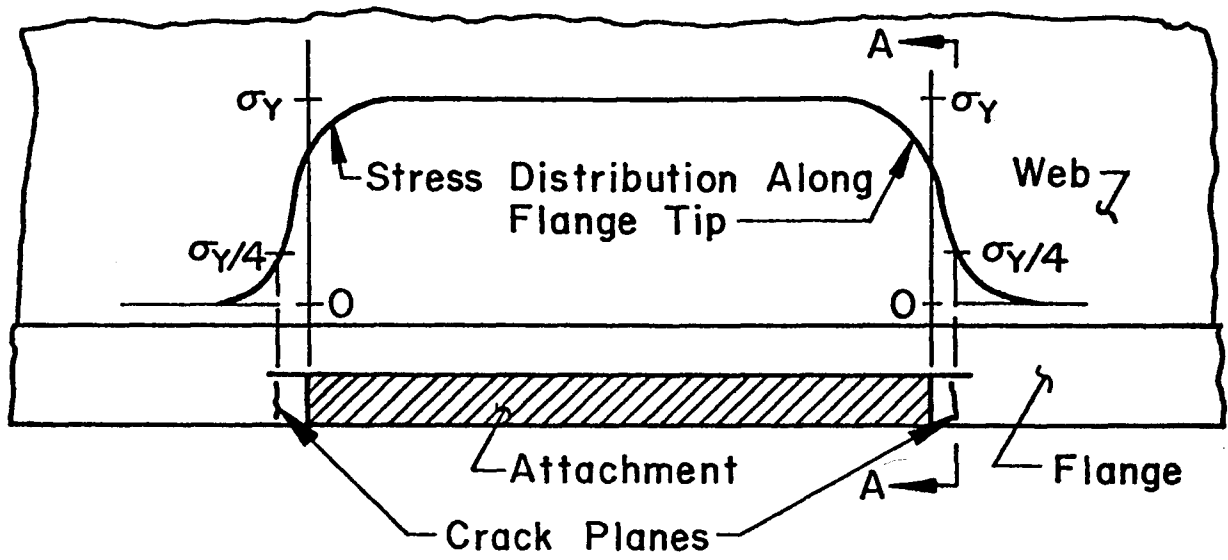-164-
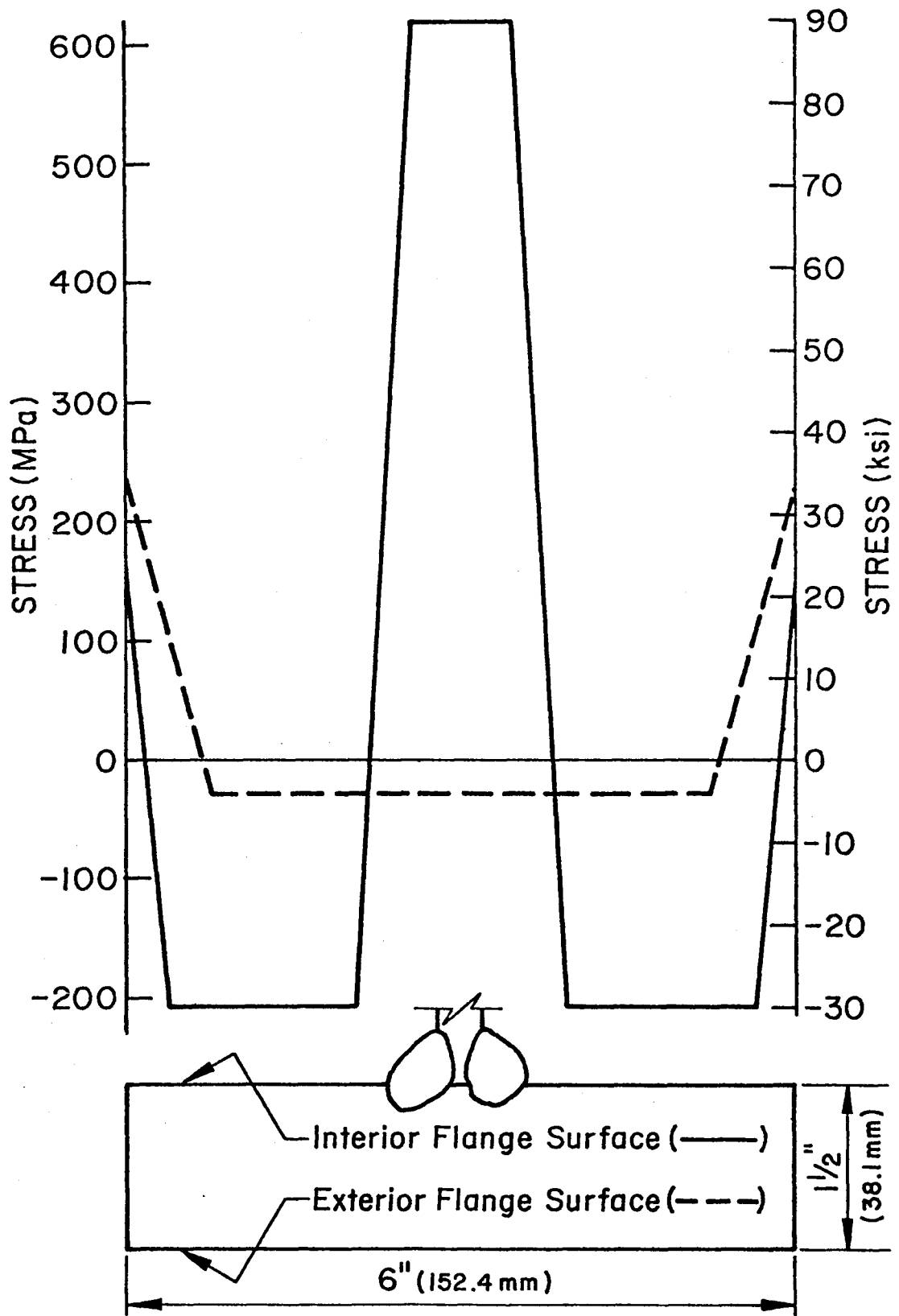
Fig. 4.27a Estimated Residual Stress Distribution for A514 Flange
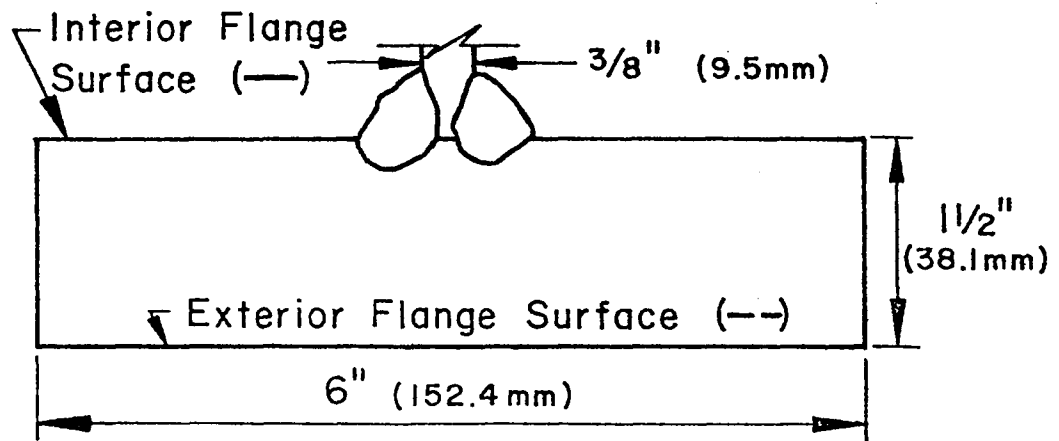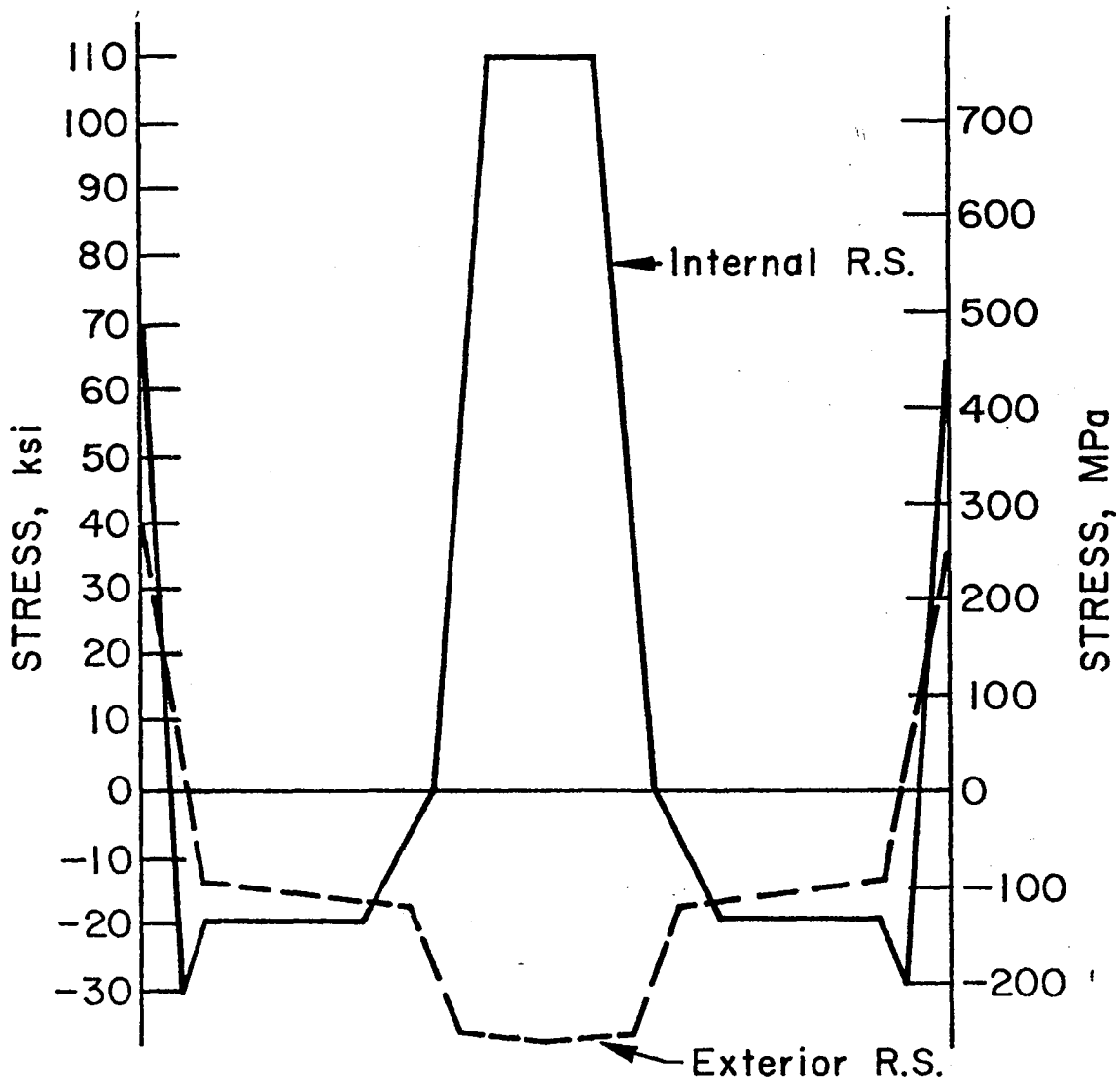
Fig. 4.27b   Measured Residual Stress Distribution for A514 Flange
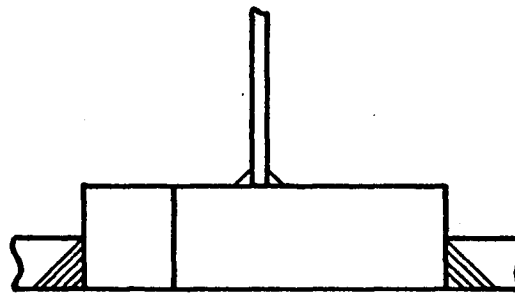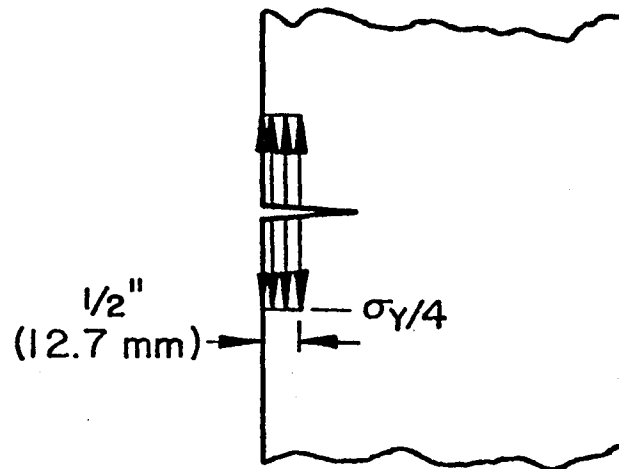
Fig. 4.28 Assumed Residual Stress Distribution Along
Flange Tip for Groove Weld Lateral Attachment
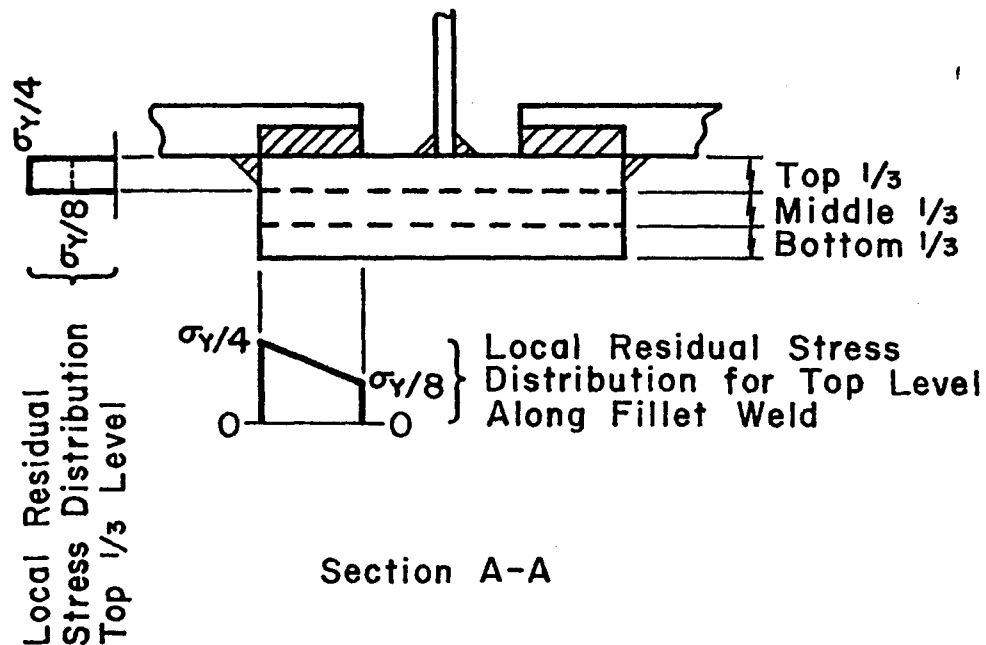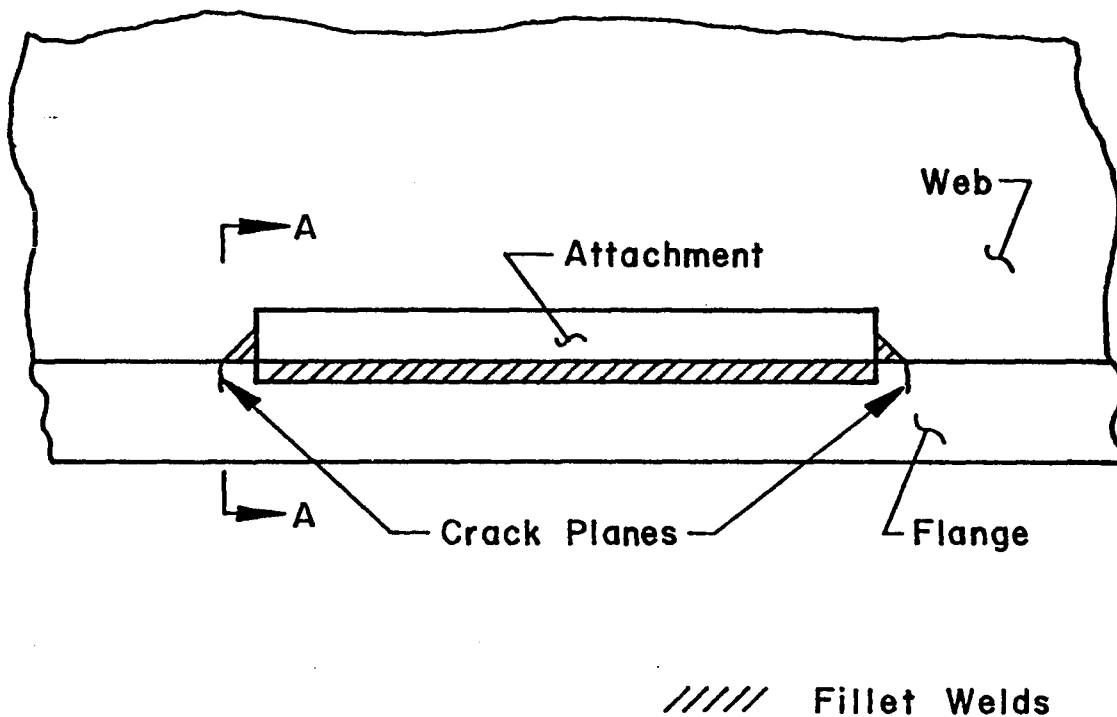
//// Fillet Welds

Fig. 4.29 Assumed Local Residual Stress Distribution
for Fillet Weld Lateral Attachment

Critical Detail

Beam B1

b

a

a
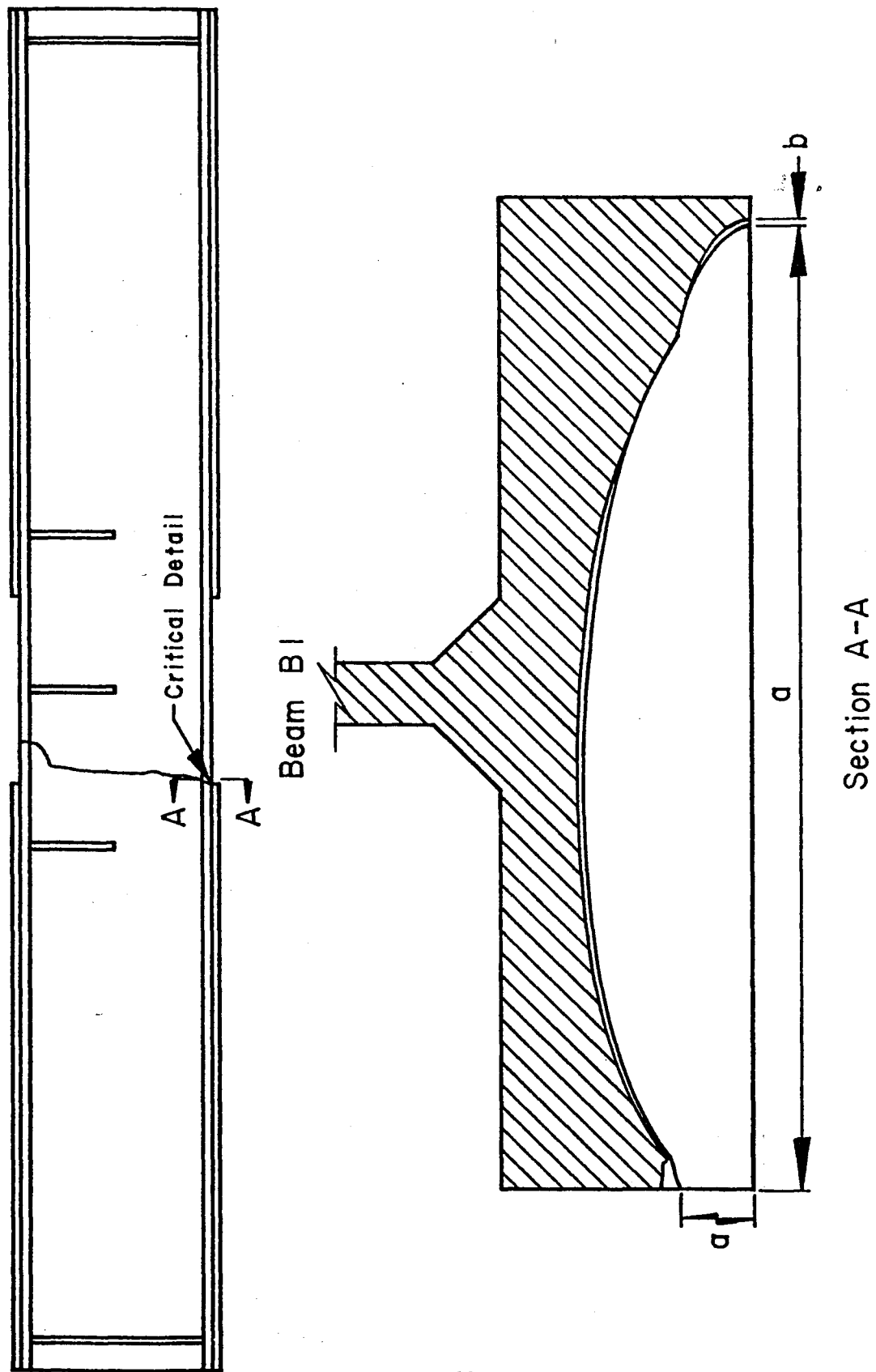
Section A-A

Fig. 5.1 Fatigue and Fracture Surface, B1 (A514)

Fig. 5.2 Fatigue and Fracture Surface, B1A (A514)

Critical Detail

A

A

Beam B3

Section A-A

a

b

c

d
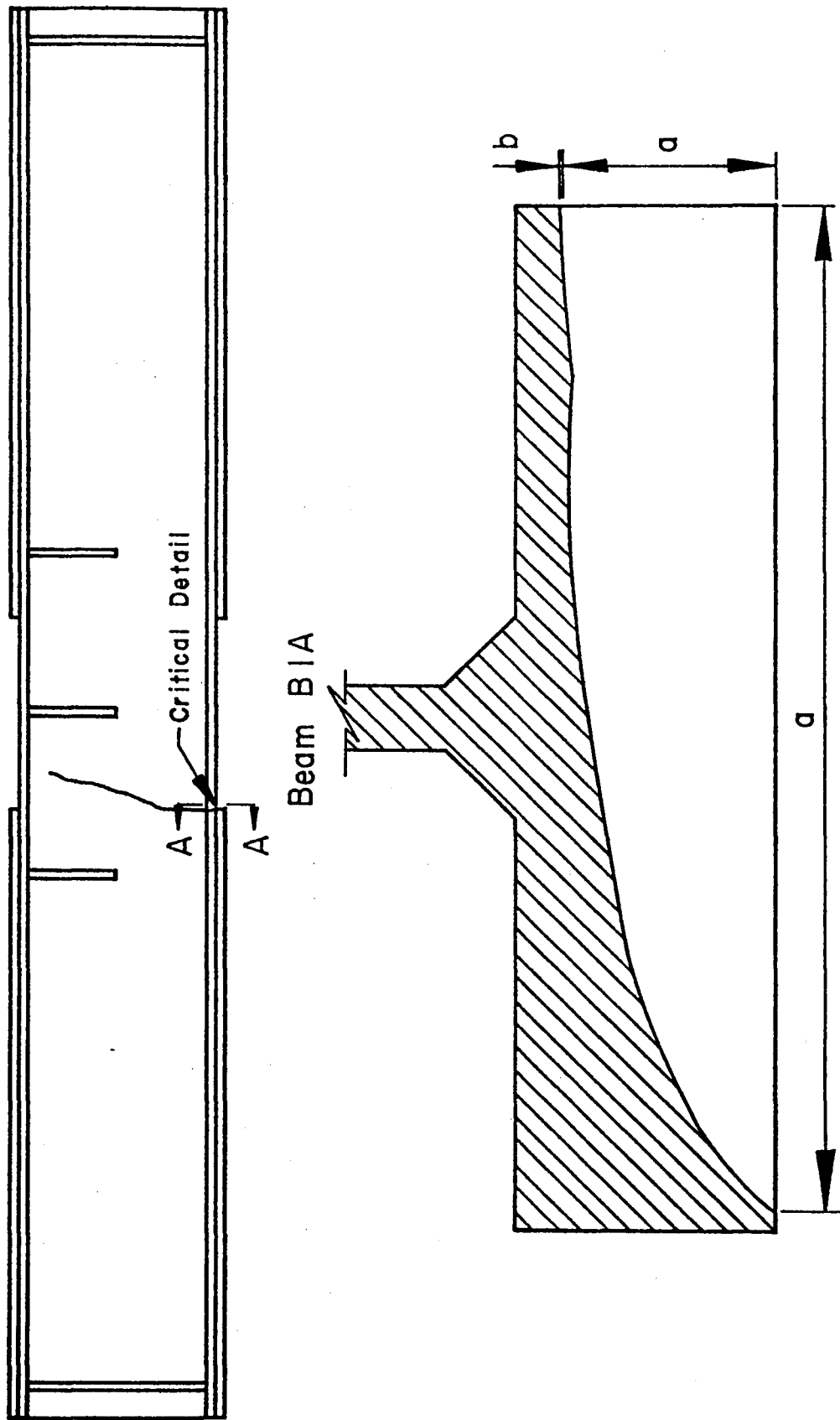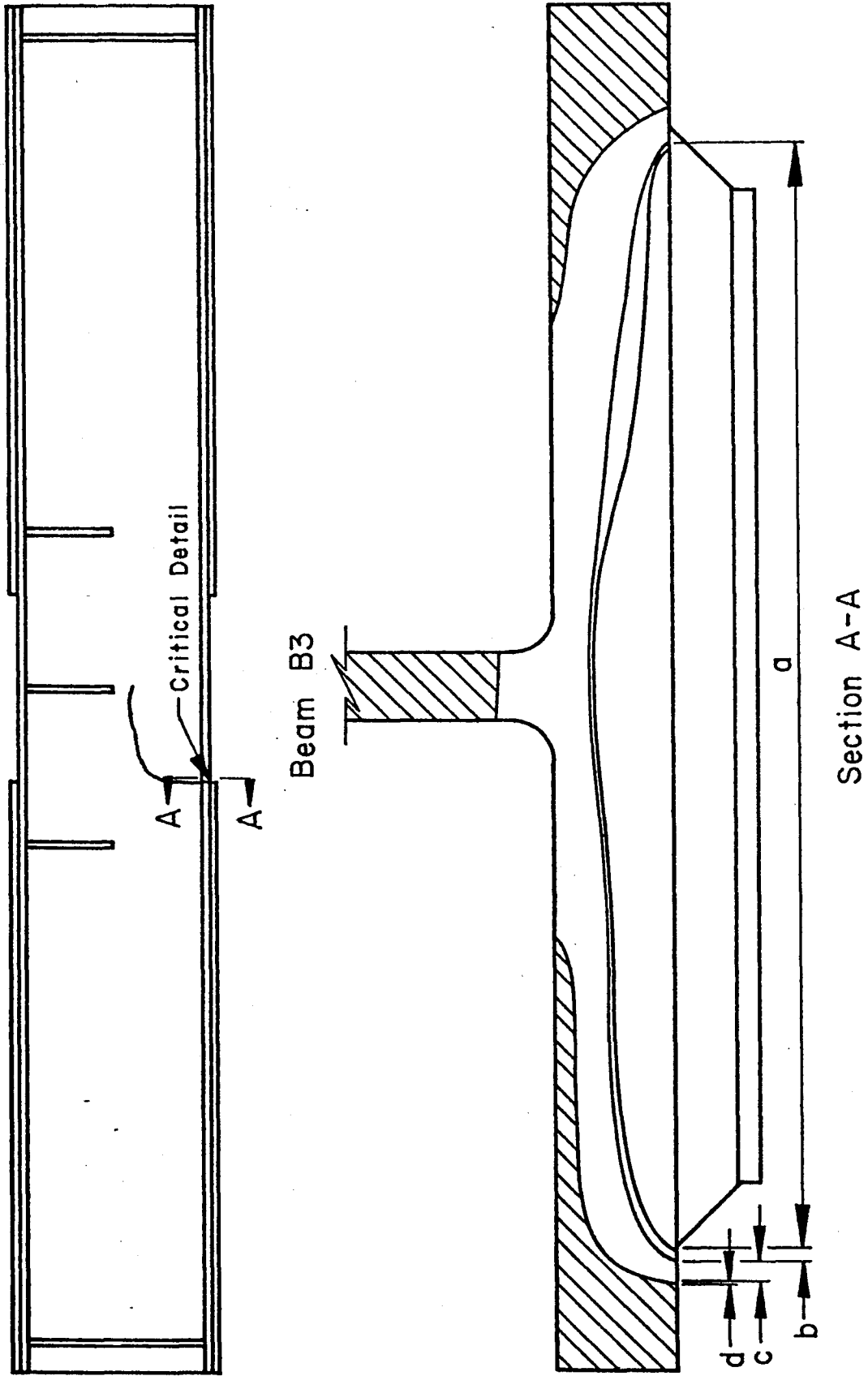
Fig. 5.3 Fatigue and Fracture Surface, B3 (A36, W36 x 260)

-171-

Critical Detail
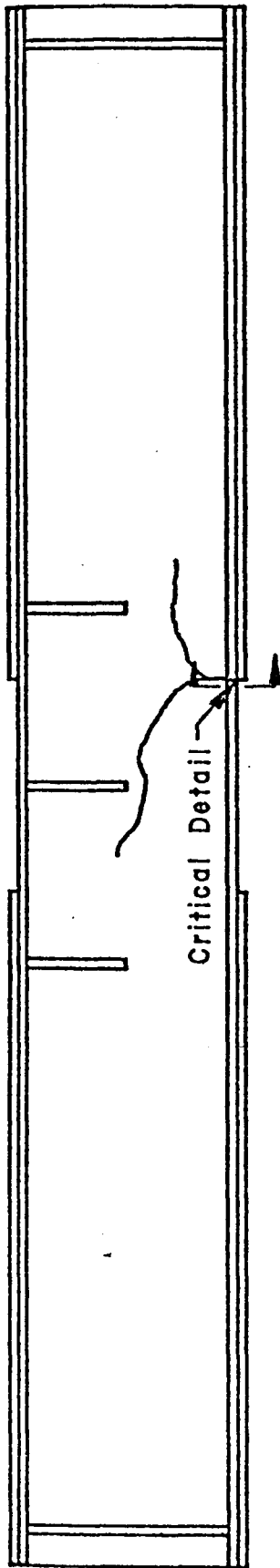
Beam B3A
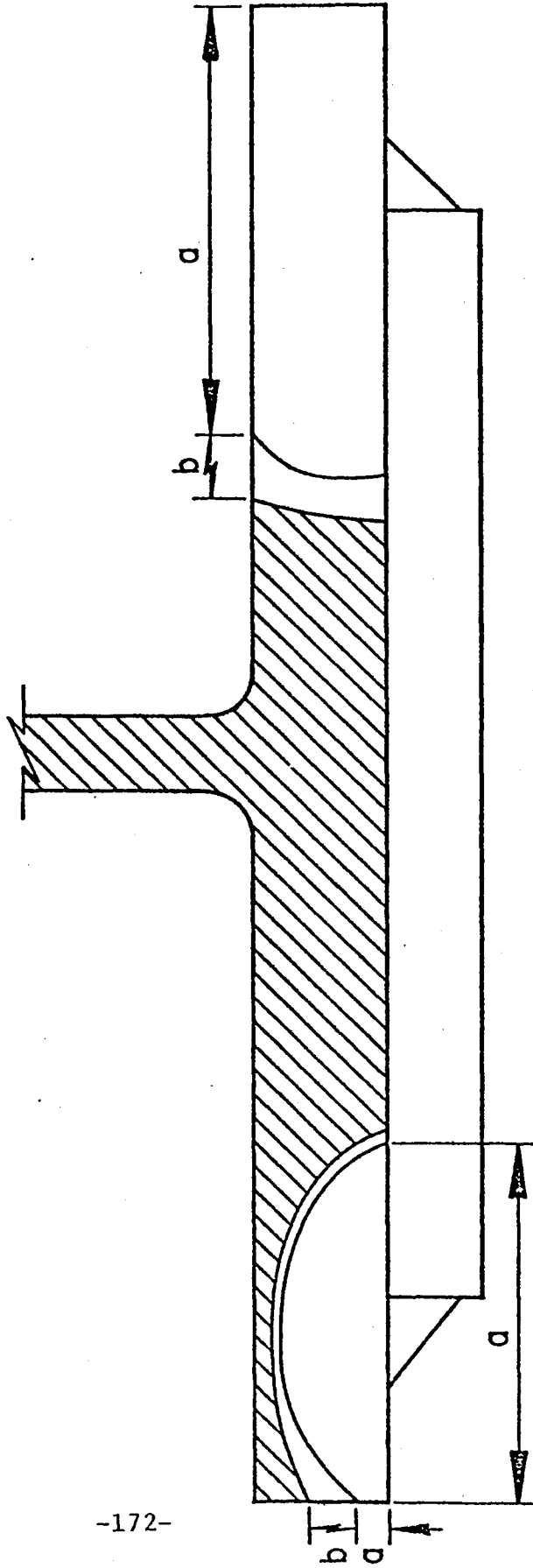
Section A–A

Fig. 5.4 Fatigue and Fracture Surface, B3A (A36, W36 x 260)

-172-

Critical Detail

Beam B5
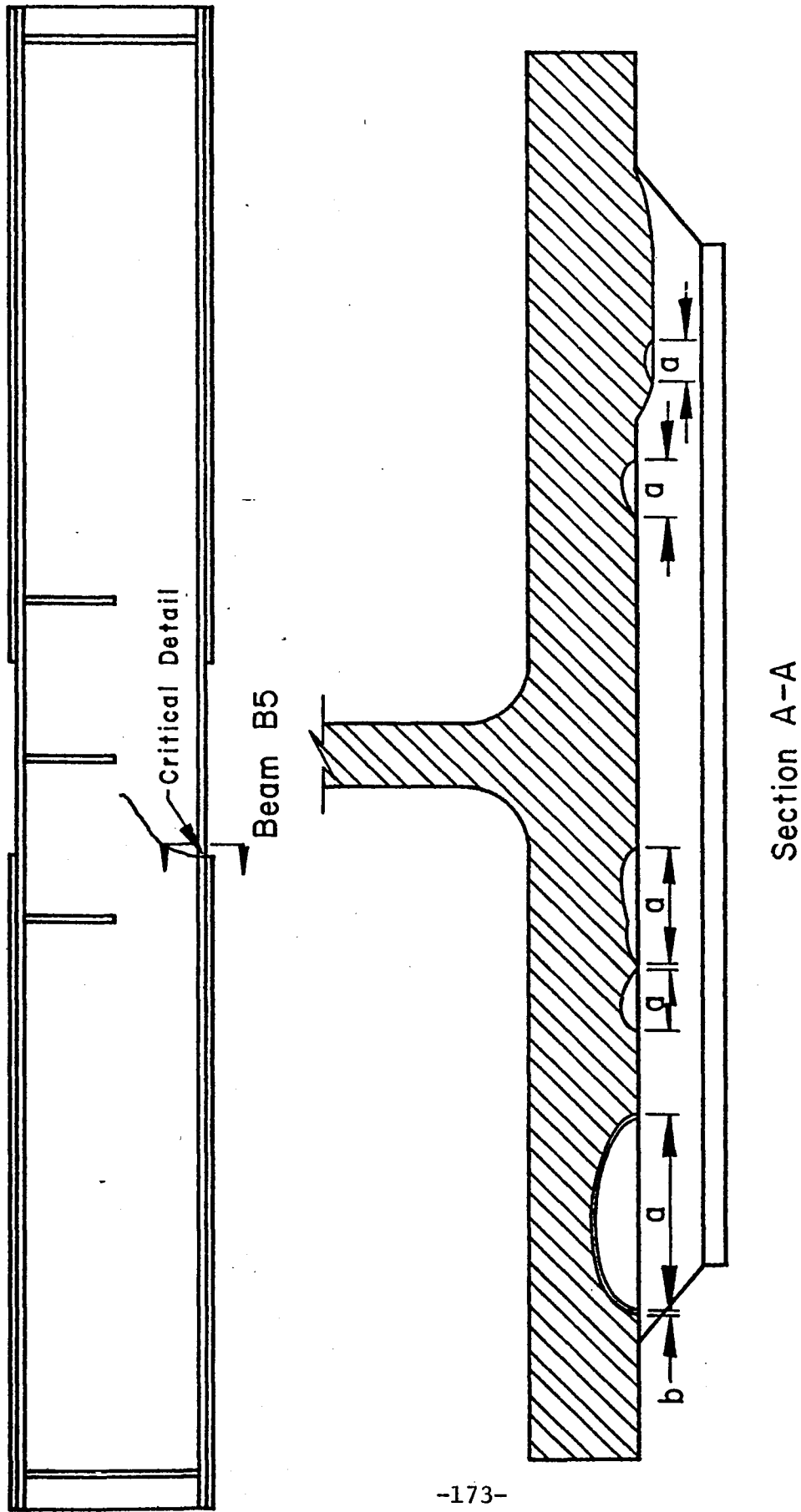
Section A-A

Fig. 5.5 Fatigue and Fracture Surface, B5 (A588, W36 x 230)
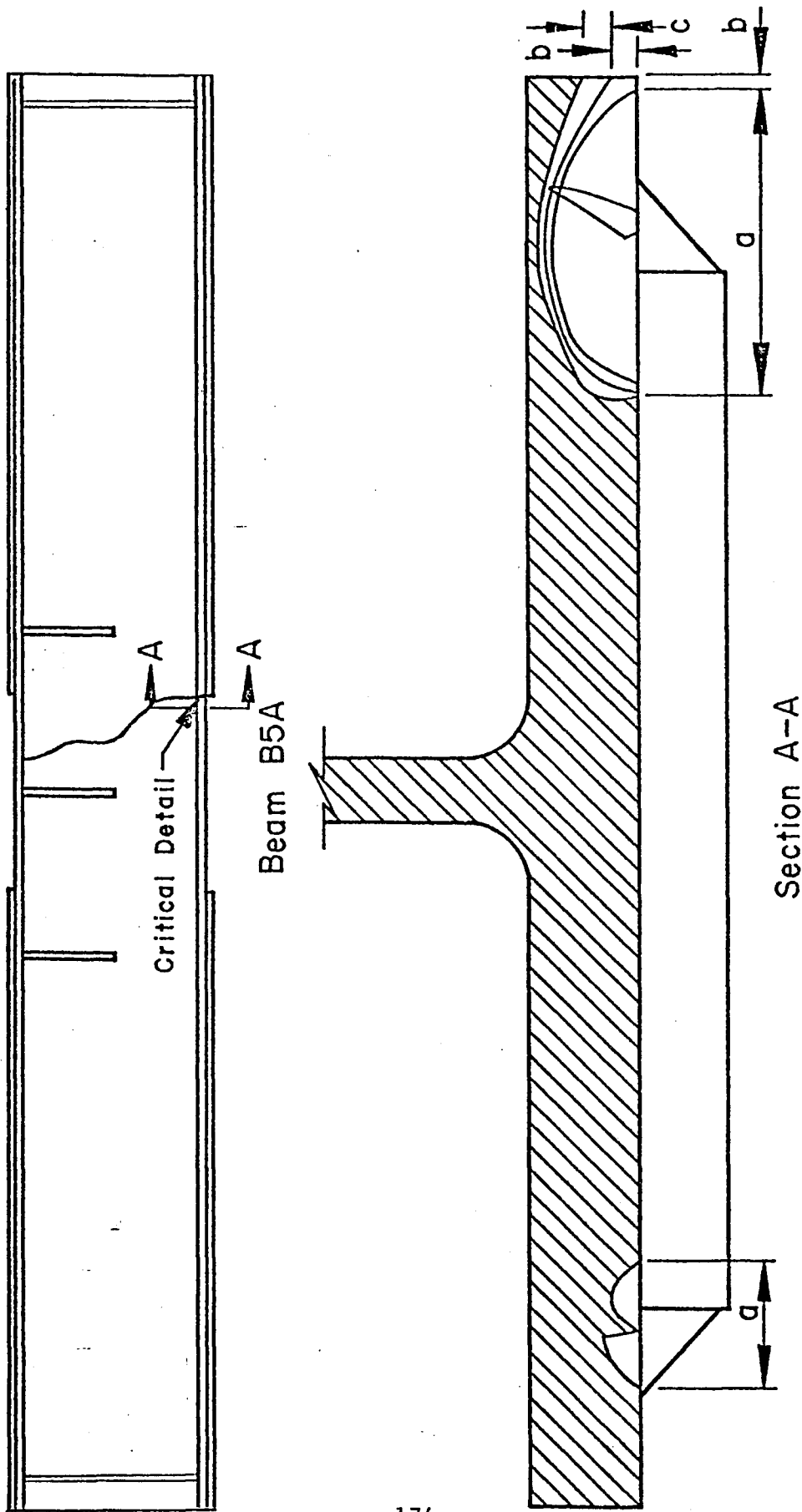
Fig. 5.6 Fatigue and Fracture Surface, B5A (A588, W36 x 230)

Section A-A

Critical Detail

Beam B5A
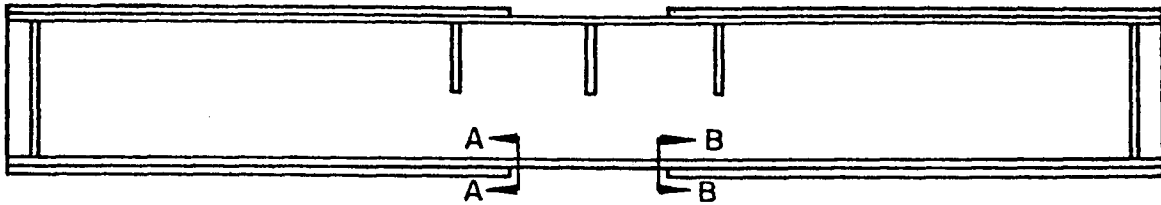
BEAM	SECTION A-A	SECTION B-B
B1	5/8" (16)	* (11) 7/16" 3/16" (5)
B1A		* 1 1/4" (32) (3) 1/8"
B3	(25) 1" 2 3/4" 2 1/4" (57) (70)	* 5 1/4" (133) 3 3/4" (95) 1" (25) (32) 1 1/4"
B3A	3/8" (10) 4 3/4" (121) * 4" (102) 5 1/4" (133)	1 3/8" 4" 5" (35) (102) (127)
B5	1 1/4" (32)	* 2 5/8" 2 5/8" 1/2" (67) (67) (13)
B5A	* (6) 1/4" 3 1/2" 1 1/4" (32) (89)	2 3/8" (60)

X Denotes Critical Detail
Measurements In Brackets, In mm

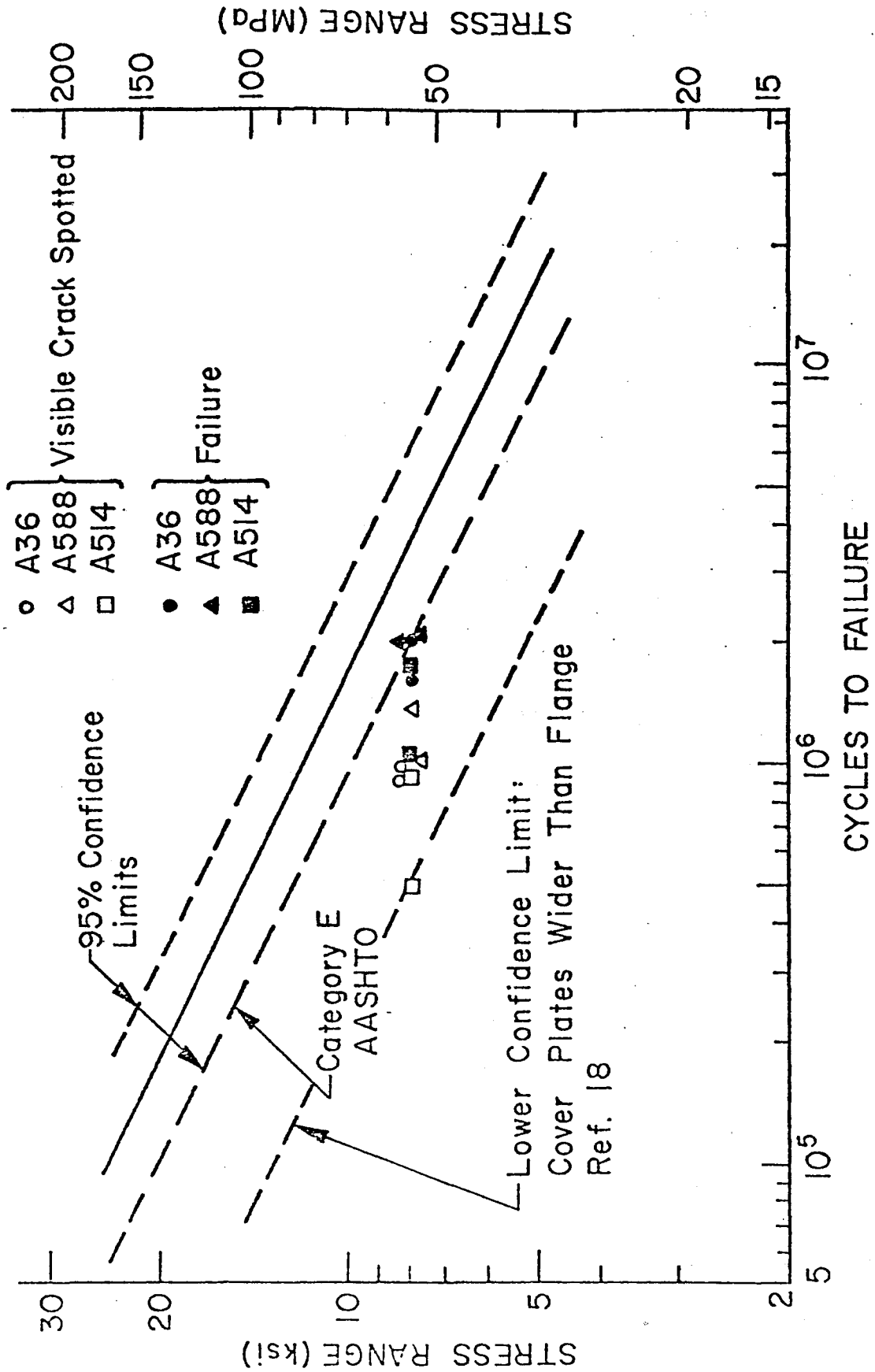Fig. 5.7 Fatigue Cracks Prior to Last Fracture Test
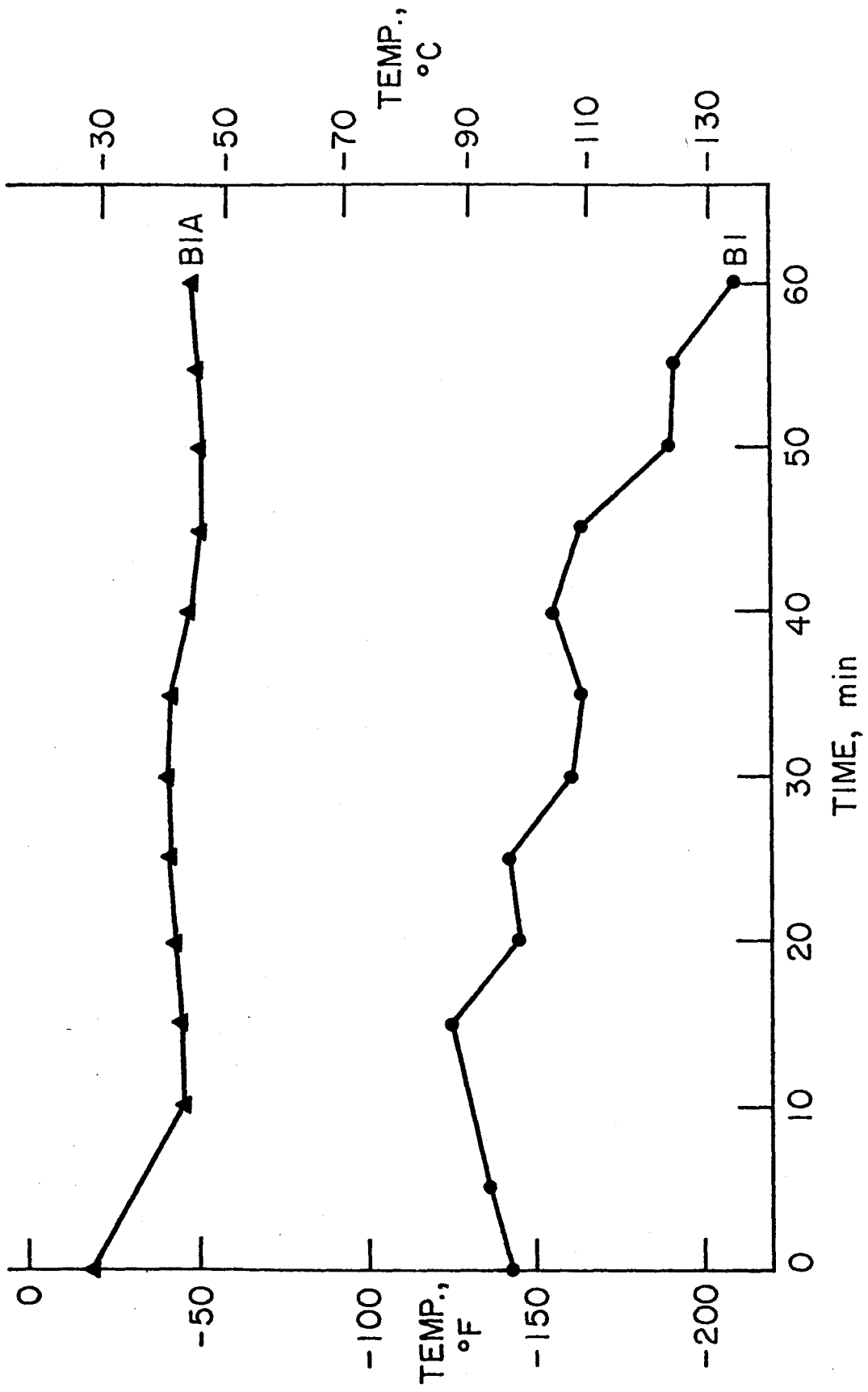
Fig. 5.8 Category E S-N Plot, Cover Plate Beams

-176-

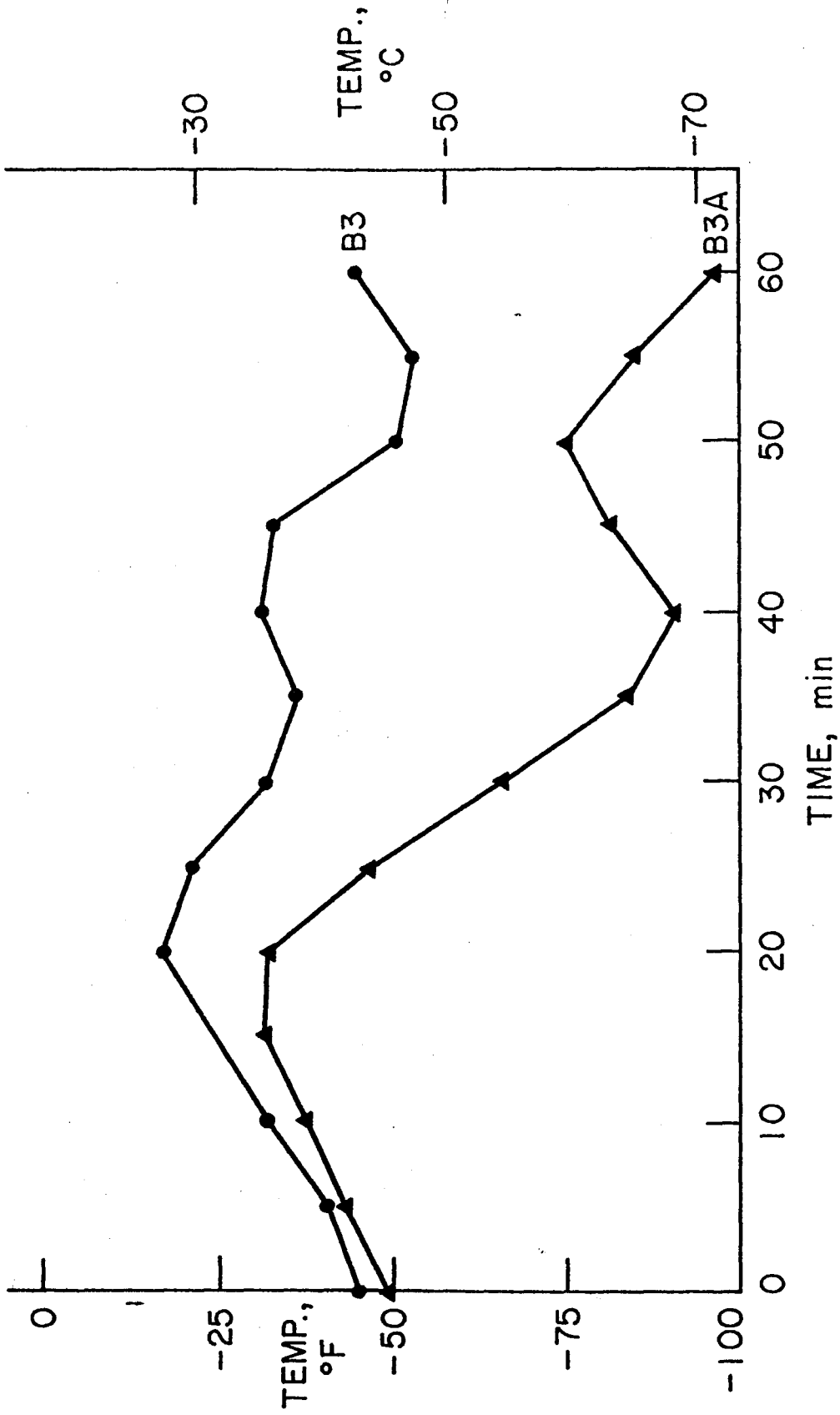Fig. 5.9 Critrical Detail Temperature/60 Minutes Prior to Fracture (A514)

Fig. 5.10 Critical Detail Temperature/60 Minutes Prior to Fracture (A36, W36 x 260)
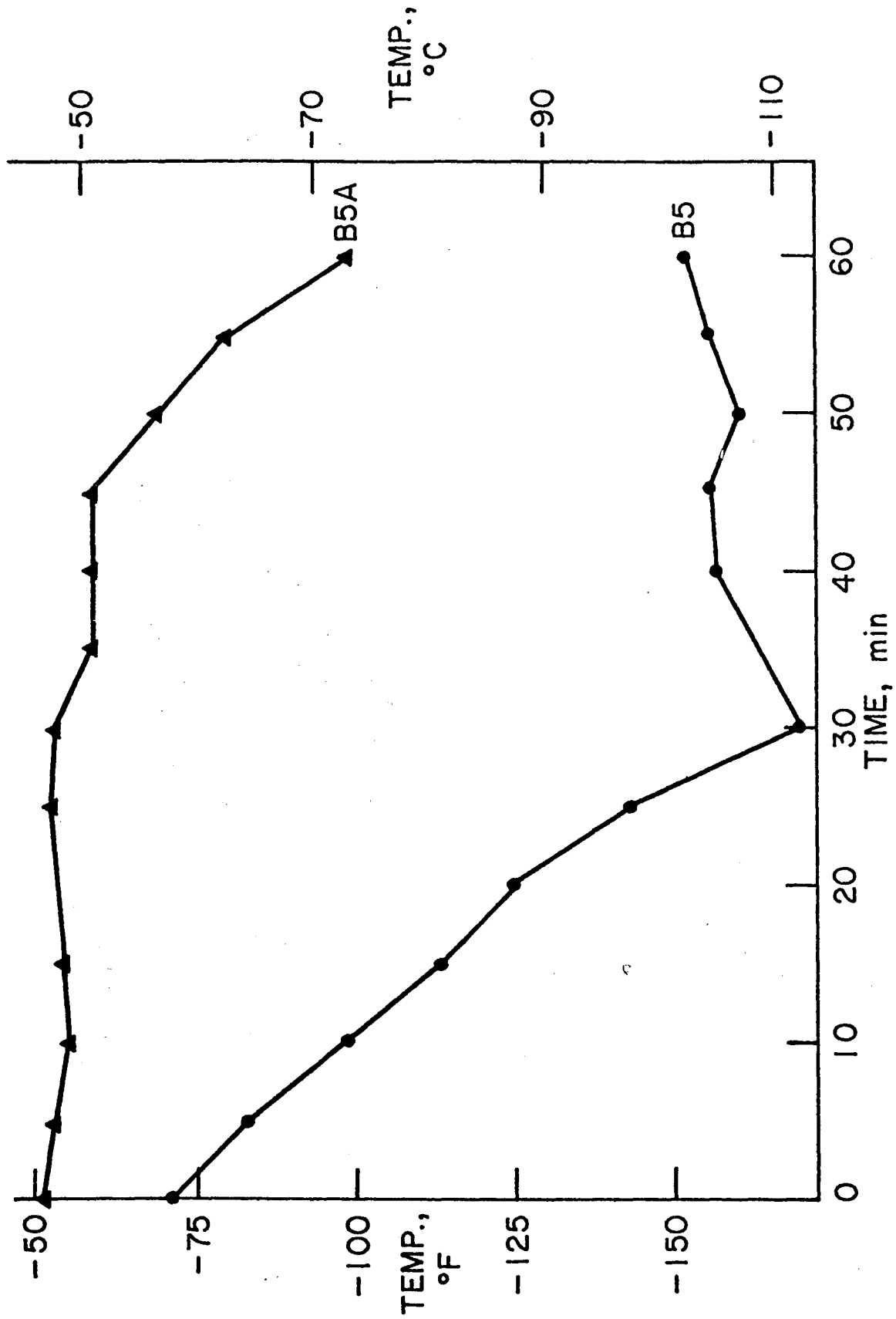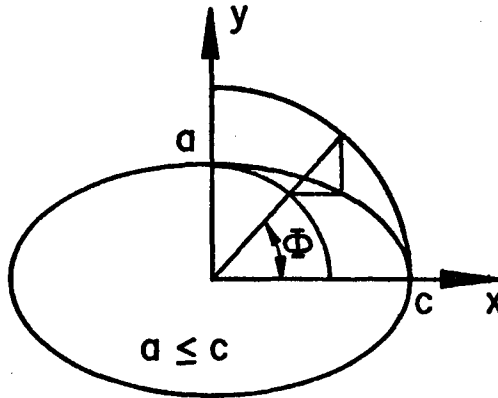
Fig. 5.11 Critical Detail Temperature/60 Minutes Prior to Fracture (A588, W36 x 230)

$$K^2 = \frac{\sigma^2 \pi a}{E_k^2} \sqrt{1 - k^2 \cos^2 \Phi}$$

$$x = c \cos \Phi, \quad y = a \sin \Phi$$

$$k^2 = 1 - (a/c)^2$$

$$E_k = \int_0^{\pi/2} \sqrt{1 - k^2 \sin^2 u} \, du$$

Fig. 5.12 Stress Intensity Model for Elliptical Crack
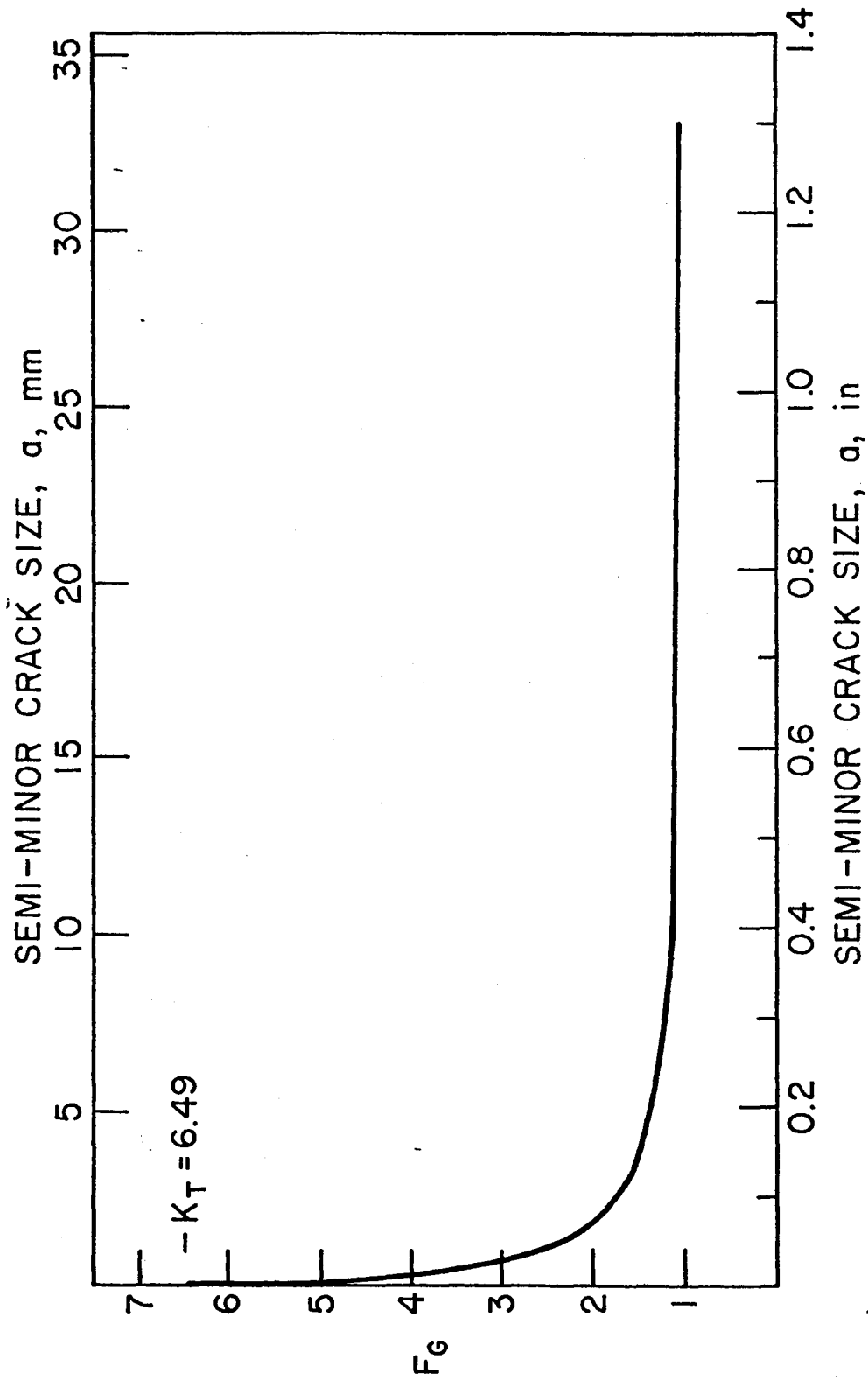Under Uniform Applied Stress

Fig. 5.13 Stress Concentration Decay With Crack Size (Beam B3)
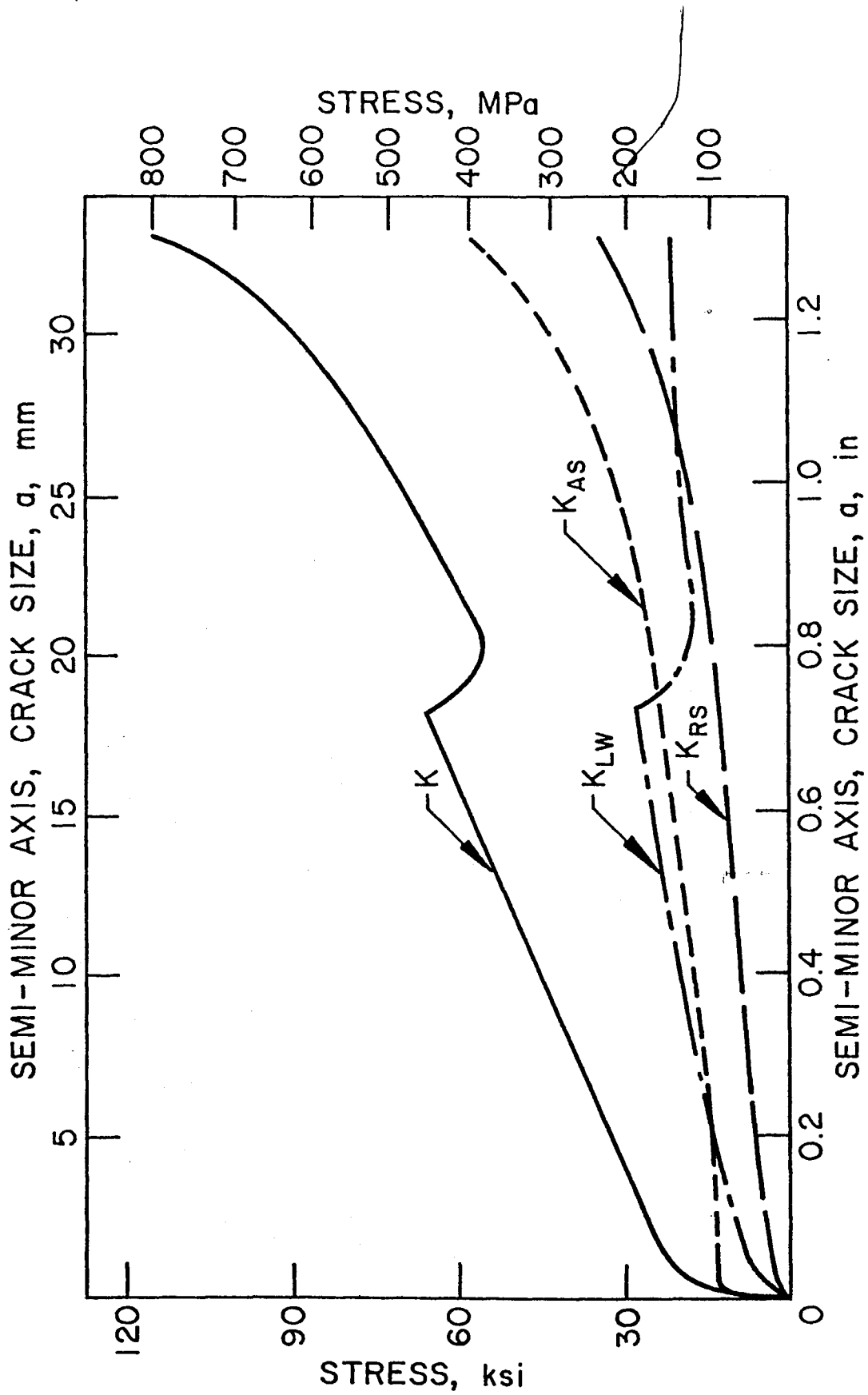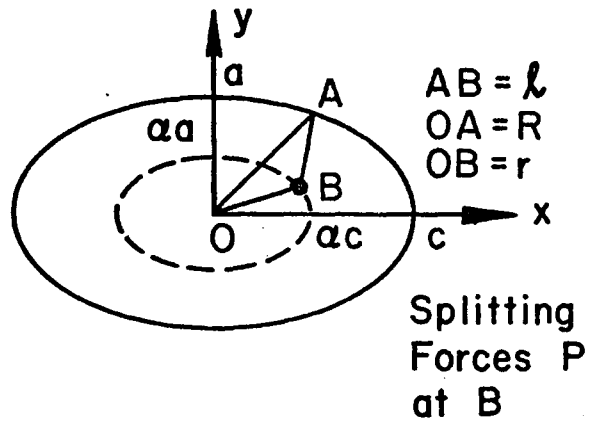
Fig. 5.14 Stress Intensity vs. Crack Size for Elliptical Surface Cracks (B3, A36, W36 x 260)

$$K = \frac{P\sqrt{a}}{\pi^{3/2} \ell^2} \sqrt{\frac{r}{R}} \; \frac{\sqrt{\frac{1}{\alpha^2} - 1}}{\left\{1 - k^2 \cos^2 \Phi\right\}^{1/4}}$$

$$x = \alpha c \; \cos \; \Phi_1, \quad y = \alpha a \; \sin \; \Phi_1$$

Fig. 5.15 Residual Stress Point Load Model for Elliptical Cracks

σ_{max}	= 55.0 ksi	= 379 MPa
σ_{YD}	= 159 ksi	= 1096 MPa
a	= 1.05 in	= 26.7 mm
r_y	= N.A.	
T_c	= $-200°F$	= $-129°C$
K_c	= 233 ksi $\sqrt{in}$	= 256 MPa $\sqrt{m}$
N	= 1,806,300	

B2 (A514)

σ_{max}	= ~55 ksi	= 379 MPa
σ_{YD}	= 133 ksi	= 917 MPa
a	= 1.25 in	= 31.8 mm
r_y	= N.A.	
T_c	= $-48°F$	= $-44°C$
K_c	= 300 ksi $\sqrt{in}$	= 330 MPa $\sqrt{m}$
N	= 1,134,200	

B2A (A514)

σ_{max}	= 17.2 ksi	= 119 MPa
σ_{YD}	= 71 ksi	= 490 MPa
a	= 2.1 in	= 53 mm
r_y	= N.A.	
T_c	= $-45°F$	= $-43°C$
K_c	= 193 ksi $\sqrt{in}$	= 212 MPa $\sqrt{m}$
N	= 2,170,700	

B3 (A36 Rolled)

σ_{max}	= 19.8 ksi	= 136 MPa
σ_{YD}	= 78 ksi	= 538 MPa
a	= 5.63 in	= 143 mm
r_y	= 0.47 in	= 11.9 mm
T_c	= $-96°F$	= $-71°C$
K_c	= 116 ksi $\sqrt{in}$	= 128 MPa $\sqrt{m}$
N	= 1,817,200	

B3A (A36 Rolled)

σ_{max}	= 27.5 ksi	= 190 MPa
σ_{YD}	= 96 ksi	= 662 MPa
a	= 0.56 in	= 14.2 mm
r_y	= 0.05 in	= 1.3 mm
T_c	= $-150°F$	= $-101°C$
K_c	= 62 ksi $\sqrt{in}$	= 68 MPa $\sqrt{m}$
N	= 2,012,500	

B5 (A588 Rolled)

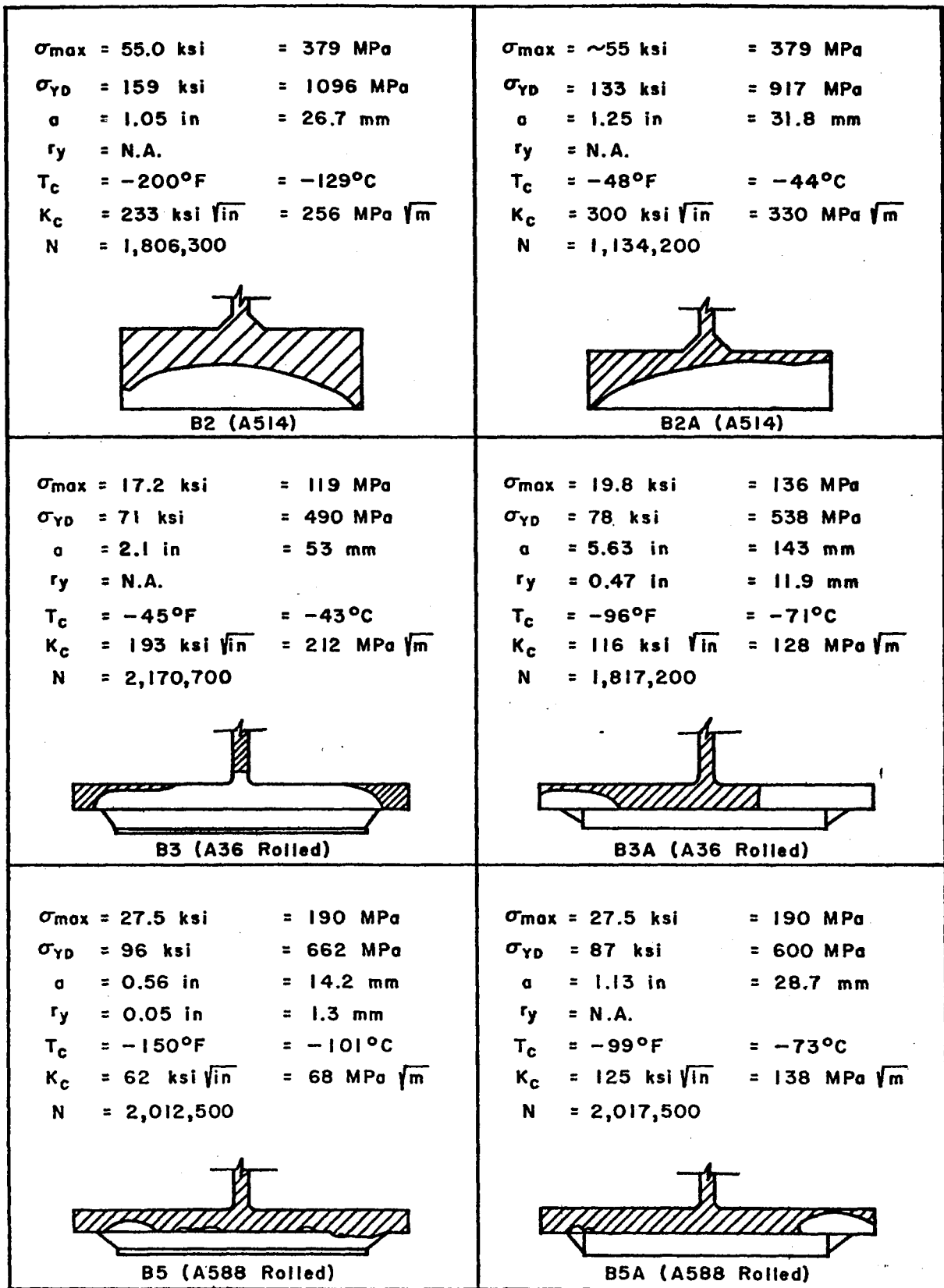| σ_{max}	= 27.5 ksi	= 190 MPa
σ_{YD}	= 87 ksi	= 600 MPa
a	= 1.13 in	= 28.7 mm
r_y	= N.A.	
T_c	= $-99°F$	= $-73°C$
K_c	= 125 ksi $\sqrt{in}$	= 138 MPa $\sqrt{m}$
N	= 2,017,500	

B5A (A588 Rolled)

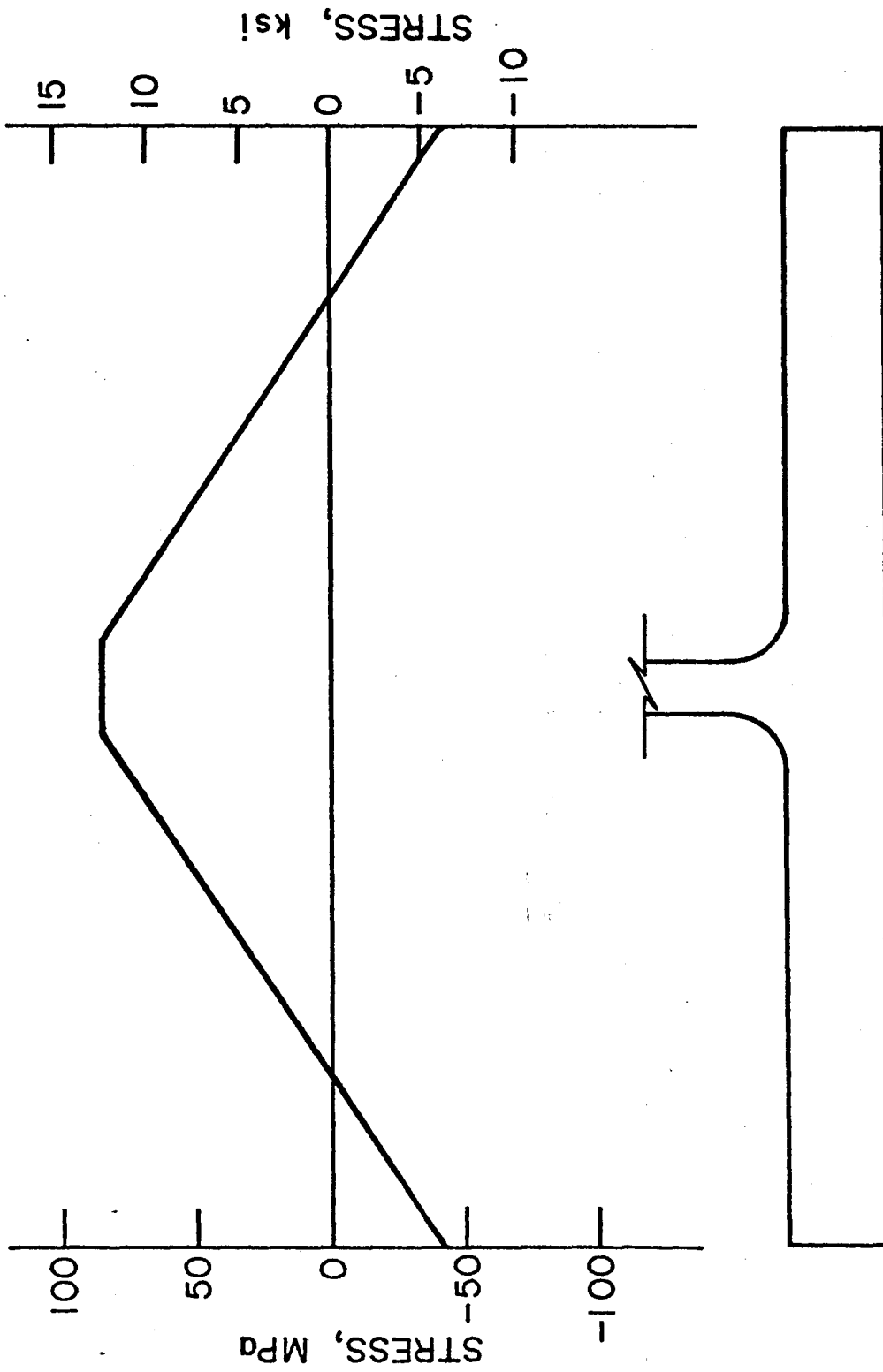Fig. 5.16   Fracture Surface Sketches and Data Summary

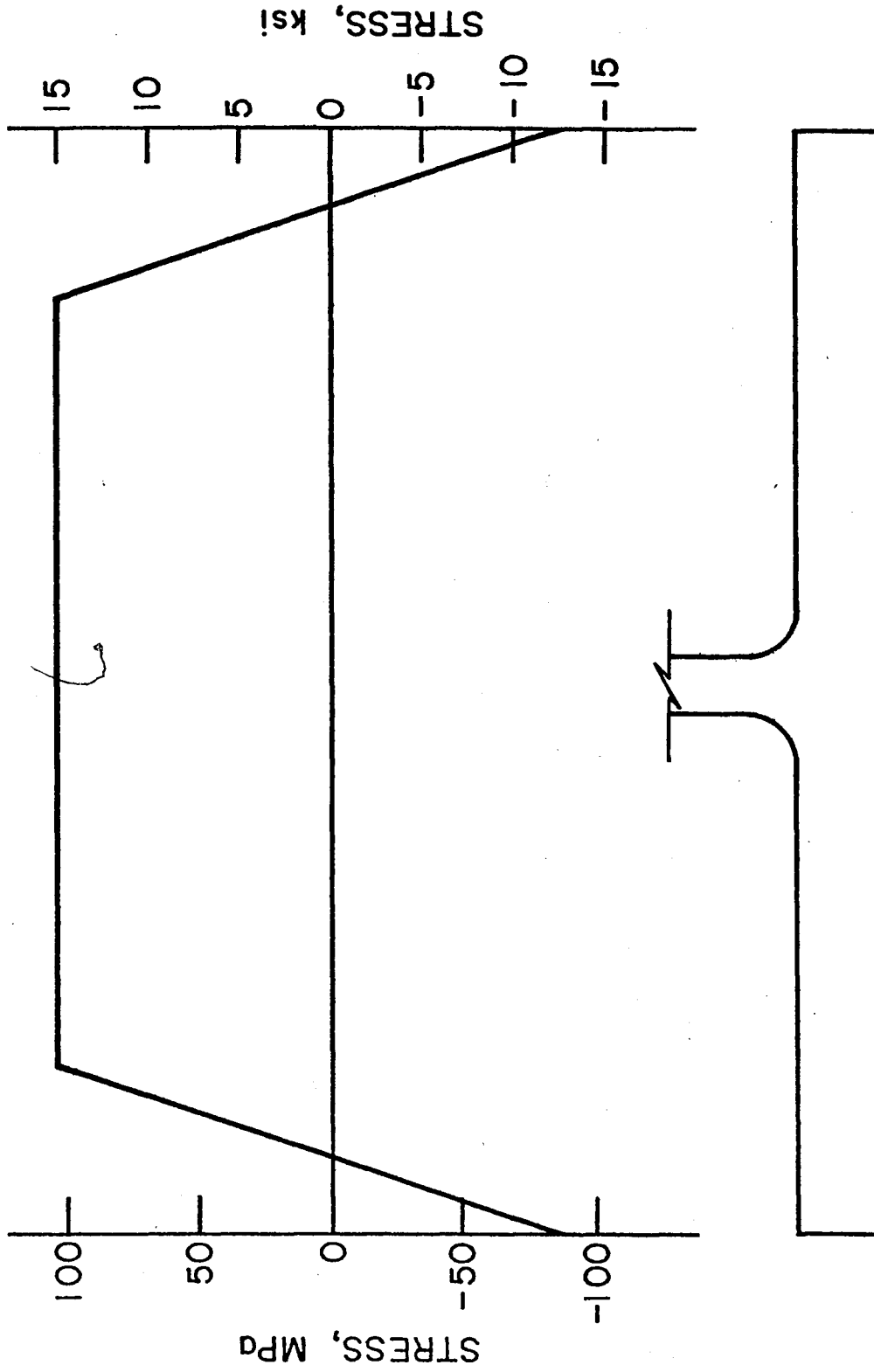Fig. 5.17 Measured Residual Stress Distribution for A36, W36 x 260, Flange

Fig. 5.18 Measured Residual Stress Distribution for A588, W36 x 230, Flange
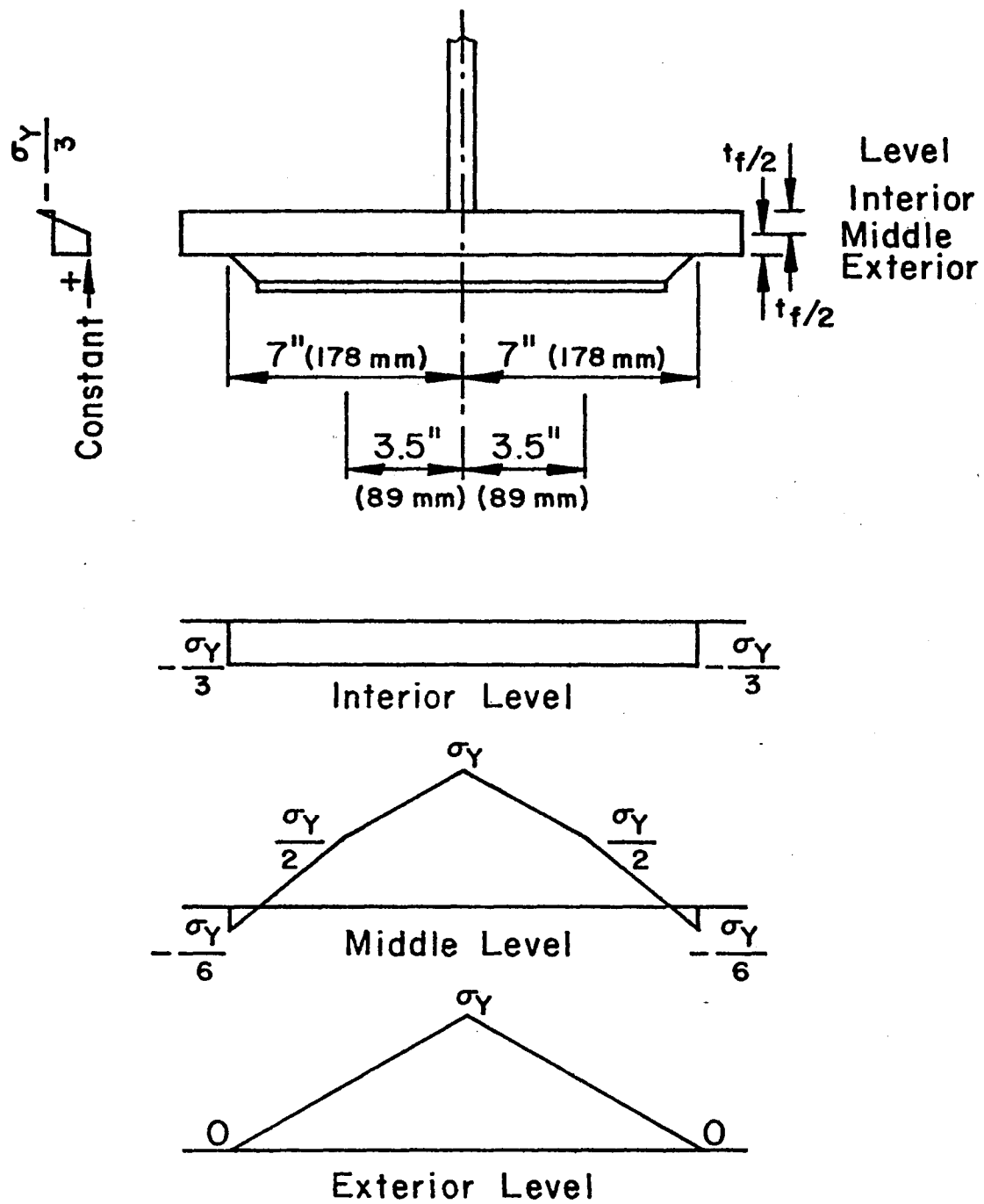
Fig. 5.19 Local Weld Residual Stress Distribution
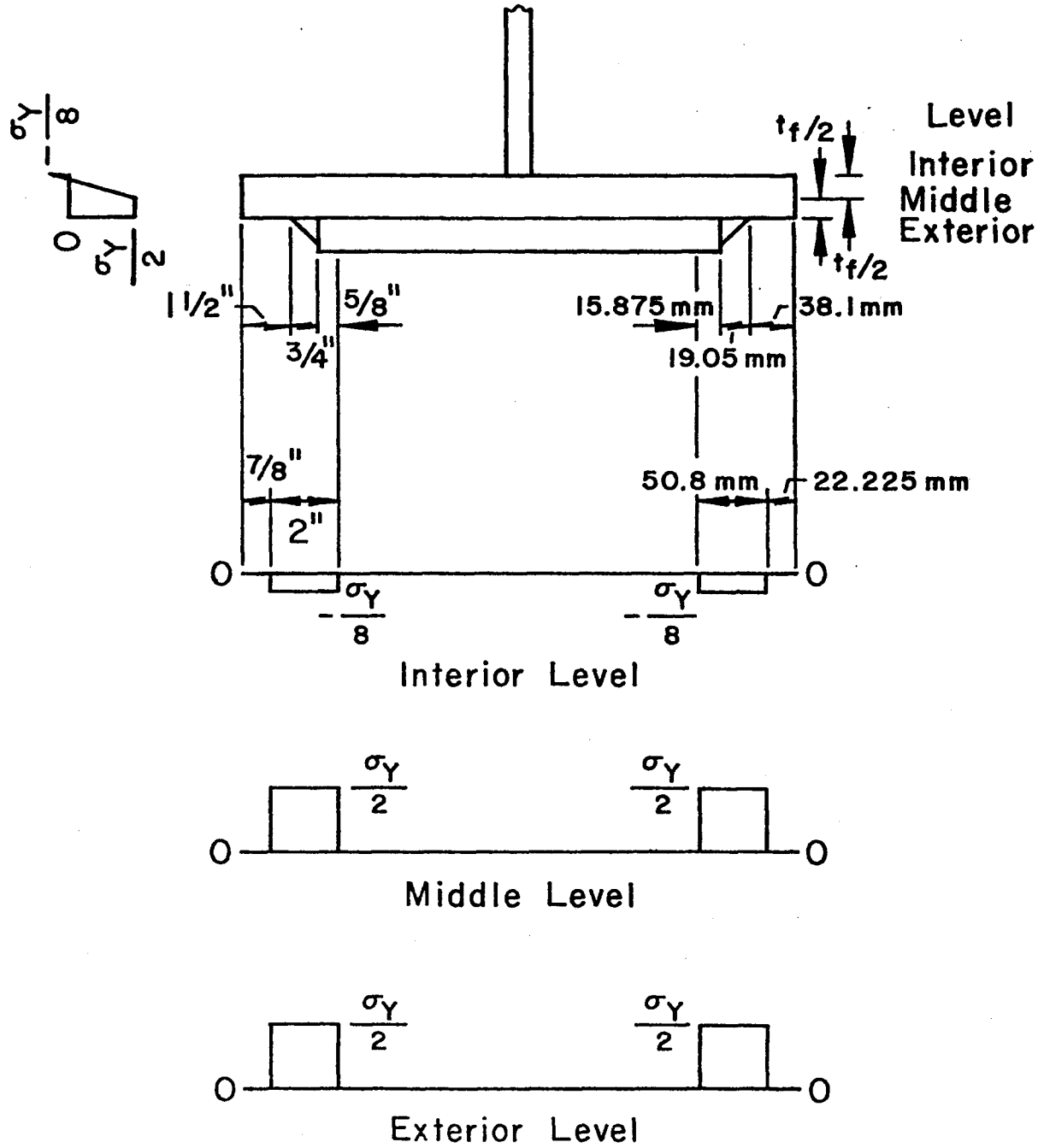for End Weld Cover Plate Detail (A36, A588)

Fig. 5.20 Local Weld Residual Stress Assumptions for
          No-End-Weld Cover Plate Detail (A36,.A588)
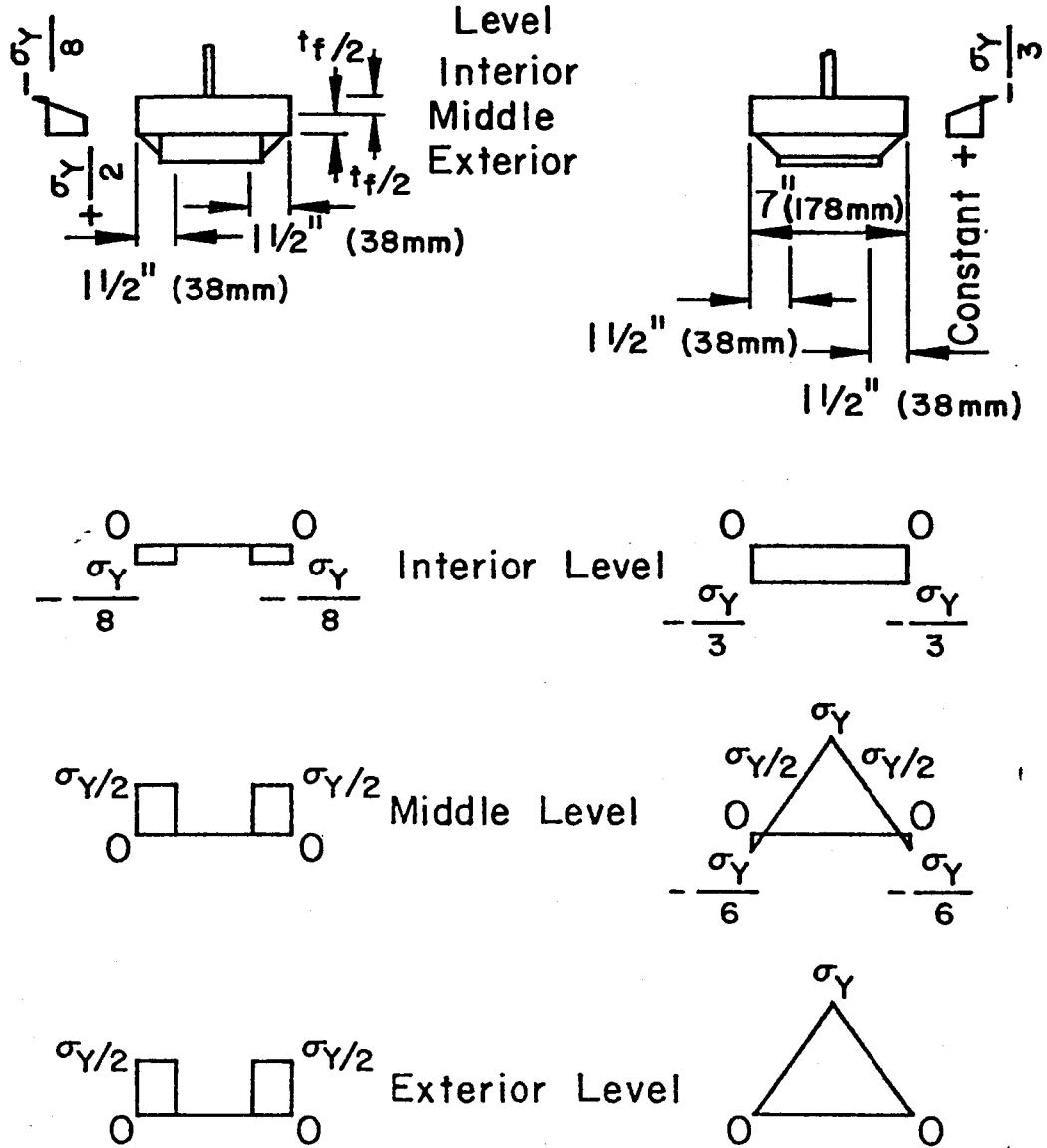
No-End-Weld Cover Plate　　　　End-Weld Cover Plate

Fig. 5.21　Local Weld Residual Stress Assumptions
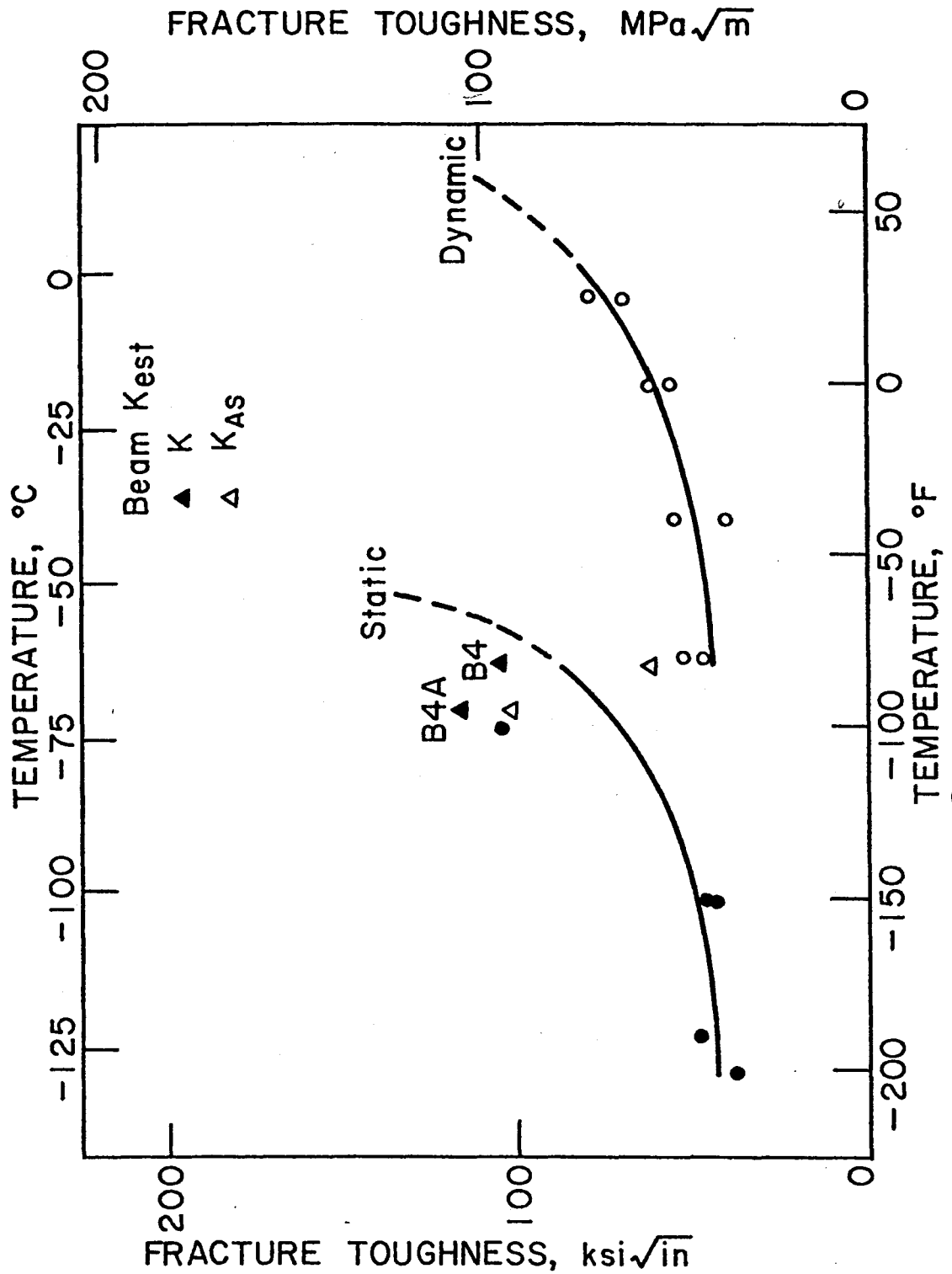for A514 Cover Plate Detail (B2, B1A)

Fig. 6.1 Correlation of Beam K_{est} and Material Toughness Characterization, B4, B4A (A36)
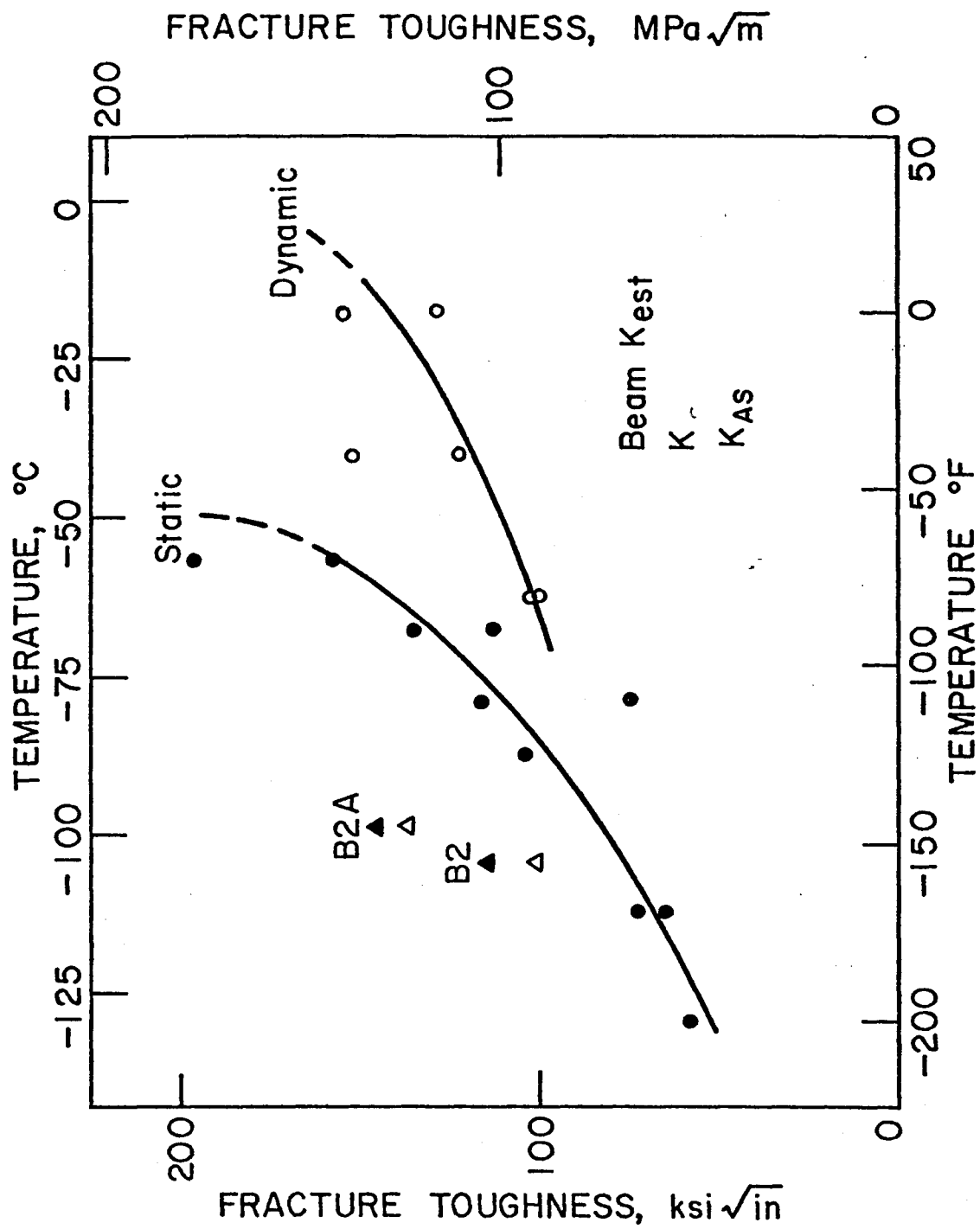
Fig. 6.2 Correlation of Beam K_{est} and Material Toughness Characterization, B6, B6A (A588)

Fig. 6.3 Correlation of Beam K_{est} and Material Toughness Characterization, B2, B2A (A514)
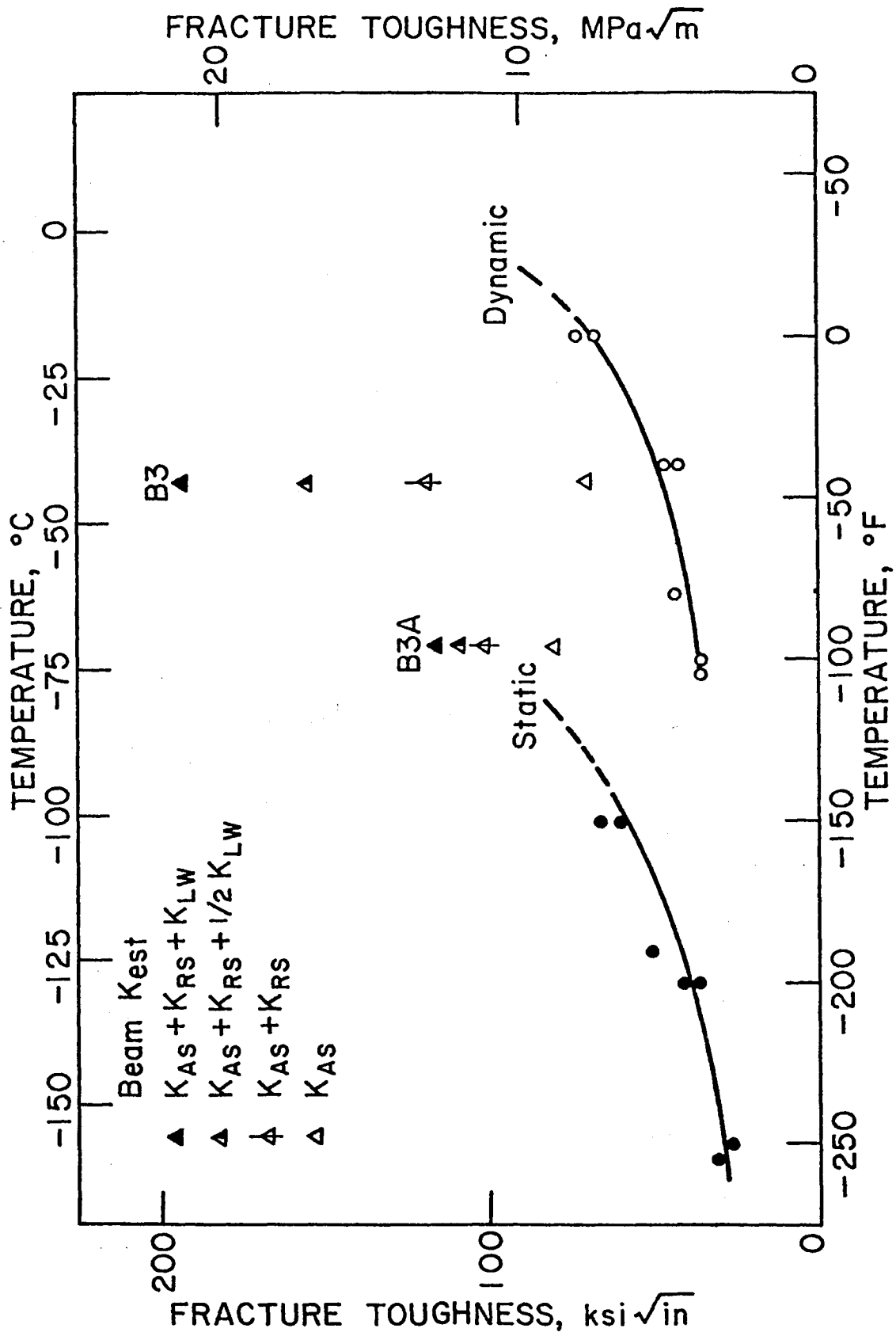
Fig. 6.4 Correlation of Beam K_{est} and Material Toughness Characterization, B3, B3A (A36, Rolled)
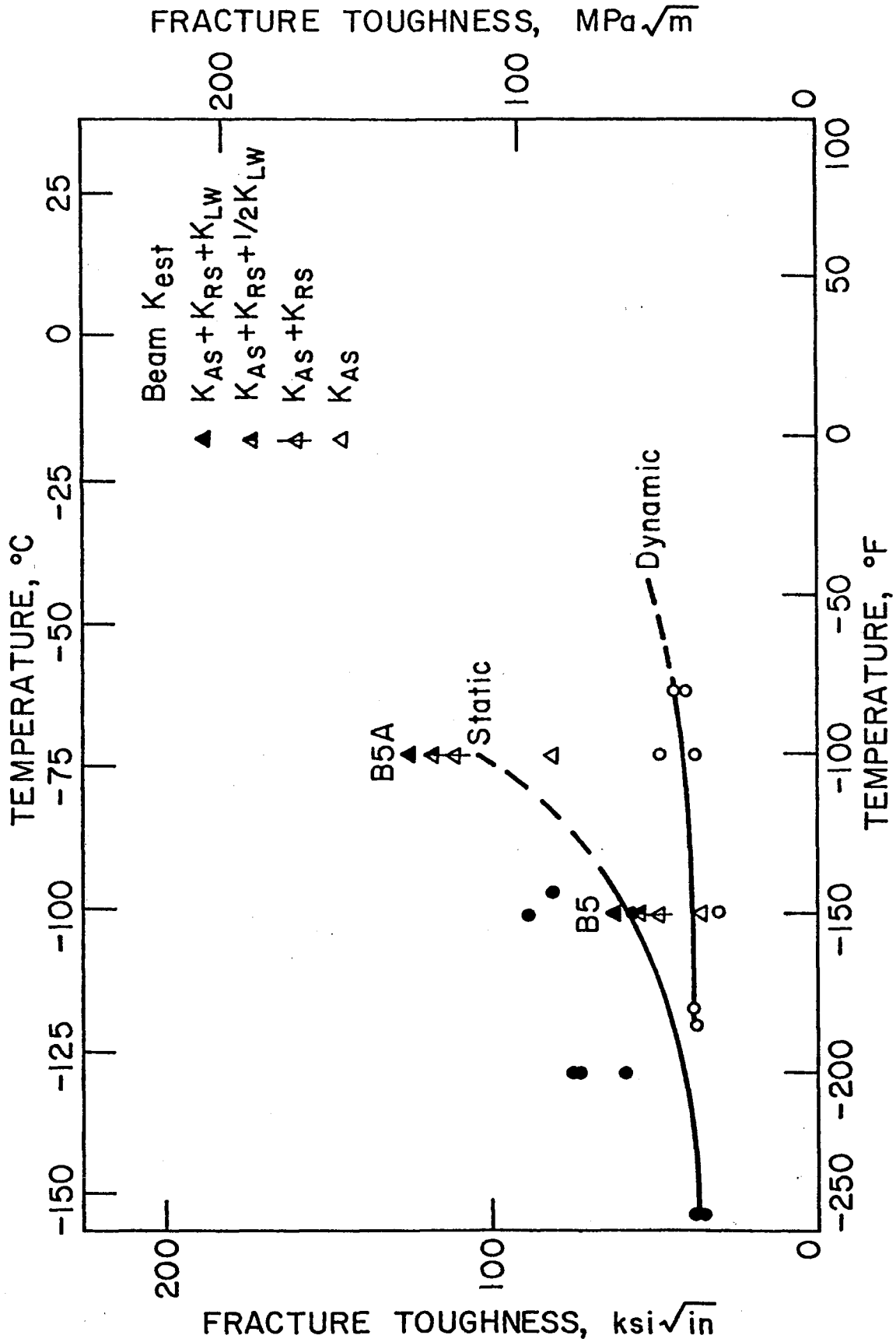
Fig. 6.5 Correlation of Beam K_{est} and Material Toughness Characterization, B5, B5A (A588, Rolled)

Fig. 6.6 Correlation of Beam K_{est} and Material Toughness Characterization, B1, B1A (A514)

Web Crack Opening
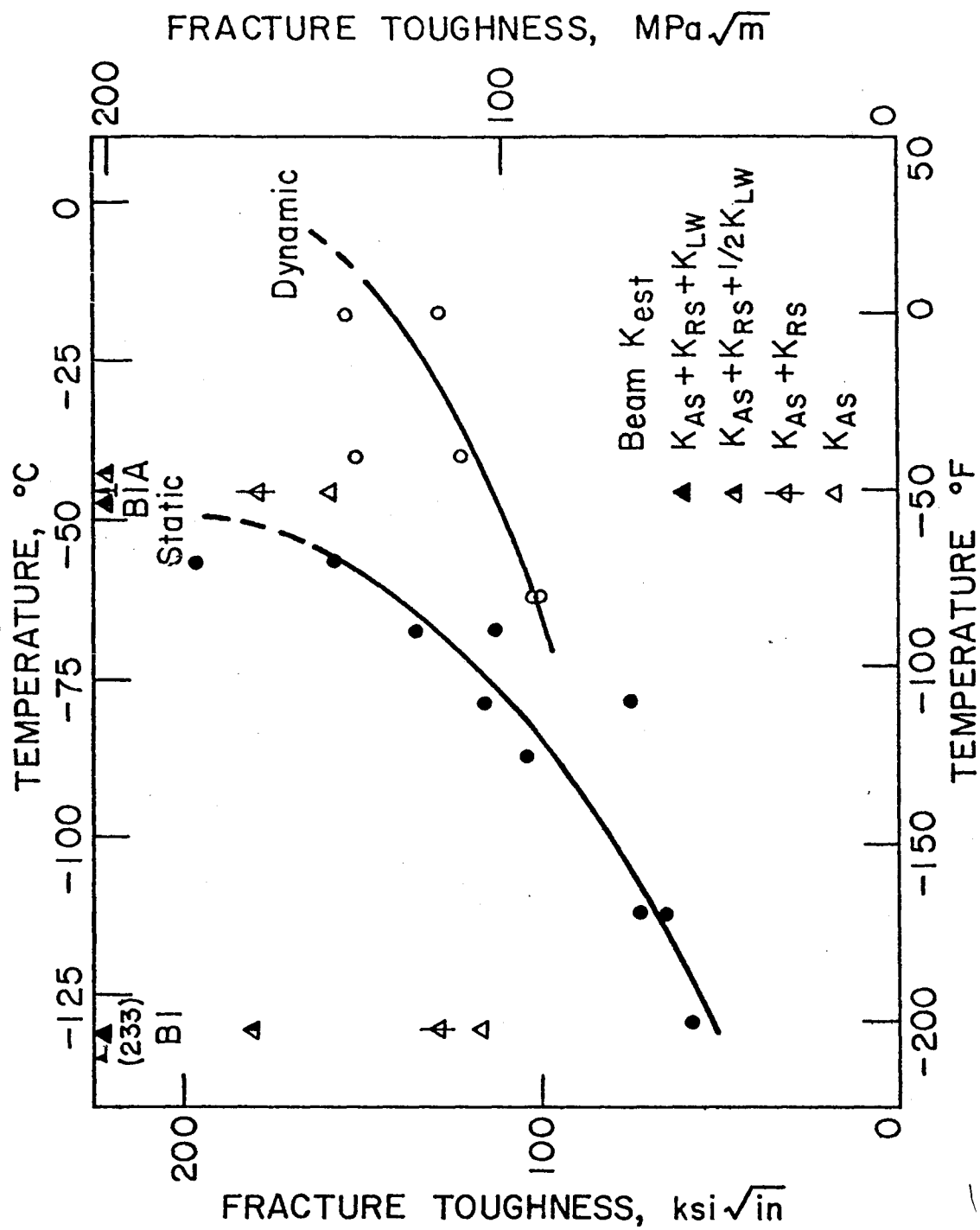
V_w (Applied Stress, Res. Stress)

V_f

σ

Web $\mathcal{C}_L$

$V_f = f$(Applied Stress, Res. Stress)
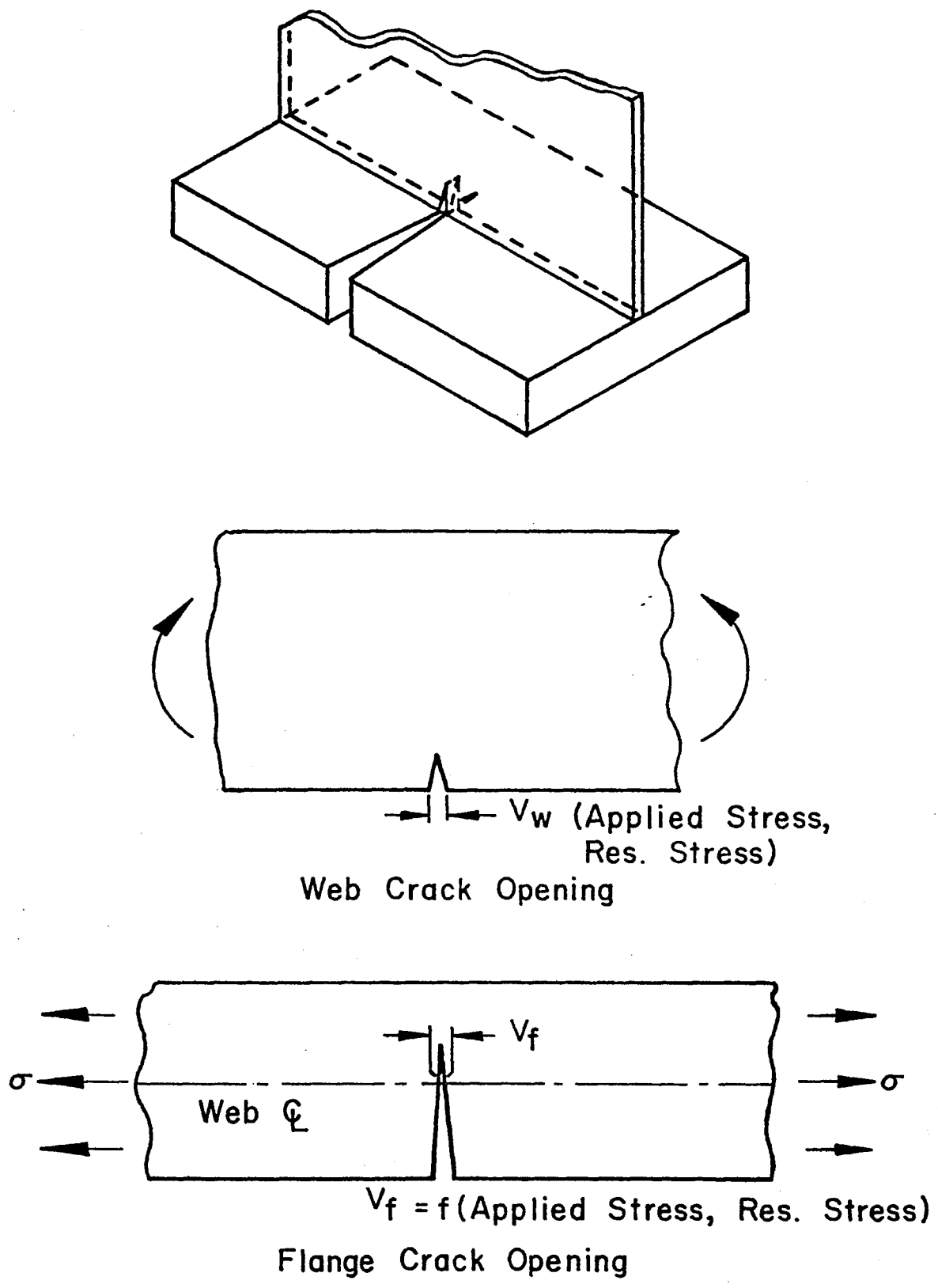
Flange Crack Opening
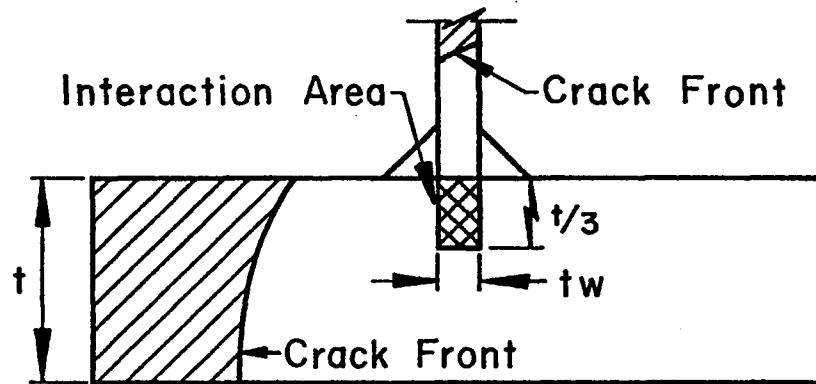
Fig. A.1   Flange and Web Crack Interaction

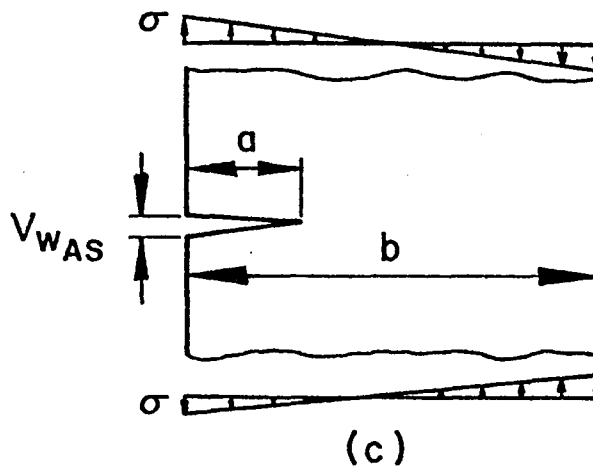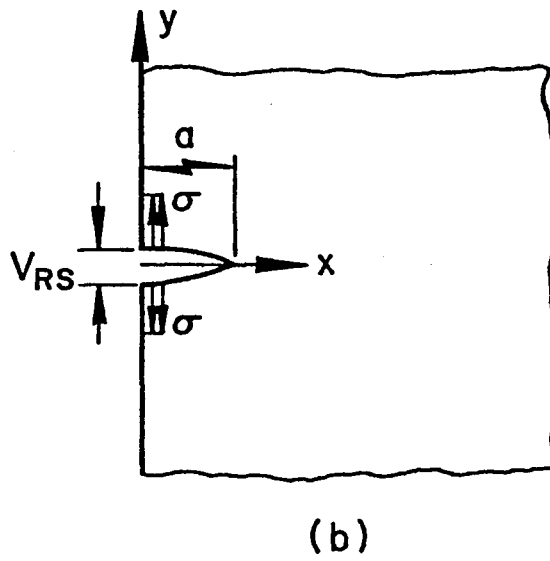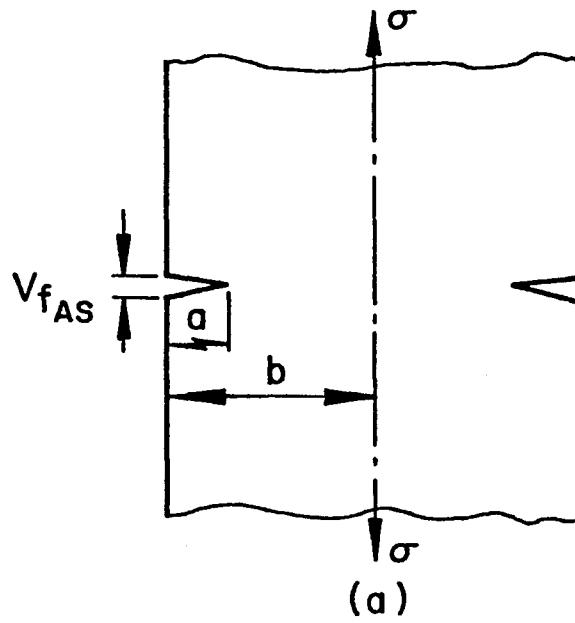Fig. A.2 Assumed Interaction Area for Web Restraint Analysis

Fig. A.3 Models Used for Web Restraint Analysis

10. REFERENCES

1. Fisher, J. W., Frank, K. H., Hirt, M. A. and McNamee, B. M.
   EFFECT OF WELDMENTS ON THE FATIGUE STRENGTH OF STEEL BEAMS,
   NCHRP Report No. 102, Highway Research Board, National
   Academy of Science – National Research Council,
   Washington, D.C., 1970.

2. Fisher, J. W., Albrecht, P. A., Yen, B. T., Klingerman, D. J.
   and McNamee, B. M.
   FATIGUE STRENGTH OF STEEL BEAMS WITH TRANSVERSE STIFFENERS
   AND ATTACHMENTS, NCHRP Report No. 147, Highway Research
   Board, National Academy of Science – National Research
   Council, Washington, D.C., 1974.

3. American Association of State Highway Officials
   STANDARD SPECIFICATIONS FOR HIGHWAY BRIDGES, AASHTO,
   Washington, D.C., 1973.

4. Tada, H. and Irwin, G. R.
   K-VALUE ANALYSIS FOR CRACKS IN BRIDGE STRUCTURES, Fritz
   Engineering Laboratory Report No. 399.1, Lehigh University,
   June 1975.

5. Brothers, A. J. and Yukawa, S.
   THE EFFECT OF WARM PRESTRESSING ON NOTCH FRACTURE STRENGTH,
   Paper No. 62-Met-1, ASME Headquarters, January 1962.

6. Succop, L. N., Pense, A. W. and Stout, R. D.
   THE EFFECTS OF WARM OVERSTRESSING ON PRESSURE VESSEL STEEL
   PROPERTIES, Welding Journal Research Supplement, August 1970.

7. Barsom, J. M.
   INVESTIGATION OF TOUGHNESS CRITERIA FOR BRIDGE STEELS,
   U.S.S. Research Laboratory Report No. 97.018-001(5),
   February 1973.

8. Roberts, R., Irwin, G. R., Krishna, G. V. and Yen, B. T.
   FRACTURE TOUGHNESS OF BRIDGE STEELS, Federal Highway
   Administration Report No. FHWA RD-74-57, September 1974.

9. Luft, D. E., Madison, R. B. and Irwin, G. R.
    MEASUREMENT OF DYNAMIC K_c FROM DROP-WEIGHT TEAR TEST, Fritz
    Engineering Laboratory Report 335.1, Lehigh University, 1969.

10. Irwin, G. R.
    LINEAR FRACTURE MECHANICS, FRACTURE TRANSITION AND FRACTURE
    CONTROL, Engineering Fracture Mechanics, Vol. 1, pp. 241-257,
    1968.

11. ASTM Tentative Standard
    TENTATIVE METHOD OF TEST FOR PLAIN STRAIN FRACTURE TOUGHNESS
    OF METALLIC MATERIALS, E399-70T.

12. Paris, P. D., Gomez, M. P. and Anderson, W. E.
    A RATIONAL ANALYTICAL THEORY OF FATIGUE, The Trend in
    Engineering, University of Washington, Vol. 13, No. 1,
    January 1961.

13. Albrecht, P. and Yamada, K.
    RAPID CALCULATION OF STRESS INTENSITY FACTORS, Paper
    submitted for publication in the Journal of the Structural
    Division, ASCE.

14. Zettlemoyer, N.
    STRESS CONCENTRATION AND FATIGUE OF WELDED DETAILS,
    Ph.D. Dissertation in preparation, 1976.

15. Tada, H., Paris, P. and Irwin, G.
    THE STRESS ANALYSIS OF CRACKS HANDBOOK, Del Research
    Corporation, Hellertown, Pennsylvania, 1973.

16. Alpsten, G. A. and Tall, L.
    RESIDUAL STRESSES IN HEAVY WELDED SHAPES, Welding Journal,
    Vol. 49, March 1970.

17. McFalls, R. K. and Tall, L.
    A STUDY OF WELDED COLUMNS MANUFACTURED FROM FLAME-CUT PLATES,
    Welding Journal, Vol. 43, April 1969.

18. Fisher, J. W., Frank, K. H., Hirt, M. A. and McNamee, B. M.
    EFFECT OF WELDMENTS ON THE FATIGUE STRENGTH OF STEEL BEAMS,
    NCHRP Report No. 102, Highway Research Board, National Academy
    of Science-National Research Council, Washington, D.C., 1970.

19. Tebedge, N., Alpsten, G. and Tall, L.
    RESIDUAL-STRESS MEASUREMENT BY THE SECTIONING METHOD,
    Experimental Mechanics, Vol. 13, No. 2, pp. 88-96,
    February 1973.

20. Tebedge, N., Alpsten, G. and Tall, L.
    MEASUREMENT OF RESIDUAL STRESSES, A STUDY OF METHODS, Fritz
    Engineering Laboratory Report No. 337.8, Lehigh University,
    February 1971.

21. Madison, R. B.
    APPLICATIONS OF FRACTURE MECHANICS TO BRIDGES, Fritz
    Engineering Laboratory Report No. 335.2, Lehigh University,
    June 1969.

11. APPENDICES

The two-ended crack shown in Fig. A.1 was analyzed by using a method similar to that proposed by Madison[21]. The crack openings of the flange and web crack at the web-to-flange junction are known to be equal. Therefore, to satisfy compatibility, a closing force was applied to the flange crack and an opening force is applied to the web crack.

The flange crack opening at the compatibility point is a function of the applied stress and the residual stress. Local weld effects can be neglected since the crack tip is distant from the detail welds.

$$v_f = v_{f_{AS}} + v_{f_{RS}} \tag{A1}$$

$v_{f_{AS}}$ was obtained from the formulation presented in Ref. 15 (see Fig. A.1

$$v_{f_{AS}} = \frac{4 \sigma a}{E} V_1 \left(\frac{a}{b} \right) \tag{A2}$$

$$V_1 \left(\frac{a}{b} \right) = \frac{1}{\left(\frac{\pi a}{2b} \right)} \left\{ 0.459 \left(\sin \frac{\pi a}{2b} \right) - 0.065 \left(\sin \frac{\pi a}{2b} \right)^3 - 0.007 \left(\sin \frac{\pi a}{2b} \right)^5 + \cosh^{-1} \left(\sec \frac{\pi a}{2b} \right) \right\}$$

$v_{f_{RS}}$ was derived following the formulation presented by Madison[21] for a partially loaded edge crack (see Fig. A.3)

$$x < c: \quad V_{RS} = \frac{4\sigma}{E\pi} \left(V_1 \left(\frac{a}{b} \right) \right) \left\{ \sqrt{a^2 - x^2} \sin^{-1} \frac{c}{a} + c \coth^{-1} \sqrt{\frac{a^2 - x^2}{a^2 - c^2}} \right.$$

$$\left. - x \coth^{-1} \frac{c}{x} \sqrt{\frac{a^2 - x^2}{a^2 - c^2}} \right\}$$

$$x > c: \quad V_{RS} = \frac{4\sigma}{E\pi} \left(V_1 \left(\frac{a}{b} \right) \right) \left\{ \sqrt{a^2 - x^2} \sin^{-1} \frac{c}{a} + c \tanh^{-1} \sqrt{\frac{a^2 - x^2}{a^2 - c^2}} \right.$$

$$\left. - x \tanh^{-1} \frac{c}{x} \sqrt{\frac{a^2 - x^2}{a^2 - c^2}} \right\} \tag{A3}$$

$$x = 0$$

$$V_{RS} = \frac{4\sigma}{E\pi} \left(V_1 \left(\frac{a}{b} \right) \right) \left\{ a \sin^{-1} \frac{c}{a} + c \coth^{-1} \left(1 - \frac{c^2}{a^2} \right)^{-1/2} \right\} \tag{A4}$$

The web crack opening at the compatibility point is also a function of the applied stress and the residual stress[15].

$$v_w = v_{w_{AS}} + v_{w_{RS}}$$

$v_{w_{AS}}$ was estimated following the formulation presented in Ref. 15 for the in-plane bending case (see Fig. A.3 for the diagram)

$$v_{w_{AS}} = \frac{4 \sigma a}{E} V_2 \left(\frac{a}{b} \right)$$

$$V_2 \left(\frac{a}{b} \right) = 0.8 - 1.7 \left(\frac{a}{b} \right) + 2.4 \left(\frac{a}{b} \right)^2 + \frac{0.66}{\left(1 - \frac{a}{b} \right)^2} \tag{A5}$$

-204-

$V_{w_{RS}}$ was derived in a manner identical to $v_{f_{RS}}$

If $v_f < v_w$ there is no web restraint and the stress intensity can be computed by analyzing the flange edge crack alone. If $v_f > v_w$, there is a web restraining effect.

The difference between v_f and v_w, Δv, has to equal zero to meet the compatibility conditions

$$\Delta v = v_f - v_w \tag{A6}$$

After defining an interaction area (see Fig. A.2) a closing force was applied to the flange crack. Similarly, an opening force is applied to the web crack. This force must be defined as a stress acting over an interaction area since crack displacement at a point load is not defined. The flange closing, v_{f_c}, and the web opening, v_{w_o}, are defined by Eqs. A1 and A5 as a function of stress σ_f and σ_w.

$$v_{f_c} = f(\sigma_f) \tag{A7}$$

$$v_{w_o} = f(\sigma_w)$$

Since the interaction area is assumed to be common to both the flange and web then

$$|\sigma_f| = |-\sigma_w| \tag{A8}$$

By the compatibility condition

$$v_{f_c} + v_{w_o} = \Delta v \tag{A9}$$

σ_{f_c} or σ_{w_o} can be solved directly from Eqs. A7 and A9. From the stress in the flange σ_f, and the assumed interaction area a restraining value of K can be determined through Eq. 14 in Section 4.5.4.

Ideally this procedure should be an iterative one using the plane stress plastic zone correction

$$r_y = \frac{1}{2\pi} \left(\frac{K_c}{\sigma_Y} \right)^2$$

Since the fracture toughness, K_c, of the material from the material characterization is known, a first approximation of r_y can be obtained and thus a good estimate of K_{WR}. This was the case for analysis of beam B4A. Only one iteration was needed since the interaction area was in the top one-third of the flange thickness as shown in Fig. A.2. The restraint was decreased linearly to the bottom one-third. Thus K_{WR} was -12, -6, 0 for top, middle and bottom levels of the flange thickness.

a   = edge crack size; semi-minor axis crack size for an elliptical crack

a' = $a + r_y$

B   = 3 point bend specimen width

b   = flange width

C   = semi-major axis crack size for an elliptical crack

c   = dimension from the plate edge to the end or beginning of the approximated block of residual stress (see Fig. 4.17)

E   = Young's Modulus, 29000 ksi

E_k = elliptical integral of the second kind

$F(a') =$ $F_E \ F_G \ F_S \ F_W$

F_E = elliptical crack front correction, $\dfrac{1}{E_R}$ for $\Phi = 90°$

F_G = stress concentration correction

F_S = free surface correction

F_W = finite width correction

K   = linear elastic fracture mechanics stress intensity factor

      = $K_{AS} + K_{RS} + K_{LW} + K_{WR}$

K_{AS} = stress intensity contributions from the applied stress

K_{RS} = stress intensity contribution from the nominal section residual stresses

K_{LW} = stress intensity contribution from the local weld residual stresses

K_{WR} = stress intensity contribution from the web restraint

K_c = fracture toughness value

K_{Id} = fracture toughness value from the dynamic material test

K_T = stress concentration factor

$$k = \left[1 - \left(\frac{a}{c}\right)^2\right]^{-1/2}$$

P = applied load

r_y = plastic zone size

t = loading time to maximum load

t_o = time of load application for a static tensile test

T = testing temperature

T_{cp} = cover plate thickness

T_f, t_f = flange thickness

v_f = flange crack opening, $= v_{f_{AS}} + v_{f_{RS}}$

$v_{f_{AS}}$ = flange crack opening from the applied stress

$v_{f_{RS}}$ = flange crack opening from the residual stress

v_w = web crack opening

$v_{w_{AS}}$ = web crack opening from the applied stress

$v_{w_{RS}}$ = web crack opening from the residual stress

z = fillet weld leg size

σ_{AS} = applied stress

σ_Y = yield stress

σ_{YD} = yield stress as a function with loading rate and temperature

σ_r = stress range

σ_{rs} = residual stress block stress

Φ = parametric angle, see Fig. 5.12

12. <u>VITA</u>

Keith Dale Boyer, the son of Eleanor and Lee D. Boyer, was born on January 24, 1952 in Ashland, Pennsylvania. The author grew up in Lebanon, Pennsylvania and was graduated from Lebanon Senior High School in 1969.

His undergraduate studies were conducted at Lehigh University where he received two undergraduate degrees. In 1973 he received a Bachelor of Arts in Applied Science and in 1974 he received a Bachelor of Science in Civil Engineering. Continuing his education at Lehigh University, he was awarded a Research Assistantship in Civil Engineering at Fritz Engineering Laboratory, Lehigh University, in September 1974 and received his Master of Science in Civil Engineering, with a structures major, in May 1976.

The author has co-authored Fritz Engineering Laboratory Report No. 399-2(76), "Fracture Analyses of Full Size Beams with Welded Lateral Attachments".